INSTANTANEOUS AND FREQUENCY-WARPED SIGNAL PROCESSING TECHNIQUES FOR AUDITORY SOURCE SEPARATION

A DISSERTATION
SUBMITTED TO THE DEPARTMENT OF ELECTRICAL ENGINEERING
AND THE COMMITTEE ON GRADUATE STUDIES
OF STANFORD UNIVERSITY
IN PARTIAL FULFILLMENT OF THE REQUIREMENTS
FOR THE DEGREE OF
DOCTOR OF PHILOSOPHY

By
Avery Li-Chun Wang
August, 1994

Abstract

This thesis summarizes several contributions to the areas of signal processing and auditory source separation. The philosophy of *Frequency-Warped Signal Processing* is introduced as a means for separating the AM and FM contributions to the bandwidth of a complex-valued, frequency-varying sinusoid $p[n]$, transforming it into a signal with slowly-varying parameters. This transformation facilitates the removal of $p[n]$ from an additive mixture while minimizing the amount of damage done to other signal components. The average winding rate of a complex-valued phasor is explored as an estimate of the instantaneous frequency. Theorems are provided showing the robustness of this measure.

To implement frequency tracking, a *Frequency-Locked Loop* algorithm is introduced which uses the complex winding error to update its frequency estimate. The input signal is dynamically demodulated and filtered to extract the envelope. This envelope may then be remodulated to reconstruct the target partial, which may be subtracted from the original signal mixture to yield a new, quickly-adapting form of notch filtering. Enhancements to the basic tracker are made which, under certain conditions, attain the Cramér-Rao bound for the instantaneous frequency estimate.

To improve tracking, the novel idea of *Harmonic-Locked Loop* tracking, using N harmonically constrained trackers, is introduced for tracking signals, such as voices and certain musical instruments. The estimated fundamental frequency is computed from a maximum-likelihood weighting of the N tracking estimates, making it highly robust. The result is that harmonic signals, such as voices, can be isolated from complex mixtures in the presence of other spectrally overlapping signals. Additionally, since phase information is preserved, the resynthesized harmonic signals may be removed from the original mixtures with relatively little damage to the residual signal.

Finally, a new methodology is given for designing linear-phase FIR filters which require a small fraction of the computational power of conventional FIR implementations. This design strategy is based on truncated and stabilized IIR filters.

These signal-processing methods have been applied to the problem of auditory source separation, resulting in voice separation from complex music that is significantly better than previous results at far lower computational cost.

Acknowledgments

There are many people who were involved in providing an environment in which this thesis and the ideas contained within could be realized.

I would like to extend my profound gratitude to my advisor, Julius O. Smith, III, for infinite patience, kindness, encouragement, friendship, enthusiasm, and encyclopedic knowledge of signal processing. Despite being in high demand, he always made the time to advise and share his broad-band wisdom in matters beyond just signal processing. His excellent advising during the two years I have been at CCRMA were among the salient factors motivating the most creative and productive months of my research career to date.

My appreciation goes to the faculty, staff, and students at the Center for Computer Research in Music and Acoustics, John Chowning, Chris Chafe, and Heidi Kugler, and many others. The interdisciplinary blend of musicians and engineers from all over the world created an open, friendly, and relaxed environment in which to work. I would especially like to thank Fernando Pablo Lopez-Lezcano, our jack-of-all-trades, resident composer, and Unix sysadmin, who helped greatly and showed great patience and trust as I continually performed minor surgeries on our NeXT network. I am grateful for the CCRMA DSP Seminar, organized by Julius, and its participants. It was in this relaxed, friendly, and well-informed forum that I was able to beta-test my craziest ideas without fear of unconstructive criticism. Thanks, also, go to Malcolm Slaney for running the CCRMA Hearing Seminar.

I would like to honor the memory of the late Allen M. Peterson, who was my advisor during the early, amorphous stage of my graduate student career. Professor Peterson was always flexible and encouraging, allowing me to explore many different areas while I was trying to decide on my specialization. This freedom enabled me to masquerade as a neuroscientist for some time with no pressure to find a direct link with Electrical Engineering, letting me explore new horizons and form new insights. Professor Peterson will be remembered for his unfailing kindness, encouragement, and humor, and for his many achievements, including his leadership of STAR Lab.

I would also like to acknowledge the Stanford Neurobiology Department, and especially Bill Newsome, Ken Britten,[1] who provided a great opportunity for an outsider to learn about the fascinating world of neurobiology. Ken and Bill were patient and friendly with me while I worked in their lab doing data analysis.

I would like to thank the National Science Foundation for their generous graduate fellowship which allowed me three years of no-strings-attached funding, during which I was free to explore many different areas inside and outside of Electrical Engineering. The creativity expressed in this thesis may not have been possible without that freedom. I would also like to thank the CCRMA Affiliates, whose generosity, along with that of the Stanford Electrical Engineering Department, provided funding for my last 6 months of graduate work.

[1] Presently at UC Davis.

I extend my gratitude to Professor Christoph von der Malsburg of the *Institut für Neuroinformatik* at the *Ruhr-Universität Bochum*, in Bochum, Germany, under whom I studied from August of 1990 to September of 1992 while on a Fulbright scholarship. I would like to thank him, the German Fulbright Kommission, and its director, Reiner Rohr, for generously providing me the opportunity to learn about another culture and language, as well as giving me free reign and resources to pursue my scientific interests. I also express my thanks to Christoph for being patient with me while I experienced culture shock and went off in directions which were orthogonal to his group's main research focus. I would also like to acknowledge my colleagues and friends there, especially Martin Lades (now at Lawrence Livermore), the *Halbausländer* whose openness and friendship I value highly, and René Doursat, the amazing and unconventional Frenchman whose kindness, creativity, humor, irreverence and discussions I will always cherish. Thanks also to Michael Neef, the patient sysadmin who ruled over a large, heterogeneous network with heterogeneous users.

My gratitude goes to the members of my orals committee: Julius Smith, Stephen Boyd, John Chowning, Constance Chang-Hasnian, and the late Allen Peterson. Also, my appreciation goes to my reading committee: Julius Smith, Stephen Boyd, and especially Gene Franklin, who kindly and personally took on the responsibility of covering for Dr. Peterson on very short notice.

I would like to express my thanks to my friends: you know who you are. Special thanks go to Francisco Marquez, Robert Sage, and Jim Spencer, who were my housemates during this project. Their support, flexibility, and friendship were valuable in keeping me sane.

I would like to extend my great appreciation to Timothy J. Hawks, who is among the most multi-dimensionally talented people I have had the privilege to befriend. Tim kept me focussed on the immediate goals when I didn't know which of many directions to take in my research. His comments and insights were always deep and valuable. I am profoundly thankful for his quick advice, proofreading, and suggestions.

I would like to express my great thanks and love to my dear Katja Andrea Rault, who is enthusiastic, positive, curious, generous, infinitely loving, and supportive. I would like to thank her for her patient understanding and flexibility, especially during the time this thesis was finally being condensed from vague notions into its final draft.

My greatest thanks are to my parents, who made all this possible through their incredible support. I am proud to be able to dedicate this dissertation to them.

Preface

This dissertation is one continuing step in the evolution of my excursion through the various domains of knowledge related to my life-long interest in how the mind works. The material presented here may seem rather removed from the problems of the philosophy of mind. Let me confirm that it is indeed largely irrelevant to such musings. However, let me also try to explain my perspective that makes the research presented here a plausible, if haphazard, continuation of my prime interest.

If I were not as lazy as I am, I most likely would have studied biology as an undergraduate and continued with neurosciences in graduate school. Upon arriving at Stanford as an undergraduate I had decided to study psychology, and not mathematics, since I felt that I had had enough of math in high school and wanted to pursue something more directly related to my most burning interest. After sitting in on a few sessions of Psych 1 I decided that biology would suit my goals better and shortly thereafter declared biology to be my major. I took the Bio Core at Stanford and found that I was worse at photographically memorizing pages out of biology texts than at organic chemistry, despite my enthusiasm and fascination for the mechanisms of life and the mind. My lack of discipline in forcing myself to memorize finally led me to the path of least resistance, whereupon I finally changed my major to mathematics–the subject in which most things are "obvious by inspection" or "left as an exercise to the reader."

My interest in the inner workings of the mind persisted in the background, leading me to courses in the Department of Electrical Engineering. I was interested in problems in cybernetics and thought that knowledge in the fields of control theory, information theory, and signal processing could be applied to problems in biological information processing. I felt that if I took this angle I could have a well-informed approach to the challenge of understanding how the mind works. Indeed, in order to study the mind effectively nowadays, one must have a thorough grounding in biology, psychology, statistics, electrical engineering, philosophy of mind, and several other related subjects.

My initial area of interest as a graduate student in Electrical Engineering was in the field of neural networks. I had enough familiarity with neural networks to know that I did not want to follow the beaten path of back-propagation and set forth on the search for biologically realistic models of neural functioning. I joined Allen M. Peterson's lab in 1988 with the intention of doing research in a VLSI implementation of a neural net model. The problem then was to find a model I liked enough to want to implement in silicon. I promptly enrolled in several classes in the Neurosciences program, reviving my dormant interests. Despite the largely empirical and somewhat disconnected nature of the field I saw that there has been much recent progress in developing a well-founded basis of understanding on which to hang the many empirical observations. Indeed, one estimate has it that over 90% of what is known about the brain has been discovered in the last 5-10 years. I believe that this statement will remain true for many decades to come. With the explosion of new techniques and technologies in functional imaging, electrophysiology, neurochemistry, anatomical tracing, developmental neurobiology, psychophysics, biophysics, and molecular genetics, just to name a few areas, optimism about finally being able to understand how the brain works has never been

higher.

Unfortunately, I found that the time was not yet ripe for collaboration between the fields of neurobiology and electrical engineering at Stanford in 1989. In neurobiology, I found serious biologists who were interested in serious biology. Interdisciplinary cooperation with engineers was generally not feasible, perhaps mostly because of the lack of common goals, knowledge, approaches to scientific problem solving, and culture.

My short stay as a data analysis programmer in William T. Newsome's systems neurobiology laboratory of during the academic year of 1989-1990 was valuable in showing me a different, more intellectually disciplined approach to problem solving than I was used to. In neurobiology, one cannot often afford to be as hypothetical and speculative as in the mathematical sciences. The length of time and effort it takes to set up an experiment leads one to be more cautious about going off on exploratory "fishing trips" where it isn't clear what the goal is. The kind of experiments that are more likely to be attempted are ones where the outcomes are expected to fall within a small set of well thought-out possibilities.

In contrast, those who practice "computational neurosciences" are fortunate to be able to set up experiments and obtain results rather quickly. Hence, one has more freedom to try out wild, speculative experiments. However, as Florentin Wörgötter, a researcher at the *Ruhr-Universität Bochum* and Caltech, once said, "simulations are doomed to success." Indeed, those who do this kind of research usually find what they are looking for, after choosing their mathematical models and setting the boundary conditions to attain the desired results.

Not having a clear idea of what I wanted to write my dissertation on, I decided to apply for a Fulbright grant to Germany. Mike Stryker of UCSF recommended looking at the research that Christoph von der Malsburg was doing. He was in the process of founding a new division of the "Institut für Neuroinformatik" in Bochum, Germany. This was to be a center for research into new theories of neural pattern matching based on von der Malsburg's "Dynamical Link Architecture" (DLA) theory, which was a "biologically realistic" neural net model. I received the Fulbright grant and found myself in Germany from August of 1990 to September of 1992. My goal was to find a thesis topic while I was in Germany.

I did achieve this goal after taking several more serpentine paths. I initially studied the dynamics of von der Malsburg's DLA theory, writing some computer simulations. However, I became disenchanted with the idea of amorphous self-organizing systems, and turned my attentions towards studying the literature in neurobiology. I eventually became interested in the field of auditory perception. I saw clear advantages in focusing on this area:

1. The state of knowledge in auditory research is perhaps over a decade behind vision. For example, it is currently known that there are at least 35 visual areas in the visual cortex [53]; on the other hand, the layout of the auditory cortex is vaguely known to consist of a small number of auditory fields. Perhaps the most extensively studied part of the auditory system is the cochlea. To this day, the proportion of efforts in auditory physiology and modeling research devoted to studying the cochlea is rather large. My rough impression is that there is proportionally more research being done on the cochlea relative to the rest of the auditory system than there is research being done on the eye relative to the rest of the visual system. Hence, there is much unexplored territory waiting to be discovered, especially in the central auditory system.

2. Auditory perception is an extremely interesting problem. Accurately or not, it is relatively easy to be introspective and imagine how we process visual information. We can imagine movies being fed in frame by frame through various stages of feature extractors which form retinotopically mapped representations of the visual scene. For most of us, however, it is

relatively difficult to imagine the kinds of cortical representations that auditory stimuli must be mapped onto. The representations are most likely time-based, since sound is, by nature, a temporal entity. I believe that understanding the auditory system may help us to understand better how the visual system works. My belief is that the focus on the retinotopy in the visual system has lead many researchers astray from the temporal aspects of visual processing. Since the neocortex is evolutionarily relatively recent and has a common 6-layered motif over its entire extent, one might expect intuitively that the auditory and visual cortices might have some functional characteristics in common.

3. Finally, there are far fewer researchers studying psychoacoustics and auditory physiology than those studying vision. The advantage of this is that one is less anonymous.

My thesis topic, then, was to study the problem of auditory scene analysis. Specifically, I wanted to pull apart sounds into distinct, conceptually grouped "sources." Hence, a complex auditory scene would be decomposed into separate channels, each of which would represent a separate voice, musical instrument, a barking dog, or other self-coherent sound source.

Auditory science is a "second class" discipline compared to visual science.[2] Indeed, the emphasis in Bochum was on vision, and in von der Malsburg's group, it was focussed on face recognition. I was half of the auditory research team[3] there amongst about 50 workers in visual science whose interests ranged among visual neurophysiology, computational modeling of the visual cortex, and computer vision.

Two years in Germany were sufficient for me, so I returned to Stanford in October of 1992. Having acquired an interest in acoustics and auditory source separation, I became affiliated with CCRMA, the Center for Computer Research in Music and Acoustics. I became associated with Julius Smith and benefitted greatly from his advice and knowledge of signal processing. Although Julius's main research interests during this time were in musical sound synthesis using the Waveguide technique he invented, he encouraged me greatly in my forays into bizarre methods of audio signal processing, providing plenty of fruitful discussions, one of which gave rise to the fast FIR algorithm presented in Appendix G. It was in this fertile environment at CCRMA during the previous two years that I developed the ideas contained in this dissertation, bringing to a close my six-year random walk as a PhD student.

[2] Tactile and olfactory research is even less prestigious!

[3] Christian Kaernbach was the other half.

Contents

Appendices

List of Tables

List of Figures

Chapter 1

Introduction

Imagine sitting at a busy college cafe. A man sits in the corner with his manual typewriter clacking away constantly. There are dozens of people milling about, holding a jumble of conversations. You eavesdrop on some of them as you sip your coffee. Some students are discussing strategies for staging another protest against the school's admissions policies. Some teaching assistants are discussing the grading scale for a recent exam. A student is fervently advocating the most radical waves to be surfed in the Western hemisphere. You fade back to your lunch partner, who is still describing his weekend spiritual retreat in the Santa Cruz mountains. The music catches your attention. It's Peter Gabriel singing something about a sledgehammer. You shift your restless auditory attention around effortlessly to listen selectively to any of these streams of conversation or music. In your boredom, you are performing *auditory source separation*–dissecting the energy from your complex acoustical environment which impinges upon your two ears into streams of sensation corresponding to conceptually grouped auditory events.

What is one person's boredom can be another's fascination. How do we do it? Technically, it is a very difficult problem. We are required to parse a very complex superposition of many overlapping, broad-band, and non-stationary signals into independent, meaningful constituents. Auditory source separation, also known as "auditory scene analysis," "auditory streaming," and "auditory grouping," is currently the focus of a growing number of researchers around the world. Ever since about the mid 1960's there has been a rising interest in the problem of how we group sounds together. We still do not know exactly what kinds of computation are involved in the execution of auditory source separation, although much progress is being made. The problem is being approached from many different directions. The process of auditory perception has been studied by neurobiologists, psychologists, musicians, physicists, engineers, and computer scientists.

There seem to be two main goals of the research in auditory source separation. The first is to provide understanding of how we, as psychological and biological organisms, perceive sounds. This line of inquiry concerns primarily neurobiologists and psychologists. The other goal is to create an artificial system which can take a recorded sound and automatically separate it into representations of component auditory streams which can be played back in isolation. This line of inquiry is not restricted to implementing models of auditory function, though many researchers try to incorporate some form of physiological realism into their models.

It is not clear at all if our brains actually do sort out auditory sources into separate channels for our inner homonculus's selective listening pleasure. Indeed, those studying the philosophy of mind generally agree that such a homonculus is unnecessary since it just puts off explanations to a higher level. Positing the separation of sounds into separate channels corresponds to our auditory phenomenology. After all, we believe that we hear separated sounds, so sound separation is what

must go on in our auditory system, right? Not necessarily. We do not exactly perceive reality, but rather, an interpreted version of it. A good example is the rather large blind spot all humans have lateral to the fovea in each eye. Most people go through life never noticing this huge hole in their visual experience since the brain seems to "fill in" the gap. The philosopher Daniel C. Dennett argues that filling in is not necessary because that would presume the existence of a homonculus to observe the filled-in region [48]. The point here is that what we perceive does not necessarily reflect what is really there. Hence, the fact that we believe we can hear separate streams does not necessarily imply that we actually do produce those streams anywhere within our auditory system. Given this somewhat pessimistic outlook on the phenomenology of streaming, we cannot conclude that there exists a general way to separate mixtures of acoustical energy into their conceptually distinct component sources. Hence the goal of creating a source separation system may actually be impossible. It may be possible, however, to create an interpretive system that can resynthesize streams of sound that it believes it has detected. Such a system would be susceptible to illusions and hallucinations, as are we.

We present an extremely brief summary of research in auditory scene analysis. The history of auditory scene analysis stretches back many years. Among the first to write about the phenomenon was the great psychophysicist and physicist, Hermann von Helmholtz [28, 65], who, in 1859, was concerned about the grouping of harmonics in complex piano tones into coherent percepts.

In 1953, Cherry identified the "Cocktail-party effect," in which a listener deprived of binaural information can nonetheless attend selectively to one out of a mixture of several speakers [31]. More recently, Bregman [23] has compiled a wonderful tome summarizing the known facts (in 1990) about psychoacoustical grouping and the perceptual organization of sound, much of which has been determined in the last 25 years.

Ideas from *gestalt* perceptual psychology for grouping have been used by some researchers [26, 40, 50, 51, 96, 145] as guidelines for implementing artificial systems which can segment sounds into meaningful streams. Some examples of strong cues for grouping auditory events are: common location, harmonicity, common onsets, common frequency modulation, and common amplitude modulation. Generally, if events in auditory channels occur simultaneously or are modulated coherently it is likely that they have some common origin, and therefore should be grouped together [23]. Technical approaches to auditory source separation usually consist of decomposing sounds into some kind of filterbank representation, constructing feature maps of some subset of qualities listed above, and then using some kind of high-level grouping scheme to sort out the features in each map.

For a more complete survey of the literature and history on auditory scene analysis, the curious reader should refer to Bregman's book [23] on psychoacoustical factors of auditory scene analysis. Brown [26], and Cooke [40] also contain good discussions of the history of psychoacoustical as well as computational approaches.

1.1 Previous Work in Auditory Source Separation

In this section, we give a quick survey of the relevant work in creating an artificial auditory source separation system. Work is reported in which resynthesis and separation was reported.

1.1.1 Spatial Approaches

A number of researchers have attempted to segment ambient sound mixtures into streams based on spatial location. We mention two approaches in this direction.

1.1.1.1 Phase-Array Detectors

In a broad sense, phase-array detectors may be seen as a long-standing solution to the problem of source separation based on spatial location. The literature on such devices is vast, spanning many decades, and covering many related areas such as radar, adaptive beamforming, adaptive noise cancellation, and ultrasound imaging [90]. An excellent book by Haykin which covers these topics in detail is [63].

The principle is simple: given a large array of microphones in a rectangular lattice, the spatial location of a sound may be estimated from the relative phases of the signals received at each point in the array. Additionally, a weighted average of the microphone array elements can be computed which results in a selective sensitivity to signals from specific locations in space. This is a process called *beamforming*. If the beamforming process is servoed to the location of the source, the process is called *adaptive beamforming*.

1.1.1.2 Blauert and Lindemann

The phase-array approach does not address the issue of human spatial hearing. For one thing, since the weighted summation over the microphone array is a linear summation equivalent to performing an inverse two-dimensional Fourier transform on the array values, the spatial resolution is proportional to the number of elements. Hence, a large number of "ears" are necessary for meaningful spatial localization using this method. Since humans nominally have two ears, the phase-array method must be ruled out as a strategy used by humans for spatial hearing.

Jens Blauert and Werner Lindemann at the Ruhr-Universität Bochum in Germany have developed a model of auditory spatial localization based on cross-correlations between the two ears [16, 86]. Their approach is to use a model of the medial superior olivary (MSO) nucleus in the medulla. The MSO is thought to compute spatial information from the relative arrival times of neural impulses from the two ears using a kind of anti-parallel ladder network [71, 77]. In his dissertation, Lindemann computes a two-dimensional map of filterbank channels versus interaural time disparity and groups according to peaks in the cross-correlation. The result is a 15 dB relative enhancement of one of two simultaneously speaking voices in differing spatial locations. The spatial selectivity had to be set by hand, however; no automatic localization was known to be available as of this writing.

1.1.2 Periodicity-and Harmonicity-Based Methods

A number of researchers have used periodicity pitch information towards the goal of auditory source separation.

1.1.2.1 Stockham

Tom Stockham, the pioneer of digital audio technology, was among the first to apply signal-processing techniques to separate a voice from a musical recording. Stockham used homomorphic deconvolution [20, 105, 106, 116] to pull out the voice of the singer Caruso from the background noise as well as the orchestral accompaniment [131]. RCA records has published a set of restorations and original recordings made after 1906, entitled "The Complete Caruso."

1.1.2.2 Parsons

Parsons used an FFT approach to analyze frames of sampled speech [109]. The peaks of each time frame were tabulated and a first fundamental frequency was determined using a method by Schroeder [125] to account for one set of harmonics. The identified harmonics were then sorted out

and the process repeated to identify the harmonics due to the second speaker. The two voices were resynthesized frame-by-frame using their respectively tagged FFT bins. The quality of separation was reported as being good.

1.1.2.3 Weintraub

Mitchel Weintraub provided an early computational model of monaural source separation for speech [145]. His work is based on grouping together autocorrelation peaks with similar periodicities across channels of a cochlear filterbank. Once a salient correlation peak across channels is found, a score is computed to determine how much of the energy in each channel contributes to that common periodicity peak. For resynthesis, the time-aligned, reconstructed waveform for each filterbank channel is weighted with the score for the target peak autocorrelation period and summed together.

1.1.2.4 de Cheveigné

Alain de Cheveigné based his work on voice separation on minimizing the output power of a comb filter [42–46]. To separate two voices, de Cheveigné processed frames of sampled speech using an exhaustive search of all combinations of comb filter delays τ_A and τ_B, with $\tau_{\max} > \tau_B > \tau_A > 0$ [43]. The pair that minimized the filter's output energy were then assumed to be the pitch periods of the two target voices during that speech frame. The output of the algorithm was fed to a speech recognition system; improved recognition rates were claimed [42]. de Cheveigné's technique is similar to that studied by J. A. Moorer [97, 98].

A further discussion of comb filtering is given in Section 1.2.4.

1.1.2.5 Holdsworth

John Holdsworth was able to perform separation by calculating envelope modulation maps of voice signals. He effectively calculated a filterbank analysis of the envelope of each output channel of a filterbank, thereby generating a two-dimensional map of modulation frequency versus filter center frequency. He then grouped the signals on the map across filterbank channels for a fixed modulation frequency and resynthesized the signal according to the energy in each channel. For resynthesis, the grouped modulation frequency channel had to be picked by hand. The result was somewhat intelligible separated speech.

This work is similar to that of Weintraub [145]. Weintraub finds peaks in the autocorrelation of each channel, whereas Holdsworth finds peaks in the modulation envelope power spectrum. The two works are thus related by a Fourier transform. Holdsworth's method is advantageous because the periodic peaks in the autocorrelogram collapse onto a single peak in the modulation envelope power spectrum.

1.1.2.6 HBSS

Tomohiro Nakatani, Hiroshi G. Okuno, and Takeshi Kawabata of NTT Basic Research Laboratories, Japan, have pursued a grouping strategy based on tracking harmonic signals, called "HBSS" (Harmonic-Based Stream Segregation) [99]. Speech signals are analyzed with a 512-point FFT, yielding 256 frequency channels. Each channel monitors signal onsets, creating a "tracer" agent to track its target signal for onsets that exceed a dynamically determined power threshold. The tracked signal is subtracted from the global input source in order to minimize interference between tracer units; ideally, each tracer should not see the others' target signals. If each component harmonic signal is accounted for perfectly by the corresponding number of tracers the residual signal should

have no residual energy. This cross-signal cancellation scheme is similar to the "RSA" (Residual Signal Analysis) strategy introduced by Costas [41] in 1981 and its successor called "RISC" (Residual Interfering Signal Canceler) by Kumaresan, *et al* [78, 79, 117].

The HBSS method accounts for contention among tracers for the same signal by providing a monitoring agent for each tracer. Tracers that are trying to track a signal which is already accounted for are eliminated.

HBSS has been demonstrated on the separation of simultaneous male and female voices speaking continuous vowel sequences plus noise, achieving clear and intelligible results.

1.1.3 Marrian Approaches

The work of David Marr [93] has been quite influential in the evolution of research towards a technical solution to auditory source separation. Marr defines three fundamental levels of perceptual information processing:

1. The *implementation*, or *mechanism* level. This level focuses on the low-level details of what is known about a perceptual phenomenon. In perceptual psychology, this would correspond to the study of neurons, ion channels, and gene expression. In a technical solution this would correspond to the specific software and hardware used.

2. The *algorithm and representation*, or *process* level. This is one level of abstraction higher than the previous level, and focuses on block diagrams, incorporating clearly labeled inputs and outputs of well-defined functional blocks.

3. The *computational theory*, or *functional model* level. This is the highest level of abstraction and focuses on the problem to be solved rather than the method used to solve it.

Marr emphasizes this last approach, reasoning that

> "The nature of the computations that underlie perception depends more upon the computational problems that have to be solved than upon the particular hardware in which their solutions are implemented..." [93, p. 27]

Marr argues that the three levels of abstraction are only loosely related, and that explanations at one level should be independent of the explanations at the other two levels.

Marr also advocates four principles for the organization of complex computational processes. They are:

1. *The principle of explicit naming.* Any data to be processed must be given a name to abstract it for symbolic computational purposes.

2. *The principle of modular design.* A large computation should be broken up into small functional units which are as independent of each other as possible.

3. *The principle of least commitment.* Nothing should be done which may later have to be undone.

4. *The principle of graceful degradation.* The system should break down in a robust manner as the data become corrupted.

We cite some examples of technical work influenced by Marr.

1.1.3.1 Sheffield Work

Martin Cooke [40] and Guy Brown [26] at the University of Sheffield have done work on computational auditory scene analysis based on Gestalt grouping principles and AI techniques, following the Marrian school of thought.

Cooke Cooke attempts to give consideration to biological models by filtering sound signals through a physiologically modeled complex-valued cochlear filterbank [110]. In each channel, this is followed by the calculation of the instantaneous frequency by taking the time derivative of the phase of the each complex filterbank channel, followed by zero-crossing detection of the derivative across frequency of the smoothed distribution of instantaneous frequency minus the center frequency of each channel. Each zero-crossing then corresponds to a spectral peak. This is called "place group" extraction. Once the place groups have been extracted, the place groups which are continuous across time are aggregated together to form "synchrony strands." These synchrony strands are then passed to an AI-based search using Marr's hierarchical heuristics. Strands which have common onsets, harmonicities, AM, continuity, and other common *gestalt* grouping properties are placed together. Cooke provides for resynthesis of extracted signal components.

Brown Brown continues the line of research at Sheffield in the Marrian style by using a variety of maps, based on periodicity, onsets and offsets, and frequency transition. The extracted feature maps are given to an AI-based heuristic search to group signal components based on *gestalt* grouping rules.

The results of Brown's auditory source separation analyses may be retrieved by anonymous FTP to sound.media.mit.edu, and is in the directory /pub/Sounds. The relevant files are

- brn1_16k.aiff,
- brn2_16k.aiff,
- brn3_4_16k.aiff, and
- brn5_16k.aiff.

1.1.3.2 Dan Ellis–MIT Media Lab

[50, 51] The work by Ellis is has a similar approach to that of the Sheffield group. He preprocesses his sounds by with a cochleogram transform and picks peaks across frequencies using a sinusoidal peak-picking algorithm by McAulay and Quatieri [94]. The results are then sorted out by a grouping rules based on harmonicity, FM, onsets, AM, continuity, and proximity.

His sound results may be retrieved at the same FTP site and directory under the names

- clacan.aif,
- cla.sep.aif, and
- can.sep.aif.

The sound example is that of a clarinet mixed with a dropped can. The separated clarinet and can are presented in their respective sound files.

1.2 Related Signal Processing Areas

We mention here a few topics that are either related to auditory source separation or other signal processing topics addressed in this thesis.

1.2.1 De-noising

While de-noising technology is not commonly thought of from the perspective of auditory scene analysis, it has everything to do with it. The goal in signal de-noising in commercial audio applications, such as provided by the No-Noise$^{\text{tm}}$ process by Sonic Solutions, Inc., is to distill the signal from noise so as to produce a perceptually higher quality copy of a recording than the original. Recordings may be corrupted by either the imposition of interfering noise (e.g. coughing in a concert hall) or system noise (e.g. from analog tape noise, surface noise on gramophone recordings, nonlinear distortions in the recording equipment, etc.). One must model the desired signal and be able separate it from the noise.

1.2.2 Compression and Synthesis Techniques

Compression techniques are also not commonly thought of in terms of auditory scene analysis. Lossy compression, however, depends on the use of psychoacoustic data to preserve the aspects of sound which are perceptually relevant and discard or ignore those components which do not contribute to auditory perception. "Psychoacoustic" frequency masking effects are used in many audio compression algorithms such as MPEG audio compression [69]. Such simple masking thresholds may be thought of as a first step in narrowing down the contributors to auditory perception. Better models of psychoacoustically relevant signal components can provide better compression performance.

If a signal can be described using a small number of high-level parameters, it can be compressed greatly with little perceptible loss of quality. The best compression is resynthesis. This is most apparent in synthesized electronic music. If we take an arranged piece of music and convert the score into a MIDI data stream to represent the sequencing of notes, we have compressed the sound greatly by reducing the performance to a sparse set of playback parameters. Some previous efforts at CCRMA for performing automatic transcription of musical performances [30] could be thought of as an attempt to compress sound data by reducing it to a sequence of note values.

1.2.3 Adaptive Notch Filtering

Adaptive notch filtering is not normally associated with auditory scene analysis. Indeed, there has been little connection. However, adaptive notch filters are relevant to this thesis because of their ability to track changing sinusoidal signals through time. A *notch filter* is a filter with a zero, or null, at its notching frequency, which may or may not be fixed. It passes all signal components except for those near the selected frequency. An *adaptive notch filter* is one which may adaptively change its notching frequency to track and cancel a frequency-varying narrow-band signal component. There is a large amount of literature on adaptive notch filtering (ANF). Some examples are given by [13, 29, 62, 88, 102, 103, 118, 127, 133, 134]. To study the literature one may follow the usual technique of applying the transitive closure operation to the bibliographies of these references. Notch filters may be used to remove strong interfering sinusoidal signals.

A notch filter is usually realized by placing a zero of its transfer function $H(z)$ on the unit circle at the point corresponding to the frequency of the notching frequency f_n. In the usual case where real-valued signals are concerned, the notch filter has zeros at both $+f_n$ and $-f_n$. If the sampling rate is f_s, the zeroes are then located at $\exp(\pm j2\pi f_n/f_s)$. In order to balance out the notch response, a pole is placed near the notch at the same frequency, but slightly within the circle, with a radius $\rho < 1$. Hence, the poles are located at $\rho\exp(\pm j2\pi f_n/f_s)$. Thus, the notch transfer function is

$$H(z) = \frac{(1 - z^{-1}\exp(j2\pi f_n/f_s))(1 - z^{-1}\exp(-j2\pi f_n/f_s))}{(1 - z^{-1}\rho\exp(j2\pi f_n/f_s))(1 - z^{-1}\rho\exp(-j2\pi f_n/f_s))} \tag{1.1}$$

$$= \frac{1 - 2\cos(2\pi f_n/f_s)z^{-1} + z^{-2}}{1 - 2\rho\cos(2\pi f_n/f_s)z^{-1} + \rho^2 z^{-2}} \tag{1.2}$$

$$= \frac{1 - 2\alpha z^{-1} + z^{-2}}{1 - 2\rho\alpha z^{-1} + \rho^2 z^{-2}}, \tag{1.3}$$

where α is defined implicitly. The value of ρ is usually taken to be close to 1, usually between 0.95 and 0.995, with the closeness to 1 determining the tightness of the spectral notch in the transfer function $H(z)$.

An adaptive notch filter is usually formulated so as to constrain the zeroes to be on the unit circle. The parameters α and ρ may be varied at will. The usual goal is to try to move the notch to follow the center frequency of a narrow band signal. Hence, the ANF attempts to estimate (implicitly) the instantaneous frequency $f[n]$ of the target signal $p[n]$ given as

$$p[n] = a[n] \exp\left(\frac{2\pi}{f_s}\sum_{k=1}^{n} f[n] + \phi_0\right). \tag{1.4}$$

The notion of instantaneous frequency and the structure of signals of the form in Eqn. (1.4) will be discussed in more detail in Section 2.1.

The conventional ANF algorithm uses some kind of error feedback, usually gradient descent, to adjust the value of α so as to minimize the output signal energy of the filtered signal

$$\epsilon[n] = h * p[n]. \tag{1.5}$$

While the filter seeks to adapt to the signal frequency, one may set ρ to have a small value, say 0.95, in order to have a shorter filter impulse response, thereby facilitating tracking speed. Once the filter has adapted to the desired center frequency, ρ may be set to be closer to 1, say 0.995, in order to make the notch narrow. The value of the signal center frequency may then be estimated from α as

$$\hat{f}[n] = f_n[n] \tag{1.6}$$

$$\triangleq \frac{f_s}{2\pi}\cos^{-1}(\alpha[n]). \tag{1.7}$$

At steady-state, the ANF is no different from its fixed-coefficient instantiation given by Eqn. (1.1), and is thus a linear, time-invariant filtering system. However, when the coefficients, i.e. α and ρ, change with time, the filter is obviously no longer time-invariant. If α and ρ change in a way dependent on the input signal, then the system is non-linear.

One problem with the conventional formulation of the ANF is that the state variables are not guaranteed to have any easily understandable properties when the coefficients of the filter change with time. In particular, if α and ρ change rapidly, energy may be pumped into the system in such a way as to cause the filter to become unstable, even if their instantaneous values always correspond to a stable filter, i.e., if $\rho < 1$ at all times. Hence, the ANF tracking and filtering performance are not guaranteed to be meaningful for signals with rapidly-varying frequency. Empirically, the conventional ANF cannot track signals whose slew rate is moderately large [149].

Another problem with the ANF, as defined in Eqn. (1.1), is that the filter has a large group delay near the notch. If ρ is very close to 1 then signal components with frequencies near f_n are subjected to a long delay, whereas signal components far from f_n have a relatively short group delay. In many applications, such as audio signal processing, the resulting temporal distortion may be unacceptable.

1.2.4 Comb Filtering

Comb filtering has been used as a strategy either to selectively pass or block harmonic signals. The conventional formulation for a simple comb filter is of the form

$$H(z) = 1 - z^{-M}, \tag{1.8}$$

which corresponds to the system

$$y[n] = x[n] - x[n - M]. \tag{1.9}$$

We see immediately that the zeroes of this filter are the M-th roots of unity:

$$r_k = \exp\left(\frac{2\pi jk}{M}\right), \text{ for } k = 0, \cdots, M-1. \tag{1.10}$$

Hence, the spectral nulls are at frequencies

$$f_k = kf_s/M. \tag{1.11}$$

Moorer [97, 98] has studied the problem of finding the delay parameter M which minimizes the mean-square error of the filtered response of the filter over a block of length N:

$$\text{MSE}[n] = \frac{1}{N}\sum_{i=0}^{N} y[n-i]^2 \tag{1.12}$$

$$= \frac{1}{N}\sum_{i=0}^{N} (x[n] - x[n-M])^2 \tag{1.13}$$

given a periodic input.

A problem with comb filtering is that frequency is constrained to being of the form in Eqn. (1.11), for $M = 2, 3, 4, \ldots$. Hence, frequency quantization is non-linear and quite bad at higher frequencies, with increasing resolution as M approaches infinity. The frequency resolution is given by

$$f_s\left(\frac{1}{M} - \frac{1}{M+1}\right) = f_s\frac{1}{M(M+1)}. \tag{1.14}$$

There are, however, ways around integer delays implied in Eqn. (1.8). Cook and Smith have studied the problem [39, p. 60] and have proposed a method by which to extract a non-integer pitch delay. Their method consists of finding the best integer period P by an error-minimizing search, using a predictive filter giving

$$\hat{x}[n] = \sum_{i=-M} Mx[n - P + 1]c[i]. \tag{1.15}$$

After the best P is found, the phase delay is computed via

$$\text{Phase Delay} = \frac{1}{\omega}\arctan\left(\frac{\sum_{i=-M}^{M} c[i]\sin(\omega i)}{\sum_{i=-M}^{M} c[i]\cos(\omega i)}\right) \tag{1.16}$$

where $\omega = 2\pi f_s/P$. The period is then given as

$$\text{Period} = \frac{P}{f_s} + \text{Phase Delay}. \tag{1.17}$$

Nehorai has also studied the adaptive comb filter [103]. A related topic is delay estimation, studied by Abatzoglou [1], for example.

1.2.5 Phase- and Frequency-Locked Loops

Conventional applications of PLLs are widespread and an essential part of our modern technological world. Some examples are television color burst synchronization, FM radio tuners, digital clock rate multipliers, and so on. Without PLLs these and other appliances would be virtually impossible. In practically all these applications, the need for phase and frequency lock is served by conventional techniques which are simple and easy to implement in either analog or digital hardware. The common assumptions in these cases are that the signal being followed is very stable in its frequency and phase, dominated by the pure oscillatory component to be tracked, and that only a small amount of correction for synchronization needs to be applied.

These assumptions, though valid in most applications, often fail in the context of tracking of sinusoidal components (partials) in audio signals, particularly speech or other natural sounds. Audio signals are nonstationary mixtures of partials and non-periodic components. In addition, the partials are hardly ever stable in frequency or phase. Hence, phase-locked loops have not been widely applied to the analysis of sound signals. An early example of an attempt to use phase-locked loops was by Costas [41], who applied the technique to analyzing submarine sounds, and not to speech or musical sounds. More recently, a number of researchers have revived interest in phase- and frequency-locked loops for sound processing [22, 78, 79, 117, 140, 149].

There are two major classes of PLLs in general use today: the *analog* and *digital* forms. These conventional formulations of phase-locked loops rely on the assumptions of signal stability and high signal-to-noise ratios. In all PLL circuits, including the one being described in this document, there is a reference signal generated by the PLL which follows the input signal. In the simple analog version, this follower signal is 90° out of phase with the input signal, and is multiplied with the input signal, whose target signal is assumed to be a sine wave. The result is low-pass filtered so that the output voltage is approximately the sine of the difference of the phases of the two signals. This error signal is used to adjust the frequency of the follower, usually some kind of voltage-controlled oscillator (VCO), resulting in a negative-feedback control loop with phase as the state variable. Note, however, that the follower is assumed to be close in frequency to the input signal, and it is just the phase which needs to be synchronized, with perhaps a small frequency adjustment to be made. Phase-lock in this system divides the frequency spectrum into several regions: a lock-in region in which the frequency disparity is small and lock occurs quickly and with an exponentially decaying phase difference, a pull-in region which will lock slowly and non-linearly, and a region which has too great a frequency disparity and cannot lock. There are many books that address the lock-in dynamics of analog PLLs, for example [14, 87, 146]. The problem with the analog PLL technique is that phase-lock is fragile so it is suitable for only relatively stable input signals. Nevertheless, it is simple and low cost, and is widely used because the majority of applications fulfill the operating requirements.

The other major kind of PLL is the digital PLL. Actually, there are various formulations of this, which range from semi-analog to completely digital. The "digital" aspect of these PLLs comes from the zero-crossing detector which is common to this class of PLLs. The follower and input signals are assumed to have some regular waveform (not necessarily sinusoidal), but with clean zero-crossings. There is some sort of counter which increments each time the input signal makes a zero-crossing, and decrements whenever the reference signal makes a zero-crossing. The value of this counter is the frequency control parameter to the reference signal generator, which may be analog or digital. When the counter value reaches steady state, frequency lock is achieved. Also, phase-lock is attained because the asynchronies in the zero-crossings of the input signal and reference signal cause fluctuations in the frequency which serve to reduce the phase difference.

The problem with this formulation of PLL occurs when there is enough noise in the input to cause spurious zero crossings, or if harmonic components of the input signal are subject to nonlinear phase

distortion, so that the waveform has multiple zero-crossings per cycle. This can be seen in Figures B.3 and B.4. Figures B.1–B.4 all have the same power spectra, but the phases of the corresponding partials are different. Refer to Appendix B for more details on this.

As mentioned above, acoustical signals are usually non-stationary, noisy, and may not have good phase coherence. Hence, phase-lock tracking of audio signals is difficult, fragile, and noise sensitive. For some audio purposes, exact phase tracking is not necessary; rather, it is the ability to track the *frequency* which is important. Frequency-locked loops (FLLs), as the name suggests, do this and furthermore can be made to be fairly insensitive to noise and phase drift. Hence, FLLs should have wide application in audio signal processing.

An FLL simply attempts to center the *change* in relative phase between the input signal and reference signal to zero; a PLL, on the other hand, centers the relative phase itself. Hence, in the analog case, the frequency discriminator is simply the derivative of the phase detector function with respect to time. Since PLLs are used more widely throughout industry than FLLs, there are many more references in the literature to PLLs than to FLLs. FLLs are handled as a special case of PLLs since they are sometimes employed to help speed up lock-in for PLLs. Some references to FLLs are given by [54, 100].

1.3 Time-Frequency Analysis

In this section we present a brief and highly incomplete survey of time-frequency representations of signals. One may classify frequency estimation procedures as either parametric or non-parametric. The former attempts to describe a signal through a small number of conceptually meaningful parameters such as frequency and amplitude. The latter provides some multidimensional space and maps the signal into some kind of density distribution or point within that space.

1.3.1 Non-Parametric Representations

Transforms such as MUSIC [70, 124, 129, 132, 142, 150, 151], the Wigner-Ville Distribution [17–19, 35, 66], the short-time Fourier Transform, and constant-Q filterbanks, for example, may be thought of as non-parametric representations. A key property of non-parametric estimation is that signals are represented in a distributed fashion in some multi-dimensional feature space. No decisions are made to summarize or interpret the result. Some non-parametric representations are invertible.

The reader is undoubtedly familiar with Fourier transforms and all its variants, including the DFT and STFT [21]; hence, there is no need to mention its well-known properties. A generalization of the STFT is the wavelet, of which there are many popular references, for example [33, 138]. Wavelets provide a multi-resolution, self-similar way of tiling the time-frequency plane, as opposed to the STFT, which only provides a uniform, rectangular tiling.

Unto Laine has proposed an orthogonal "FAM" class of functions for time-frequency analysis [81–83]. "FAM" stands for "Frequency-Amplitude Modulated" complex exponential functions. The FAM family of basis functions is defined as

$$\Phi_g(f, a) = \sqrt{|g'(f)|}\exp[j2\pi a g(f)], \tag{1.18}$$

where $g(f)$ is the "generative," "scale," or "resolution" function. The quantity a is an integer index into the family of functions generated by $g(f)$. Here, the function $g(f)$ serves as a warping mapping of the frequency axis, and the factor $\sqrt{|g'(f)|}$ is the appropriate weighting to confer orthogonality. In the time domain, the functions become a kind of basis of orthogonal wavelet-like functions which are modulated in frequency, as well as amplitude: hence the name. FAMlets are useful for designing non-uniform filter banks, among other things [80].

The well-known Wigner-Ville distribution is the result of calculating the Fourier transform of the instantaneous cross-correlation:

$$\mathrm{WVD}\{s\}(t,f) \triangleq \int_{-\infty}^{\infty} s(t+\tau/2)s^*(t-\tau/2)\exp(-j2\pi f\tau)\,d\tau \tag{1.19}$$

The result is a high-resolution time-frequency function. A problem with the Wigner-Ville distribution is the presence of cross-terms; every pair of wave packets in the time-frequency plane generates an oscillatory cross-term centered at their midpoint in the time-frequency plane. Generalized time- and frequency-shift invariant time-frequency distributions derived by Cohen are related to the Wigner-Ville distribution by a convolution kernel $K(t,f)$ [34]:

$$\mathrm{C}_K\{s\}(t,f) \triangleq K * \mathrm{WVD}\{s\}(t,f), \tag{1.20}$$

where the convolution is understood to be over both time and frequency. There are several other generalizations of the Wigner-Ville distribution, such as the *affine* class, defined by:

$$\begin{aligned}\mathrm{A}_K\{s\}(t,f) &\triangleq \\ &\int_{-\infty}^{\infty}\int_{-\infty}^{\infty}\int_{-\infty}^{\infty} K(f\{t-t'\}, f'/f) \\ &\qquad \times s(t'+\tau/2)s^*(t'-\tau/2)\exp(-j2\pi f'\tau)\,d\tau\,dt'\,df'.\end{aligned} \tag{1.21}$$

The reason for having the various kinds of quadratic time-frequency representations is to smooth out the oscillatory cross-terms. The WVD suffers from fairly high computational cost, and is easily seen to be non-causal. To make it causal, a time-limiting kernel is necessary to localize the temporal distribution; this is known as the *pseudo-Wigner distribution.* An excellent review of quadratic time-frequency distributions is [66]. As a side note, the Wigner-Ville distribution is related to the cyclostationary distribution via a Fourier Transform in the t argument, yielding a bi-frequency distribution studied extensively by Gardner, *et al* [27, 55–58, 120].[1] Additionally, the WVD is related to the radar ambiguity function via a Fourier transform along both the t and f dimensions.

The MUSIC (MUltiple SIgnal Classification) technique is a super-resolution method which represents a signal's spectrum as the reciprocal of quadratic function $\boldsymbol{\omega}^H \boldsymbol{V}\boldsymbol{V}^H\boldsymbol{\omega}$, where $\boldsymbol{V}$ is the matrix composed of the "noise" eigenvectors of the correlation matrix of a signal, and $\boldsymbol{\omega}$ represents a column vector whose k-th entry is $\exp(jk\omega)$. Component signal frequencies are thus not explicitly represented. The MUSIC technique performs poorly for non-stationary signals, however, due to the long time-averaging necessary to form an accurate estimate of the covariance matrix.

1.3.2 Parametric Representations

Parametric estimation may be thought of as providing a concise summary of interesting features of a signal. Some examples of parametric descriptions of a signal include the power of a signal, the average frequency of a signal as a function of time, and the number of voices present in a mixture. Parametric estimators of the frequency characteristics of a signal include the Maximum-Likelihood estimator [25, 119], phase-difference frequency estimators [75, 137], Maximum *a-priori* Line Estimation (MAPLE) [147]

Non-parametric representations may be made to be parametric by further processing, such as peak estimation or other kinds of post processing. Some examples of parameterization of a Short-Time Fourier Transform (STFT) are given by Wolcin's MAPLE [73, 147], Serra's SMS [126],

[1] The actual definition of the cyclostationary function requires an expectation operator.

McAulay and Quatieri's FFT peak-picking [94, 95]. Wolcin showed that finding the peak of the discrete-time Fourier transform is equivalent to finding the maximum-likelihood frequency estimate for stationary sinusoidal signals in Gaussian white noise. However, MAPLE does not provide an optimal frequency estimate for nonstationary signals. Indeed, a slewing sinusoidal signal does not have a well-defined spectral peak in a DFT or STFT representation, but, rather, a broad-band smear. The signal energy cannot accumulate in any particular frequency bin; the bins to which it does contribute can be distorted with relatively low-power additive noise. Changing the frame of reference, as discussed in Chapter 3, can enhance the signal-to-noise ratio greatly, allowing the signal energy to accumulate in a given FFT bin.

Another example of converting a non-parametric representation to a parametric one is provided by the MUSIC algorithm. Peak detection on the MUSIC spectrum described above yields the parametric frequency representations.

In reality, the parametric/non-parametric dichotomy is not absolute. Estimation schemes such as Linear Predictive Coding (LPC) [63, 73, 105] can be thought of as a parametric estimation procedure in which one tries to find the predictive filter coefficients $a_1, \cdots, a_N$ which minimize the estimation error. Hence, one obtains N parameters. On the other hand, in order to get more accurate estimates one must use higher estimation orders, so N may be large. As N increases one does not gain much insight into the structure of the input signal. One may then consider LPC to be a non-parametric estimation procedure. One may regain the parametric aspect of LPC by finding the roots of the corresponding whitening filter. One may then extract the phases and residues of the poles and thus obtain a parametric representation of the most salient peaks as a measure of the sinusoidal components of the signal. In practice LPC is a rather poor method for frequency estimation, especially for non-stationary signals for the same reason MUSIC suffers.

Another parametric signal representation results from estimating the instantaneous phase as a polynomial function of time. Peleg, Porat, and Friedlander derive the Cramér-Rao bounds on polynomial fits to the phase of a complex signal over an interval of time [111]. Here, the first few polynomial coefficients at $t = 0$ may be understood (with appropriate scaling factors) as the phase offset, instantaneous frequency, slew, and frequency acceleration of the complex signal. Again, if the order of the polynomial becomes large, the coefficients cease to hold such conceptual significance; the polynomial representation my then be thought of as being non-parametric.

There are many more kinds of time-frequency representations and estimation procedures besides the ones mentioned here. To treat the subject with the care it deserves would consume many pages and go beyond the scope of this thesis. The curious reader is encouraged to refer to the citations given above and apply the usual procedure of collecting the references recursively until closure is attained.

1.4 Goals

The primary of the research described in this dissertation is to provide one further step towards solving the problem of auditory source separation. Since we are approaching the problem from a signal-processing engineering point of view, we are not constrained by biology. No attempt will be made to attain biological realism; we will use physiological or psychoacoustical knowledge only where it can help, and never when it puts us at a disadvantage. In order to attain the best quality separation possible we will attempt to maintain a high *statistical efficiency*, i.e., we want to use the information present in the signal to produce the highest-quality parameter estimates possible of target signals embedded in a mixture. Furthermore, in order to make auditory source separation a practical tool, we will attempt to make the algorithms as *computationally efficient* as possible; the goal is to have real-time separation performance. A further goal is to maintain a firm understanding

of the algorithms involved; hence, black-box architectures and self-organizing techniques such as "neural nets" and genetic algorithms will be avoided.

John R. Pierce says that there is a world of difference between what will make the CIA happy and what will make the musical world happy. The aim of this research is to satisfy the latter.

In contrast to the Marrian approach, which is often interpreted to advocate high-level symbolic auditory scene understanding, the philosophy taken in this thesis focuses on *low-level* signal processing techniques.

1.4.1 Scope of Work

What is provided in this dissertation is a theory of monoaural sound separation based on tracking filters suitable for continuous voice or musical instruments. The only cues used are harmonicity and common-FM information. Spatial cues such as from inter-channel time and level differences are not taken into account.

1.5 Overview

Chapter 2 contains a collection of useful signal-processing concepts for non-stationary signal analysis. First, we present some concepts about instantaneous signal parameters, such as instantaneous frequency, instantaneous bandwidth, and instantaneous spectrum. The motivation behind these concepts is to recognize that natural, meaningful signals are nonstationary. The concepts of frequency, bandwidth, and spectrum are traditionally associated with second-order stationary signals in the context of Fourier transforms. Given a parameterized model of a signal, we assume that the parameters of the model change with time. We wish to characterize and track those parameters as they change. The second part of Chapter 2 advocates the perspective of an audio signal as an *analytic signal*. An analytic signal is a complex-valued signal which may be constructed from a real-valued signal by deleting the negative-frequency half of its Fourier transform and then applying the inverse Fourier transform. The real part of the resulting signal is proportional to the original signal. We provide a number of results that show the conditions under which a robust estimate of the instantaneous frequency of a sinusoid may be made from the average winding rate of the analytic signal around the time axis. We provide an analysis of the error and show the conditions under which the Cramér-Rao bound on the variance may be attained.

Chapter 3 discusses the philosophy of *frequency-warped signal processing*. Frequency-warping simply consists of dynamically modulating a signal in order to shift the instantaneous frequencies of its components. All signals may be considered to have AM and FM mean-square bandwidth components, σ^2_{AM} and σ^2_{FM}. By choosing the appropriate frequency-warping transform it is possible to eliminate the FM-component of the mean-square bandwidth, leaving only the envelope modulation component of the mean-square bandwidth. For signals which consist of time-varying sinusoidal components (i.e., *partials*), such a transformation may make a wideband signal extremely narrowband. This transformation makes it easy to remove a targeted partial from a mixture while minimizing the damage done to other signal components in a mixture. The utility of the frequency-warped signal processing strategy is contingent upon having a good estimate of the instantaneous frequency of targeted time-varying sinusoidal signal components. Various formulations of frequency-warped signal processing are discussed, along with some applications and examples.

In Chapter 4 we provide the means for tracking and estimating the instantaneous frequency of a target partial in a signal based on a frequency-locked loop algorithm. We provide an analysis of the tracking and convergence properties in the presence of noise and interfering partials, including the case of real-valued input signals. We discuss various issues concerning loop filter design, group delay,

and loop stability. We present a variation of the basic tracking loop which returns a high-quality estimate of the instantaneous frequency of the target partial, which attains the Cramér-Rao bound under certain conditions. Finally, we show some applications of the frequency-locked loop tracker, including resynthesis of partials and adaptive notch filtering.

The tracking algorithm in Chapter 4 works well for tracking sinusoidal signals with high signal-to-noise ratios. However, for analyzing sounds in natural environments in the presence of significant noise, the basic FLL algorithm performs poorly. In Chapter 5 we take advantage of the harmonic structure of many natural acoustical signals to improve greatly the robustness of tracking, making the frequency-locked loop approach to auditory source separation practical. Each harmonic is tracked by its own FLL tracker, and the frequency update estimates are combined by a maximum-likelihood weighting scheme to form a robust estimate of the fundamental frequency update. The combined estimate is then used to update each of the trackers in the harmonic tracking set. This improved tracking scheme is called the *harmonic-locked loop* (HLL) tracking algorithm. Some variations on the HLL theme are discussed, including multiple harmonic tracking and inharmonic tracking. Finally, we discuss a few extensions to the harmonic tracker, such as resynthesis, harmonic notch filtering, and some applications.

Chapter 6 summarizes the contributions made in this dissertation. We describe some sound separation examples generated using techniques described in this thesis. We discuss several potential applications and mention some future directions.

A number of miscellaneous topics have been relegated to the Appendices. Most notable among them is Appendix G, which describes the fast FIR algorithm. Truncated IIR (TIIR) filters are created by subtracting the tail off an IIR response. A linear-phase response filter is then created by cascading the truncated filter and a time-reversed copy of itself. This filter can be 10-100+ times faster than an equivalent conventional FIR filter implemented as a tapped delay-line.

Chapter 2

Instantaneous and Analytic Signal Descriptions

This chapter lays the foundation for our approach to signal analysis. We first present some concepts regarding instantaneous signal parameters, such as instantaneous frequency, instantaneous bandwidth, and instantaneous spectrum. The motivation behind these concepts is to recognize that natural, meaningful signals are nonstationary. The concepts of frequency, bandwidth, and spectrum are traditionally associated with second-order stationary signals in the context of Fourier transforms. Given a parameterized model of a signal, we assume that the parameters of the model change with time. We wish to characterize and track those parameters as they change in time. In the second part of this chapter, we explore some properties of *analytic signals*. We provide a minor theorem and some corollaries that show the conditions under which a robust estimate of the instantaneous frequency of a sinusoid may be made from the average winding rate of the analytic signal around the time axis. We provide an analysis of the error and show the conditions under which the Cramér-Rao bound on the variance may be attained.

2.1 Instantaneous Signal Parameterization

Any real signal $s(t) \in \mathrm{L}_1(-\infty, \infty)$[1] defined on $t \in (-\infty, \infty)$ may be represented as a magnitude and phase spectrum $S_{\mathrm{mag}}(f)$ and $S_\phi(f)$, respectively, such that[2]

$$s(t) \doteq \int_0^\infty S_{\mathrm{mag}}(f) \cos\{2\pi f t + S_\phi(f)\}\, df. \tag{2.1}$$

$S_{\mathrm{mag}}(f)$ is a non-negative-valued function

$$S_{\mathrm{mag}}(f) \triangleq \begin{cases} 2\,|S(f)| & : \quad f > 0 \\ |S(0)| & : \quad f = 0 \end{cases} \tag{2.2}$$

[1] A signal $s(t)$ is a member of $\mathrm{L}_p(X)$ if

$$\left[\int_X |s(t)|^p\, dt\right]^{1/p} < \infty,$$

where X is some subset of the interval $(-\infty, \infty)$.

[2] The "$\doteq$" symbol denotes "equality in the mean." Cf. page 53.

and

$$S_\phi(f) \stackrel{\triangle}{=} \arg S(f), \tag{2.3}$$

where $S(f)$ is the Fourier transform of $s(t)$ defined by [21]

$$S(f) \stackrel{\triangle}{=} \int_{-\infty}^{\infty} s(t) e^{-j2\pi f t}\, dt. \tag{2.4}$$

Neither the Fourier spectral representation nor the representation in Eqn. (2.1) lends itself easily to an intuition about the dynamic behavior of non-stationary signals [17]. What we would like to have is a more dynamic representation of a signal providing an estimate of the instantaneous frequency, phase, and amplitude at each point in time.

The *frequency* of a general signal is not a well-defined quantity. The very concept of frequency has traditionally been tied to the Fourier transform. Attempting to speak about *the* frequency of a signal in the context of a Fourier representation is a conceptual error because the Fourier transform is a *non-parametric* distribution, whereas asking for the frequency of a signal presumes a parametric model which has frequency as one of its parameters. Most natural signals are mixtures of signals from many sources, and, as implied by the Fourier representation, may have a rich spectral composition. Thus, a general signal has no well-defined single frequency.

For the analysis of non-stationary signals, a suitable signal model must be chosen in which time-varying frequency is one of the parameters. As a counterexample, the concept of an instantaneous frequency does not exist in the Fourier framework. Casual inspection of the definition of the Fourier transform in Eqn. (2.4) will reveal that there is nothing time-varying about it. Hence we must extend the concept of frequency in order to include frequency-varying signals.

Chapter 3 discusses some time-varying extensions to the definition of the Fourier transform, providing a more flexible framework for signal analysis.

2.1.1 Definition of Instantaneous Frequency

It makes sense to think about *the* frequency of a signal when given a parametric signal model in which frequency is a parameter. Thus, we quickly depart from the world of Fourier analysis into the well-defined problem of parameter estimation. If the signal is being synthesized, we know *a priori* what the value of the frequency parameter is (provided that it has been appropriately labeled). Otherwise, given the data, we must estimate the value of the frequency parameter. In agreement with the Fourier notion of frequency, we choose the signal model to be the class of signals which are the complex sinusoids of the form

$$p(t) = \exp(j2\pi f t + j\phi_0), \quad \text{for all t}, \tag{2.5}$$

where ϕ_0 is the phase at time $t = 0$. In this case, it is clear that the parameter f is the frequency of the signal $p(t)$. Thus, one may define the frequency of this signal as

$$f \stackrel{\triangle}{=} \frac{1}{2\pi} \frac{d \arg\{p(t)\}}{dt} \tag{2.6}$$

Since the frequency of this signal model is defined to be constant, the derivative may be taken at any time t.

We depart from the constant-frequency philosophy by modifying the signal model of Eqn. (2.5) to be

$$p(t) = \exp\left(j2\pi \int_0^t f(\tau)\, d\tau + j\phi_0\right), \quad \text{for all t}. \tag{2.7}$$

We now have a time-dependent *instantaneous* frequency definition:

$$f(t) \triangleq \frac{1}{2\pi}\frac{d\arg\{p(t)\}}{dt}, \tag{2.8}$$

which is consistent with Eqns. (2.5) and (2.6). It is important to keep in mind that this definition of instantaneous frequency applies only to signals of the form given by Eqn. (2.7).

In the discrete case, Eqn. (2.7) becomes

$$p[n] = \exp\left(\frac{j2\pi}{f_s}\sum_{k=1}^{n} f[k] + j\phi_0\right), \quad \text{for all n} \geq 0, \tag{2.9}$$

and the discrete-time version of Eqn. (2.8) is

$$f[n] \triangleq \frac{f_s}{2\pi}\arg(p[n]p^*[n-1]), \tag{2.10}$$

2.1.1.1 Pitfalls

In practice, attempting to apply the definition Eqn. (2.8) directly to the analysis of sampled data leads to some pitfalls. First of all, there is no guarantee that any sampled signal will be of the form given in Eqn. (2.9). One obvious hazard is that the derivative is extremely sensitive to noise and discontinuities. Simply adding white noise to the signal in Eqn. (2.7) yields a signal which is nowhere differentiable.

Another example of how the phase derivative fails to yield meaningful results when applied to the wrong kind of signal model is given by the simple signal

$$z(t) = a_1\exp(j\omega_1 t) + a_2\exp(j\omega_2 t), \quad \text{where } \omega_1 \neq \omega_2. \tag{2.11}$$

This signal is obviously bandwidth limited in the Fourier sense. Mandel [91] argues that the IF estimate given by the phase derivative is biased towards ω_1 if $a_1 > a_2$ and towards ω_2 if $a_1 < a_2$. In an extension to his argument, we show here that the phase derivative is unbounded. At time t we have

$$z(t) = a_1\cos(\omega_1 t) + a_2\cos(\omega_2 t) + j\left\{a_1\sin(\omega_1 t) + a_2\sin(\omega_2 t)\right\} \tag{2.12}$$

and thus the phase derivative is

$$\frac{d\phi(t)}{dt} = \mathrm{Im}\left\{\frac{d\log(z)}{dt}\right\} \tag{2.13}$$

$$= \mathrm{Im}\left\{\frac{1}{z}\frac{dz}{dt}\right\} \tag{2.14}$$

$$= \mathrm{Im}\left\{\frac{z^*}{|z|^2}\frac{dz}{dt}\right\} \tag{2.15}$$

$$= \frac{a_1^2\omega_1 + a_2^2\omega_2 + a_1a_2(\omega_1+\omega_2)\cos\{(\omega_1-\omega_2)t\}}{a_1^2 + a_2^2 + 2a_1a_2\cos\{(\omega_1-\omega_2)t\}} \tag{2.16}$$

$$= \frac{\omega_1+\omega_2}{2} + \frac{\omega_1-\omega_2}{2}\frac{a_1^2-a_2^2}{a_1^2+a_2^2+2a_1a_2\cos\{(\omega_1-\omega_2)t\}}. \tag{2.17}$$

To illustrate the point, let $t_0 = \pi/(\omega_1-\omega_2)$ so that

$$\left.\frac{d\phi(t)}{dt}\right|_{t=t_0} = \frac{\omega_1+\omega_2}{2} + \frac{\omega_1-\omega_2}{2}\frac{a_1+a_2}{a_1-a_2}. \tag{2.18}$$

We see that as a_1 approaches a_2 this quantity becomes unbounded. Thus, naïvely applying the phase derivative to general signals may lead to questionable results.

It is not the case, however, that the phase derivative is a useless mathematical curiosity. We will use the discrete-time phase difference extensively in the following sections as the basis of our partial tracker. The important point here is that the phase derivative can only be applied to an isolated frequency-varying sinusoid, e.g. obtained after bandpass filtering a signal to remove signal components other than the desired partial. Also, Kay derives a linear frequency estimator based on the optimal weighted average of the discrete-time phase difference in [75]. The main results of that work are summarized in Appendix E

2.1.1.2 Frequency Moments

It is interesting to note that the power-weighted, time-averaged instantaneous frequency given by the phase derivative and the first moment of the Fourier power spectrum are identical. This may be seen in an adaptation of the result by Ville [17, 139]. For a signal $z(t) \in L_1(-\infty, \infty)$ we have

$$\frac{\int_{-\infty}^{\infty} f\,|Z(f)|^2\,df}{\int_{-\infty}^{\infty} |Z(f)|^2\,df} = \frac{\left[\frac{1}{j2\pi}\frac{d}{dt}\int_{-\infty}^{\infty} z^*(\tau)z(t+\tau)\,d\tau\right]_{t=0}}{\int_{-\infty}^{\infty} |z(t)|^2\,dt} \tag{2.19}$$

$$= \frac{\frac{1}{j2\pi}\int_{-\infty}^{\infty} z^*(t)z'(t)\,dt}{\int_{-\infty}^{\infty} |z(t)|^2\,dt} \tag{2.20}$$

$$= \frac{\frac{1}{j2\pi}\int_{-\infty}^{\infty} |z(t)|^2\,d\log\{z(t)\}}{\int_{-\infty}^{\infty} |z(t)|^2\,dt} \tag{2.21}$$

$$= \frac{\frac{1}{j2\pi}\int_{-\infty}^{\infty} |z(t)|^2\,d\left\{\log|z(t)| + j\arg\{z(t)\}\right\}}{\int_{-\infty}^{\infty} |z(t)|^2\,dt} \tag{2.22}$$

$$= \frac{\frac{1}{j4\pi}\int_{-\infty}^{\infty} d|z(t)|^2 + \int_{-\infty}^{\infty} f(t)|z(t)|^2\,dt}{\int_{-\infty}^{\infty} |z(t)|^2\,dt} \tag{2.23}$$

$$= \frac{\int_{-\infty}^{\infty} f(t)|z(t)|^2\,dt}{\int_{-\infty}^{\infty} |z(t)|^2\,dt} \tag{2.24}$$

where in Eqn. (2.19) we have used the autocorrelation, derivative, and Rayleigh theorems [21], and in Eqn. (2.24) we have used the assumption that $z(t)$ is integrable, hence $|z(t)|^2 = 0$ for $|t| \to \infty$.

2.1.2 Instantaneous Amplitude

Signals of the form given in Eqn. (2.7) are fixed in amplitude and may be broadened in scope to include signals of the form

$$p(t) = a(t)\exp\left(j2\pi\int_0^t f(\tau)\,d\tau + j\phi_0\right), \quad \text{for all t.} \tag{2.25}$$

with a time-varying envelope $a(t) \geq 0$. The introduction of $a(t)$ to the definition of a partial presents yet another twist to the definition of the instantaneous frequency of a signal. The instantaneous frequency of such a signal, especially in the context of a mixture of signals, may become ambiguous. For example, if $a(t)$ is a sinusoidally varying envelope of the form

$$a(t) = 1 + \cos(2\pi\mu t), \tag{2.26}$$

we see that the partial $p(t)$ may then be interpreted as the sum of *three* instantaneous frequency tracks:

$$p_1(t) = \frac{1}{2}\exp\left(j2\pi\int_0^t \{f(\tau)+\mu\}\,d\tau + j\phi_0\right), \tag{2.27}$$

$$p_2(t) = \exp\left(j2\pi\int_0^t f(\tau)\,d\tau + j\phi_0\right), \text{ and} \tag{2.28}$$

$$p_3(t) = \frac{1}{2}\exp\left(j2\pi\int_0^t \{f(\tau)-\mu\}\,d\tau + j\phi_0\right). \tag{2.29}$$

Since we restrict the envelope $a(t)$ to functions which are non-negative in value, we see that the Fourier spectrum $A(f)$ is Hermitian (i.e., having even real part and odd imaginary part). We see also that $a(t)$ has a unique spectral peak at $f = 0$ if $a(t)$ is not identically zero[3],

$$A(0) = \int_{-\infty}^{\infty} a(t)\,dt \tag{2.30}$$

$$= \int_{-\infty}^{\infty} |a(t)|\,dt \tag{2.31}$$

$$= \int_{-\infty}^{\infty} \left|a(t)e^{-j2\pi ft}\right|\,dt \tag{2.32}$$

$$\geq \left|\int_{-\infty}^{\infty} a(t)e^{-j2\pi ft}\,dt\right| \tag{2.33}$$

$$= |A(f)|, \tag{2.34}$$

with equality only at $f = 0$. Hence, if we modulate a pure-frequency carrier $c(t)$ by $a(t)$, we see that the spectral peak of the resulting signal remains the frequency of the original carrier. We expect the same result to apply to the instantaneous frequency of a frequency-varying carrier. Indeed, we see that where $a(t) > 0$, Eqn. (2.8) still applies for signals $p(t)$ of the form in Eqn. (2.25) since the phase does not change, though the magnitude is scaled. For a complex signal of the form Eqn. (2.25), we call $a(t)$ the *instantaneous amplitude* (IA) of $p(t)$ at time t.

Another restriction on $a(t)$ is that if the bandwidth of $a(t)$ is greater than the instantaneous frequency of the carrier then one encounters the ambiguity of whether $a(t)$ is the modulator or the carrier. This is a consequence of the Bedrosian Product Theorem [12] discussed in Appendix A. Another problem here is that the signal will then contain negative frequency components, violating the assumptions in Section 2.3 that the signal $p(t)$ is an analytic signal, i.e., having only positive frequencies in a Fourier-transform representation.

2.1.3 Instantaneous Bandwidth

In addition to the notions of instantaneous frequency (IF) and instantaneous amplitude (IA), there is also the idea of *instantaneous bandwidth* (IB). The IB of a time-varying carrier $p(t)$ of the form in Eqn. (2.7) is not easily defined. One may consider the usual width of the support of the Fourier transform, but this concept is non-local. Mandel [17, 91] derived an expression for the second moment of the frequency of a signal $z(t)$:

$$\sigma_{\text{BW}}^2 \triangleq \frac{\int_{-\infty}^{\infty}(f-\langle f\rangle)^2|Z(f)|^2\,df}{\int_{-\infty}^{\infty}|Z(f)|^2\,df} \tag{2.35}$$

[3] More precisely, if $a(t)$ has its support on a set of non-zero measure.

$$= \frac{\int_{-\infty}^{\infty} \left[(f(t) - \langle f \rangle)^2 + \left[\frac{a'(t)}{2\pi a(t)} \right]^2 \right] |z(t)|^2 \, dt}{\int_{-\infty}^{\infty} |z(t)|^2 \, dt} \tag{2.36}$$

$$= \sigma_{\mathrm{FM}}^2 + \sigma_{\mathrm{AM}}^2, \tag{2.37}$$

where

$$\langle f \rangle \triangleq \frac{\int_{-\infty}^{\infty} f |Z(f)|^2 \, df}{\int_{-\infty}^{\infty} |Z(f)|^2 \, df} \tag{2.38}$$

and σ_{FM}^2 and σ_{AM}^2 are respectively the FM and AM contributions to the total mean-square bandwidths.

This suggests that there are two components to the bandwidth: one component due to the variance of the IF, and one due to the variation of the amplitude envelope. We see that if the instantaneous frequency is constant, the term $(f(t) - \langle f \rangle)^2$ vanishes and the second moment is determined by the second term. Similarly, if the envelope function is constant, the right term is zero and the second moment is determined solely by the distribution of the instantaneous frequency. We see that the instantaneous second moment of frequency at time t is given by

$$\sigma_{\mathrm{BW}}^2(t) \triangleq \left[\frac{a'(t)}{2\pi a(t)} \right]^2. \tag{2.39}$$

This is the same expression arrived at by Cohen and Lee for the frequency spread of certain Cohen-class time-frequency distributions [36, 37]. We adopt

$$\mathrm{IB}_a(t) = \left| \frac{a'(t)}{2\pi a(t)} \right| \tag{2.40}$$

as our measure of root-mean-square IB, as advocated by Cohen and Lee [38].

We see that if the envelope changes amplitude quickly in relation to its value the instantaneous bandwidth moment may be very large. In fact, if the envelope passes through zero, the instantaneous bandwidth may be unbounded. This is another way of looking at the results of the signal example given in Eqn. (2.11) since that signal may come arbitrarily close to zero in amplitude as a_1 approaches a_2. The amplitude of $z(t)$ is

$$a(t) \triangleq |z(t)| \tag{2.41}$$

$$= \sqrt{a_1^2 + a_2^2 + 2a_1 a_2 \cos\{(\omega_1 - \omega_2)t\}}. \tag{2.42}$$

It follows that

$$\sigma_{\mathrm{BW}}^2(t) = \left[\frac{-2a_1 a_2 (\omega_1 - \omega_2) \sin\{(\omega_1 - \omega_2)t\}}{4\pi \left(a_1^2 + a_2^2 + 2a_1 a_2 \cos\{(\omega_1 - \omega_2)t\} \right)} \right]^2. \tag{2.43}$$

For the case that $a_2 = a_1 > 0$,

$$\sigma_{\mathrm{BW}}^2(t) = \frac{(\omega_1 - \omega_2)^2}{16\pi^2} \left[\frac{\sin\{(\omega_1 - \omega_2)t\}}{1 + \cos\{(\omega_1 - \omega_2)t\}} \right]^2 \tag{2.44}$$

$$= \frac{(\omega_1 - \omega_2)^2}{16\pi^2} \tan^2 \left(\frac{\omega_1 - \omega_2}{2} t \right). \tag{2.45}$$

We see that, as t approaches $\pi/(\omega_1-\omega_2)$, $\sigma^2_{\rm BW}(t)$ becomes unbounded, just as the IF of $z(t)$ becomes unbounded, even though the signal $z(t)$ is bandwidth-limited in the Fourier sense.

Like the IF, the IB in the form of $\sigma^2_{\rm BW}(t)$ is not appropriate for describing mixtures of signals, but, rather, makes sense only for pure signals $p(t)$ of the form given by Eqn. (2.25), and for which $a(t) > 0$ for all t. The positive-real condition on the amplitude envelope restricts the available kinds of modulation to those which have no effect on the phase, specifically abrupt changes of π radians, and hence the IF, of the signal. The previous example has $a(t) = 0$ periodically, thus violating the positive-real condition. It is interesting to note that if the envelope does not vary in time $\sigma^2_{\rm BW}(t)$ is identically zero.

In reality, we never encounter the instantaneous bandwidth expression of Eqn. (2.39) because we must take several samples of the signal in order to compute the derivative of the signal. In this case, the *windowing function* $h(t)$, which peaks at $t = 0$, for the instantaneous bandwidth calculation plays an important role in determining the value of the measured instantaneous bandwidth of the signal at a given time t. Generally, the signal $z(t)$ is weighted by an analysis window $h(t)$ to provide time localization in Eqn. (2.35), so that the Fourier transform $Z(f)$ is replaced by its windowed version

$$Z_t(f) \triangleq \int_{\Re} z(\tau)h(\tau - t)e^{-j2\pi f\tau}\, d\tau. \tag{2.46}$$

Cohen and Lee [38] provide an excellent analysis of the contribution of the time moments of the window to the measured instantaneous bandwidth. In the windowed case, we have [38]

$$\sigma^2_{\rm BW}(t) = \frac{1}{P(t)} \int_{\Re} (f - \langle f\rangle_t)^2 \left|Z_t(f)\right|^2\, df, \tag{2.47}$$

where

$$P(t) \triangleq \int_{\Re} \left|Z_t(f)\right|^2\, df \tag{2.48}$$

and

$$\langle f\rangle_t \triangleq \frac{1}{P(t)} \int_{\Re} f\left|Z_t(f)\right|^2\, df. \tag{2.49}$$

Cohen and Lee arrive at the general expression for the windowed mean-square bandwidth in terms of the derivatives of the phase as [38]

$$\begin{aligned}\sigma^2_{\rm BW}(t) = {} & \frac{1}{P(t)} \int_{\Re} \left(\frac{1}{2\pi}\frac{d}{d\tau}a(\tau)h(\tau - t)\right)^2 d\tau \\ & + \sum_{n=2}^{\infty}\left(\frac{1}{2\pi^2}\sum_{k=1}^{\lfloor (n-1)/2\rfloor} \phi^{(n-k+1)}(t)\phi^{(k+1)}(t)\frac{M_n(t) - M_{n-k}(t)M_k(t)}{(n-k)!k!} + \delta_n\right),\end{aligned} \tag{2.50}$$

where $\phi^{(k)}(t)$ denotes the k-th derivative of $\phi(t)$,

$$M_n(t) \triangleq \frac{\int_{\Re} a^2(\tau + t)h^2(\tau)\tau^n\, d\tau}{\int_{\Re} a^2(\tau + t)h^2(\tau)\, d\tau}, \tag{2.51}$$

and

$$\delta_n \triangleq \begin{cases} \frac{1}{4\pi^2}\frac{M_n(t) - M^2_{n/2}(t)}{(n/2)!^2}\left(\phi^{(n/2+1)}\right)^2, & \text{if } n \text{ is even} \\ 0, & \text{if } n \text{ is odd.}\end{cases} \tag{2.52}$$

The first few terms of this expansion are

$$\sigma^2_{\rm BW}(t) \approx \frac{1}{P(t)} \int_{\Re} \left(\frac{1}{2\pi}\frac{d}{d\tau}a(\tau)h(\tau - t)\right)^2 d\tau + \frac{M_2(t) - M_1^2(t)}{4\pi^2}\phi''^2(t). \tag{2.53}$$

2.1.3.1 Discrete-Time Case

We may use the finite difference as an approximation to the continuous-time equations given above, so that Eqn. (2.40) becomes

$$\mathrm{IB}[n] = \frac{f_s}{2\pi}\left|\frac{a[n]-a[n-1]}{a[n]}\right|. \tag{2.54}$$

In general, we may replace the k-th phase derivatives in the above expressions with the k-th finite difference operator

$$f_s^k \Delta^k \phi[n] \triangleq f_s^k \sum_{\ell=0}^{k} (-1)^\ell \binom{k}{\ell} \phi[n-k] \tag{2.55}$$

$$\approx \left.\frac{d^k \phi(t)}{dt^k}\right|_{t=n/f_s}, \tag{2.56}$$

and the integrals may be approximated by the appropriate summations.

2.1.4 Instantaneous Spectrum

The *instantaneous spectrum* of a signal is another concept for which there are many interpretations. For example, one may consider the windowed Fourier transform of a signal, e.g. with diminishing weight given to past samples. The various filter-bank approaches and short-time FFT are examples of this interpretation.

In the context of instantaneous frequency, one may define the instantaneous spectrum $Z(f,t)$ of a signal

$$z(t) = \sum_{k=1}^{N} p_k(t), \tag{2.57}$$

where the $p_k(t)$ are of the form in Eqn. (2.25) and thus individually have a well-defined instantaneous frequencies, to be the discrete distribution on the instantaneous frequencies $f_1(t), \ldots, f_N(1)$ weighted by their instantaneous amplitude envelopes $a_1(t), \ldots, a_N(t)$, such that

$$Z(f,t) = \sum_{k=1}^{N} a_k(t) \exp(j\phi_{k,0})\delta\{f - f_k(t)\}. \tag{2.58}$$

Similarly, we define the *discrete-time instantaneous spectrum* to be

$$Z[f,n] = \sum_{k=1}^{N} a_k[n] \exp(j\phi_{k,0})\delta\{f - f_k[n]\}. \tag{2.59}$$

Clearly, this definition of instantaneous spectrum assumes the model in Eqn. (2.57), which has well-defined time-varying partials. This definition does not take into account signals which cannot be characterized as such, and therefore has limited utility. However, vocalized speech and many musical sounds fit well with Eqn. (2.57). An extension of this result would be to factorize any arbitrary signal into a deterministic component described by Eqn. (2.57) and a stochastic component, in a practical application of the Wold decomposition theorem [73, 84, 148]. The deterministic component could then be modeled as an instantaneous spectrum, and the stochastic component may be modeled as an ARMA system with white noise input [89]. Xavier Serra [126] explores this factorization in his dissertation. The modeling of the stochastic component is beyond the scope of this dissertation.

One may invert the instantaneous spectrum of a single partial by extracting its instantaneous frequency at each point in time, integrating with respect to time to obtain the phase, and then multiplying by its envelope. In order to invert the instantaneous spectrum of a mixture of components, it is necessary to sort out the individual contributing terms originating from each $p_k(t)$ and then to apply the inversion procedure to each one.

There are some problems with this formulation of the instantaneous spectrum. Intersecting partials present some problems with respect to the invertibility of the instantaneous spectrum. Crossed partials may lead to ambiguity about the direction a particular partial takes. This matters since the phase of the partial depends on its history. The reader may also notice that the instantaneous spectrum of a signal is not unique. Trivially, one may represent any instantaneous spectrum as

$$Z^0(f,t) = z(t)\delta\{f\}. \tag{2.60}$$

Section 3.6 illustrates several examples of instantaneous spectra, for example, Eqns. (3.77) and (3.95).

2.2 Parametric Signal Description Goals

To apply the above definition of instantaneous frequency to sampled signals it is necessary to decompose the signals into components of the form given in Eqn. (2.9) before attempting to extract the phase derivative. In this context we must enumerate, identify, and parameterize the complex-valued sinusoidal partials. The main parameters we would like to extract from each partial are its instantaneous frequency and amplitude. Since complex information is generally not available in sampled signals, we must solve the slightly more difficult problem where only the real part of the complex signal is available.

We model the real signal $s(t)$ as the sum of frequency-modulated sinusoidal components:

$$s(t) = \sum_{k=1}^{N} a_k(t) \cos\left(2\pi \int_0^t f_k(\tau)\, d\tau + \phi_{k,0}\right) \tag{2.61}$$

where N is the number of partials, $a_k(t) \geq 0$ is the amplitude of the k-th partial at time t, $f_k(t) > 0$ is its instantaneous frequency and $\phi_{k,0}$ is its phase offset at time zero. In the discrete-time case we have

$$s[n] = \sum_{k=1}^{N} a_k[n] \cos\left(\frac{j2\pi}{f_s} \sum_{\ell=1}^{n} f_k[\ell] + j\,\phi_{k,0}\right) \tag{2.62}$$

where $a_k[n] \geq 0$.

Signals which conform to this model are, of course, only a small subset of all possible signals, but a useful enough subset to merit our interest. Signals that are composed of non-deterministic "noise" are not suitable for this kind of analysis, as opposed to signals composed of slowly-varying frequency-modulated sinusoids. As mentioned above, Xavier Serra [126] studied such a decomposition of signals into stochastic and deterministic components. Many sound sources such as wind and string instruments, human voices, and bird songs may be modeled as being composed of of frequency-modulated sinusoids [68, 112]. Other sources, such as percussive instruments and non-vocal speech do not have well-localized Fourier spectral peaks and do not project easily onto a small number of complex sinusoidal partials with slowly-varying frequencies and amplitudes.

In general, the parameterization is an ill-posed problem. If we have N partials, we must extract $3N$ parameters for each input sample (frequency, phase, and amplitude), and hence the problem is highly under-determined. If we decimate our parameter estimates sufficiently, the problem may

then be well-posed. Additionally, the input samples are generally real-valued since they stem from physical measurements. Consequently, for every complex partial with instantaneous frequency $f(t)$ there must be another partial of equal amplitude at frequency $-f(t)$. Because of this symmetry, we ignore the partials with negative instantaneous frequencies.

2.2.1 Number of Partials: Model Selection

It is important to know how many partials there are in the input signal. This is a first step in the direction of finding how many coherent structures there are in the signal mixture. Clearly, if the estimated number of partials is too low we would expect loss of performance in any identification or segmentation task dependent on the extracted parameters. On the other hand, if the number of partials is overestimated, there may be problems in forming robust estimates of the parameters of the partials. Estimating the number of partials N is a difficult problem. Ljung outlines several general approaches for model selection in [89]:

1. Examining the spectral analysis estimate of the transfer function
2. Testing ranks in sample covariance matrices
3. Correlating variables
4. Examining the information matrix

For our application, approach (1) is not practical because it is subjective and we wish to automate the estimation procedure.

Approach (2) suggests determining the rank of the covariance matrix

$$R^s(N) = \frac{1}{N}\sum_{t=1}^{N} \phi_s(t)\phi_s^T(t) \tag{2.63}$$

where

$$\phi_s(t) = [-y(t-1)\ldots - y(t-s) \quad u(t-1)\ldots u(t-s)]^T, \tag{2.64}$$

and where the system equation is assumed to be describable as

$$\begin{aligned} y(t) + a_1 y(t-1) + \ldots + a_n y(t-n) \\ = b_1 u(t-1) + \ldots + b_n u(t-n) + \nu_0(t) \end{aligned} \tag{2.65}$$

for some n, and where $\{\nu_0(t)\}$ is some noise sequence [89]. Then $R^s(N)$ will be nonsingular for $s \leq n$ (provided that $\{u(t)\}$ is persistently exciting), and singular for $s > n$. Of course, in reality this is only an approximation and notions of "singularity" must be developed since any uncorrelated noise in the input will always cause the system to become nonsingular; one way of computing the approximate rank of $R^s(N)$ is to define a threshold $\hat{\sigma}^2$ and count the number of singular values of the *singular value decomposition* [59] of $R^s(N)$ which exceed $\hat{\sigma}^2$. One way of determining a suitable value of $\hat{\sigma}^2$, and hence n, is to vary it continuously and observe the thresholded rank. As $\hat{\sigma}^2$ decreases, the rank should rise slowly until a critical range, at which the thresholded rank starts to rise sharply.

Approach (3), that of "correlating variables," attempts to determine whether a variable $w(t)$ makes a meaningful contribution to a model in predicting the output $y(t)$ of a system. To this end, the correlation between $w(t)$ and $y(t)$ is measured. To discount redundant information, the correlation should be taken between $w(t)$ and the prediction error $\varepsilon(t, \hat{\theta_N}) = y(t) - y(t|\hat{\theta_N})$. The variable is accepted if it makes a significant contribution to explaining the residual. This process is known as *canonical correlation* or *partial correlation* [49, 89].

The fourth model order estimation method makes use of the *Fisher information matrix*,

$$M_N \triangleq E\left[\frac{d}{d\theta_N} log\{f_y(\theta_N; y^N)\}\right]\left[\frac{d}{d\theta_N} log\{f_y(\theta_N; y^N)\}\right]^T \Big|_{\theta_N=\theta_{N,0}}, \tag{2.66}$$

where $\theta_{N,0}$ is assumed to be the "true" value of θ_N and $f_y(\cdot)$ is the "true" probability distribution of the observations $\{y(t)\}$, given θ_N [89]. The information matrix must be inverted to use the Gauss-Newton method of parameter estimation, hence M_N must be non-singular. The number of parameters is taken to be the largest order N of M_N for which it is well-conditioned. Akaike has proposed an information-theoretic criterion for estimating the number of parameters in a model [4]. Wax and Kailath have described some methods for estimating the number of signals based on various information theoretic measures [143, 144].

The problem with any form of spectral analysis based on correlation matrices is that the signals are assumed to be fixed-frequency sinusoids mixed in with stationary Gaussian noise. Such signals almost never exist in reality except as test signals. Correlation methods depend on some range of time-averaging in order to accumulate meaningful statistics. However, nonstationary signals do not stay still long enough for any meaningful averaging to occur. If correlation methods are used they are assumed to have fixed-frequency spectra over some time window. Signals with even moderate frequency slew, although well-characterizable, introduce a tradeoff between poor frequency localization due to long time averaging and poor noise rejection due to short time averaging.

In general, model order prediction is a difficult problem; obtaining an order estimate in a computationally efficient manner is even more difficult. The problem of estimating the number of nonstationary, frequency-modulated sinusoids is even more challenging. Much work on this topic needs to be done.

2.3 Analytic Signal Representation

A key idea in this thesis is to view the signal $s[n]$ as the real part of an analytic signal. We may obtain the analytic signal $z_H[n]$ by replacing $\cos(\cdot)$ in Eqn. (2.1) by the complex exponential function so that

$$z_H(t) = \int_0^\infty S_{\text{mag}}(f) \exp\left(j2\pi ft + jS_\phi(f)\right)\, df \tag{2.67}$$

This is equivalent to adding together the signal and $-j$ times its Hilbert-transformed complement function

$$q_H(t) = \mathcal{H}\{s(t)\} \tag{2.68}$$

which has a Fourier spectrum:

$$\mathcal{F}\{\mathcal{H}\{s(t)\}\} = \begin{cases} jS(f) & : \quad f > 0 \\ 0 & : \quad f = 0 \\ -jS(f) & : \quad f < 0 \end{cases} \tag{2.69}$$

where $\mathcal{H}\{\cdot\}$ is the Hilbert transform operator, whose kernel is seen to have an infinite extent in time [21]:

$$\mathcal{H}\{s(t)\} = s(t) * \frac{-1}{\pi t}. \tag{2.70}$$

Then, $z_H(t) = s(t) - jq_H(t)$. The spectrum of $z_H(t)$ is

$$Z_H(f) = \begin{cases} 2S(f) & : \quad f > 0 \\ S(0) & : \quad f = 0 \\ 0 & : \quad f < 0 \end{cases} \tag{2.71}$$

Ideally, one would like to construct the complex signal $z(t) = s(t) - jq(t)$, in which the imaginary part $-q(t)$ is composed of components which are in quadrature with their corresponding components in $s(t)$, based on the signal model of Eqn. (2.61), i.e.,

$$q(t) = -\sum_{k=1}^{N} a_k(t) \sin\left(2\pi \int_0^t f_k(\tau)\, d\tau + \phi_{k,0}\right) \tag{2.72}$$

The minus sign for $q(t)$ is for agreement with the convention linking the Hilbert transform and the analytic signal [21].

It is by no means guaranteed that $q(t) = q_H(t)$. Under the reasonable assumptions given by the Bedrosian product theorem, summarized in Appendix A and [12, 17], which require that the lowest frequency component of the spectrum of the carrier signal be greater than the cut-off frequency of the spectrum of the modulating function, such a signal $q(t)$ may be obtained by a Hilbert transform as above for the stationary signal, i.e., $q(t) = q_H(t) = \mathcal{H}\{s(t)\}$.

For the remainder of this paper we will assume that the conditions of the Bedrosian product theorem hold, so that the analytic signal $z_H(t) = s(t) - jq_H(t)$ and the model-based real-plus-quadrature signal $z(t) = s(t) - jq(t)$ are the same.

Under these conditions, the signal $z(t) = s(t) - jq(t)$ may be thought of as the sum

$$z(t) = \sum_{k=1}^{N} p_k(t) \tag{2.73}$$

where the $p_k(t)$ are counterclockwise-rotating complex phasors,

$$p_k(t) = a_k(t) \exp\left(j2\pi \int_0^t f_k(\tau)\, d\tau + j\phi_{k,0}\right), \tag{2.74}$$

or in the discrete-time case,

$$z[n] = \sum_{k=1}^{N} p_k[n] \tag{2.75}$$

and

$$p_k[n] = a_k[n] \exp\left(\frac{j2\pi}{f_s} \sum_{\ell=1}^{n} f_k[\ell] + j\,\phi_{k,0}\right), \quad a_k[n] \geq 0. \tag{2.76}$$

The real part of each such term $p_k(t)$ or $p_k[n]$ corresponds to a partial of the real signal $s(t)$.

As mentioned above, we would like to extract the instantaneous frequency and amplitude of each partial. Some estimation methods for instantaneous frequency consider calculating the derivative $d\phi(t)/dt$, or equivalently, the finite difference $\phi[n] - \phi[n-1]$, where $\phi(t)$ is the phase of the complex phasor $z(t) = a(t)\exp\{j\phi(t)\}$ at time t [17]. However, this method is extremely susceptible to noise and is furthermore unbounded, as was shown in Section 2.1.1.1, even if the spectrum $Z(f)$ is bandwidth-limited. See Section 2.1.1.1 for more details on this behavior. This estimate of the instantaneous frequency must be filtered to be of any use.

2.3.1 Phase Winding Measure

A more robust estimation method than using the phase derivative or phase difference directly is to count the frequency of windings of $z(t)$ around the time axis. This procedure is equivalent to low-pass filtering the derivative of $\phi(t)$. We are helped by the following definition and theorem:

Definition 2.1 *We define the* winding number $W_z(t_0, t_1)$ *of a complex phasor* $z(t)$ *over a time interval* $t \in (t_0, t_1)$ *as*

$$W_z(t_0, t_1) \stackrel{\triangle}{=} \frac{1}{2\pi} \int_{t_0}^{t_1} d \arg\{z(t)\}. \tag{2.77}$$

This is simply the number of times the phasor has wrapped counterclockwise around the time axis between time t_0 and t_1. This formulation avoids the branch ambiguity of the $\arg(\cdot)$ function, which has range $(-\pi, \pi)$. Formally,

$$W_z(t_0, t_1) = \frac{1}{2\pi} \left[\mathrm{Arg}\{z(t_1)\} - \mathrm{Arg}\{z(t_0)\} \right], \tag{2.78}$$

where $\mathrm{Arg}(\cdot)$ returns the absolute phase of its argument.

Definition 2.2 *For the discrete-time case we similarly define the* discrete-time winding number $W_z[n_0, n_1]$ *of a complex phasor* $z[n]$ *over a time interval* $n \in \{n_0, \ldots, n_1\}$ *as*

$$W_z[n_0, n_1] \stackrel{\triangle}{=} \frac{1}{2\pi} \sum_{k=n_0+1}^{n_1} \arg\{z[k] z^*[k-1]\} \tag{2.79}$$

$$= \frac{1}{2\pi} \left[\mathrm{Arg}\{z[n_1]\} - \mathrm{Arg}\{z[n_0]\} \right]. \tag{2.80}$$

Since $z[n]$ is assumed to be critically sampled we are guaranteed that the phase cannot change by more than $\pm\pi$ radians between samples so that $\arg\{z[k] z^*[k-1]\}$ is well-defined and there is no branch ambiguity.

Theorem 2.1 (Winding Theorem) *Let* $z(t)$ *be the sum of two complex signals* $p(t)$ *and* $\nu(t)$ *such that*

$$p(t) = a(t) \exp\left(j 2\pi \int_0^t f(\tau)\, d\tau + j\, \phi_0 \right), \quad a(t) \geq 0, \tag{2.81}$$

and also the $\mathcal{M}_1$*-condition*[4]

$$a(t) > |\nu(t)| \tag{2.82}$$

hold over the interval $t \in (t_0, t_1)$*. It follows that the winding numbers* $W_z(t_0, t_1)$ *of the signal* $z(t)$ *and* $W_p(t_0, t_1)$ *of* $p(t)$ *over the interval* (t_0, t_1) *have the relation*

$$|W_z(t_0, t_1) - W_p(t_0, t_1)| < 1/2. \tag{2.83}$$

[4] In general, the $\mathcal{M}_p$ metric of instantaneous signal strength, where $p \geq 1$, in an additive mixture of orthogonal signals as in Eqn. (2.73) is

$$\mathcal{M}_p\{z(t)\} = \left[\sum_{k=1}^{N} |p_k(t)|^p \right]^{1/p}.$$

Notice that the value of $\mathcal{M}_p\{z(t)\}$ completely depends on how the signal is modeled. In the present context $z(t)$ is comprised of functions of the form given in Eqn. (2.25). For $p = 1$ this measure may be seen the maximum value that the sum in Eqn. (2.57) could attain at time t, given that the phases $\phi_k(t)$ of each partial $p_k(t)$ are unknown and assuming the worst possible case. This is not to be confused with the L_p measure (cf. footnote 1, page 17).

Proof:

$$z(t) = p(t) + \nu(t) \tag{2.84}$$

$$= \exp\left(j2\pi \int_0^t f(\tau)\, d\tau + j\phi_0\right) \left\{a(t) + e^{j\alpha(t)}|\nu(t)|\right\} \tag{2.85}$$

where $\alpha(t)$ is an unimportant phase factor. We examine the phase perturbation factor[5]

$$K(t) \triangleq a(t) + e^{j\alpha(t)}|\nu(t)|. \tag{2.86}$$

From Eqn. (2.82), we see that $K(t)$ is complex with positive real part, and therefore its phase is in the range $(-\pi/2, \pi/2)$ for all $t \in (t_0, t_1)$ so that

$$|\arg\{K(t)\}| < \pi/2. \tag{2.87}$$

By definition,

$$W_z(t_0, t_1) = \frac{1}{2\pi} \int_{t_0}^{t_1} d\arg\{z(t)\} \tag{2.88}$$

$$= \frac{1}{2\pi} \int_{t_0}^{t_1} d\left[\arg\{p(t)\} + \arg\{K(t)\}\right] \tag{2.89}$$

$$= W_p(t_0, t_1) + \frac{1}{2\pi} \int_{t_0}^{t_1} d\arg\{K(t)\} \tag{2.90}$$

$$= W_p(t_0, t_1) + \frac{1}{2\pi} \left[\arg\{K(t_1)\} - \arg\{K(t_0)\}\right] \tag{2.91}$$

where in the last line we note that $K(t)$ never winds around the time axis so there is no branch ambiguity (see Figure 2.7). Thus,

$$|W_z(t_0, t_1) - W_p(t_0, t_1)| = \frac{1}{2\pi} |\arg\{K(t_1)\} - \arg\{K(t_0)\}| \tag{2.92}$$

$$< 1/2. \quad \text{Q.E.D.} \tag{2.93}$$

The obvious extension to the discrete case for the signal

$$z[n] = p[n] + \nu[n] \tag{2.94}$$

is given here:

Theorem 2.2 (Discrete Winding Theorem) *Let $z[n]$ be the sum of the complex signals $p[n]$, which is of the form in Eqn. (2.76), and $\nu[n]$ and also the $\mathcal{M}_1$-condition*

$$a[n] > |\nu[n]| \tag{2.95}$$

hold over the interval $n \in \{n_0, \ldots, n_1\}$. It follows that the winding numbers $W_z[n_0, n_1]$ of the signal $z[n]$ and $W_p[n_0, n_1]$ of $p[n]$ over the interval $n \in \{n_0, \ldots, n_1\}$ have the relation

$$|W_z[n_0, n_1] - W_p[n_0, n_1]| < 1/2. \tag{2.96}$$

We give a partial proof in order to define some terms for the discrete case.

[5] We have cast the noise here as a multiplicative phase factor. However, this multiplicative factor cannot cause aliasing, i.e., violating the Nyquist criterion, because it describes an *additive* perturbation to the signal. Therefore $K(t)$ does not act like independent multiplicative noise.

Proof:

$$z[n] = p[n] + \nu[n] \tag{2.97}$$

$$= \exp\left(\frac{j2\pi}{f_s}\sum_{k=1}^{n} f[k] + j\phi_0\right)\left\{a[n] + e^{j\alpha[n]}|\nu[n]|\right\} \tag{2.98}$$

where $\alpha[n]$ is an unimportant phase factor. We define the discrete-time phase perturbation factor

$$K[n] \triangleq a[n] + e^{j\alpha[n]}|\nu[n]|. \tag{2.99}$$

The rest of the proof is virtually identical to the previous theorem.

2.3.1.1 Average Instantaneous Frequency

The winding number allows us to approximate the average instantaneous frequency of $p(t)$ for $t \in (t_0, t_1)$ as

$$\bar{f}_p(t_0, t_1) \triangleq \frac{W_p(t_0, t_1)}{t_1 - t_0} \tag{2.100a}$$

$$\approx \frac{W_z(t_0, t_1)}{t_1 - t_0} \tag{2.100b}$$

$$\triangleq \bar{f}_z(t_0, t_1). \tag{2.100c}$$

The discrete-time average instantaneous frequency of $p[n]$ for $n \in \{n_0, \ldots, n_1\}$ is analogous:

$$\bar{f}_p[n_0, n_1] \triangleq \frac{W_p[n_0, n_1]}{n_1 - n_0} \tag{2.101a}$$

$$\approx \frac{W_z[n_0, n_1]}{n_1 - n_0} \tag{2.101b}$$

$$\triangleq \bar{f}_z[n_0, n_1]. \tag{2.101c}$$

2.3.1.2 Corollaries

Theorems 2.1 and 2.2 and Eqns. (2.100) and (2.101) suggest a powerful method for estimating the instantaneous frequency of the strongest partial $p_k(t)$ or $p_k[n]$ in a mixture $z(t)$ or $z[n]$, respectively, provided that the signal-to-noise ratio in the $\mathcal{M}_1$-sense be greater than one, as implied by Eqn. (2.82) and (2.95). Since the relations between the discrete and continuous cases are obvious we focus only the discrete cases here.

We may immediately infer from Theorem 2.2:

Corollary 2.1 (Multi-Partial Winding Corollary) *Let $z[n]$ be the sum of complex signals*

$$z[n] = \sum_{\ell=1}^{N} p_\ell[n] + \nu[n] \tag{2.102}$$

where each $p_\ell[n]$ is of the form given in Eqn. (2.76) and $\nu[n]$ is some signal such that for some fixed k the $\mathcal{M}_1$-condition

$$a_k[n] > \sum_{\substack{\ell=1 \\ \ell \neq k}}^{N} a_\ell[n] + |\nu[n]| \tag{2.103}$$

is satisfied on the interval $n \in \{n_0, \ldots, n_1\}$. *Then, the winding numbers* $W_z[n_0, n_1]$ *of the signal* $z[n]$ *and* $W_{p_k}[n_0, n_1]$ *of* $p_k[n]$ *over the interval* $n \in \{n_0, \ldots, n_1\}$ *have the relation*

$$|W_z[n_0, n_1] - W_{p_k}[n_0, n_1]| < 1/2.$$

Proof: This follows from Theorem 2.2 and the triangle inequality:

$$\sum_{\substack{\ell=1 \\ \ell \neq k}}^{N} a_\ell[n] + |\nu[n]| = \sum_{\substack{\ell=1 \\ \ell \neq k}}^{N} |p_\ell[n]| + |\nu[n]| \tag{2.104}$$

$$> \left| \sum_{\substack{\ell=1 \\ \ell \neq k}}^{N} p_\ell[n] + \nu[n] \right|, \tag{2.105}$$

and thus, with the appropriate substitutions, Eqn. (2.95) is satisfied and the desired result is immediate. Q.E.D.

The conditions given above in Eqns. (2.95) and (2.103) provide criteria for guaranteeing frequency lock on the sinusoidal signal with the maximum amplitude over the entire spectrum. We usually want to track a *local* maximum-amplitude partial rather than the global maximum-amplitude partial. We may replace a signal $z[n]$ with a filtered version $h * z[n]$, where $h[n]$ is the impulse response of some linear filter with transfer function $H(f)$. Naturally, the Discrete Winding Theorem and the Multi-Partial Winding Corollary apply to the filtered signal as well. We state the obvious result which follows immediately from the Winding Theorem:

Corollary 2.2 (Filtered Winding Corollary) *If* $z[n]$ *is of the form given by Eqn. (2.94) and*

$$|h * p[n]| > |h * \nu[n]| \tag{2.106}$$

is satisfied in the interval $n \in \{n_0, \ldots, n_1\}$, *where* $h[n]$ *is the impulse response of some linear filter, then the winding numbers* $W_{h*z}[n_0, n_1]$ *of the signal* $h * z[n]$ *and* $W_{h*p}[n_0, n_1]$ *of* $h * p[n]$ *over the interval* $n \in \{n_0, \ldots, n_1\}$ *have the relation*

$$|W_{h*z}[n_0, n_1] - W_{h*p}[n_0, n_1]| < 1/2.$$

The obvious extension to the Multi-Partial Winding Corollary is:

Corollary 2.3 (Filtered Multi-Partial Winding Corollary) *If* $z[n]$ *is of the form given by Eqn. (2.102) and for some* k

$$|h * p_k[n]| > \sum_{\substack{\ell=1 \\ \ell \neq k}}^{N} |h * p_\ell[n]| + |h * \nu[n]| \tag{2.107}$$

is satisfied in the interval $n \in \{n_0, \ldots, n_1\}$, *where* $h[n]$ *is the impulse response of some linear filter, then the winding numbers* $W_{h*z}[n_0, n_1]$ *of the signal* $h * z[n]$ *and* $W_{h*p_k}[n_0, n_1]$ *of* $p_k[n]$ *over the interval* $\{n_0, \ldots, n_1\}$ *have the relation*

$$|W_{h*z}[n_0, n_1] - W_{h*p_k}[n_0, n_1]| < 1/2.$$

Eqns. (2.106) and (2.107) are the *filtered* $\mathcal{M}_1$*-conditions.*

If the group delay of $H(f)$ is small for $f = f[n]$, $n \in \{n_0, \ldots, n_1\}$, then

$$\varepsilon_W = |W_{h*p}[n_0, n_1] - W_p[n_0, n_1]| \tag{2.108}$$

is small so that, using the triangle inequality,

$$\begin{aligned} |W_{h*z}[n_0, n_1] - W_p[n_0, n_1]| &< |W_{h*z}[n_0, n_1] - W_{h*p}[n_0, n_1]| && \text{(2.109a)} \\ &\quad + |W_{h*p}[n_0, n_1] - W_p[n_0, n_1]| && \text{(2.109b)} \\ &< 1/2 + \varepsilon_W && \text{(2.109c)} \\ &\approx 1/2, && \text{(2.109d)} \end{aligned}$$

and thus we see that $W_{h*z}[n_0, n_1]$ may be used as an approximation to $W_p[n_0, n_1]$.

Corollaries 2.2 and 2.3 have applications in determining the winding number of a partial $p[n]$ in noise. For example, if $z[n]$ is of the form Eqn. (2.94) and if $H(f)$ is a bandpass filter which passes frequencies $f \approx +f[n]$ and attenuates signals at frequencies away from $f[n]$, then the signal-to-noise ratio can be greatly increased and the error in the winding number may be reduced, as will be seen in Section 2.3.2. Additionally, if $z[n]$ is of the form Eqn. (2.102) and Eqn. (2.103) does not hold, then if a filter can be found such that Eqn. (2.107) holds then we may use Corollary 2.3 and Eqns. (2.109) to approximate the measurement of $W_{p_1}[n_0, n_1]$. Generally, we may use a bandpass filter which passes frequencies $f \approx +f_k[n]$ and assume that the instantaneous frequency tracks $f_\ell[n]$, $\ell \neq k$ are outside the passband so that the partials $p_\ell[n]$ are sufficiently attenuated for Eqn. (2.107) to hold.

We notice that if $s[n]$ is a real signal and

$$H(f) = 0 \text{ for } f \leq 0 \tag{2.110}$$

then the signal $h * s[n]$ is an analytic signal. If $z[n]$ is the analytic complement of $s[n]$, i.e., if $z[n] = s[n] - j\, q_H[n]$, where $q_H[n]$ is the discrete-time Hilbert transform of $s[n]$, then

$$W_{h*s}[n_0, n_1] = W_{h*z}[n_0, n_1]. \tag{2.111}$$

This result obviates the need to perform an explicit Hilbert transform on the signal $s[n]$ to obtain $z[n]$ for the purpose of performing a winding analysis.

Thus, if the real signal $s[n]$ is of the form given in Eqn. (2.62) and the Bedrosian conditions (cf. Theorem A.1) hold, its analytic counterpart

$$z[n] = s[n] - j\, q_H[n] \tag{2.112}$$

may be described as

$$z[n] = \sum_{k=1}^{N} a_k[n] \exp\left(\frac{j2\pi}{f_s} \sum_{\ell=1}^{n} f_k[\ell] + j\, \phi_{k,0} \right). \tag{2.113}$$

We may then approximate the winding of a given partial $p_k[n]$ as

$$\begin{aligned} W_{p_k}[n_0, n_1] &\approx W_{h_k * p_k}[n_0, n_1] && \text{(2.114)} \\ &\approx W_{h_k * z}[n_0, n_1] && \text{(2.115)} \\ &= W_{h_k * s}[n_0, n_1], && \text{(2.116)} \end{aligned}$$

given that the filter $H_k(f)$ satisfies Eqn. (2.107) for $p_k[n]$ and that Eqn. (2.110) holds.

2.3.1.3 Examples

Figures 2.1–2.6 illustrate the winding concept.

2.3.2 A Sharper Estimate of the Winding Error

The bound of 1/2 in Eqn. (2.82) in Theorem 2.1 and its corollaries is a bit generous and may be tightened up considerably. The result of Theorem 2.1 is that the winding numbers $W_z[n_0, n_1]$ of the signal $z[n]$ and $W_p[n_0, n_1]$ of $p[n]$ over the interval $[n_0, n_1]$ have the relation

$$|W_z[n_0, n_1] - W_p[n_0, n_1]| < 1/2.$$

However, this inequality is the limiting value in the worst possible case where the signal $\nu[n]$ has magnitude approaching $a[n]$ in Eqn. (2.99):

$$K[n] \triangleq a[n] + e^{j\alpha[n]}|\nu[n]|.$$

The bound in Eqns. (2.83) and (2.96) may be improved upon dramatically when the signal-to-noise ratio in the $\mathcal{M}_1$-sense is greater than one (see footnote 4 on page 29).

Define the $\mathcal{M}_1$ signal-to-noise ratio

$$\mathrm{SNR}_1[n] \triangleq \frac{a[n]}{r[n]}, \tag{2.117}$$

where

$$r[n] \triangleq |\nu[n]|. \tag{2.118}$$

Given that the phase $\varphi[n] \triangleq \arg(\nu[n])$ is unknown, we know that $K[n]$ is located somewhere on a circle of radius $r[n]$. We may divide $K[n]$ by $r[n]$ so that the locus of $K[n]$ is a unit circle centered at $\mathrm{SNR}_1[n]$ (see Figure 2.7). Define the phase error

$$\begin{aligned}
\zeta[n] &\triangleq \arg(K[n]) && (2.119)\\
&\leq \sin^{-1}\left(\frac{r[n]}{a[n]}\right) && (2.120)\\
&= \sin^{-1}\left(\frac{1}{\mathrm{SNR}_1[n]}\right) && (2.121)\\
&\approx \frac{1}{\mathrm{SNR}_1[n]}. && (2.122)
\end{aligned}$$

where in Eqn. (2.120) we use the fact that the tangent to the circle makes a right triangle with the radius at the contact point, and Eqn. (2.122) holds for large $\mathrm{SNR}_1[n]$. Hence, the bound of 1/2 in Eqn. (2.96) may be replaced by β/π, where

$$\beta \triangleq \max_{n\in\{n_0,\ldots,n_1\}} \sin^{-1}\left(\frac{1}{\mathrm{SNR}_1[n]}\right), \tag{2.123}$$

so that

$$\begin{aligned}
|W_z[n_0, n_1] - W_p[n_0, n_1]| &< \beta/\pi && (2.124)\\
&\approx \frac{1}{\pi\,\mathrm{SNR}_1}, \quad \text{for large } \mathrm{SNR}_1. && (2.125)
\end{aligned}$$

2.3.2.1 Mean and Variance of the Phase Error $\zeta[n]$

The maximum phase error for the interval $n \in \{n_0, \ldots, n_1\}$ is 2β, assuming $\mathrm{SNR}_1 < 1$. However, the mean and variance may give an even more optimistic measure of performance. Assuming that the phase $\varphi[n]$ is a random variable independent of $p[n]$ and uniformly distributed over the interval $[-\pi, \pi]$, we see that

$$\mathrm{E}\{\zeta[n]\} = \int_{-\pi}^{\pi} \arg\left(r[n] + \cos(\theta) + j\sin(\theta)\right)\, d\theta \tag{2.126}$$

$$= 0 \tag{2.127}$$

by noting that the integrand is an odd function of θ. Therefore, the winding number $W_z[n_0, n_1]$ of the signal $z[n]$ is an unbiased estimator of the winding number $W_p[n_0, n_1]$ of $p[n]$.

The variance is computed as

$$\mathrm{E}\left\{\zeta^2[n]\right\} - \mathrm{E}^2\left\{\zeta[n]\right\} = \sigma_\zeta^2\left(r[n]\right) \tag{2.128}$$

$$\stackrel{\triangle}{=} \frac{1}{2\pi}\int_{-\pi}^{\pi} \arg^2\left(r[n] + \cos(\theta) + j\sin(\theta)\right)\, d\theta. \tag{2.129}$$

No exact closed form expression of this integral could be found with reasonable effort.[6] The solid curve in Figure 2.8 shows a log-log plot of $\sigma_\zeta^2(r)$ vs. $\log(r)$, revealing an slope of -2 for large SNR_1. This may be seen intuitively from Eqn. (2.129) by realizing that for large r the argument to the $\arg(\cdot)$ function is dominated by $\sin(\theta)/r$:

$$\sigma_\zeta^2\left(r\right) = \frac{1}{2\pi}\int_{-\pi}^{\pi} \arctan^2\left(\frac{\sin(\theta)}{r + \cos(\theta)}\right)\, d\theta, \text{ for } r \geq 1 \tag{2.130a}$$

$$\approx \frac{1}{2\pi}\int_{-\pi}^{\pi} \arctan^2\left(\frac{\sin(\theta)}{r}\right)\, d\theta, \text{ for } r \gg 1 \tag{2.130b}$$

$$= \frac{1}{2\pi}\int_{-\pi}^{\pi} \left\{\sum_{k=0}^{\infty} \frac{(-1)^k}{2k+1}\left(\frac{\sin(\theta)}{r}\right)^{2k+1}\right\}^2\, d\theta \tag{2.130c}$$

$$\approx \frac{1}{2\pi}\int_{-\pi}^{\pi} \left\{\frac{\sin(\theta)}{r}\right\}^2\, d\theta \tag{2.130d}$$

$$= \frac{1}{2r^2}, \tag{2.130e}$$

where in Eqn. (2.130d) we have used the small-angle approximation, $\arctan(x) \approx x,\ |x| \ll 1$. We see in Figure 2.8 that, for $\mathrm{SNR}_1 < 1$, $\sigma_\zeta^2(r)$ reaches an asymptote of about $\pi^2/3$ as r approaches zero. This is because the phase error $\zeta[n]$ is bounded above by π, due to the $\arg(\cdot)$ function returning only the principal branch. *Therefore, for* $\mathrm{SNR}_1 \leq 1$, *the measure of phase variance* $\sigma_\zeta^2(r[n])$ *given by Eqn. (2.129) is not a reliable indicator of winding error because it is biased towards smaller values.* On the other hand, when $\mathrm{SNR}_1 > 1$ phase winding errors due to spurious loops around the time axis do not occur so that there is no branch ambiguity in $\zeta[n]$ so that $\sigma_\zeta^2(r[n])$ is a reliable measure of the phase error due to $\nu[n]$.

The approximation is plotted with the dashed curve in Figure 2.8. We see that for larger values of r Eqn. (2.130e) provides an excellent approximation.

[6] This is left as an exercise for the reader!

2.3.2.2 Comparison Between the SNR_1 and SNR_2 Error Metrics

The SNR_1 defined in Eqn (2.117) seems like an unusual signal-to-noise measure. SNR_2, defined as

$$\mathrm{SNR}_2 \triangleq \frac{\text{signal power}}{\text{noise power}} \tag{2.131}$$

$$= \frac{A^2}{\sigma_\nu^2}, \tag{2.132}$$

is the more traditional measure, where σ_ν^2 is assumed to be Gaussian white noise,

It is instructive to see the role each has in predicting system performance. Eqns. (2.130) and Figure 2.8 show the significance of the SNR_1 metric. We ask what role SNR_2 plays in the winding analysis. We note that the statistics of the noise $\nu[n]$ can give quite different values for SNR_1 for a given value of SNR_2. SNR_1 gives the maximum magnitude of the error at any given time n and predicts the breakdown of the winding count when $\mathrm{SNR}_1 < 1$. On the other hand, given Gaussian noise with $\mathrm{SNR}_2 = \sigma_\nu^2$, the maximum value of $|\nu[n]|$ is effectively unbounded and we have to resort to a probabilistic analysis of the error rate.

We refer to Kay's results in simulating the unweighted phase averager [75], which is identical to the average winding number measure given by $\bar{f}_z[n_0, n_1]$ (cf. Eqn. (2.101c)). Figure 2.9 shows that the unweighted phase averager has a threshold of $\mathrm{SNR}_2 = 6$ dB. This fact seems to fit with a SNR_1 threshold of 1. To see this we note that in Kay's analysis $\nu[n]$ is complex white noise of variance σ_z^2 and the signal amplitude is given by A so that, at threshold,

$$\frac{A^2}{\sigma_z^2} = 2. \tag{2.133}$$

The radial component of the white noise has variance $\sigma_r^2 = \sigma_z^2/2$. This means that at the SNR_2 threshold

$$A = 2\sigma_r \tag{2.134}$$

so that the signal amplitude must be two standard deviations greater than the noise. At this amplitude the probability of a spurious crossing is $(1 - \mathrm{erf}(2/\sqrt{2}))/2 = 0.0228$, where [2]

$$\mathrm{erf}(x) \triangleq \frac{2}{\sqrt{\pi}} \int_0^x e^{-t^2}\, dt,$$

implying that at least 97% of the time there is no winding error due to the noise causing the rotating phasor to make a spurious loop around the time axis. Figure 2.10 shows the expected probability of spurious winding as a function of SNR_2, and knee of the curve seems to fit well with Kay's empirical observation of a 6 dB threshold.

Finally, we note that, if SNR_2 is small and the phase of $\nu[n]$ is uniformly distributed over $(-\pi, \pi)$, we may use the small-angle approximation and Eqn. (2.130e) to find that, to a very good approximation,

$$\mathrm{SNR}_2 \approx \mathrm{SNR}_1^2. \tag{2.135}$$

The problem of phase and frequency modulation signal detection thresholds in the presence of noise has been studied in considerable detail. The preceeding analysis is similar to the study of the so-called "capture effect" carried out by Panter [107, Ch. 14].

2.3.3 Weighted Winding Measurement

According to Theorem 2.2, the winding number $W_z[n_0, n_1]$ of the signal $z(t)$ gives an estimate of the winding number $W_p[n_0, n_1]$ of the signal $p(t)$, where $p(t)$ and $z(t)$ satisfy the appropriate conditions Eqns. (2.76) and (2.95). The difference given by Eqn. (2.96) is bounded by 1/2. If we apply Eqn. (2.80) we see that the estimate $W_z[n_0, n_1]$ effectively results from two data points! Hence, the estimate of $\bar{f}_p[n_0, n_1]$ given by Eqns. (2.101) is rather noisy. Assuming that $\nu[n]$ is independent Gaussian white noise, we have from Eqn. (2.101c) that

$$\begin{aligned}
\mathrm{var}\left\{\bar{f}_z[n_0, n_1]\right\} &= \mathrm{var}\left\{\frac{W_z[n_0, n_1]}{n_1 - n_0}\right\} && \text{(2.136a)}\\
&= \frac{f_s^2}{4\pi^2(n_1 - n_0)^2}\mathrm{var}\left[\arg\{K[n_1]\} - \arg\{K[n_0]\}\right] && \text{(2.136b)}\\
&= \frac{f_s^2}{4\pi^2(n_1 - n_0)^2}\mathrm{var}\left[\arg\{K[n_1]\}\right] + \mathrm{var}\left[\arg\{K[n_0]\}\right] && \text{(2.136c)}\\
&\approx \frac{f_s^2}{4\pi^2(N-1)^2}\left\{\frac{\sigma_\nu^2}{2a^2[n_0]} + \frac{\sigma_\nu^2}{2a^2[n_1]}\right\} && \text{(2.136d)}\\
&\approx \frac{f_s^2}{4\pi^2(N-1)^2}\frac{\sigma_\nu^2}{A^2}, && \text{(2.136e)}
\end{aligned}$$

where in the last equation we presume that the envelope satisfies $a[n_0] \approx A \approx a[n_1]$. Thus, we see that the variance of $\bar{f}_z[n_0, n_1]$ diminishes as $O(1/N^2)$, where $N = n_1 - n_0 + 1$, the number of data samples. We know, however, that the Cramér-Rao bound on the variance of the frequency estimate from N samples is about $O(1/N^3)$ (cf. Appendix E, Eqn. (E.41), and refs. [24, 75, 111, 119]). Therefore the phase-winding measure of Section 2.3.1 is suboptimal.

However, the results from the previous sections (2.3.1) and (2.3.2) are instructive. If we know that the $\mathcal{M}_1$-condition, Eqn. (2.95), holds, Theorem 2.1 tells us that the unknown signal $\nu[n]$ does not cause $W_z[n_0, n]$ to fail catastrophically as an estimate of $W_p[n_0, n]$, and thus the estimate $\bar{f}_z[n_0, n_1]$ is robust. Under these conditions, it follows that any *weighted average* of the phase differences

$$\bar{f}_z^w[n_0, n_1] \triangleq \frac{f_s}{2\pi}\sum_{m=n_0+1}^{n_1} w[m - n_0]\arg\left\{z[m]z^*[m-1]\right\} \tag{2.137}$$

is also a robust frequency estimator of the weighted average frequency

$$\begin{aligned}
\bar{f}_p^w[n_0, n_1] &\triangleq \frac{f_s}{2\pi}\sum_{m=n_0+1}^{n_1} w[m - n_0]\arg\left\{p[m]p^*[m-1]\right\} && \text{(2.138)}\\
&= \frac{f_s}{2\pi}\sum_{m=n_0+1}^{n_1} w[m - n_0]f[m]. && \text{(2.139)}
\end{aligned}$$

To see this, we first provide a definition.

Definition 2.3 (Total Variation) *The* total variation *of a sequence* $w[k]$, $0 \le k \le N$ *is*

$$\mathrm{TV}\{w\} \triangleq \sum_{m=0}^{N-1}\left|w[m+1] - w[m]\right|. \tag{2.140}$$

Now we prove the following theorem:

Theorem 2.3 (Weighted Winding Theorem) *Let $\{w[k]\}_{k=0}^{N}$ be a set of non-negative weighting coefficients such that*

$$\sum_{k=0}^{N} w[k] = 1 \tag{2.141a}$$

and additionally, the endpoints satisfy

$$w[0] = w[N] = 0. \tag{2.141b}$$

Also suppose that the conditions of Theorem 2.2 hold for the signal $z[n] = p[n] + \nu[n]$. Then

$$\left|\bar{f}_z^w[n_0, n_1] - \bar{f}_p^w[n_0, n_1]\right| < \frac{f_s}{4}\mathrm{TV}\{w\}. \tag{2.142}$$

Proof:

$$z[n] = \exp\left(\frac{j2\pi}{f_s}\sum_{k=1}^{n} f[k] + j\phi_0\right)\left\{a[n] + e^{j\alpha[n]}|\nu[n]|\right\} \tag{2.143}$$

where $\alpha[n]$ is an unimportant phase factor. We remember that

$$K[n] \stackrel{\triangle}{=} a[n] + e^{j\alpha[n]}|\nu[n]|. \tag{2.144}$$

Then

$$\bar{f}_z^w[n_0, n_1] = \frac{f_s}{2\pi}\sum_{m=n_0+1}^{n_1} w[m-n_0]\left\{f[m] + \arg\left(K[m]\right) - \arg\left(K[m-1]\right)\right\} \tag{2.145}$$

$$= \bar{f}_p^w[n_0, n_1] + \varepsilon \tag{2.146}$$

where the error term,

$$\varepsilon = \frac{f_s}{2\pi}\sum_{m=n_0+1}^{n_1} w[m-n_0]\left\{\arg\left(K[m]\right) - \arg\left(K[m-1]\right)\right\}, \tag{2.147}$$

satisfies

$$|\varepsilon| = \frac{f_s}{2\pi}\left|\sum_{m=n_0+1}^{n_1} w[m-n_0]\left\{\arg\left(K[m]\right) - \arg\left(K[m-1]\right)\right\}\right| \tag{2.148}$$

$$\leq \frac{f_s}{2\pi}\left\{w[N-1]\left|\arg\left(K[n_1]\right)\right| + w[1]\left|\arg\left(K[n_0]\right)\right|\right\} \tag{2.149}$$

$$+ \frac{f_s}{2\pi}\sum_{m=n_0+1}^{n_1-1}\left|w[m-n_0+1] - w[m-n_0]\right|\left|\arg\left(K[m]\right)\right|$$

$$< \frac{f_s}{4}\left\{w[1] + w[N-1] + \sum_{m=1}^{N-2}\left|w[m+1] - w[m]\right|\right\} \tag{2.150}$$

$$= \frac{f_s}{4}\sum_{m=0}^{N-1}\left|w[m+1] - w[m]\right| \tag{2.151}$$

$$= \frac{f_s}{4}\mathrm{TV}\{w\} \tag{2.152}$$

where in Eqn. (2.150) we have used the fact that Eqn. (2.95) gives us

$$|\arg(K[m])| < \frac{\pi}{2}. \tag{2.153}$$

Q.E.D.

The weighted extensions to Corollaries 2.1, 2.2 and 2.3 are obvious and are stated without proof:

Corollary 2.4 (Weighted Multi-Partial Winding Corollary) *If $z[n]$ and $p_k[n]$ satisfy Eqn. (2.103) of Corollary 2.1, and if $w[k]$, $k \in \{0,\ldots,N\}$, satisfy Eqns. (2.141) then*

$$\left|\bar{f}_z^w[n_0,n_1] - \bar{f}_{p_k}^w[n_0,n_1]\right| < \frac{f_s}{4}\mathrm{TV}\{w\}. \tag{2.154}$$

Corollary 2.5 (Weighted Filtered Winding Corollary) *If $z[n]$ and $h[n]$ satisfy Eqn. (2.106) of Corollary 2.2, and if $w[k]$, $k \in \{0,\ldots,N\}$, satisfy Eqns. (2.141) then*

$$\left|\bar{f}_{h*z}^w[n_0,n_1] - \bar{f}_{h*p}^w[n_0,n_1]\right| < \frac{f_s}{4}\mathrm{TV}\{w\}. \tag{2.155}$$

Corollary 2.6 (Weighted Filtered Multi-Partial Winding Corollary) *If $z[n]$, $p_k[n]$ and $h[n]$ satisfy Eqn. (2.107) of Corollary 2.3, and if $w[k]$, $k \in \{0,\ldots,N\}$, satisfy Eqns. (2.141) then*

$$\left|\bar{f}_{h*z}^w[n_0,n_1] - \bar{f}_{h*p_k}^w[n_0,n_1]\right| < \frac{f_s}{4}\mathrm{TV}\{w\}. \tag{2.156}$$

2.3.3.1 A Tighter $\mathcal{M}_1$-Bound for the Weighted Case

The bound in Eqn. (2.156) of is rather conservative and assumes the worst case since it uses the pessimistic bound of $1/2$ in Eqn. (2.153). Recall in Section 2.3.2 Eqn. (2.123) gives a tighter bound on the phase error $\arg(K[n])$. Thus, we may substitute β in Eqn. (2.150) and obtain

$$\left|\bar{f}_{h*z}^w[n_0,n_1] - \bar{f}_{h*p_k}^w[n_0,n_1]\right| < \frac{\beta f_s}{2\pi}\mathrm{TV}\{w\} \tag{2.157}$$

$$\approx \frac{f_s}{2\pi\mathrm{SNR}_1}\mathrm{TV}\{w\}, \quad \text{for large } \mathrm{SNR}_1. \tag{2.158}$$

2.3.3.2 Minimum-Variance Frequency Estimate

Kay derives the optimal weighting coefficients for calculating the estimated frequency from a block of $N-1$ phase-differences in [75, 76]. The coefficients are given as

$$w_{\mathrm{Kay}}[k] = \frac{3N}{2\left(N^2-1\right)}\left\{1 - \left[\frac{2k-N}{N}\right]^2\right\}, \quad k = 1,\ldots,N-1. \tag{2.159}$$

These coefficients yield the Cramér-Rao bound for estimating a single stationary complex sinusoid in Gaussian white noise for $\mathrm{SNR}_2 > 6$ dB [75]. Computing the weighted average of the phase difference using these coefficients is equivalent to solving for the slope in the linear regression problem for the absolute phase of the signal [115]. The derivation of this weighting function is given in Appendix E and may also be found in [75].

Thus, for a given estimate under the condition given by Eqn. (2.95), we may use Kay's weighting coefficients and rewrite Eqn. (2.100c) as

$$\bar{f}_z^{\dagger}[n_0,n_1] \triangleq \frac{f_s}{2\pi}\sum_{k=n_0+1}^{n_1} w_{\mathrm{Kay}}[k-n_0]\arg(z[k]z^*[k-1]). \tag{2.160}$$

The absolute error in $\bar{f}_z^\dagger[n_0, n_1]$, given Eqn. (2.95), may be found using Theorem 2.3:

$$\left|\bar{f}_z^\dagger[n_0, n_1] - \bar{f}_p^\dagger[n_0, n_1]\right| < \frac{f_s}{4}\mathrm{TV}\{w_{\mathrm{Kay}}\} \tag{2.161}$$

$$= \frac{6f_s}{4(N^3 - N)} \sum_{k=0}^{N-1} |1 + 2k - N| \tag{2.162}$$

$$= \begin{cases} \frac{f_s}{4}\frac{3}{N}, & \text{if } N \text{ is odd} \\ \frac{f_s}{4}\frac{3N}{N^2-1}, & \text{if } N \text{ is even} \end{cases}. \tag{2.163}$$

Using Eqn. (2.157), we may tighten the inequality (2.161) to

$$\left|\bar{f}_z^\dagger[n_0, n_1] - \bar{f}_p^\dagger[n_0, n_1]\right| < \begin{cases} \frac{\beta f_s}{2\pi}\frac{3}{N}, & \text{if } N \text{ is odd} \\ \frac{\beta f_s}{2\pi}\frac{3N}{N^2-1}, & \text{if } N \text{ is even} \end{cases} \tag{2.164}$$

$$\approx \begin{cases} \frac{f_s}{2\pi\mathrm{SNR}_1}\frac{3}{N}, & \text{if } N \text{ is odd} \\ \frac{f_s}{2\pi\mathrm{SNR}_1}\frac{3N}{N^2-1}, & \text{if } N \text{ is even} \end{cases}, \tag{2.165}$$

for large SNR_1.

The variance of this estimator is given by [75] (cf. Appendix E, Eqn. (E.41)) as

$$\mathrm{var}\left\{\bar{f}_z^\dagger[n_0, n_1]\right\} \approx \frac{3f_s^2\sigma_\nu^2}{2\pi^2 A^2 N\left(N^2 - 1\right)} \tag{2.166}$$

$$= \frac{3f_s^2}{2\pi^2 \mathrm{SNR}_2 N\left(N^2 - 1\right)}, \tag{2.167}$$

where it is presumed that

$$a[k] \approx A, k \in \{n_0, \ldots, n_1\}. \tag{2.168}$$

Comparing this result with Eqn. (2.136d) we see that the Kay weighting gives an extra order of magnitude of variance suppression.

Kay's weighted estimation method also falls away rapidly from the Cramér-Rao bound when the SNR_2 of the signal falls below a threshold of about 6 dB, as seen in Figure 2.9, similar to the unweighted phase difference averager as discussed in Section 2.3.2.2. This similar SNR_2 threshold for the Kay estimator is also due to the unreliability of the winding measure when the $\mathcal{M}_1$ condition given by Eqn. (2.95) is violated so the conditions for Theorem 2.3 no longer hold.

We will use the results from this section in Section 4.8.1 in order to form an "optimal," minimum-variance estimate of the average frequency of a signal.

2.4 Summary

In this chapter, we have presented some concepts which attempt to break away from the conventional signal processing paradigm in which signals are assumed to be (second-order) stationary. By focussing on concept of instantaneous frequency, we are able to characterize more accurately many natural signals such as speech and music, in which signal parameters vary quickly. The ideas of instantaneous bandwidth and amplitude may also be useful in describing signals. The discussion on analytic signals and winding provides us with some powerful tools for non-stationary signal analysis which we will use extensively in the remainder of this dissertation.

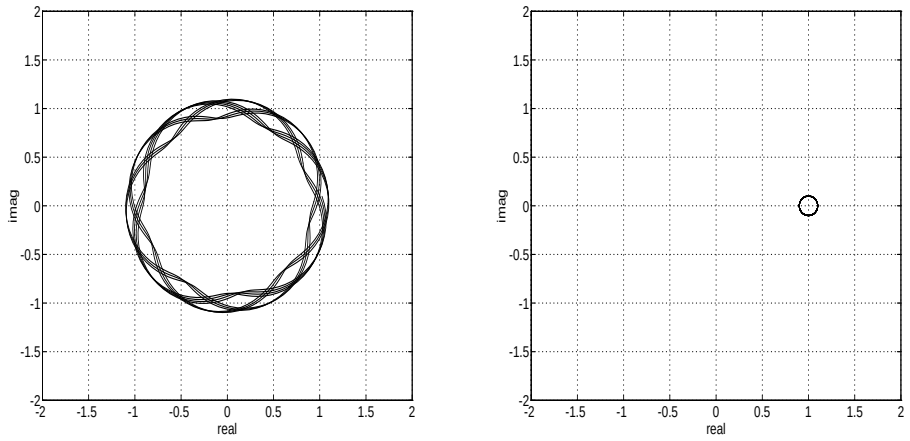

(a)

(b)

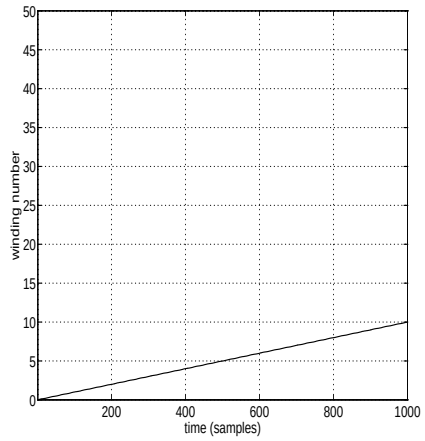

(c)

Figure 2.1: $z[n] = \exp(j\,2\pi 10n/1000) + 0.10\exp(j\,2\pi 43.21n/1000)$. **(a)** Argand plot of $z[n]$. **(b)** Argand plot of $z[n]$ demodulated by multiplying by the phase factor $\exp(-j\,2\pi 10n/1000)$ so the target component is at DC. **(c)** Cumulative windings = $\mathrm{Arg}(z[n])/2\pi$. The total number of windings is 10.0150. It is clear that the 10 Hz signal dominates the winding.

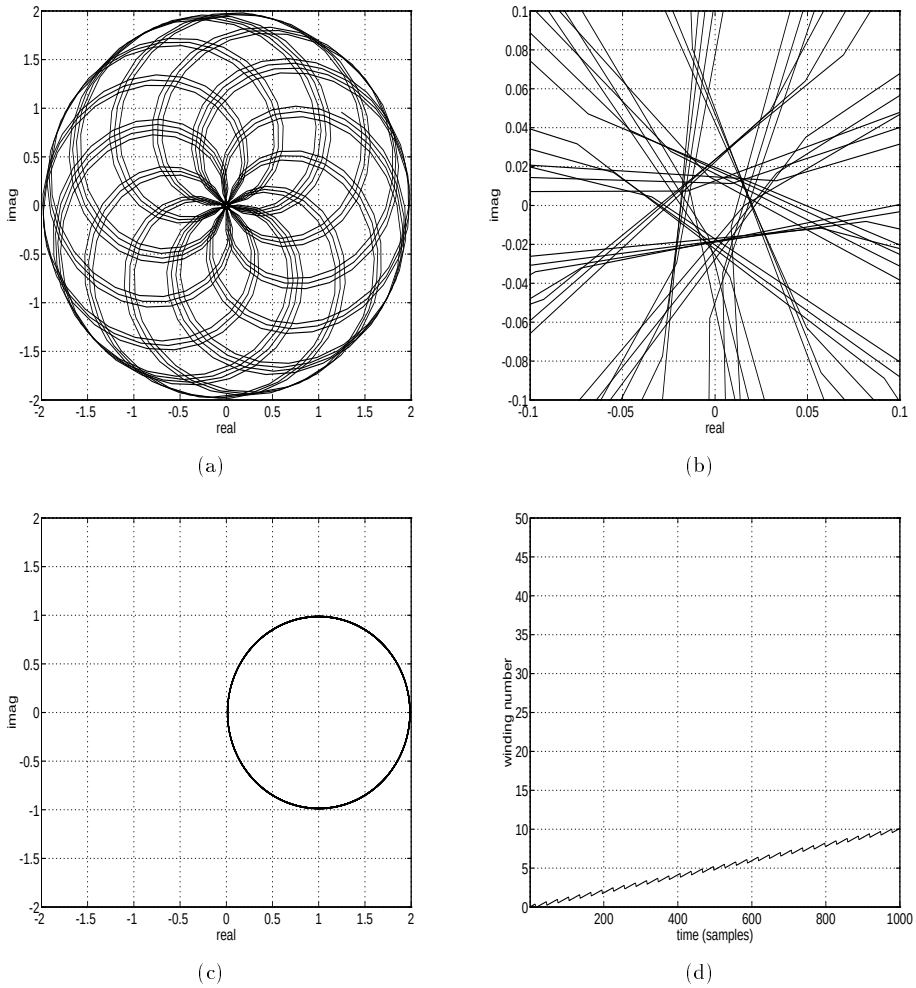

Figure 2.2: $z[n] = \exp(j\,2\pi 10n/1000) + 0.99\exp(j\,2\pi 43.21n/1000)$. **(a)** Argand plot of $z[n]$. **(b)** Detail of (a). **(c)** Argand plot of $z[n]$ demodulated by multiplying by $\exp(-j\,2\pi 10n/1000)$ so the target component is at DC. **(d)** Cumulative windings $= \mathrm{Arg}(z[n])/2\pi$. The total number of windings is 10.1044. The 10 Hz signal dominates the winding even though the 43.21 Hz has amplitude 0.99 because the $\mathcal{M}_1$-condition obtains. Compare with Figure 2.3.

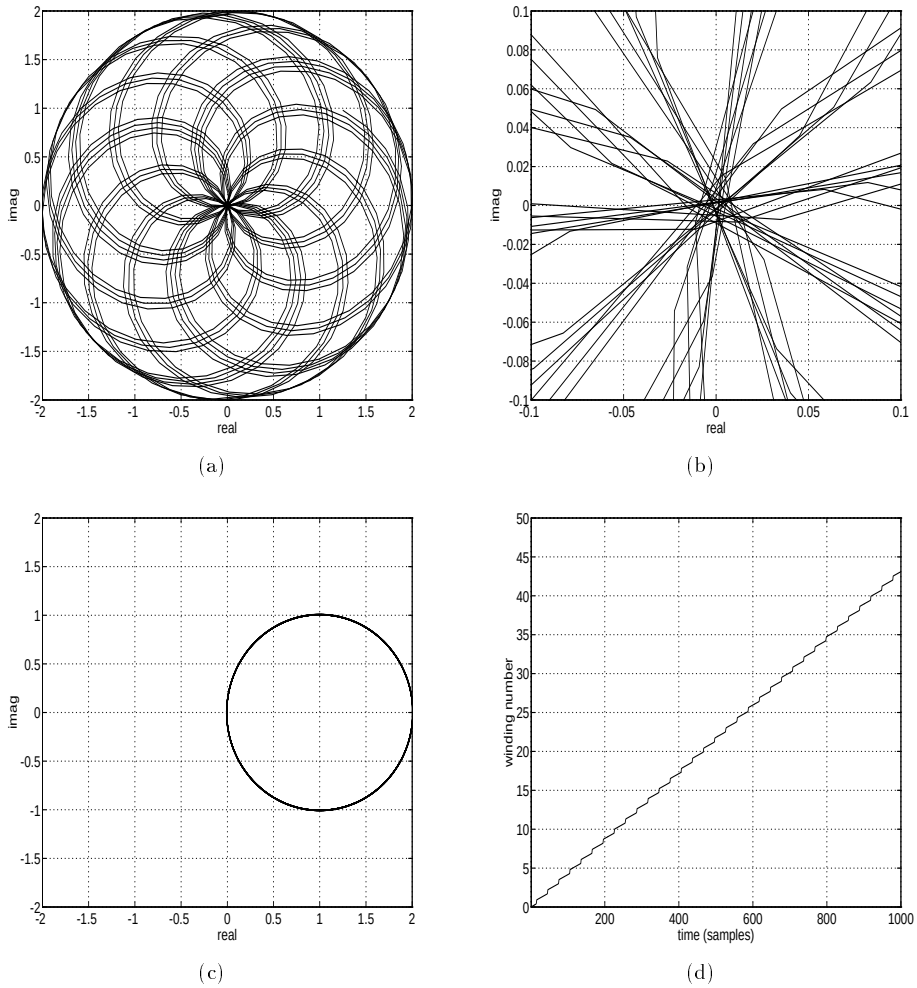

Figure 2.3: $z[n] = \exp(j\,2\pi 10n/1000) + 1.01\exp(j\,2\pi 43.21n/1000)$. **(a)** Argand plot of $z[n]$. **(b)** Detail of (a). **(c)** Argand plot of $z[n]$ demodulated by multiplying by $\exp(-j\,2\pi 10n/1000)$ so the target component is at DC. **(d)** Cumulative windings = $\mathrm{Arg}(z[n])/2\pi$. The total number of windings is 43.1056. The 43.21 Hz signal dominates the winding now because its amplitude is greater than that of the 10 Hz signal. Compare with Figure 2.2.

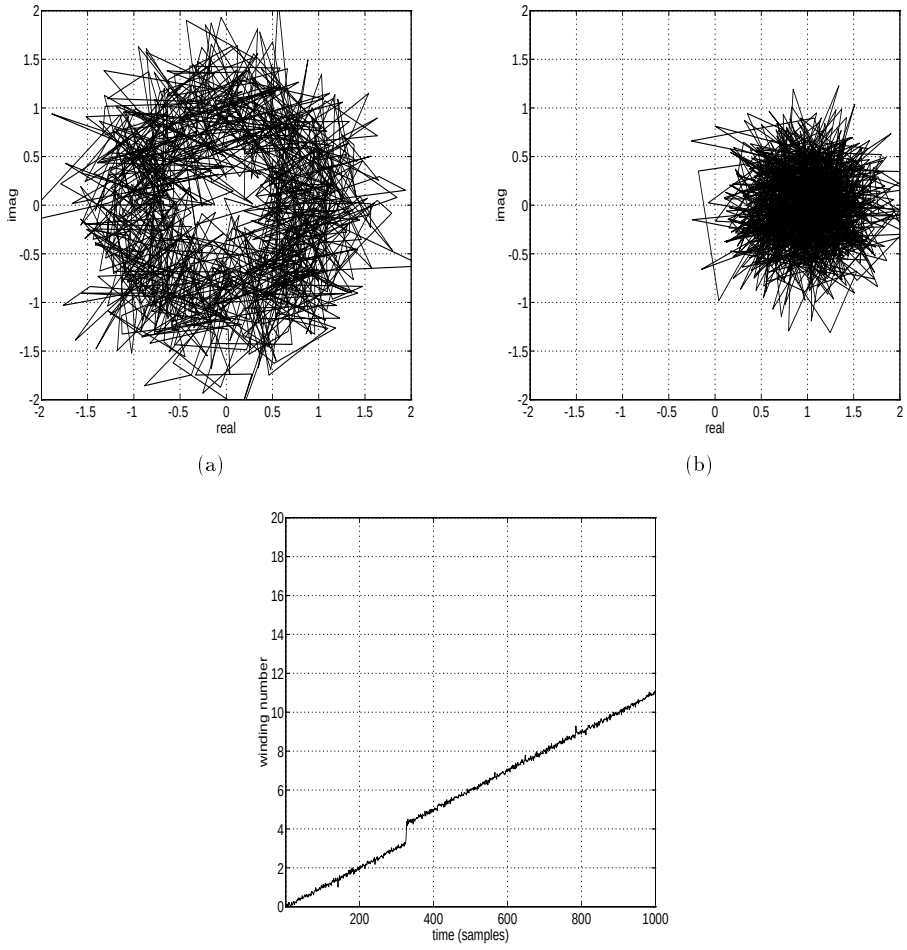

Figure 2.4: $z[n] = \exp(j\,2\pi 10n/1000) + \nu[n]$, where $\nu[n]$ is complex Gaussian white noise with variance 0.32, putting the SNR_2 above Kay's 6 dB threshold shown in Figure 2.9. **(a)** Argand plot of $z[n]$. **(b)** Argand plot of $z[n]$ demodulated by multiplying by $\exp(-j\,2\pi 10n/1000)$ so the target component is at DC. **(c)** Cumulative windings = $\mathrm{Arg}(z[n])/2\pi$. The total number of windings is 11.0221. The 10 Hz signal dominates the winding but there is one spurious loop which adds one to the winding count. This Gaussian $\nu[n]$ does not strictly obey the $\mathcal{M}_1$-condition, but winding violations are few.

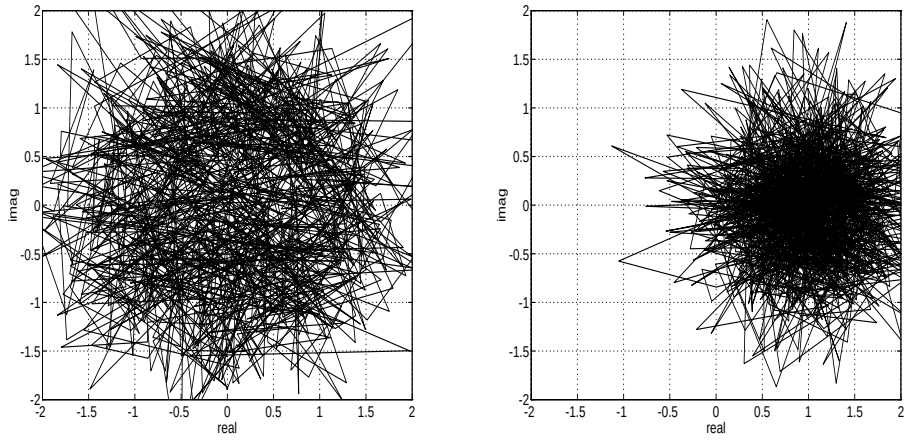

(a)

(b)

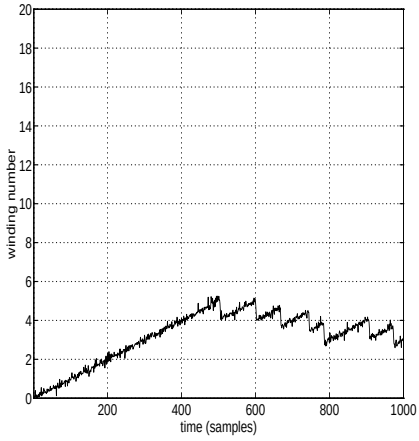

(c)

Figure 2.5: $z[n] = p[n] + \nu[n]$, where $p[n] = \exp(j\,2\pi 10n/1000)$ and $\nu[n]$ is complex Gaussian white noise with variance 0.72, which puts the SNR_2 below Kay's 6 dB threshold shown in Figure 2.9 [76]. **(a)** Argand plot of $z[n]$. **(b)** Argand plot of $z[n]$ demodulated by multiplying by $\exp(-j\,2\pi 10n/1000)$ so the target component is at DC. **(c)** Cumulative windings = $\mathrm{Arg}(z[n])/2\pi$. The total number of windings is 2.9343. The 10 Hz signal dominates the winding but there are many spurious loops which cause the winding count to be an unreliable measure of the phase of $p[n]$.

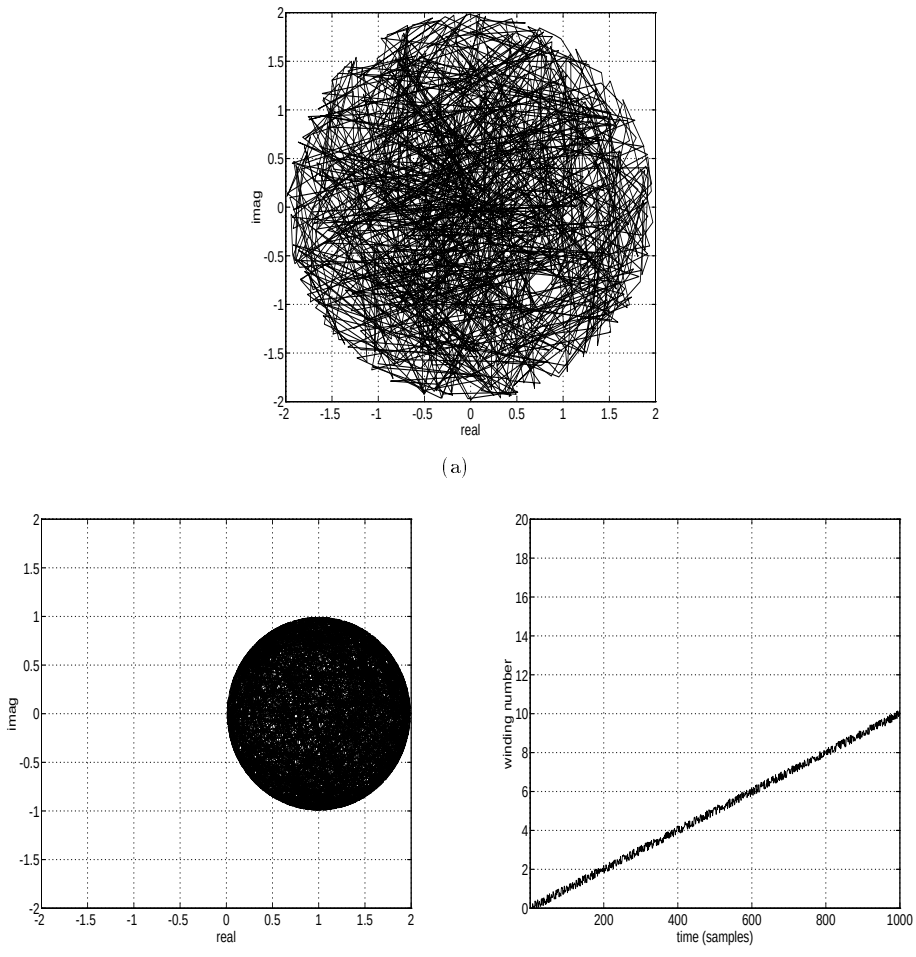

(a)

(b)

(c)

Figure 2.6: $z[n] = \exp(j\,2\pi 10n/1000) + \nu[n]$, where $\nu[n]$ is complex white noise with amplitude 0.99 and uniformly distributed phase. **(a)** Argand plot of $z[n]$. **(b)** Argand plot of $z[n]$ demodulated by multiplying by $\exp(-j\,2\pi 10n/1000)$ so the target component is at DC. **(c)** Cumulative windings = $\mathrm{Arg}(z[n])/2\pi$. The total number of windings is 10.1852. The 10 Hz signal dominates the winding and there are no spurious loops. In this case, $\sigma_\nu^2 = 0.9801$, which puts the SNR_2 above Kay's 6 dB threshold for Gaussian white noise, as seen in Figure 2.9 [76].

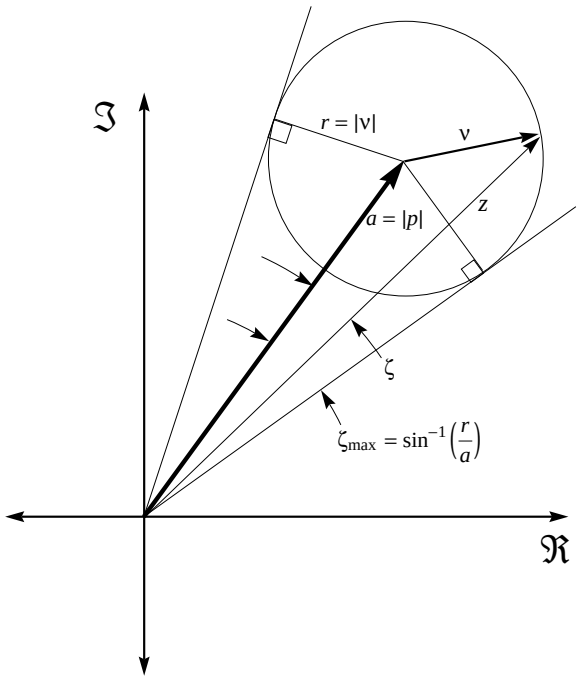

Figure 2.7: Bound on the phase error $\zeta[n]$. The signal is $z[n] = p[n]+\nu[n]$, where $p[n]$ is the dominant partial with magnitude $a[n]$ and $\nu[n]$ is an unknown signal with magnitude $r[n]$ and unknown phase. Notice that if $\mathrm{SNR}_1 > 1$ then the disturbance $\nu[n]$ can never cause a spurious winding.

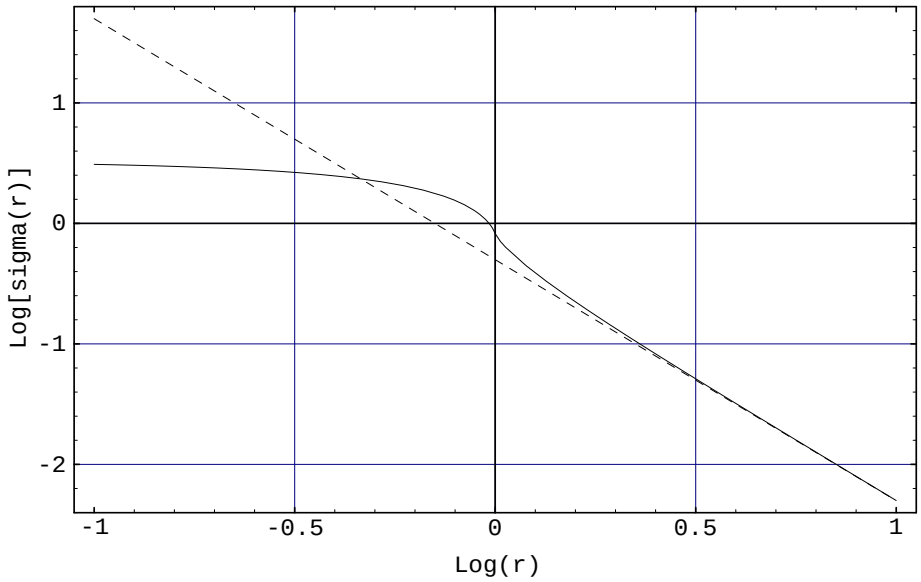

Figure 2.8: Variance of σ_ζ^2 as a function of SNR_1, (cf. Eqn. (2.129)). The solid line is $\sigma_\zeta^2(r)$ and the dashed line is $1/2r^2$. Logs are to base 10.

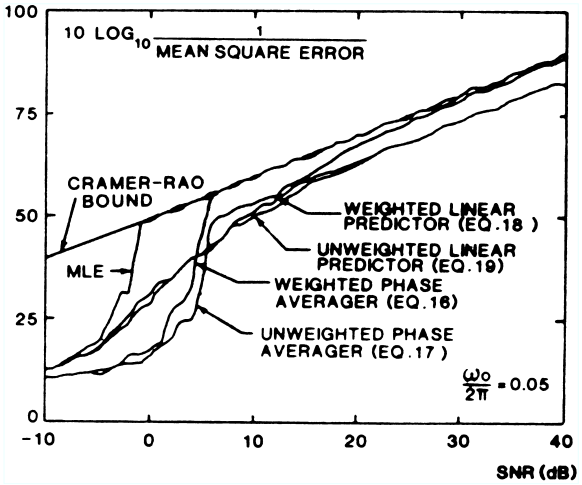

Figure 2.9: Comparison of performance of frequency estimators. Formerly Figure 2 of Kay [76]. Reprinted with permission, ©1989 IEEE.

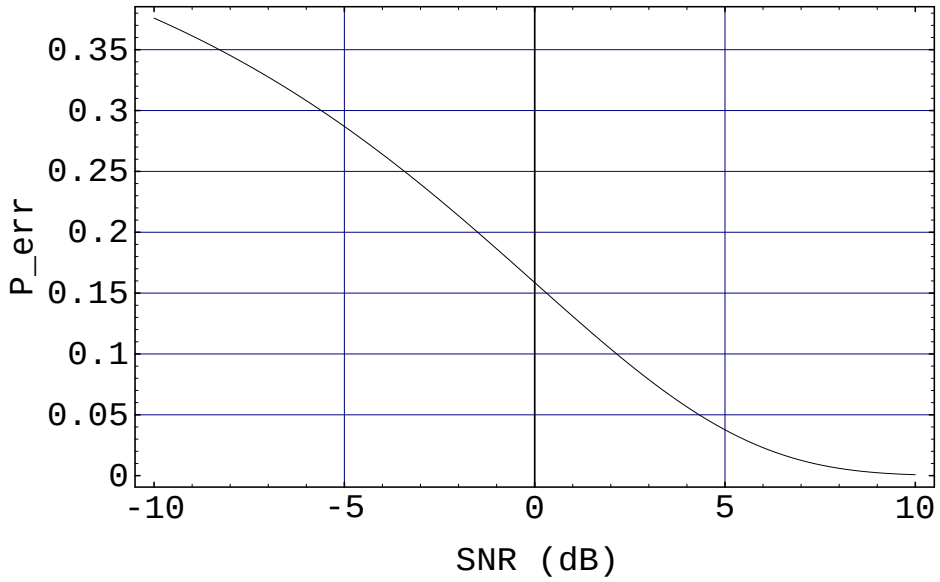

Figure 2.10: Probability of spurious windings as a function of SNR_2, (cf. Eqn. (2.133)). $P_{\mathrm{err}}(r) = [1 - \mathrm{erf}(r/\sqrt{2})]/2$.

Chapter 3

Frequency-Warped Signal Processing

In this chapter we discuss the theory and applications of *frequency-warped signal processing*. Conventional signal processing techniques often make use of the Fourier transform, which is suited for the spectral analysis of stationary signals, i.e., signals whose statistics are time-independent [21, 74]. However, as discussed in Section 2.1, the Fourier transform is ill-suited for analyzing signals with rapidly varying parameters. By frequency warping a signal, i.e., selectively frequency modulating it, it may be possible to transform it so that the resulting signal is stationary and has a simplified spectrum which is more amenable to analysis. Frequency warping may be thought of as attempting to "straighten out" nonstationarities due to continuous variations in the instantaneous frequency of a signal.

Consider, for example, the chirp signal with a Gaussian envelope

$$z(t) = \exp\left\{\pi(\alpha + j\beta)t^2\right\}, \tag{3.1}$$

where $\alpha, \beta \in \Re$, and $\alpha < 0$. The instantaneous frequency, as defined by Eqn. (2.8) is

$$\begin{aligned} f(t) &= \frac{1}{2\pi}\frac{d\arg\{z(t)\}}{dt} \\ &= \beta t. \end{aligned} \tag{3.2}$$

We derive the Fourier transform of $z(t)$ to illustrate the difficulty in attempting to apply Fourier analysis directly to this nonstationary signal.

$$Z(f) = \int_{-\infty}^{\infty} \exp\{\pi(\alpha + j\beta)t^2 - j2\pi ft\}\, dt \tag{3.3}$$

$$= \exp\left\{\frac{\pi f^2}{\alpha + j\beta}\right\} \int_{-\infty}^{\infty} \exp\left\{\pi(\alpha + j\beta)t^2 - j2\pi ft - \frac{\pi f^2}{\alpha + j\beta}\right\} dt \tag{3.4}$$

$$= \exp\left\{\frac{\pi f^2}{\alpha + j\beta}\right\} \int_{-\infty}^{\infty} \exp\left\{\pi(\alpha + j\beta)\left(t - j\frac{f}{\alpha + j\beta}\right)^2\right\} dt \tag{3.5}$$

$$= \exp\left\{\frac{\pi f^2}{\alpha + j\beta}\right\} \int_{-\infty}^{\infty} \exp\left\{\pi(\alpha + j\beta)t^2\right\} dt, \tag{3.6}$$

where in Eqn. (3.6) we have used the Cauchy Integral Theorem [3] and the fact that $\exp(\cdot)$ has no singularities in the complex plane. To evaluate the integral in Eqn. (3.6) we use the usual trick of evaluating the square:

$$\left\{\int_{-\infty}^{\infty} \exp\left\{\pi(\alpha+j\beta)t^2\right\}\,dt\right\}^2 = \int_{-\infty}^{\infty}\int_{-\infty}^{\infty} \exp\left\{\pi(\alpha+j\beta)(s^2+t^2)\right\}\,ds\,dt \tag{3.7}$$

$$= \int_0^{2\pi}\int_0^{\infty} \exp\left\{\pi(\alpha+j\beta)r^2\right\} r\,dr\,d\theta \tag{3.8}$$

$$= \frac{1}{\alpha+j\beta}\int_0^{\infty} \exp\left\{\pi(\alpha+j\beta)r^2\right\}\,d\pi(\alpha+j\beta)r^2 \tag{3.9}$$

$$= \frac{-1}{\alpha+j\beta}, \tag{3.10}$$

therefore

$$Z(f) = \frac{1}{\sqrt{-\alpha-j\beta}}\exp\left\{\frac{\pi f^2}{\alpha+j\beta}\right\} \tag{3.11}$$

$$= \frac{1}{\sqrt{-\alpha-j\beta}}\exp\left\{\frac{\pi(\alpha-j\beta)f^2}{\alpha^2+\beta^2}\right\}, \tag{3.12}$$

where we take the value of the square root to have $\left|\arg\left(\sqrt{-\alpha-j\beta}\right)\right| < \pi/4$.

The power spectrum of $z(\cdot)$ is thus

$$|Z(f)|^2 = \frac{1}{\sqrt{\alpha^2+\beta^2}}\exp\left\{\frac{2\pi\alpha f^2}{\alpha^2+\beta^2}\right\}, \tag{3.13}$$

We cannot easily tell from either Eqns. (3.12) or (3.13) what the character of the signal's time evolution is since the signal energy distribution is represented as a broad-band smear. Figures 3.1(c) and 3.1(e) illustrate the broadband character of the Gaussian chirp signal.

Recalling the definition of mean-square bandwidth $\sigma^2_{\rm BW}$, Eqns. (2.36) and (2.37) show the breakdown of contributors to bandwidth. Using the *frequency-warped* signal processing techniques described in this chapter, it is possible to eliminate the FM bandwidth component $\sigma^2_{\rm FM}$ due to the instantaneous frequency modulation of the carrier and collect all the energy of $z(t)$ in Eqn. (3.1) into a relatively narrow distribution with minimized smearing, provided that the form of frequency modulation is known.

3.1 Frequency-Warping

Let $\xi(t)$ be a continuous, real-valued function specifying the *ξ-frequency warp factor* defined by

$$\Xi(t) \stackrel{\triangle}{=} \exp\left(j2\pi\int_0^t \xi(\tau)\,d\tau\right). \tag{3.14}$$

When the frequency warping function is $\alpha(t)$ instead of $\xi(t)$ we make the dependence on $\alpha(t)$ explicit by defining

$$\Xi_\alpha(t) \stackrel{\triangle}{=} \exp\left(j2\pi\int_0^t \alpha(\tau)\,d\tau\right). \tag{3.15}$$

Intuitively, the frequency-warping factor $\Xi^*(t)$ demodulates a signal (cf. Eqn. (2.25))

$$p(t) = a(t) \exp\left(j2\pi \int_0^t f(\tau)\, d\tau + j\phi_0\right) \tag{3.16}$$

by displacing its instantaneous frequency $f(t)$ by $-\xi(t)$. This is easy to see because

$$\Xi^*(t)p(t) = \exp\left(-j2\pi \int_0^t \xi(\tau)\, d\tau\right) a(t) \exp\left(j2\pi \int_0^t f(\tau)\, d\tau + j\phi_0\right) \tag{3.17}$$

$$= a(t) \exp\left(j2\pi \int_0^t \{f(\tau) - \xi(\tau)\}\, d\tau + j\phi_0\right), \tag{3.18}$$

and, by Eqn. (2.8), the instantaneous frequency is

$$\frac{1}{2\pi}\frac{d \arg\{\Xi^*(t)p(t)\}}{dt} = f(t) - \xi(t).$$

Hence, we see the motivation for the name "frequency-warping". We introduce the notation

$$\langle p \wr \alpha \rangle(t) \stackrel{\triangle}{=} \Xi^*_\alpha(t)p(t) \tag{3.19}$$

and call this the *α-frequency-warped transform* of the signal $p(t)$, where $\alpha(t)$ is a continuous function.

We note that if we set $\xi(t)$ to be the instantaneous frequency $f(t)$ of a signal, the signal $p(t)$ is then demodulated by $\Xi^*_f(t)$ to a constant-phase signal

$$\langle p \wr f \rangle(t) = \Xi^*_f(t)p(t) \tag{3.20}$$

$$= a(t) \exp\left(j2\pi \int_0^t \{f(\tau) - f(\tau)\}\, d\tau + j\phi_0\right) \tag{3.21}$$

$$= a(t) \exp\left(j\phi_0\right). \tag{3.22}$$

In this case the demodulating function $\Xi_f(t)$ is *frequency-matched* to $p(t)$.

We see that frequency warping a signal $p(t)$ is nothing more than multiplying it by a unit-amplitude phase factor $\Xi^*(t)$. To invert the frequency warping we simply multiply the result by $\Xi(t)$. Notationally, the inversion can be stated as

$$p(t) = \langle \langle p \wr \xi \rangle \wr -\xi \rangle(t) \tag{3.23}$$

Another obvious fact is the linearity in the first argument of frequency warping:

$$\langle w + z \wr \xi \rangle(t) = \langle w \wr \xi \rangle(t) + \langle z \wr \xi \rangle(t). \tag{3.24}$$

Also,

$$\langle \langle p \wr \xi \rangle \wr \eta \rangle(t) = \langle p \wr \xi + \eta \rangle(t), \tag{3.25}$$

which generalizes Eqn. (3.23).

3.1.1 Discrete-Time Case

The discrete-time case follows from the continuous-time case in the obvious way. For a discrete-time function $\xi[n]$ defined for $n \in 0, \ldots, N-1$ we may define the *discrete-time ξ-frequency warp factor* as

$$\Xi[n] \stackrel{\triangle}{=} \exp\left(\frac{j2\pi}{f_s} \sum_{k=1}^{n} \xi[k]\right). \tag{3.26}$$

As in the continuous case, we see that the factor $\Xi^*[\cdot]$ frequency warps the signal

$$p[n] = a[n] \exp\left(\frac{j2\pi}{f_s} \sum_{k=1}^{n} f[k] + j\phi_0\right)$$

by displacing its instantaneous frequency by $-\xi[n]$. This may be seen from

$$\Xi^*[n]p[n] = a[n] \exp\left(\frac{j2\pi}{f_s} \sum_{k=1}^{n} (f[k] - \xi[k]) + j\phi_0\right), \tag{3.27}$$

so that the discrete instantaneous frequency, as defined by Eqn. (2.10), is

$$\begin{aligned} &\frac{f_s}{2\pi} \arg\left(\Xi^*[n]p[n]\,\Xi[n-1]p^*[n-1]\right) &(3.28)\\ &\quad = \frac{f_s}{2\pi} \arg\left\{a[n]a[n-1] \exp\left(\frac{j2\pi}{f_s}\left(f[n] - \xi[n]\right)\right)\right\} \\ &\quad = f[n] - \xi[n] - f_s\beta[n], &(3.29)\end{aligned}$$

where $\beta[n]$ is an integer such that the discrete instantaneous frequency lies within the range $(-f_s/2, f_s/2)$.[1] We see that one aspect in which discrete-time frequency warping differs from the continuous case is that frequency wrap-around occurs in the former. The discrete instantaneous frequency axis may be thought of as a circle which is rotated by $-2\pi\xi[n]/f_s$ radians at time n.

The discrete-time *α-frequency-warped transform* of $p[n]$ is then

$$\langle p \,\wr\, \alpha \rangle[n] \stackrel{\triangle}{=} \Xi_\alpha^*[n]p[n]. \tag{3.30}$$

3.2 Frequency-Warped Fourier Transforms

The usual Fourier basis functions used in spectral analysis are complex exponentials of the form

$$\mathbf{e}(f,t) = \exp(j2\pi ft), \quad \forall f,t \in \Re. \tag{3.31}$$

As is well known, the Fourier basis is a complete orthonormal basis for the space of functions in $L_1(\Re)$ [21, 72]. However, the Fourier basis is certainly not the only possible basis set for signal analysis. Of the many possibilities, we focus on the somewhat unconventional class of *frequency-warped Fourier bases*. We define the *frequency-warped Fourier basis functions*

$$\begin{aligned} \mathbf{e}_\xi(\varphi,t) &\stackrel{\triangle}{=} \Xi(t)\mathbf{e}(\varphi,t) &(3.32)\\ &= \exp\left\{j2\pi\left(\varphi t + \int_0^t \xi(\tau)\,d\tau\right)\right\} &(3.33)\end{aligned}$$

for all φ and t. We have used "φ" to index the transform domain of the kernel rather than "f" since it is not exactly a "frequency," although it is analogous. φ may be seen as a constant frequency displacement of the frequency warping function $\xi(\cdot)$ so that the $\mathbf{e}_\xi(\varphi,t)$, indexed by φ, form a family

[1] The value at the endpoints is not well-defined because it could equally well be either $+f_s/2$ or $-f_s/2$, depending on whether the principal branch of the $\arg(\cdot)$ function is in $[-f_s/2, f_s/2)$ or $(-f_s/2, f_s/2]$.

of functions of time whose instantaneous frequencies are parallel to $\xi(t)$. The function $\mathbf{e}_\xi(\varphi,t)$ defines a kernel for the *frequency-warped Fourier transform* $Z_\xi(\varphi)$ of $z(t) \in L_1(-\infty,\infty)$ such that

$$Z_\xi(\varphi) \stackrel{\triangle}{=} \int_{-\infty}^{\infty} z(t)\mathbf{e}_\xi^*(\varphi,t)\,dt \tag{3.34}$$

$$= \int_{-\infty}^{\infty} z(t)\Xi^*(t)\exp\left(-j2\pi\varphi t\right)\,dt. \tag{3.35}$$

Thus, we see that the transform $Z_\xi(\varphi)$ is simply the Fourier transform of $\langle z \,\rceil\, \xi\rangle(t)$.

We introduce here the functional notation

$$\mathcal{F}_\xi\{z(t)\} \stackrel{\triangle}{=} Z_\xi(\varphi). \tag{3.36}$$

The transform is invertible:

$$\int_{-\infty}^{\infty} Z_\xi(\varphi)\mathbf{e}_\xi(\varphi,t)\,d\varphi = \int_{-\infty}^{\infty}\int_{-\infty}^{\infty} z(\tau)\mathbf{e}_\xi^*(\varphi,\tau)\,d\tau\,\mathbf{e}_\xi(\varphi,t)\,d\varphi \tag{3.37}$$

$$= \left\{\int_{-\infty}^{\infty}\int_{-\infty}^{\infty} z(\tau)\Xi^*(\tau)\mathbf{e}^*(\varphi,\tau)\,d\tau\,\mathbf{e}(\varphi,t)\,d\varphi\right\}\Xi(t) \tag{3.38}$$

$$\doteq z(t)\Xi^*(t)\,\Xi(t) \tag{3.39}$$

$$= z(t), \tag{3.40}$$

where in Eqn. (3.39) we have used the fact that the bracketed expression in Eqn. (3.38) is the inversion of the Fourier transform of $\Xi^*(t)z(t)$. The "$\doteq$" symbol denotes "equality in the mean," i.e., the left and right sides are equal except for possibly a set of measure zero [121, 122]. It follows that for any fixed $\xi(\cdot)$ the functions $\mathbf{e}_\xi(\varphi,t)$ indexed by φ form a complete orthonormal basis, which may be seen by considering the inner product[2]

$$\int_{-\infty}^{\infty} \mathbf{e}_\xi(\varphi,t)\mathbf{e}_\xi^*(\varphi',t)\,dt = \int_{-\infty}^{\infty} \mathbf{e}(\varphi,t)\Xi(t)\Xi^*(t)\mathbf{e}^*(\varphi',t)\,dt \tag{3.41}$$

$$= \int_{-\infty}^{\infty} \mathbf{e}(\varphi,t)\mathbf{e}^*(\varphi',t)\,dt \tag{3.42}$$

$$= \delta(\varphi-\varphi') \quad \text{(formally)}. \tag{3.43}$$

3.2.1 Frequency-Matched Frequency-Warped Fourier Transform

If $\Xi(t)$ is frequency-matched to a signal $p(t)$ given in Eqn. (3.16), i.e., if $\xi(t) = f(t)$ then we see that

$$P_f(\varphi) = \mathcal{F}_f\{p(t)\} \tag{3.44}$$

$$= A(\varphi)\exp(j\phi_0). \tag{3.45}$$

Thus, the frequency-matched frequency-warped Fourier transform is simply a phase factor times the Fourier transform of its envelope function. From Eqn. (2.36) we see that the frequency-matched frequency-warped Fourier transform $P_f(\varphi)$ of a signal $p(t)$ has the minimum mean-square bandwidth σ^2_{BW} over all frequency-warped Fourier transforms $P_\xi(\varphi)$ for continuous frequency-warping functions $\xi(t)$.

[2] Technically, this integral does not make sense since the functions $\mathbf{e}_\xi(\varphi,t), \mathbf{e}(f,t) \in L_\infty(-\infty,\infty)$, not $L_1(-\infty,\infty)$ and thus the Fourier integral does not converge. A discussion on delta distributions may be found in Arfken [7] and Bracewell [21]. A mathematically rigorous approach to Fourier integrals may be found in Katznelson [72]. Royden [121] and Rudin [122] provide classic mathematical treatments of measure theory and Lebesgue integration.

3.2.2 Conservation of Energy

The frequency-warped Fourier transform conserves the energy, i.e., the squared L_2-norm, of a signal. That is, for a signal $z(t) \in L_2(-\infty, \infty)$,

$$\int_{-\infty}^{\infty} |Z(f)|^2 \, df = \int_{-\infty}^{\infty} |z(t)|^2 \, dt \tag{3.46}$$

$$= \int_{-\infty}^{\infty} |\Xi^*(t) z(t)|^2 \, dt$$

$$= \int_{-\infty}^{\infty} |Z_\xi(\varphi)|^2 \, d\varphi. \tag{3.47}$$

This is a simple consequence of the fact that phase-modulating a signal does not change its power, even though its spectrum may change.

3.2.3 Discrete-Time Formulation

The discrete-time version of the frequency-warped Fourier transform is a straightforward analog to the continuous case. The usual discrete-time basis functions for an N-point Fourier transform are of the form [21, 105]

$$\mathbf{e}[k, n] = \exp\left(\frac{j2\pi kn}{N}\right), \quad \forall n, k \in \{0, \ldots, N-1\}. \tag{3.48}$$

Recalling Eqn. (3.26), we define the discrete-time frequency-warped Fourier kernel as

$$\mathbf{e}_\xi[\kappa, n] \stackrel{\triangle}{=} \Xi[n]\mathbf{e}[\kappa, n] \tag{3.49}$$

$$= \exp\left\{ j2\pi \left(\frac{\kappa n}{N} + \frac{1}{f_s} \sum_{k=1}^{n} \xi[k] \right) \right\} \tag{3.50}$$

for all $\kappa, n \in \{0, \ldots, N-1\}$. We use "$\kappa$" here instead of "$k$" for the same reasons we use "φ" instead of "f" in the continuous case. The discrete-time warped Fourier transform is

$$\mathcal{F}_\xi\{z[n]\} = Z_\xi[\kappa] \tag{3.51}$$

$$\stackrel{\triangle}{=} \sum_{n=0}^{N-1} z[n]\mathbf{e}_\xi^*[\kappa] \tag{3.52}$$

$$= \sum_{n=0}^{N-1} z[n]\Xi^*[n]\mathbf{e}^*[\kappa, n], \tag{3.53}$$

which may be seen as the DFT of $\langle z \wr \xi \rangle[n]$. The inverse discrete-time warped Fourier transform is

$$\mathcal{F}_\xi^{-1}\{Z_\xi[\kappa]\} \stackrel{\triangle}{=} \frac{1}{N} \sum_{\kappa=0}^{N-1} Z_\xi[\kappa]\mathbf{e}_\xi[\kappa, n] \tag{3.54}$$

$$= \Xi[n] \left(\frac{1}{N} \sum_{\kappa=0}^{N-1} Z_\xi[\kappa]\mathbf{e}[\kappa, n] \right) \tag{3.55}$$

$$= \Xi[n]\Xi^*[n]z[n] \tag{3.56}$$

$$= z[n] \tag{3.57}$$

3.3 Warped Instantaneous Spectra

Let a signal $z(t)$ have the form (cf. Eqn. (2.57))

$$z(t) = \sum_{k=1}^{N} p_k(t), \tag{3.58}$$

where each $p_k(\cdot)$ has the form

$$p_k(t) = a_k(t) \exp\left(j2\pi \int_0^t f_k(\tau)\, d\tau + j\phi_{k,0}\right) \quad \text{for all t,} \tag{3.59}$$

and $a_k(t) \geq 0$, so that its instantaneous spectrum is (cf. Section 2.1.4)

$$Z(f,t) = \sum_{k=1}^{N} a_k(t) \exp(j\phi_{k,0})\, \delta(f - f_k(t)),$$

as in Eqn. (2.58). Then, its ξ-frequency-warped instantaneous spectrum will be shifted by $-\xi(t)$.

$$Z_\xi(\varphi,t) = \sum_{k=1}^{N} a_k(t) \exp(j\phi_{k,0})\, \delta(\varphi - f_k(t) + \xi(t)). \tag{3.60}$$

This fact stems from the linearity of the frequency warping operation in Eqn. (3.17).

3.3.1 Discrete-Time Formulation

If $z[n]$ is a multicomponent signal such that

$$z[n] = \sum_{k=1}^{N} p_k[n],$$

with instantaneous spectrum given by (cf. Eqn. (2.59))

$$Z[f,n] = \sum_{k=1}^{N} a_k[n] \exp(j\phi_{k,0})\, \delta\{f - f_k[n]\},$$

then the warped discrete-time instantaneous spectrum is given by

$$Z_\xi[\varphi,n] = \sum_{k=1}^{N} a_k[n] \exp(j\phi_{k,0})\, \delta\{\varphi - f_k[n] + \xi[n]\}, \tag{3.61}$$

similar to the continuous-time case given above.

Instantaneous Spectrum of a frequency-matched frequency-warped signal. We continue by examining the effect of frequency warping a signal $z(t)$ using a frequency-warping function $\Xi^*_{f_1}(t)$

which is frequency-matched to a signal component $p_1(t)$ with instantaneous frequency $f_1(t)$. From Eqn. (3.60) we see that

$$Z_{f_1}(\varphi, t) = \sum_{k=1}^{N} a_k(t) \exp(j\phi_{k,0})\, \delta(\varphi - f_k(t) + f_1(t)) \tag{3.62}$$

$$= a_1(t) \exp(j\phi_{1,0})\, \delta(\varphi) + \sum_{k=2}^{N} a_k(t) \exp(j\phi_{k,0})\, \delta(\varphi - f_k(t) + f_1(t)) \tag{3.63}$$

We see that if we can notch out the component of the warped instantaneous spectrum at $\varphi = 0$ then we may eliminate the partial $p_1(t)$ from $z(t)$. In this idealized signal representation we have ignored dealing with the bandwidth components due to the envelope modulation functions $a_k(t)$.

3.4 Applications to the Separation of Partials

Frequency-warped signal processing is useful for the analysis of sinusoidal signals with varying frequency. In particular, frequency-modulated signals with narrow instantaneous bandwidth (cf. Section 2.1.3) may be easily notched out or isolated. We present the following material in the continuous-time format with the recognition that the discrete-time case is directly analogous.

3.4.1 Fourier Transform Notching

If there is a mixture of different frequency-modulated partials as in Eqn. (3.58), with each $p_k(t)$ of the form in Eqn. (3.59), then, if the instantaneous frequency function $f_1(t)$ for one of the partials, say $p_1(t)$, is known, we may set $\xi(t) = f_1(t)$ and thus obtain the frequency-warped Fourier transform

$$Z_{f_1}(\varphi) = \int_{-\infty}^{\infty} z(t) \mathbf{e}^{*}_{f_1}(\varphi, t)\, dt \tag{3.64}$$

$$= \sum_{k=1}^{N} \int_{-\infty}^{\infty} a_k(t) \exp\left(j2\pi \int_0^t \{f_k(\tau) - f_1(\tau)\}\, d\tau + j\phi_{k,0} - j2\pi\varphi t \right) dt \tag{3.65}$$

$$= A_1(\varphi) \exp(j\phi_{1,0}) \tag{3.66}$$

$$+ \sum_{k=2}^{N} \int_{-\infty}^{\infty} a_k(t) \exp\left(j2\pi \int_0^t \{f_k(\tau) - f_1(\tau) - \varphi\}\, d\tau + j\phi_{k,0} \right) dt,$$

where $A_1(\varphi)$ is the Fourier transform of the envelope function $a_1(t)$. We may then simply set the values of the transform to zero for $\varphi \approx 0$, so that

$$\langle Z_{f_1} \setminus 0 \rangle(\varphi) = \begin{cases} 0 & : \quad |\varphi| < \mathrm{BW}_{a_1} \\ Z_{f_1}(\varphi) & : \quad \text{otherwise,} \end{cases} \tag{3.67}$$

where the "$\langle \cdot \setminus \cdot \rangle$" symbol denotes a notch filtering operation on the left argument in which the notch frequency as a function of time is given by the right argument. If we regard z to be a set of signals and p as an element of that set with instantaneous frequency $f(t)$, then $\langle z \setminus f \rangle$ is the set z without the signal element p.

In the case that $a_1(t)$ is a constant, so that its bandwidth is exactly zero, we see that we simply set only the point at $\varphi = 0$ to zero. Thus, Eqn. (3.67) yields

$$\langle Z_{f_1} \setminus 0 \rangle(\varphi) \approx \sum_{k=2}^{N} \int_{-\infty}^{\infty} a_k(t) \exp\left(j2\pi \int_0^t \{f_k(\tau) - f_1(\tau) - \varphi\}\, d\tau + j\phi_{k,0} \right) dt. \tag{3.68}$$

We assume now that the contributions from $p_2(t), \ldots, p_N(t)$ to $\langle Z_{f_1} \setminus 0 \rangle(\varphi)$ near $\varphi = 0$ are negligible, so that Eqn. (3.68) holds in the mean. If we inverse transform this result, we obtain

$$\langle z \setminus f_1 \rangle(t) = z(t) - p_1(t) \tag{3.69}$$

$$= \sum_{k=2}^{N} p_k(t) \tag{3.70}$$

$$\approx \mathcal{F}_{f_1}^{-1} \left\{ \langle Z \setminus f_1 \rangle(\varphi) \right\}. \tag{3.71}$$

3.4.2 Isolation by Filtering

As an alternative to zeroing bins of the frequency-matched frequency-warped Fourier transform $P_f(\varphi)$ of a signal $p(t)$ with instantaneous frequency $f(t)$, it is also possible to low-pass filter the frequency-warped signal $\langle p \wr f \rangle(t)$. If we have a low-pass filter **LPF** with an impulse response $h(t)$ and a passband equal in width to the bandwidth of the amplitude envelope $a(t)$ of $p(t)$ then we may isolate $p(t)$ from an additive mixture $z(t) = p(t) + \nu(t)$, where $\nu(t)$ is some unknown signal. We simply calculate

$$\hat{p}(t) = \langle h * \langle z \wr f \rangle \wr -f \rangle(t), \tag{3.72}$$

where we have neglected the group delay of the low-pass filter.

To the extent that the frequency-warped interfering signal $\langle \nu \wr f \rangle(t)$ does not intersect the bandwidth of the filter **LPF** we may isolate $p(t)$ relatively cleanly, due to its decreased bandwidth after frequency-matched frequency warping.

We may, similarly, *high-pass* filter the signal $\langle z \wr f \rangle(t)$ with a filter **HPF** whose stop band coincides with the pass band of **LPF**. The resulting signal after unwarping (remodulating) the high-passed signal should be a signal without $p(t)$.

Thus, we see that component signals that have relatively small instantaneous bandwidth can be separated from a mixture by the above procedures. The effect of multiplying the signal $z(t)$ by the conjugate of the frequency warping factor $\Xi_{f_1}(t)$ is to reduce the overall bandwidth of the signal $p_1(t)$ since, as seen in Eqn. (2.36), the component due to frequency modulation is eliminated, leaving only the component due to the bandwidth of $a_1(t)$. By minimizing the bandwidth spread of $p_1(t)$, we decrease the frequency spread of any spectral alterations to $Z_{f_1}(\varphi)$ necessary to isolate or remove $p_1(t)$ from the mixture $z(t)$, hence minimizing the "damage" done to other signal components other than $p_1(t)$. For these applications it is necessary to obtain a good estimate of the instantaneous frequency $f_k(t)$ for each partial $p_k(t)$ we wish to isolate. The frequency-lock algorithm of Section 4.2 provides a way of doing this.

3.5 Related Work

We briefly cite some previous work related to frequency warping.

3.5.1 Shear Madness

Baraniuk and Jones [8–10] have described wavelet transforms based on chirp functions. They advocate transforming the rectilinear time-frequency tilings of conventional wavelets into "fan bases" through their "axis warping operator" Λ_c, which transforms a basis function $z(\cdot)$ to

$$\left(\Lambda_c z\right)(v) \stackrel{\triangle}{=} |c|^{1/2} |v|^{(c-1)/2} z\left\{ |v|^c \mathrm{sign}(v) \right\}, \tag{3.73}$$

where $c \in \Re$ and $c \neq 0$. The new bases then provide a new kind of frequency- and time-varying tessellation of the time-frequency plane. Baraniuk and Jones point out correctly that "the energy of a frequency modulated signal will be spread over many basis coefficients in [proportional-bandwidth and constant-bandwidth] expansions, since it traces a path in the time-frequency plane that is not well modeled by either of the basis tilings..." [8].

One disadvantage with the wavelet approach is that it gives a non-parametric representation of the energy distribution in the time-frequency plane. Once the wavelet transform has been performed, sheared or not, one must still extract peaks in the non-parametric distribution in order to localize the signal energies.

Our approach in this dissertation is to provide a *model-based* representation of signals through time.

3.5.2 Time Warping

Another approach to frequency-warping has been proposed by Wulich, Plotkin, Swamy, and Tong [149]. Their approach to analyzing frequency-varying signals is to *time-warp* the input signal. Their strategy consists of acquiring lock on a continuous-time interfering FM signal using a phase-locked loop, and then using the zero-crossing rate of the PLL to control a *variable rate* of sampling of the signal, i.e., with non-uniformly spaced samples in time, in order to stabilize the discrete-time frequency of the sampled interfering signal. The resulting signal is then notch-filtered with a conventional adaptive notch filter [118], which then removes the interfering FM signal.

One major problem with their approach is that variable-rate sampling is incompatible with processing of signals which have already been sampled at a fixed rate. Additionally, frequency components near $f_s/2$, where f_s is taken to be the average sampling rate, will be aliased when the sampling rate decreases. However, they are able to improve significantly upon the tracking ability of the adaptive notch filter and the removal the interfering FM signal.

Functional Time-Warping Almeida, *et al*, viewed voiced speech as being composed of a time-varying harmonic signal [5]. They introduced a time-warping function $\phi^{-1}(t)$ used to make component frequencies stationary in time. Calculating $\phi^{-1}(t)$ proved to be a difficult task. Stettiner, *et al* [130] have found a tractable way to calculate $\phi^{-1}(t)$ using a method based on maximum likelihood.

3.5.3 RISC

Kumaresan, *et al*, [78, 79] have used time-varying demodulation similar to the technique described in this chapter to reduce the bandwidth of an frequency-modulated sinusoid signal in their "RISC" (Residual Interfering Signal Canceler) algorithm for tracking partials. In [78], they minimize the squared error between a signal

$$s(t) = \sum_{k=1}^{M} a_k(t) \cos[k\phi(t) + \phi_k(t)], \tag{3.74}$$

presumed to be harmonic, and a model

$$\hat{s}(t) = \sum_{k=1}^{M_1} a_k \cos[2\pi k \tilde{f}_0 t], \tag{3.75}$$

where M_1 is the number of partials below 1 KHz. For each short segment of sampled speech data, the parameters a_k and $\tilde{f}_0$ are the values which attain the minimum mean-square error. The estimated

frequency function $\tilde{f}_0(t)$ is then calculated from the f_0 estimates for the segments by using a spline to interpolate the instantaneous frequency.

In [79], they adopt a frequency-locked loop similar to [140],[3] and others [54, 100] to estimate the fundamental frequency. The resulting frequency estimate is then used to frequency-warp the input signal.

3.6 Examples

In this section, we illustrate some examples of how frequency-warped Fourier transforms and frequency-warped instantaneous spectra may be useful.

3.6.1 Gaussian Chirp Example

Recall the chirp with a Gaussian envelope in Eqn. (3.1). We may separate the envelope and frequency functions by defining

$$a(t) = \exp\left(\pi\alpha t^2\right), \quad (\alpha < 0) \tag{3.76}$$

and recalling the expression Eqn. (3.2) for instantaneous frequency. We find that the instantaneous spectrum is

$$\begin{aligned} Z(f,t) &= a(t)\,\delta(f-\beta t) && (3.77)\\ &= \exp\left(\pi\alpha t^2\right)\,\delta(f-\beta t). && (3.78) \end{aligned}$$

We note that $a(t)$ has an RMS instantaneous bandwidth (cf. Eqn. (2.40)) of

$$\begin{aligned} \mathrm{IB}_a(t) &= \left|\frac{a'(t)}{2\pi a(t)}\right| && (3.79)\\ &= |\alpha t|. && (3.80) \end{aligned}$$

The somewhat non-intuitive fact that the instantaneous bandwidth effectively goes to infinity with increasing $|t|$ is mitigated by the fact that the instantaneous power decreases to zero extremely rapidly.

Using $\xi(t) = \beta t$, we find that the ξ-frequency warping factor is

$$\Xi(t) = \exp\left(j\pi\beta t^2\right) \tag{3.81}$$

and the frequency-warped Fourier transform is

$$\begin{aligned} Z_\xi(\varphi) &= \mathcal{F}\{z(t)\} && (3.82)\\ &= \mathcal{F}\left\{\exp\left(\pi\alpha t^2\right)\right\} && (3.83)\\ &= \frac{1}{\sqrt{|\alpha|}}\exp\left(\pi\varphi^2/\alpha\right). && (3.84) \end{aligned}$$

Note that this is narrower than the Fourier spectrum given in Eqn. (3.12) since

$$|Z(f)| = \frac{1}{\sqrt[4]{\alpha^2+\beta^2}}\exp\left\{\frac{\pi\alpha f^2}{\alpha^2+\beta^2}\right\}. \tag{3.85}$$

[3] see the following chapter for details

By inspection, we see that the variance of f with respect to $Z(f)$ is

$$\sigma_f^2 = \frac{\alpha^2 + \beta^2}{2\pi|\alpha|} \tag{3.86}$$

and the variance of φ with respect to $Z_\xi(\varphi)$ is

$$\sigma_\varphi^2 = \frac{|\alpha|}{2\pi}. \tag{3.87}$$

We see from the following numerical example that σ_φ^2 can be much less than σ_f^2. We choose $\alpha = -10$, $\beta = 2000$. Thus, the signal is a sweep of about 0.8 seconds in length from about -1600Hz to 1600Hz. We see that $\sigma_f^2 = 63663.6$ and $\sigma_\varphi^2 = 1.5915$, a relative ratio of about 40000 to 1. The results are presented in Figure 3.1 The real part of the signal $z(t)$ is plotted in Figure 3.1(a) and $a(t) = |\Xi^*(t)z(t)|$ in Figure 3.1(b). The magnitude of the Fourier transform $Z(f)$ of $z(t)$ plotted in Figure 3.1(c). Noting that the instantaneous frequency function is $f(t) = \beta t = 2000t$, we obtain $Z_f(\varphi)$, whose magnitude is plotted in Figure 3.1(d). In Figure 3.1(e) we display a density plot of the short-time discrete-time spectrogram of $z(t)$ on a decibel scale. Figure 3.1(e) shows the ξ-frequency-warped spectrogram of the same signal using $\xi(t)$ set to the instantaneous frequency $f(t)$ of $z(t)$. Note that the density is concentrated near DC. Figure 3.1(f) is the spectrogram of Figure 3.1(e) with DC shifted to the instantaneous frequency $f(t)$. The FFT bins are simply wrapped around modulo 512 to perform the frequency shift. All simulations here were done using a 4096 Hz sampling rate, 512-point FFT, 16-point hop size, and a Hanning window, where applicable.

3.6.2 FM Signal Example

A frequency modulated signal with fixed amplitude is of the form

$$z(t) = A \exp\{j2\pi f_0 t + jm \sin(2\pi f_m t)\}, \tag{3.88}$$

where A is the amplitude, f_0 is the carrier frequency, f_m is the modulation frequency, and m is the modulation index defined as

$$m = \frac{d}{f_m}, \tag{3.89}$$

with d being the peak frequency deviation. It is well known that the Fourier spectrum of $z(t)$ may be quite complex. The FM-synthesis algorithm by Chowning [32] takes advantage of this fact, providing a computationally efficient way of producing musical sounds. In particular, $z(t)$ may be represented as a Fourier series expansion

$$z(t) = A \exp(j2\pi f_0 t) \exp\{jm \sin(2\pi f_m t)\} \tag{3.90}$$

$$= A \exp(j2\pi f_0 t) \sum_{k=-\infty}^{\infty} J_k(m) \exp(j2\pi k f_m t), \tag{3.91}$$

where the $J_k(m)$ are the Bessel functions of the first kind [60]. Thus, the frequency component at $f_0 + kf_m$, for all integer k, has amplitude $J_k(m)$. This is certainly a complex spectrum! If the modulation frequency is sufficiently slow, the significant support of the spectrum will be band-limited, and the distinction between modulator and carrier will be unambiguous. Hence ideas from the Bedrosian product theorem [12] may be applied to disambiguate the instantaneous frequency of this signal.

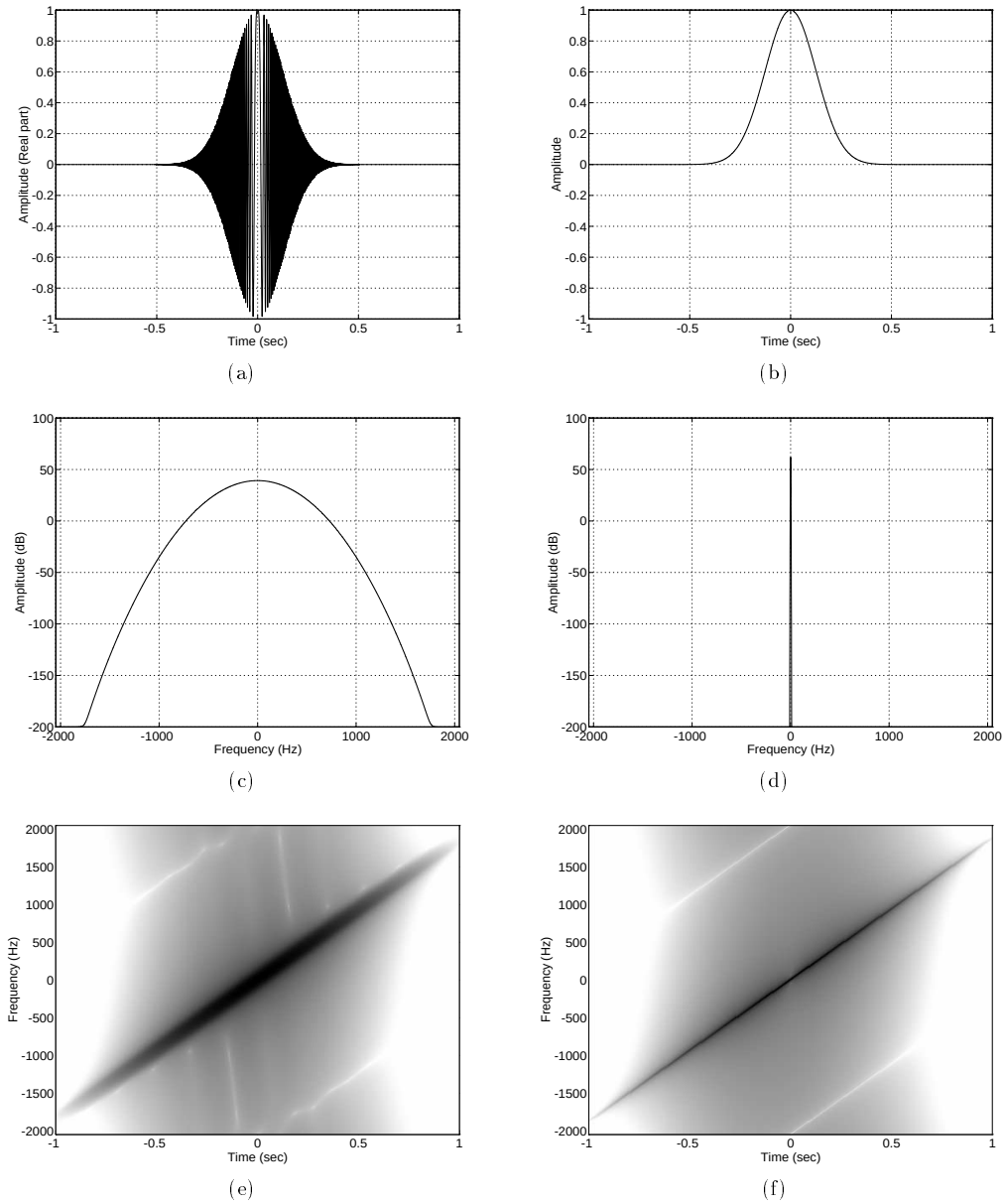

Figure 3.1: Frequency-warped complex Gaussian chirp example. See text for details. **(a)** Real part of the chirp signal $z(t)$. **(b)** The magnitude envelope of the chirp signal is what remains after frequency-matched frequency-warping. **(c)** FFT of the original signal $z(t)$. **(d)** FFT of $\langle z \wr f \rangle(t)$. Notice that it is quite narrow-band. **(e)** Spectrogram of $z(t)$. **(f)** Spectrogram of $\langle z \wr f \rangle(t)$, but DC shifted so as to match the instantaneous frequency $f(t)$. This "artificial" spectrogram illustrates how well the signal energy may be localized if the FM-bandwidth component can be factored out, leaving only the AM-bandwidth.

Using Eqn (2.8), we find that the instantaneous frequency is

$$f(t) = \frac{1}{2\pi}\frac{d\arg\{z(t)\}}{dt} \tag{3.92}$$
$$= f_0 + m f_m \cos(2\pi f_m t) \tag{3.93}$$
$$= f_0 + d\cos(2\pi f_m t). \tag{3.94}$$

The instantaneous spectrum of $z(t)$ is then (cf. Eqn. (2.58))

$$Z(f,t) = A\,\delta\left\{f - f_0 - d\cos(2\pi f_m t)\right\}. \tag{3.95}$$

Since the envelope function is a constant $a(t) = A$, we see that the instantaneous bandwidth of this demodulated signal (cf. Eqn. (2.40)) is $\mathrm{IB}_a(t) = 0$.

When we set $\xi(t) = f(t)$ we find that

$$\Xi_f(t) = \exp\left(j2\pi\int_0^t f(\tau)\,d\tau\right) \tag{3.96}$$
$$= \exp\left(j2\pi f_0 t + jm\sin(2\pi f_m t)\right). \tag{3.97}$$

It follows trivially that

$$\mathcal{F}_f\{z(t)\} = Z_f(\varphi) \tag{3.98}$$
$$= A\,\delta(\varphi). \tag{3.99}$$

Thus, we see that the f-frequency-warped Fourier spectrum of $z(t)$ is much simpler than its Fourier spectrum, as given implicitly by Eqn. (3.90).

We illustrate this example with numerical simulations. We set $A = 1$, $f_0 = 1000$, $f_m = 20$, and $d = 200$, so that $m = d/f_m = 10$. $z(t)$ is then sampled at 4096 Hz. The Fourier transform is plotted in Figure 3.2(a). Noting that the instantaneous frequency function is $f(t) = 1000 + 200\cos(2\pi 20t)$, we obtain $Z_f(\varphi)$, which is plotted in Figure 3.2(b). In Figure 3.2(c) we display the spectrogram of $z(t)$ on a decibel scale. Figure 3.2(c) shows the frequency-warped spectrogram of the same signal using $\xi(t)$ set to the instantaneous frequency $f(t)$ of $z(t)$. Note that the density is concentrated exactly at DC since the instantaneous bandwidth is zero. Figure 3.2(d) is the spectrogram of Figure 3.2(c) with DC shifted to the instantaneous frequency $f(t)$. Similar to the previous example, the FFT bins are simply wrapped around modulo 256 to perform the frequency shift. All simulations here were done using a 4096 Hz sampling rate, 256-point FFT, 8-point hop size, and a Hanning window, where applicable.

3.6.3 FM and Chirp Example

We now apply the frequency-warped technique to remove a broad-band signal from a mixture. We have two signals, $z_1(t)$ and $z_2(t)$, which are a Gaussian chirp and FM-signal, respectively. $z_1(t)$ is as before, with

$$z_1(t) = \exp\left\{\pi(\alpha + j\beta)t^2\right\}, \tag{3.100}$$

where $\alpha = -10$ and $\beta = 2000$, and

$$z_2(t) = A\exp\left\{j2\pi f_0 t + jm\sin(2\pi f_m t)\right\}, \tag{3.101}$$

where, as before, $A = 1$, $f_0 = 1000$, $f_m = 20$, and $d = 200$, so that $m = d/f_m = 10$. Our total signal is then $z(t) = z_1(t) + z_2(t)$. In the following, the sampling rate is 4096 Hz, the number of points in the analysis is 8192, the FFT size is 256 points per frame, and the hop size is 16 points.

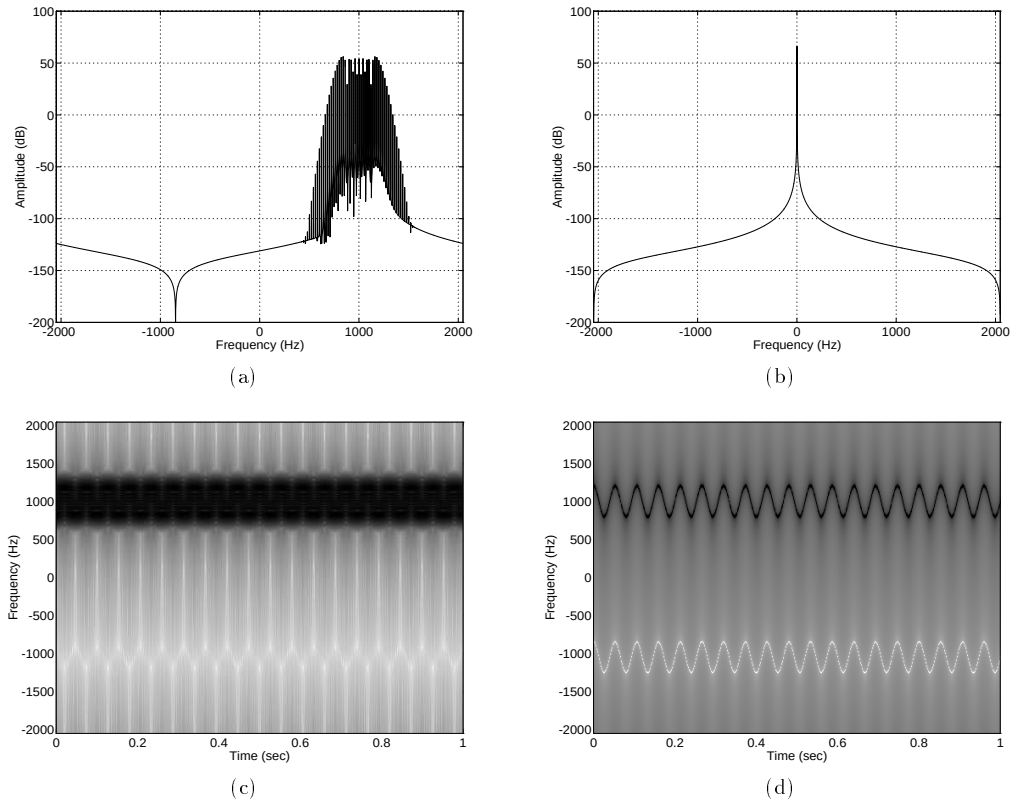

Figure 3.2: Frequency-warped frequency-modulated signal example. See text for details. **(a)** FFT of the original signal $z(t)$. Note the complicated broadband structure reflecting the Bessel-function $J_k(m)$ distribution of the modulation sidebands. **(b)** FFT of $\langle z \wr f \rangle(t)$. Notice that it is quite narrow-band. The deviation from a pure delta at 0 is due to windowing. **(c)** Spectrogram of $z(t)$. The frequency modulation is somewhat visible **(d)** Spectrogram of $\langle z \wr f \rangle(t)$, but DC shifted so as to match the instantaneous frequency $f(t)$. This "artificial" spectrogram illustrates how well the signal energy may be localized if the FM-bandwidth component can be factored out, leaving only the AM-bandwidth.

The results are shown in Figure 3.3. Figures 3.3(a) and 3.3(b) show the FFT and spectrogram, respectively, of the sum signal $z(t)$. Notice how the two signals overlap in time and frequency.

Figures 3.3(c) and 3.3(d) show the FFT and spectrogram, respectively, of the f_2-warped signal, $\langle z \wr f_2 \rangle(t)$, where $f_2(t)$ is the instantaneous frequency of $z_2(t)$. Notice how the FM signal $z_2(t)$ has been modulated to DC and how the chirp signal $z_1(t)$ has been made even more broad-band than before with some interesting frequency modulation.

Figures 3.3(e) and 3.3(f) show the result of zeroing the single bin at DC of the 8192-point FFT in Figure 3.3(c), performing an inverse-FFT on it, and then reversing the f_2-frequency-warping to restore the original instantaneous frequencies. In other words, if

$$Z^-_{f_2}[\kappa] = \begin{cases} Z_{f_2}[n], & \text{for } \kappa \in \{1, \ldots, 8191\} \\ 0, & \text{for } \kappa = 0, \end{cases} \tag{3.102}$$

is the notched f_2-warped FFT of $z[n] = z(n/f_s)$ then

$$z^-[n] = \mathcal{F}^{-1}_{f_2}\{Z^-_{f_2}[\kappa]\} \tag{3.103}$$

is the signal plotted in Figures 3.3(e) and 3.3(f). We observe that the FM signal has been attenuated by approximately 77 decibels, leaving the chirp fairly intact, even where they intersected. The remaining trace of $z_2(t)$ is due to the missing contribution of $z_1(t)$ which was lost when $Z_{f_2}[0]$ was set to zero. The fact that the extra frequency-modulation due to f_2-frequency warping caused $z_1(t)$ to become broader-band than before mitigates the damage done, thus allowing a cleaner separation. This clean signal surgery would not have been possible if the $z(t)$ had not been frequency-warped. This, of course, necessitates knowing the instantaneous frequency of $z_2(t)$, which we know *a priori* in this case.

3.7 Summary

We have seen in this chapter how frequency warping may be applied to a signal $p(t)$ with a known time-varying instantaneous frequency $f(t)$ to transform it to a relatively narrow-band signal whose bandwidth is determined solely by its amplitude envelope. This transformation makes it relatively easy to remove a target signal $p(t)$ out of an additive mixture $z(t)$ composed of various other signals. This removal may be done by either zeroing the low-frequency components of the frequency-matched frequency-warped Fourier transform of a signal or by low- or high-pass filtering the frequency-warped signal and unwarping. Removing a signal in this way minimizes the damage done to other signals in the mixture, especially when the target signal has a significantly broad-band FM bandwidth component σ^2_{FM}. All this, of course, is contingent on knowing or having a good estimate of the instantaneous frequency of the target signal, which is the topic of the next chapter.

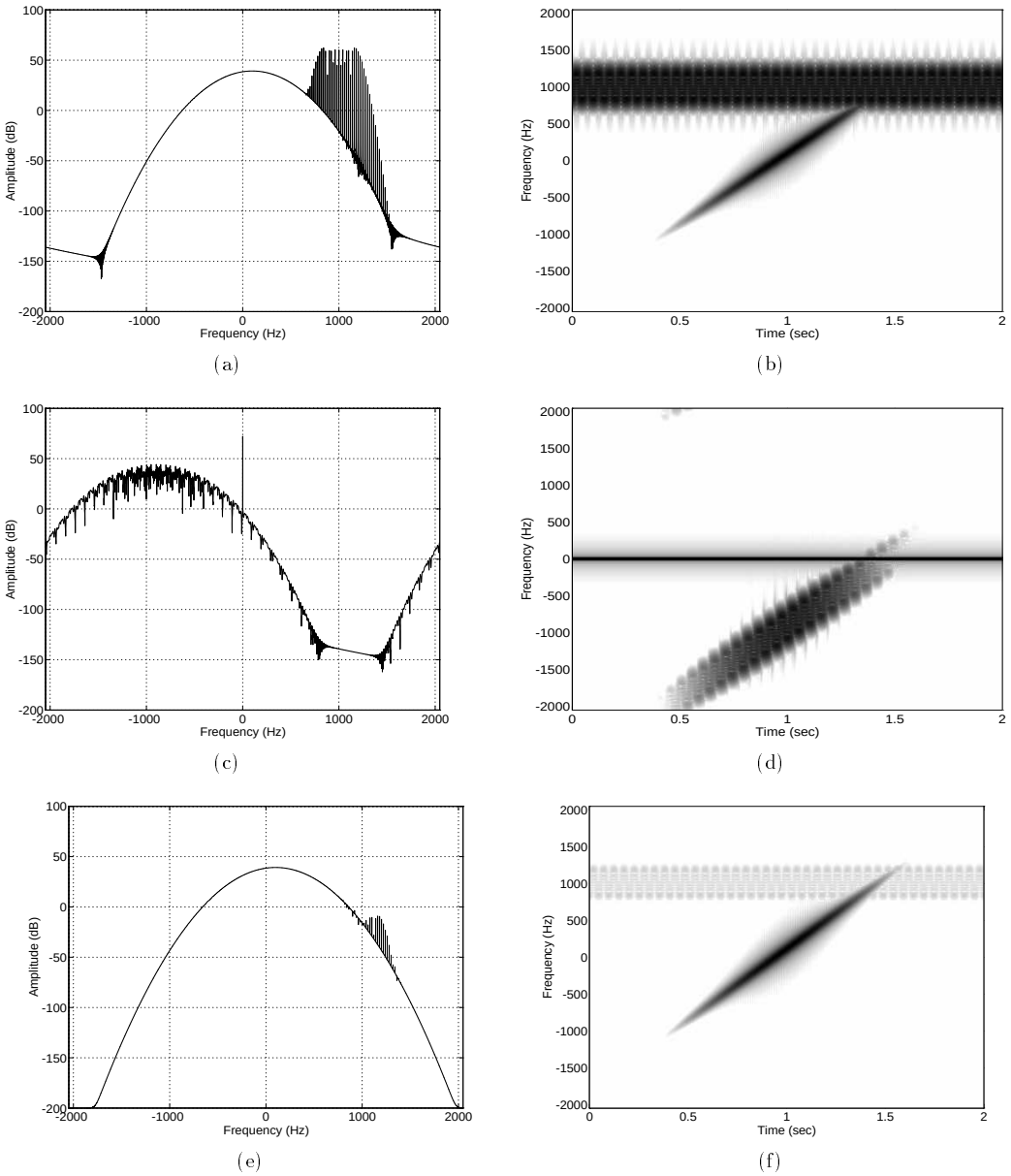

Figure 3.3: FM and chirp signal separation example. See text for details. **(a)–(b)** FFT and spectrogram, respectively, of $z(t) = z_1(t) + z_2(t)$, where $z_1(t)$ is the Gaussian chirp and $z_2(t)$ is the FM signal. **(c)–(d)** FFT and spectrogram, respectively, of $\langle z \wr f_2 \rangle(t)$. **(e)–(f)** FFT and spectrogram, respectively, of the notched signal $z^-(t)$ with $z_2(t)$ highly attenuated.

Chapter 4

Frequency-Locked Loop Signal Tracking

There are many ways to estimate and track the instantaneous frequency of a frequency-varying sinusoidal signal. Wolcin [147], McAulay and Quatieri [94], and Serra [126], for example, use frame-to-frame peak following in the FFT-magnitude spectrum. Costas [41] uses a kind of linear prediction based on a

In this section we present a basic, somewhat unconventional, discrete-time frequency-locked loop algorithm for tracking a single, complex-valued, frequency- and amplitude-varying partial $p[n]$. This algorithm provides the instantaneous frequency estimate necessary for performing frequency-warped signal processing, as described in the previous chapter. We provide an analysis of the tracking and convergence properties in the presence of noise and interfering partials, including the case of real-valued input signals. We start by sketching the basic algorithm and then follow up with a discussion of each component and the various issues involved in designing it. We discuss various issues concerning loop filter design, group delay, and loop stability. We present a variation of the basic tracking loop which returns a high-quality estimate of the instantaneous frequency of the target partial, attaining the Cramér-Rao bound under certain conditions. Finally, we show some applications of the frequency-locked loop tracker, including resynthesis of partials and adaptive notch filtering.

4.1 Assumptions

Let the target signal $p[n]$ be a complex-valued discrete-time signal defined for $n \geq 0$ with sampling frequency f_s

$$p[n] = a[n] \exp\left(\frac{j2\pi}{f_s} \sum_{k=1}^{n} f[k] + j\phi_0\right), \tag{4.1}$$

where $a[n]$ is the instantaneous amplitude envelope, $f[n] > 0$ is the instantaneous frequency, and ϕ_0 is the phase offset at time $n = 0$.

We assume that $f[n]$ and $a[n]$ are slowly varying with respect to the loop time constant of the tracking system, which will be defined later. We assume, additionally, that $a[n]$ has a limited bandwidth $\mathrm{BW}_a[k] < f[k]$ for all $k \in \{1, \ldots, n\}$, which is a condition of the Bedrosian Product Theorem, which makes the carrier/modulator factorization unambiguous (cf. [12] and Appendix A).

Define the *discrete-time slew rate* of the instantaneous frequency as

$$\dot{f}[n] \triangleq (f[n] - f[n-1])\, f_s \tag{4.2}$$

For tracking, we assume that the slew rate is bounded by a constant $\dot{f}_{\max}$, so that

$$\forall n, \quad \left|\dot{f}[n]\right| \leq \dot{f}_{\max}. \tag{4.3}$$

The relationship between the slew rate $\dot{f}_{\max}$ and tracking performance will be discussed in Section 4.3.1

The input signal $z[n]$ will be assumed to be a mixture of $p[n]$ and some unknown disturbance signal $\nu[n]$, i.e.

$$z[n] = p[n] + \nu[n]. \tag{4.4}$$

4.2 A Frequency-Locked Loop

We start the algorithm by demodulating the input signal $z[n]$ by multiplying it by the complex conjugate of the frequency-warping signal

$$\Xi[n] \triangleq \exp\left(j\hat{\phi}[n]\right), \tag{4.5}$$

where

$$\hat{\phi}[n] \triangleq \begin{cases} \hat{\phi}[n-1] + 2\pi\hat{f}[n]/f_s, & \text{for } n \geq 1 \\ 0, & n = 0 \end{cases} \tag{4.6}$$

$$= \frac{2\pi}{f_s}\sum_{k=1}^{n}\hat{f}[k], \tag{4.7}$$

and where $\hat{f}[k] \in (0, f_s/2)$, is the estimate of $f[k]$ at time step k. We assume that $\hat{f}[1]$ is reasonably close to $f[1]$ by the criterion suggested by Eqn. (4.16).

The complex demodulated signal is

$$d[n] \triangleq \Xi^*[n]z[n] \tag{4.8}$$

$$= a[n]\exp\left(\frac{j2\pi}{f_s}\sum_{k=1}^{n}(f[k] - \hat{f}[k]) + j\,\phi_0\right) + \Xi^*[n]\nu[n]. \tag{4.9}$$

This demodulated signal is subjected to a low-pass filter **LPF** which has a cut-off frequency of f_c, unity gain at DC, and is assumed, for now, to have zero group delay at all frequencies, resulting in a signal $u[n]$ such that

$$u[n] = h_{\text{LPF}} * d[n] \tag{4.10}$$

$$= h_{\text{LPF}} * \{\Xi^*[n]z[n]\} \tag{4.11}$$

$$= h_{\text{LPF}} * \{\Xi^*[n]p[n]\} + h_{\text{LPF}} * \{\Xi^*[n]\nu[n]\} \tag{4.12}$$

$$\approx h_{\text{LPF}} * \{\Xi^*[n]p[n]\} \tag{4.13}$$

$$\approx H_{\text{LPF}}(f[n] - \hat{f}[n])a[n]\exp\left(\frac{j2\pi}{f_s}\sum_{k=1}^{n}(f[k] - \hat{f}[k]) + j\,\phi_0\right) \tag{4.14}$$

$$\approx a[n]\exp\left(\frac{j2\pi}{f_s}\sum_{k=1}^{n}(f[k] - \hat{f}[k]) + j\,\phi_0\right) \tag{4.15}$$

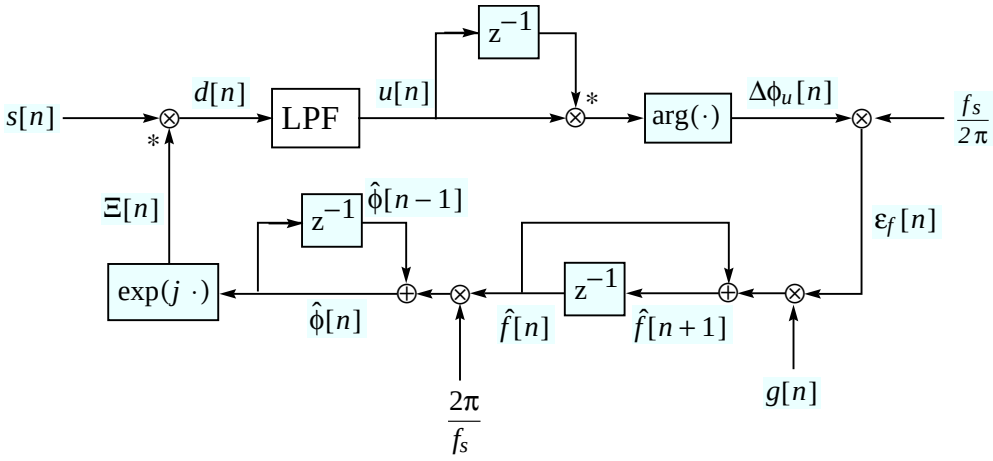

Figure 4.1: Signal flow for a basic FLL tracker. See text for explanation.

with the assumptions that the slew rate $\dot{f}[n]$ is small and that

$$\left| f[k] - \hat{f}[n] \right| < f_c. \tag{4.16}$$

In Eqn. (4.13) we have assumed that the filtered disturbance term $h_{\mathrm{LPF}} * \{\Xi^*[n]\nu[n]\}$ is negligible. The approximation in Eqn. (4.14) becomes more accurate as the slew rate $f[n]$ decreases and as the tracking by $\hat{f}[n]$ locks and stabilizes, as described below.

We see that we may attempt to estimate the amplitude envelope by setting

$$\hat{a}[n] = |u[n]|. \tag{4.17}$$

However, this expression destroys the phase error information in $u[n]$, and can cause potential problems in the context of resynthesis if frequency tracking is not exact. Also, energy leakage from other signal sources will be badly nonlinearly distorted after passing through the absolute value operation. If *phase lock* on the signal $p[n]$ is not attained, as is the case in the algorithm described here, it is desirable to keep the phase information in $u[n]$ since the phase error can compensate very well for estimation errors in tracking $f[n]$ for the purposes of resynthesis. We will explore the issues of phase-locking in Section 4.4 and signal resynthesis in Section 4.9.

In order to extract the amplitude-modulation envelope $a[n]$ and its associated phase error term in Eqn. (4.15) we require that its bandwidth $\mathrm{BW}_a[k]$ obey

$$\mathrm{BW}_a[k] < f_c, \quad \text{for all } k. \tag{4.18}$$

Additionally, the conditions for the Bedrosian Product Theorem [12] (cf. Appendix A) must hold, namely,

$$\mathrm{BW}_a[k] < f[k]. \tag{4.19}$$

If these conditions are not satisfied, the modulator-carrier decomposition may not be unique, as discussed in Appendix A. It is sufficient that this relation hold with an allowance for "forgetting" the history of the signal beyond the several tracking loop time constants. Thus, if the $a[n]$ and $f[n]$ vary with time, Eqn. (4.19) may be violated globally, but always hold locally within the time constant of the tracking loop. In practice, this determination is never carried out since the

assumption that the Bedrosian Product Theorem holds is generally valid for audio partials with slowly varying envelopes.

The exact form of **LPF** is not of immediate importance but will be discussed in more detail in Section 4.6. Its primary function is to improve the signal-to-noise ratio (SNR) by lowpass filtering the demodulated signal $d[n]$, thereby attenuating the demodulated noise signal $\Xi^*[n]\nu[n]$. **LPF** is necessary to allow the condition given by Eqn. (2.106) of the Filtered Winding Corollary to hold over a wider range of signal conditions, making the tracking performance more robust. If this condition is true, the short-time averaged winding rate of the frequency-warped signal $\Xi^*[n]z[n]$ is a robust measure of the frequency error $f[n] - \hat{f}[n]$.

We now consider the phase $\phi_u[n]$ of the signal $u[n]$,

$$\phi_u[n] \stackrel{\triangle}{=} \mathrm{Arg}(u[n]) \qquad \text{(formally)} \tag{4.20}$$

$$= 2\pi \sum_{k=1}^{n} \frac{f[k] - \hat{f}[k]}{f_s} + \phi_0 + \zeta[n] \tag{4.21}$$

$$\approx 2\pi \sum_{k=1}^{n} \frac{f[k] - \hat{f}[k]}{f_s} + \phi_0, \tag{4.22}$$

where $\zeta[n]$ is the phase-error term defined in Eqn. (2.119) and is assumed, for now, to be negligible (cf. footnote 1, page 70). The absolute phase function $\mathrm{Arg}(\cdot)$ is multi-valued (modulo 2π) and the $\arg(\cdot)$ functions commonly available to calculate it return the principal branch value in the interval $(-\pi, \pi]$ so that the absolute phase cannot be known from local measurements. This ambiguity in finding the absolute phase is known as the *phase-unwrapping problem*, and apparently some effort has been invested in tackling it directly [135]. However, there is no need to struggle with it if we choose simply to avoid it. It is better to calculate the *change* in phase

$$\Delta\phi_u[n] \stackrel{\triangle}{=} \phi_u[n] - \phi_u[n-1] \qquad \text{(formally)} \tag{4.23}$$

$$= \arg\left(u[n]u^*[n-1]\right) \tag{4.24}$$

$$= \left(2\pi \sum_{k=1}^{n} \frac{f[k] - \hat{f}[k]}{f_s} + \phi_0 + \zeta[n]\right) \tag{4.25}$$

$$- \left(2\pi \sum_{k=1}^{n-1} \frac{f[k] - \hat{f}[k]}{f_s} + \phi_0 + \zeta[n-1]\right)$$

$$= \frac{2\pi}{f_s}\left(f[n] - \hat{f}[n]\right) + \zeta[n] - \zeta[n-1] \tag{4.26}$$

$$\approx \frac{2\pi}{f_s}\left(f[n] - \hat{f}[n]\right), \tag{4.27}$$

where we assume that the disturbance is small.[1] Because the signal $s[n]$ is over-sampled, we are guaranteed that $|\Delta\phi_u[n]| \leq \pi$.[2] Consequently, $\Delta\phi_u[n]$ has a well-defined value which we may

[1] In reality, $\zeta[n] - \zeta[n-1]$ can be quite large compared to the term in Eqn. (4.27), but we may assume that it is zero-mean. What we end up with is a *stochastic difference equation* [67, 84]. Since the control loop for the $\hat{f}[n]$ updates we are constructing is a stable linear finite-difference equation, we may simply work with the expectation value of the quantities involved, giving us license to neglect the terms in $\zeta[n]$. The deviation from the noise-free equation is bounded by the variance of the ζ-noise filtered by the loop dynamics. With a sufficiently slow loop time constant τ_ℓ (cf. Eqn. (4.33)), the variance of the filtered noise in $\hat{f}[n]$ and other derived quantities becomes quite small.

[2] The bound is actually even stronger: if **LPF** has a cutoff frequency f_c then $|\Delta\phi_u[n]| \leq \pi f_c / f_s$.

calculate by using a standard complex arg(·) function. In this way, we completely avoid the phase unwrapping problem.

Define the frequency tracking error at time n as

$$\varepsilon_f[n] \stackrel{\triangle}{=} \frac{f_s}{2\pi}\Delta\phi_u[n] \tag{4.28}$$

$$= f[n] - \hat{f}[n] + \frac{f_s}{2\pi}(\zeta[n] - \zeta[n-1]) \tag{4.29}$$

$$\approx f[n] - \hat{f}[n]. \tag{4.30}$$

We see immediately that we may close the loop to form an estimate $\hat{f}[n+1]$ of $f[n+1]$ by computing

$$\hat{f}[n+1] = \hat{f}[n] + g[n]\varepsilon_f[n] \tag{4.31a}$$

$$\approx \hat{f}[n] + g[n]\left(f[n] - \hat{f}[n]\right) \tag{4.31b}$$

$$= (1 - g[n])\hat{f}[n] + g[n]f[n], \tag{4.31c}$$

where $g[n]$ is the tracking gain of the system at time step n. This system is especially nice because the frequency tracking system simply reduces to a first-order difference equation in $\hat{f}[n]$ with closed-loop gain

$$g_\ell[n] \stackrel{\triangle}{=} 1 - g[n]. \tag{4.32}$$

The tracking time constant of the system at time step n, in terms of time steps, is given by

$$\tau_\ell[n] \stackrel{\triangle}{=} \frac{-1}{\log\left(g_\ell[n]\right)} \tag{4.33}$$

$$= \frac{-1}{\log\left(1 - g[n]\right)} \tag{4.34}$$

$$\approx \frac{1}{g[n]}, \tag{4.35}$$

for small, slowly-varying $g[n]$.

Notice in Eqn. (4.31c) that $\hat{f}[n]$ is the weighted sum of the frequency estimation errors made by the tracker between time steps 1 and n. If $g[k] = 1$ then $\hat{f}[n]$ equals the total number of cycles slipped by the tracker times $f_s/2\pi$. This may be seen by observing from Eqn. (4.31a) that

$$\hat{f}[n+1] = \hat{f}[n] + g[n]\Delta\phi_u[n] \tag{4.36}$$

$$= \sum_{k=1}^{n} \frac{f_s g[k]}{2\pi}\Delta\phi_u[n] \tag{4.37}$$

$$= \frac{f_s}{2\pi}\sum_{k=1}^{n}\Delta\phi_u[n]. \tag{4.38}$$

This system will converge if

$$\forall k, \quad |g_\ell[k]| < 1 \tag{4.39}$$

which leads to[3]

$$0 < g[k] < 2. \tag{4.40}$$

[3] This condition (4.39) may be loosened considerably. For example, we could require that the RMS value of $|g_\ell[n]|$ over all intervals of a certain length be less than one. However, such elaborations are excessive and won't be pursued further here.

This condition allows a large range of possible sequences for $g[n]$. The tradeoffs are fast convergence but high noise sensitivity for small values of $|g_\ell[n]|$ on one hand, and slow convergence but less noise sensitivity for higher values on the other hand.

If the group delay of **LPF** is non-zero near DC then the foregoing analysis is inaccurate. Extra modes are introduced into the tracking dynamics and the choices for $g[n]$ are further restricted, as discussed in Section 4.6.2.

Also, $g[n]$ should be chosen to allow tracking of signals with frequency slew rates within the bound given by Eqn. (4.3). The update gain $g[n]$ may be set to a constant for simple applications, but can be set dynamically to adapt to tracking performance. Ideally, we would like to apply ideas from Kalman filtering to control the gain [6, 63, 74, 89, 114]. In order to do this, we must have a linear, state-variable model of the signal, i.e., with frequency, or perhaps the slew, given as a Gaussian random walk with known variance and stationary statistics. We must also have a model for the noise, e.g., stationary Gaussian noise, also with known variance. Given these conditions, Kalman filter theory gives the optimal estimate of the system state variables. However, since acoustical signals most commonly encountered in the natural world do not often adhere to known signal or noise models, the application of Kalman theory is somewhat difficult. It is then necessary to estimate the model parameters of the signal as well as the states of the system. Despite these difficulties, Kalman filtering theory has been used previously for speech analysis, for example, by Hedelin [64], in the form of the extended Kalman filter. The topic of adaptive gain control is pertinent to the topic of gain control in our discussion on Frequency-Locked Loops, but is beyond the scope of this dissertation.

4.3 Tracking Error and Convergence

The system is said to *converge* if $|\Delta f[n]|$ forms a monotonically decreasing sequence, where

$$\Delta f[n] \stackrel{\triangle}{=} f[n] - \hat{f}[n]. \tag{4.41}$$

Convergence is apparent when $\dot{f}[n] = 0$, i.e., when $f[n]$ is constant, since Eqn. (4.31b) leads to

$$\Delta f[n+1] = f[n+1] - \hat{f}[n+1] \tag{4.42}$$

$$= g_\ell[n]\Delta f[n] + \frac{\dot{f}[n+1]}{f_s} \tag{4.43}$$

$$= g_\ell[n]\Delta f[n]. \tag{4.44}$$

and the tracking error diminishes if $|g_\ell[n]| < 1$. As was noted in footnote 1 of page 70, the error terms due to $\zeta[n]$ may be large. Eqns. (4.42)-(4.44) actually only describe the deterministic part of the error terms $\Delta f[n]$. However, we know that, since the tracking loop is stable, the noise contribution to $\hat{f}[n]$ is bounded and small.

If $f[n]$ is slewing at a constant rate $\dot{f}_0$, and if the loop gain is $g_{\ell,0} = 1 - g_0$, where g_0 is a constant tracking gain, then we see from Eqns. (4.42) and (4.32) that

$$\lim_{n\to\infty} \Delta f[n] = \frac{\dot{f}_0}{f_s\,(1 - g_{\ell,0})} \tag{4.45}$$

$$= \frac{\dot{f}_0}{f_s g_0} \tag{4.46}$$

with time constant $1/g_{\ell,0}$. This quantity is the steady-state lag of the tracker estimate $\hat{f}[n]$ behind $f[n]$. This lag may be eliminated by using higher order tracking dynamics which estimate the slew rate as well as the frequency.

4.3.1 Frequency Lock

The tracker is considered to have ϵ-*frequency lock* on the signal $s[n]$ for $\epsilon \geq 0$ if

i.) $\left| f[n] - \hat{f}[n] \right| < \epsilon \leq f_c$, where f_c is the cutoff frequency of the low-pass filter **LPF** in Eqn. (4.10), and

ii.) the slew rate is such that $|\dot{f}[n]| \leq g_0 \epsilon f_s$,

where we assume that $g[n] \approx g_0$, and is slowly-varying. Condition (i) simply states that the signal being tracked, after demodulation, must fall within the passband of the low-pass filter **LPF**, otherwise it becomes attenuated and Eqn. (2.103) may fail.

Condition (ii) states that the algorithm cannot track the target signal within a tolerance of ϵ if it slews too quickly. The steady-state lag given in Eqn. (4.46) is greater than ϵ if condition (ii) does not hold. We see, then, that the maximum allowable slew rate for tracking to be maintained is given by

$$\dot{f}_{\max} = g_0 f_c f_s. \tag{4.47}$$

4.4 Tracking in the Presence of Noise and Interfering Partials

The analysis of the tracking loop in Section 4.2 was done with the assumption that there was a single partial in insignificant noise. The purpose of this section is to extend the robustness arguments to the case in which there is significant noise and other interfering partials.

We noted already, in footnote 1 of page 70, that Eqn. (4.31a) is a stochastic difference equation [67, 84]. In Section 4.2 we noted that that we may neglect the ζ terms if $\zeta[n]$ is zero-mean and the loop time-constant τ_ℓ is relatively long. Under these conditions, the noise contributions due to $\zeta[n]$ are minimized, due to averaging, and the resulting noise variance is bounded. As mentioned in the discussion regarding the low-pass filter **LPF** on page 70, in order for the tracking loop to form a robust estimate of $f[n]$, the demodulated disturbance $\nu[n]$ must be filtered so as to satisfy the filtered $\mathcal{M}_1$-condition

$$|h_{\text{LPF}} * \{\Xi^*[n]p[n]\}| > |h_{\text{LPF}} * \{\Xi^*[n]\nu[n]\}|. \tag{4.48}$$

When this condition is fulfilled, the Filtered Winding Corollary 2.2 on page 32 shows that the average winding rate is a robust estimator of the instantaneous frequency.

It is a simple matter to extend the analysis to interfering signals consisting of other partials. If $z[n]$ is a signal of the form given in Eqn. (2.102) and the $\mathcal{M}_1$-condition

$$|h_{\text{LPF}} * \{\Xi_k^*[n]p_k[n]\}| > \sum_{\substack{\ell=1 \\ \ell \neq k}}^{N} |h_{\text{LPF}} * \{\Xi_k^*[n]p_\ell[n]\}| + |h_{\text{LPF}} * \{\Xi_k^*[n]\nu[n]\}| \tag{4.49}$$

holds, where $p_k[n]$ is the k-th partial and $\Xi_k^*[n]$ is its associated frequency-matched frequency-warping function, then the Filtered Multi-Partial Winding Corollary (2.3) applies, guaranteeing that tracking of the k-th partial $p_k[n]$ will be robust.

4.4.1 Real-Valued Input Signals

In the case that the input signal $z[n]$ is actually a real-valued signal $s[n]$ of the form

$$s[n] = a[n]\cos\left(\frac{2\pi}{f_s}\sum_{k=1}^{n} f[k] + \phi_0\right) + \nu[n], \tag{4.50}$$

we may regard this as a sum of *two* complex-valued partials, $p_1[n]$ and $p_2[n]$ such that $p_1[n] = p[n]/2$ and $p_2[n] = p^*[n]/2$, and $p[n]$ is given by Eqn. (4.1) and $f[n] > 0$, so that

$$s[n] = p_1[n] + p_2[n] + \nu[n]. \tag{4.51}$$

Here, $\nu[n]$ is some real-valued disturbance.

The extension to the above argument for multiple partials and noise applies directly. Our target signal in this case is $p_1[n]$. We simply require **LPF** to be a filter which satisfies Eqn. (4.49) for $k = 1$, thus satisfying Eqn. (2.107) in the Filtered Multi-Partial Winding Corollary (2.3). **LPF** should have a cut-off frequency f_c such that

$$\forall k, \quad f_c < f[k] + \hat{f}[k], \tag{4.52}$$

in order to suppress $p_2[n]$.

In light of Corollary 2.3, in the presence of no other sources of interference, it is actually sufficient that the transfer function $H_{\text{LPF}}(f)$ obey

$$\forall k, \quad \left|H_{\text{LPF}}\left(-f[k] - \hat{f}[k]\right)\right| < \left|H_{\text{LPF}}\left(f[k] - \hat{f}[k]\right)\right|, \tag{4.53}$$

since $p[n]$ and $p^*[n]$ have the same magnitudes.

Notice that, after this filtering stage, the distinction in $u[n]$ between having the real signal $s[n]$ and the analytic signal $z[n] = s[n] - jq_H[n]$, where $q_H[n]$ is the discrete-time Hilbert transform of $s[n]$, as the system input is effectively lost, assuming that the response $H_{\text{LPF}}(f)$ is negligible for frequencies below $-\hat{f}[n]$ for all time steps n. This condition generally holds when $f[n]$ is sufficiently far from 0. This observation allows us to analyze the positive frequency components of a real signal $s[n]$ without having to perform a Hilbert transform off-line.

4.4.2 Tracking Bandwidth

The dynamic frequency warping provided by the Frequency-Locked Loop tracking algorithm described above reduces the bandwidth of the tracked signal $p[n]$ by factoring out the FM bandwidth component from the signal, effectively leaving only the AM bandwidth component in the demodulated signal $d[n]$ of Eqn. (4.8), where the signal $p[n]$ has been demodulated to nearly DC. This, in turn, enhances tracking performance and energy localization of the signal being tracked. The benefits of frequency warping were shown in Chapter 3.

4.5 Phase-Locked Loop

The frequency-lock algorithm described above may be easily augmented to produce a phase-locked loop. The estimation formula given by equations (4.31a)-(4.31c) integrates the *frequency tracking error* and makes no reference to absolute phase error. Phase-locked frequency tracking may be of some use in extracting spatial location from phase disparity among spatially distributed microphones.

Additionally, phase-lock may be useful for subtractive analysis, as we will comment on later in this section.

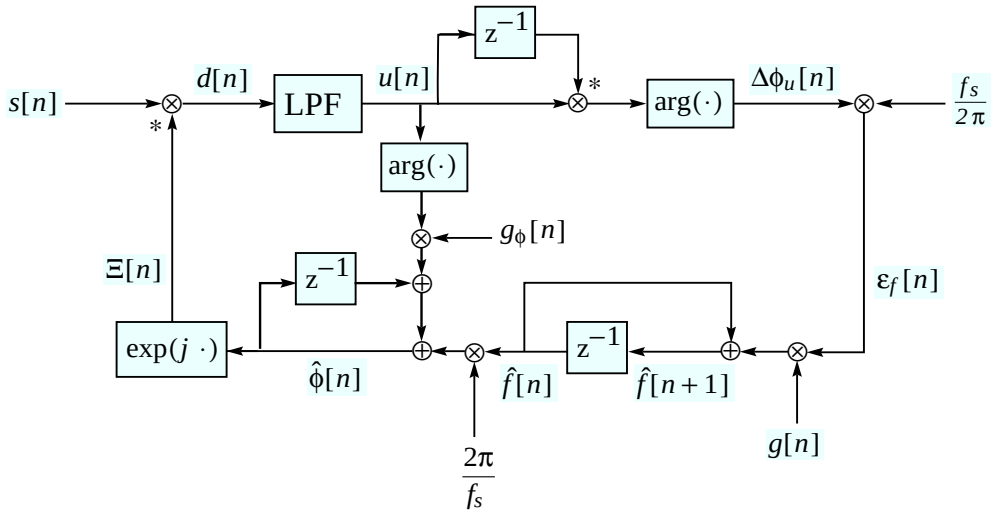

Figure 4.2: Signal flow for a basic FLL tracker with phase locking.

In the case that phase-lock is required, a simple modification to the frequency-lock method produces the desired behavior. The frequency-lock equation in equations (4.31a)-(4.31c) and Eqn. (4.6) may be augmented by adding a correction term for phase error (modulo 2π). Define the phase mismatch error between $\Xi[n]$ and $s[n]$ as

$$\phi_u^\star[n] \stackrel{\triangle}{=} \arg\left(u[n]\right). \tag{4.54}$$

The "$\star$" superscript denotes that the principal branch is taken so that $\phi_u^\star[n] \in (-\pi, \pi)$, so as not to confuse $\phi_u^\star[n]$ with $\phi_u[n]$, defined in Eqn. (4.20). We then modify the phase update term of Eqn. (4.6) to

$$\hat{\phi}[n] \stackrel{\triangle}{=} \hat{\phi}[n-1] + \frac{\hat{f}[n]}{f_s} + g_\phi[n]\Delta\phi_u^\star[n]. \tag{4.55}$$

There are two competing forces here trying to guide the tracking. We must pay attention to the relative ratios of $g[n]$ and $g_\phi[n]$. Since both $\Delta\phi_u[n]$ and $\phi_u^\star[n]$ range over $[-\pi, \pi]$, we must have $g[n] \gg g_\phi[n]$. However, as frequency lock is attained, we may want $g_\phi[n]$ to be large enough to assure quick phase tracking convergence.

Automatic gain control algorithms which monitor the status of frequency lock may be developed to adjust $g[n]$ and $g_\phi[n]$, for example, making them dependent on the variances of $\Delta\phi_u$ and $\phi_u^\star$. However simple, this topic is beyond the scope of this dissertation.

The signal flow diagram for a basic phase- and frequency-locked tracker is shown in Figure 4.2.

4.5.1 Instantaneous Amplitude Estimate–Revisited

Recall that in the misguided amplitude estimate of Eqn. (4.17) we did not have phase-lock on the partial $p[n]$ so that the phase of $u[n]$ was random. Extracting the magnitude of $u[n]$ in this case results in extreme non-linear distortion of the signal that passes through **LPF** . However, if phase-locked tracking is implemented we may represent the analytic signal $p[n]$ as being parameterized in terms of the instantaneous amplitude estimate $\hat{a}[n]$ and frequency estimate $\hat{f}[n]$. The initial phase

disparity has been absorbed into $\hat{\phi}[n]$, so that

$$\hat{p}[n] = \hat{a}[n] \exp\left(j\hat{\phi}[n]\right) \tag{4.56}$$
$$= \hat{a}[n]\Xi[n] \tag{4.57}$$
$$\approx u[n]\Xi[n] \tag{4.58}$$
$$\approx p[n]. \tag{4.59}$$

The equation

$$\hat{a}[n] = u[n] \tag{4.60}$$
$$= |u[n]| \tag{4.61}$$

holds under phase-lock with a noise-free input. In practice, $u[n]$ has an imaginary component due to noise and tracking errors, so it is better to take

$$\hat{a}[n] = \mathrm{Re}\,(u[n]) \tag{4.62}$$

to avoid the nonlinear distortion of Eqn. (4.17).

One advantage of using Eqn. (4.62) in the context of phase-locking is that it rejects the imaginary components of $u[n]$ which are due to noise components which do not exhibit real-valued (i.e., Hermitian-symmetric in the frequency-domain) modulation of the carrier at $f[n]$. In this way it is possible to distinguish the contribution of the real envelope $a[n]$ from random-phase noise.

If $\hat{a}[n]$ is estimated in this way, it enables us to implement very narrowband subtractive analysis for removing $p[n]$ from $z[n]$, effectively performing a phase-locked notch filtering operation.

4.6 Design Considerations on LPF

The form of the low-pass filter **LPF** has not yet been specified in detail. As stated previously, its primary function is to low-pass filter the demodulated signal $\Xi^*[n]\nu[n]$ so that the condition to the Filtered Winding Corollary, Eqn. (2.106), holds. The design of **LPF** involves tradeoffs among such performance issues as computational complexity, tracking lock-in range, signal isolation, phase linearity, and so forth.

One issue is whether **LPF** should be a time-varying filter. A time-varying filter is generally more complex than a time-invariant one. However, a filter with a dynamically adjustable bandwidth could adapt itself to the signal being tracked by having a wide cutoff frequency f_c before frequency lock is achieved, and then after frequency lock is attained its bandwidth could be reduced to the extent that

$$\forall k, \quad \mathrm{BW}_a[k] \leq f_c[k] \tag{4.63}$$

becomes a tight inequality, where we understand $f_c[k]$ to be the "instantaneous cut-off" of **LPF** at time step k. Dynamically altering the filter characteristics may introduce artifacts into the filter output if the changes are made suddenly, however.

A time-varying filter could be realized, for example, with a single-pole filter with a discrete time constant of

$$c[n] = \exp(-2\pi f_c[n]/f_s), \tag{4.64}$$

so that **LPF** is instantiated by

$$u[n+1] = c[n]u[n] + (1 - c[n])d[n], \tag{4.65}$$

for example.

If **LPF** is time-invariant, then we must choose f_c to balance the possible need to have a wide filter bandwidth in order to accommodate a large slew rate $\dot{f}[n]$ and to allow a wide frequency pull-in range on one hand, and a narrow bandwidth for noise rejection and to satisfy Eqn. (4.52) and the conditions for the Filtered Winding Corollaries 2.2 and 2.3 on the other. Evidently, a wide filter bandwidth leads to a wide frequency lock-in range since the algorithm tracks the strongest sinusoidal partial in the passband of **LPF** after demodulation.

4.6.1 LPF Phase Linearity and Group Delay

Additional considerations in the design of **LPF** are the issues of *group delay* and *phase linearity*. The group delay $\delta_{\mathrm{LPF}}(f)$ of a filter **LPF** at frequency f is defined from the phase of the transfer function as [108]

$$\delta_{\mathrm{LPF}}(f) \triangleq \frac{-1}{2\pi} \frac{d \arg\{H_{\mathrm{LPF}}(f)\}}{df}. \tag{4.66}$$

We see that a filter whose transfer function has a phase which is linearly proportional to frequency has a constant group delay across all frequencies. The group delay of a filter at a given frequency f is the number of time steps that a narrow-band wave packet centered at f is delayed after passing through it. Non-linear phase filters will delay wave packets at different frequencies by differing amounts of time.

For the purposes of frequency tracking alone, phase linearity of **LPF** is not a major concern. However, if we wish to remove the target signal by subtractive analysis, phase linearity is desirable for avoiding frequency-dependent group delays. Having a constant group delay facilitates phase alignment between the original and filtered signals, thus allowing the removal of the filtered signal by simple subtraction.

We consider the merits of the two classes of low-pass filters here: IIR filters and linear-phase FIR filters.

IIR Filters Recursive Butterworth filters have the nice property that an N-th order filter H_B^N has

$$\frac{d^k \left| H_B^N(f) \right|^2}{df^k} = 0 \quad \text{for} \quad k \in \{1, \ldots, 2N-1\}, \tag{4.67}$$

and thus the magnitude response is maximally flat near the origin [47]. The Butterworth filter also has a relatively linear phase function near DC. These characteristics make it ideal for constructing a wide adaptive notch filter which can be used to isolate a particular time-varying complex sinusoid. A wider passband is desirable if the tracked signal is amplitude-modulated or frequency-varying so that the signal may be effectively notched out even if the tracking is not perfect.

The Chebyshev Type II digital low-pass filters [105] also exhibit a high degree of smoothness near DC and decent phase-linearity within the pass band. The advantage of the Chebyshev Type II filter over the Butterworth filter is that it requires a smaller filter order to meet the same design specifications, due to the equiripple spreading of the error in the stop band.

FIR Filters An N-th-order FIR filter with conjugate-symmetric coefficients such that

$$h_F[k] = h_F^*[N-k] \quad \text{for} \quad k \in \{0, \ldots, N\} \tag{4.68}$$

has an exactly linear phase response with a group delay of exactly $N/2$ samples. One disadvantage of FIR filters is that, for the same design specifications, an FIR filter will have a longer group delay

than an IIR filter, causing the tracking time constant τ_ℓ to be large. Another disadvantage of FIR filters is that an FIR filter usually requires a large filter order relative to IIR implementations. The computational requirements may therefore be limiting for real-time applications, especially if large arrays of tracking filters are used for cascaded subtractive analysis. Appendix G describes a fast FIR filter implementation which has a computational complexity that is independent of the number of taps, providing phase linearity as well as a significant savings in computational effort.

4.6.2 Tracking in the Presence of LPF Group Delay

The frequency tracking algorithm described in Section 4.2 was given under the assumption that **LPF** had zero group delay for frequencies below the cutoff. In reality, all non-trivial recursive filters have some non-zero group delay $\delta_{\text{LPF}}(0)$ at DC, as defined by Eqn. (4.66). In many cases, digital systems may simulate zero group delay by delaying the rest of the system by δ time steps to allow the filter to catch up. However, in the case of the estimation algorithm given in Section 4.2, due to the recursive dependency of $\hat{f}[n+1]$ on $\hat{f}[n]$, we cannot delay the estimation procedure. Hence, given a constant group delay of $\delta > 0$ time steps, the Eqns. (4.10)-(4.15) become

$$\begin{aligned} u[n] &= h_{\text{LPF}} * d[n] && (4.69)\\ &\approx H_{\text{LPF}}(f[n-\delta] - \hat{f}[n-\delta])a[n-\delta] && (4.70)\\ &\qquad \times \exp\left(j2\pi \sum_{k=1}^{n-\delta} \frac{f[k]-\hat{f}[k]}{f_s} + \zeta[n-\delta] + j\,\phi_0\right) \\ &\approx a[n-\delta]\exp\left(j2\pi \sum_{k=1}^{n-\delta} \frac{f[k]-\hat{f}[k]}{f_s} + j\,\phi_0\right), && (4.71) \end{aligned}$$

again with the assumption of small slew rate $\dot{f}[n]$, condition (4.16), and additionally that the filter has linear phase for frequencies below f_c. As before, we neglect the effect of the phase error $\zeta[n]$.

The estimation equations become

$$\begin{aligned} \hat{f}[n+1] &= \hat{f}[n] + g[n]\frac{f_s}{2\pi}\Delta\phi_u[n] && (4.72)\\ &= \hat{f}[n] + g[n]\frac{f_s}{2\pi}\arg\left(u[n]u^*[n-1]\right) && (4.73)\\ &= \hat{f}[n] + g[n]\varepsilon_f[n] && (4.74)\\ &= \hat{f}[n] - g[n]\hat{f}[n-\delta] + g[n]f[n-\delta] + \eta[n-\delta] && (4.75)\\ &= \hat{f}[n] - g[n]\hat{f}[n-\delta] + g[n]f[n-\delta], && (4.76) \end{aligned}$$

where we account for the group delay with

$$\varepsilon_f[n] = f[n-\delta] - \hat{f}[n-\delta] + \eta[n-\delta]. \tag{4.77}$$

In Eqns. (4.72)-(4.76), we ignore the terms due to $\zeta[n]$, taking into account the discussion in footnote 1 of page 70. Instead of the first-order difference equation in Eqns. (4.31a)-(4.31c), we now have a $(\delta+1)$-th order difference equation in $\hat{f}$. If we assume that $g[n]$ varies slowly, and that $g[n] \approx g$, then the dynamics of the system are determined by the characteristic polynomial

$$\chi_g(z) = z^{\delta+1} - z^\delta + g = 0, \tag{4.78}$$

obtained from the z-transform of Eqn. (4.76). This delayed difference equation introduces δ extra modes into the tracking dynamics. We wish to find the maximum-magnitude root of Eqn. (4.78) in order to ascertain the limits on stability of the system as a function of tracking gain.

Consider the polynomial

$$P_\delta(z) \stackrel{\triangle}{=} z^\delta - z^{\delta+1} \tag{4.79}$$

$$= g - \chi_g(z). \tag{4.80}$$

We see immediately that there is a δ-fold root at $z = 0$ and a single root at $z = 1$. We see, also, that $P_\delta(z) \leq 0$ for real $z \geq 1$. Thus, for $g \leq 0$, $\chi_g(z)$ has a root z with $|z| \geq 1$, and thus the tracking dynamics are unstable. Using Descartes' rule of signs [113], we see that for positive g, $\chi_g(z)$ has two sign changes for real $z > 0$. Thus, the number of positive real roots is either two or zero. For even δ, there is one sign change for $z < 0$, therefore there is exactly one negative real root. Finally, for odd δ and $z < 0$, there are no sign changes so there are no negative real roots of $\chi_g(z)$. For real values of $z \in (0,1)$, $P_\delta(z)$ takes on positive values and has a single local maximum at

$$z_0 = \frac{\delta}{\delta+1}, \tag{4.81}$$

found by setting its derivative equal to zero, giving the local maximum as

$$M_0 = P_\delta(z_0) \tag{4.82}$$

$$= \left(\frac{\delta}{\delta+1}\right)^\delta \frac{1}{\delta+1}. \tag{4.83}$$

When $g = M_0$ we find that $\chi_g(z)$ has a double root at z_0, and thus z_0 is the minimum maximum-magnitude root of $\chi_g(z)$ over all g, i.e.,[4]

$$z_0 = \min_g \max_z \{|z| : \chi_g(z) = 0\}, \tag{4.84}$$

and thus the system is critically damped when $g = M_0$. The corresponding critically damped gain is

$$g^\dagger \stackrel{\triangle}{=} \left(\frac{\delta}{\delta+1}\right)^\delta \frac{1}{(\delta+1)}, \tag{4.85}$$

for which the system is maximally responsive. It is interesting to note that as δ increases,

$$\lim_{\delta\to\infty} \left(\frac{\delta}{\delta+1}\right)^\delta \frac{1}{\delta+1} = \frac{1}{e(\delta+1)}. \tag{4.86}$$

Using the Intermediate Value Theorem, it follows that, for $g \in (0, M_0)$, $\chi_g(z)$ has two distinct real roots z_1 and z_2 such that $z_1 \in (0, z_0)$ and $z_2 \in (z_0, 1)$. For $g > M_0$ the discriminant becomes negative, causing the two positive real roots to disappear and to be replaced by a pair of complex-conjugate roots.

As g increases beyond M_0, the $\delta+1$ complex roots of $\chi_g(z)$ increase in magnitude and eventually leave the unit circle $|z| = 1$. As soon as the first pair of complex roots touches the unit circle, the tracking system becomes unstable. To find the values of c at which the roots touch the unit circle, we assume that

$$z = e^{j\theta} \tag{4.87}$$

[4] A detailed and rigorous proof of this is left as an exercise for the reader. Hint: factor $\chi_{M_0}(z)$ using the double root at z_0.

so that

$$\chi_g(e^{j\theta}) = e^{j(\delta+1)\theta} - e^{j\delta\theta} + g = 0. \tag{4.88}$$

Since g is taken to be real,[5] we see that the imaginary component of (4.88) must be zero:

$$\sin((\delta+1)\theta) - \sin(\delta\theta) = \sin(\delta\theta)\cos(\theta) + \sin(\theta)\cos(\delta\theta) - \sin(\delta\theta) \tag{4.89}$$

$$= 0. \tag{4.90}$$

Collecting terms and using some basic trigonometric identities,

$$(1-\cos(\theta))\sin(\delta\theta) = \cos(\delta\theta)\sin(\theta) \tag{4.91}$$

$$2\sin^2(\theta/2)\sin(\delta\theta) = \cos(\delta\theta)2\sin(\theta/2)\cos(\theta/2) \tag{4.92}$$

$$\sin(\theta/2)\sin(\delta\theta) = \cos(\delta\theta)\cos(\theta/2) \tag{4.93}$$

$$\cos\left(\frac{2\delta+1}{2}\theta\right) = 0, \tag{4.94}$$

where in the (4.93) we have eliminated a factor of $\sin(\theta/2)$ from both sides, yielding $\theta = 0$ as a solution. This corresponds to the case where $z = 1$ and $g = 0$. In Eqn. (4.94) we obtain the solutions

$$\theta_k = \pi\frac{1+2k}{1+2\delta}, \quad k = 0, 1, 2, \ldots \tag{4.95}$$

The values of g which cause a pole-pair to have magnitude one are thus $g = \mathrm{Re}\left\{P_\delta(e^{j\theta_k})\right\}$, namely

$$g = -\cos\left(\frac{\pi(\delta+1)(1+2k)}{1+2\delta}\right) + \cos\left(\frac{\pi\delta(1+2k)}{1+2\delta}\right) \tag{4.96}$$

$$= \cos\left(\frac{\pi\delta(1+2k)}{1+2\delta}\right)\left(1-\cos\left(\frac{\pi(1+2k)}{1+2\delta}\right)\right) \tag{4.97}$$

$$+ \sin\left(\frac{\pi\delta(1+2k)}{1+2\delta}\right)\sin\left(\frac{\pi(1+2k)}{1+2\delta}\right)$$

$$= 2\cos\left(\frac{\pi\delta(1+2k)}{1+2\delta}\right)\sin^2\left(\frac{\pi(1+2k)}{2(1+2\delta)}\right) \tag{4.98}$$

$$+ 2\sin\left(\frac{\pi\delta(1+2k)}{1+2\delta}\right)\sin\left(\frac{\pi(1+2k)}{2(1+2\delta)}\right)\cos\left(\frac{\pi(1+2k)}{2(1+2\delta)}\right)$$

$$= 2\sin\left(\frac{\pi(1+2k)}{2}\right)\sin\left(\frac{\pi(1+2k)}{2(1+2\delta)}\right) \tag{4.99}$$

$$= 2(-1)^k\sin\left(\frac{\pi(1+2k)}{2(1+2\delta)}\right) \tag{4.100}$$

where we have used half-angle identities as well as the angle addition formulae for sine and cosine.

We need to find the smallest positive value M_1 of $g > M_0$ for which a root of $\chi_g(z)$ is on the unit circle because larger values of g yield roots outside the unit circle anyway. Therefore, for values of $g \geq M_1$, there are unstable modes. Since $\sin(x)$ is increasing for $x \in (0, \pi/2)$, we see that $k = 0$ yields the first solution,

$$M_1 \triangleq 2\sin\left(\frac{\pi}{2(1+2\delta)}\right). \tag{4.101}$$

[5] g can certainly be complex, making the analysis more difficult. However, for practical systems we only use real-valued gain.

so that the system is also stable for $g \in (M_0, M_1)$, but the modes are all oscillatory and the system is therefore over-damped.

To summarize, the system is *under-damped* when $g \in (0, M_0)$, *critically damped* when $g = M_0$, *over-damped* when $g \in (M_0, M_1)$, and *unstable* when $g \notin (0, M_1)$.

The exact value of the time constant for arbitrary $g \in (0, M_1)$ must be solved numerically. However, for the critically damped case of $g = M_0$, we know that the dominant mode has a pole at $\delta/(\delta+1)$, as given in Eqn. (4.81). The loop time constant in this case is given by

$$\tau_\ell^\dagger \triangleq -\frac{1}{\log\left(\delta/(\delta+1)\right)} \tag{4.102}$$

$$= \frac{1}{\log(\delta+1) - \log(\delta)} \tag{4.103}$$

$$\approx \delta + \frac{1}{2}, \tag{4.104}$$

in samples, which is what we would intuitively expect, and is the smallest time constant, attained when $g = g^\dagger$.

4.7 Frequency Discriminator

The frequency discriminator used in the algorithm described above uses the 4-quadrant arctangent function to detect the frequency error from the term $u[n]u^*[n-1]$. The nice thing about this particular discriminator is that the dynamical equations for convergence and tracking of $\hat{f}[n]$ become linear difference equations in $\hat{f}$. Other frequency discriminators using a small-angle approximation, or simply a 2-quadrant arctangent discriminator, may be used instead for reasons of computational efficiency or simplicity of implementation in an analog circuit. Conventional discriminators described in [100] and [54] derive their frequency references from the expression

$$\frac{d\phi}{dt} = \mathrm{Im}\left\{\frac{1}{z}\frac{dz}{dt}\right\} \tag{4.105}$$

$$= \frac{y\frac{dx}{dt} - x\frac{dy}{dt}}{x^2 + y^2}, \tag{4.106}$$

where $z = x + jy$. Conventional frequency discriminators usually use just the numerator, saving on the normalization division step. Without the division, the sign of the frequency error is always correct. Some automatic gain control can be used in place of the division. However, in applications where the amplitude of the target signal varies quickly the magnitude of the error signal changes greatly, leading to problems in tracking and convergence; a sudden increase in amplitude of the input signal would cause the frequency correction to overshoot. Hence, without normalization conventional frequency discriminators are unsuitable for applications in audio signal processing.

Other discriminators besides the 4-quadrant arctangent can be used, as long as they are suitably normalized. For example, a discrete-time version of Eqn. (4.105) may be used. However, alternative discriminators do not necessarily save computational steps over an table-reference 4-quadrant arctangent, and furthermore complicate the analysis of convergence greatly.

4.7.1 Downsampled Filtering

By effectively factoring out the FM bandwidth of the signal, the FLL algorithm yields the signal $u[n]$ which is close to DC and has a bandwidth which is limited by the low-pass filter **LPF** . This suggests

that the envelope function is oversampled. Indeed, the computational and storage requirements of the FLL system may be reduced dramatically by decimating the input after the demodulation and LPF stages. The decimation factor may be as high as

$$M = \left\lfloor \frac{f_s}{\mathrm{BW}_{\mathbf{LPF}}} \right\rfloor , \tag{4.107}$$

where $\mathrm{BW}_{\mathbf{LPF}}$ is the bandwidth of the lowpass filter. For example, a reasonable **LPF** bandwidth is 60Hz. With an input rate of 44.1 KHz, the decimation factor is over 700! A more conservative decimation factor, such as about 100-200 may allow for better tracking of changes in the instantaneous frequency trajectory of the target partial.

These calculations reduce directly the number of computations necessary in the frequency update estimation loop. The calculations, such as phase extraction in the $\arg(\cdot)$ function and, as we shall see in the next chapter, the inverse-variance-weighted averaging of fundamental update estimates need not be performed for every sample. Hence, the amount of computation may be reduced drastically.

The demodulated samples $d[n]$ must still be computed at the input sample rate f_s, however. We could either use the last value of $\hat{f}[Mk]$ for $Mk \leq n < M(k+1)$, where k is the frame number, or we could use a linearly extrapolated estimate of $\hat{f}[n]$ using the estimated slew rate for a smoother approximation. Taking the estimated slew into account allows better tracking performance and better FM bandwidth reduction, as discussed in Chapter 3.

4.8 High-Quality Frequency Tracking

In this section, we present a method for calculating a high-quality estimate of the instantaneous frequency, which reaches the Cramér-Rao minimum-variance bound under certain conditions. We implement our high-quality frequency estimator by augmenting the basic frequency tracking algorithm described in Section 4.2.

The basic algorithm does not give an optimal estimate of the instantaneous frequency $f[n]$ of a partial $p[n]$. We see this fact by noting that the optimally weighted phase-difference frequency estimator derived by Kay [75] has a parabolic impulse response.

The tracking loop, however, effectively calculates the instantaneous frequency estimate as an exponentially weighted average of previous frequency samples. To see this, if the gain $g[n]$ is a constant g_0, we have (cf. Eqn. (4.31a))

$$\begin{aligned} \hat{f}[n+1] &= \hat{f}[n] + g_0 \varepsilon_f[n] \\ &= g_\ell \hat{f}[n] + (1 - g_\ell)\left(f[n] + \eta[n]\right) , \end{aligned}$$

where $g_\ell = 1 - g_0$. This may be written as

$$\hat{f}[n+1] = (1 - g_\ell) \sum_{k=1}^{n} g_\ell^{n-k} \left(f[k] + \eta[k]\right) , \tag{4.108}$$

revealing that the estimate is simply an exponentially weighted sum of all the previous samples of $f[k]$, plus terms due to noise.

Because the optimal weighting is parabolic, the exponential weighting of Eqn. (4.108) is statistically suboptimal and cannot achieve the Cramér-Rao bound.

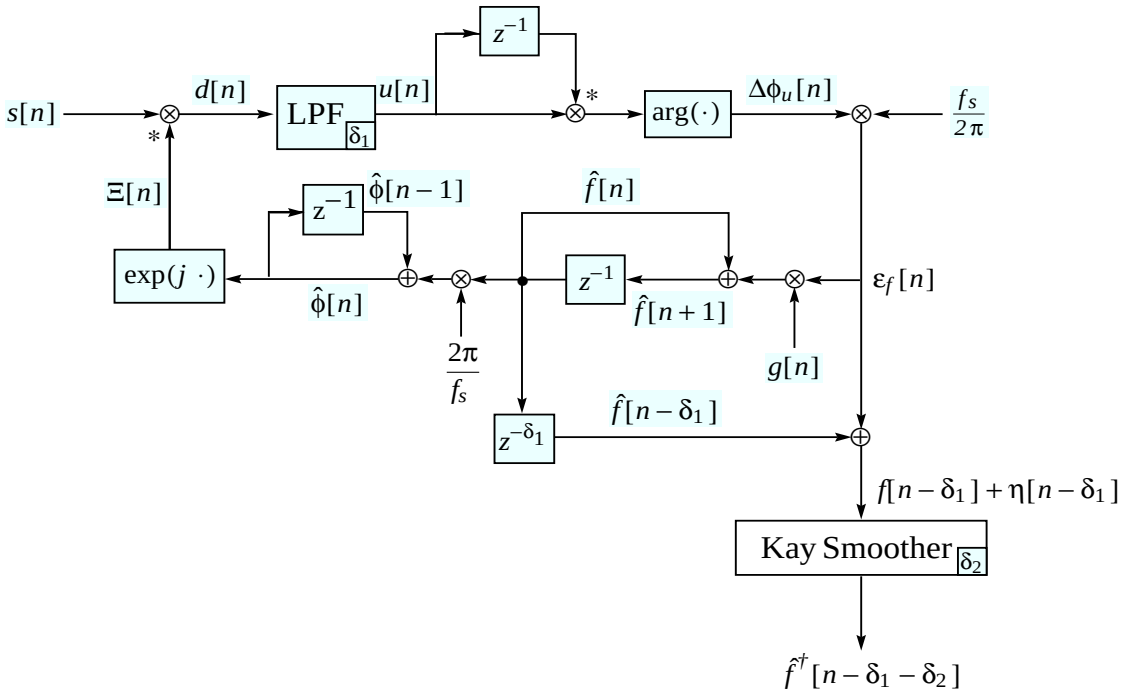

Figure 4.3: High-quality frequency tracker with Kay's optimal phase-difference smoother [75] (cf. Appendix E) outside of the control loop. The group delays δ_1 and δ_2 of the low-pass filter and Kay smoother, respectively, are taken into account. This method has the advantage of not including the group delay of the Kay smoother in the control loop and hence allows a more aggressive range of loop gains.

4.8.1 Minimum-Variance Frequency Tracking and Estimation

We now present a way to take advantage of Kay's optimal phase-difference averaging scheme [75] in the context of our tracking algorithm. The Kay frequency estimator attains the Cramér-Rao bound for the case of a constant-frequency signal in additive, zero-mean complex Gaussian noise with SNR_2 greater than 6 dB.

Figure 4.3 shows an augmented version of the tracker given in Figure 4.1. The basic tracking loop here is identical to that of Figure 4.1. However, a second frequency estimate $\hat{f}^{\dagger}[n]$ is made outside of the loop, based on the "crude" estimates $\hat{f}[n]$ from the first pass and the estimation updates $\varepsilon_f[n]$. The crude estimates are refined using Kay's optimal phase-difference smoother [75]. Since the new estimate is made outside of the loop, the new estimate does not contribute to the tracking dynamics. The discussion in Section 2.3.3.2 assures us that using Kay's weighting coefficients to estimate the average winding rate is a robust procedure, assuming that spurious windings do not occur.

To see how this improved estimator works, we first must take the group delay δ_1 of the low-pass filter **LPF** into account. We recall Eqn. (4.71), which shows that the output of the filter is group delayed by δ_1 samples.[6] After phase differencing, we see that

$$\varepsilon_f[n] = f[n-\delta_1] - \hat{f}[n-\delta_1] + \eta[n-\delta_1], \tag{4.109}$$

[6] In this section, we relabel "δ" of Eqn. (4.71) as "δ_1" since there are several different delays in the system.

where, in this case,

$$\eta[n-\delta_1] = \frac{f_s}{2\pi}(\zeta[n-\delta_1] - \zeta[n-1-\delta_1]). \tag{4.110}$$

The value of $\hat{f}[n-\delta_1]$, is made available via a delay line of length δ, as shown in Figure 4.3. Therefore, we may compute the sum

$$f^\star[n-\delta_1] \stackrel{\triangle}{=} \varepsilon_f[n] + \hat{f}[n-\delta_1] \tag{4.111}$$

$$= f[n-\delta_1] + \eta[n-\delta_1], \tag{4.112}$$

which is effectively the phase difference of the input signal $p[n-\delta_1]$, if it had not been demodulated by $\Xi^*[n-\delta_1]$. We then apply Kay's optimal smoother to the sum. The Kay smoother is simply an FIR filter with quadratic coefficients given by [75]

$$w_{\text{Kay}}[n] = \frac{6N}{N^2-1}\left\{\frac{n}{N} - \left(\frac{n}{N}\right)^2\right\} \tag{4.113}$$

for $1 \leq n \leq N-1$.

If $N = 2\delta_2 + 2$ then we have $2\delta_2 + 1$ phase differences to average. The group delay of the Kay smoother, in this case, is therefore δ_2. We then obtain the smoothed frequency estimate

$$\hat{f}^\dagger[n-\delta_1-\delta_2] = \sum_{k=0}^{N-2} w_{\text{Kay}}[k+1] f^\star[n-\delta_1-k] \tag{4.114}$$

This estimate $\hat{f}^\dagger[n]$ is advantageous in several senses. It attains the Cramér-Rao bound for $N-1$ phase-difference samples for the conditions listed above. Additionally, it is compensated for group delay and has no lag in tracking a linear slew. However, there will be some lag error in using this scheme to estimate the instantaneous frequency if there is non-zero curvature in the instantaneous frequency since the Kay smoother effectively fits a linear regressor to the absolute phase data [75]. Finally, the Kay smoother may be implemented efficiently by the Fast-FIR formulation given in Eqn. (G.120) of Appendix G.

4.9 Parametric Signal Resynthesis

Once the instantaneous amplitude and frequency information for the signal $p[n]$ have been extracted out of a mixture $z[n]$ it may be desirable to resynthesize the estimated signal $\hat{p}[n]$.

Although the relative phase information has been lost in forming the estimated instantaneous frequency $\hat{f}[n]$, we notice that the signals $\Xi[n]$ and $u[n]$ together have sufficient phase information to reconstruct $p[n]$. Ideally, the demodulated signal $d[n]$ would have no phase variation if the input signal were a stationary, pure-frequency sinusoid and tracking were exact. However, with noise and system lags, this ideal performance cannot be met perfectly, and thus the phase of $d[n]$ varies with time. To filter out extraneous noise, $d[n]$ is passed through the filter **LPF** to obtain the filtered envelope signal $u[n]$. This signal is delayed by the group delay δ_1 of **LPF** . Whatever residual frequency mismatch remains between $p[n]$ and the demodulating factor $\Xi[n]$ shows up as a phase-varying component of $u[n]$.

The signal $p[n]$ may then be reconstructed as

$$\hat{p}[n] \stackrel{\triangle}{=} \Xi[n]u[n]. \tag{4.115}$$

The flow diagram for this resynthesizer is shown in Figure 4.4 and is based on the flow diagram in Figure 4.1. A nice feature of this resynthesizer is its simplicity. It does not require anything more than two taps into the existing basic tracking loop and one additional multiply.

There are three obvious disadvantages of this method for reconstructing $p[n]$. One disadvantage is that the signal $u[n]$ is subject to lags due to the group delay δ_1 of **LPF** . If frequency tracking is nearly perfect and the amplitude envelope $a[n]$ is slowly varying, then the bandwidth of $\Xi^*[n]p[n]$ is small, and its time scale of change will be large compared to δ_1. In this case, the resynthesis method shown in Figure 4.4 is adequate for reconstructing $p[n]$. However, if tracking is not perfect, or if the bandwidth of $a[n]$ is large, then the remodulating function $\Xi[n]$ and $u[n]$ will not be synchronized. In the extreme, such asynchrony between the filtered envelope and the remodulator may cause resynthesized acoustical signals to sound noticeably different from the original. Also, even in cases where the incurred phase distortion is imperceptible, this scheme is unsuitable for subtractive analysis, as will be discussed in Section 4.9.1. An easy attempt to correct the group delay problem is simply to add a delay to the remodulator function corresponding to the group delay of the filter **LPF** . In this scheme, the signal $p[n]$ is reconstructed as

$$\hat{p}[n-\delta_1] \stackrel{\triangle}{=} \Xi[n-\delta_1]u[n], \tag{4.116}$$

which is illustrated in Figure 4.5. We note that, for an IIR implementation of **LPF** , the group delay δ_1 is not generally an integer. Hence, we must either choose **LPF** such that δ_1 is an integer or take δ_1 to be the nearest integer to the group delay of **LPF**.

The second disadvantage of the reconstruction method of Eqn. (4.115) is that if **LPF** is not linear-phase, then the group delay is not a constant. This is also a problem in the second method. In our earlier discussions regarding group delay, the given group delay of a filter is the group delay at DC, and it is expected to be relatively constant near DC. However, many signals have envelope bandwidths that are wider than the frequency range in which δ_1 is a valid approximation of the group delay. Additionally, if tracking is not exact then the envelope of the demodulated target signal may have different delays at different times. This non-linear phase distortion also causes problems for subtractive analysis.

One possible solution to this problem is to use a linear-phase filter for **LPF** . However, as mentioned in the discussion on **LPF** in Section 4.6.1, page 77, using a linear-phase filter for **LPF** may introduce excessively long delays in the tracking loop, causing the fastest time constant, i.e., the critically damped time constant $\tau_\ell^\dagger$, defined in Eqn. (4.102), to be large. The effect of having a long tracking delay is to limit the maximum value of the gain g_0 to $g^\dagger$ (cf. Eqn. (4.85)). This, in turn, limits the slew $\dot{f}$ a signal can have and still be tracked, as discussed in Section 4.3.1. The solution to this problem is given together with the solution to the third problem with the reconstruction method of Eqn. (4.115).

The third obvious flaw of the method given by Eqn. (4.115), which is also shared by the second configuration, is that the frequency estimate $\hat{f}[n]$ is not optimal in any sense. A suboptimal estimate of the instantaneous frequency $f[n]$ of $p[n]$ results in a demodulated signal $\Xi^*[n]p[n]$ which does not have all of the FM bandwidth removed. In fact, if there there is significant sample-to-sample tracking jitter, as is the case if the tracking loop is overdamped, then extra FM bandwidth can actually be injected into the demodulated signal $d[n]$, causing the energy of $p[n]$ to be splattered widely away from DC. Of course, the original input signal may be recovered from $d[n]$ by multiplying by $\Xi[n]$, no matter which frequency-warping function $\xi[n]$ is used. However, the energy in $d[n]$ due to $p[n]$ passes most efficiently through the filter **LPF** when $\Xi[n]$ is frequency-matched to $p[n]$, thereby minimizing the bandwidth of the energy due to $p[n]$ in $d[n]$. Therefore, it is best to have the most accurate estimate possible of $f[n]$ if we wish to reconstruct $p[n]$.

The estimation method described in Section 4.8 provides an easy way to obtain an "optimal"

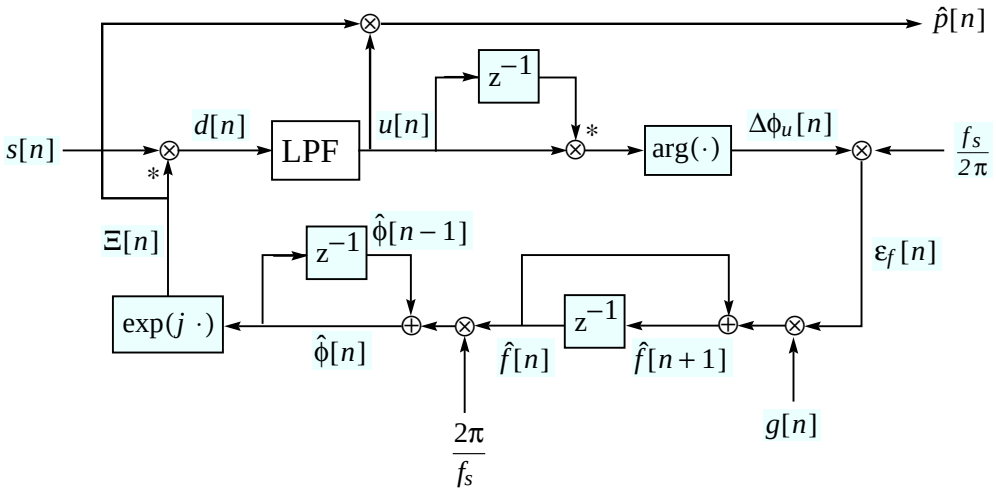

Figure 4.4: Basic resynthesis signal flow. Group delay of **LPF** is assumed to be zero.

frequency estimate which attains the Cramér-Rao bound under certain conditions. The smoothed frequency estimate $\hat{f}^{\dagger}[n]$ is then used to calculate a second frequency warping factor $\Xi^{\dagger}[n]$, which is used to demodulate the original signal, resulting in the signal $d^{\dagger}[n]$. We use a second filter, $\mathbf{LPF}_{\mathrm{R}}$, to low-pass filter $d^{\dagger}[n]$, giving $u^{\dagger}[n]$. Since the filtering is done outside of the tracking loop, long group delays are no longer an issue. Hence, the problems with non-linear phase in **LPF** are sidestepped by implementing $\mathbf{LPF}_{\mathrm{R}}$ as a linear-phase filter. To reduce computational expense, a fast-FIR filter design may be used (cf. Appendix G, [141]). Finally, $\hat{p}^{\dagger}[n]$ is derived by calculating

$$\hat{p}^{\dagger}[n] = \Xi^{\dagger}[n]u^{\dagger}[n]. \tag{4.117}$$

The resynthesis signal flow diagram for the high-resolution frequency estimator is shown in Figure 4.6. We see that group delays have been taken into account by inserting delay lines in the appropriate places in order to time-align the signals.

4.9.1 Subtractive Analysis and Adaptive Notch Filtering

The process of *notch filtering* is used to remove a narrow-band signal component out of a signal. It is an easy matter to remove a partial $p[n]$ from the original source signal, provided that it has been resynthesized, for example, using one of the methods reported above. We illustrate this idea first with the estimate of $\hat{p}[n]$ shown in Figure 4.5. In this formulation, the remodulator $\Xi[n]$ has been compensated for group delay with respect to the envelope $u[n]$. Hence, $\hat{p}[n]$ does not suffer from the asynchronous recombination inherent in Eqn. (4.115).

We simply subtract the signal $\hat{p}[n]$ from the complex input signal $z[n]$ to form the notch-filtered signal

$$\hat{z}^{-}[n] \triangleq z[n] - \hat{p}[n] \tag{4.118}$$

$$\approx z[n] - p[n] \tag{4.119}$$

$$\triangleq z^{-}[n]. \tag{4.120}$$

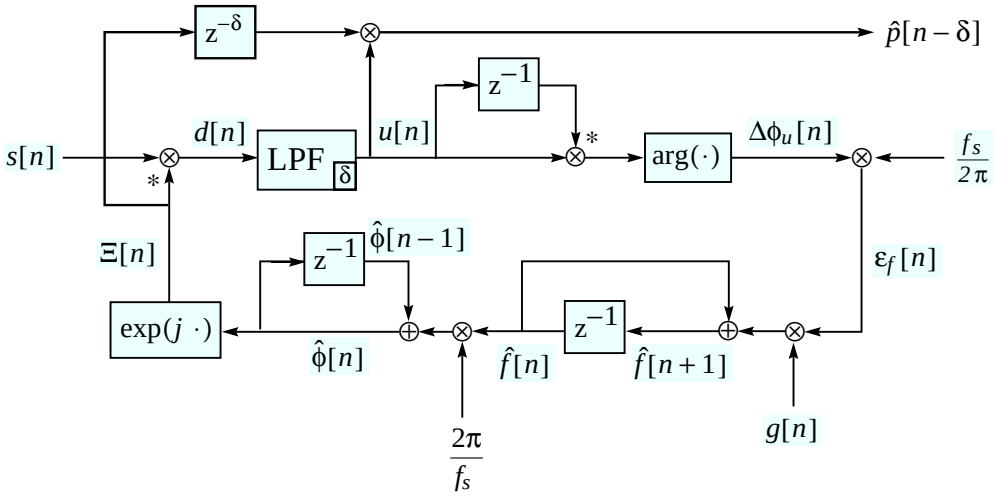

Figure 4.5: Basic resynthesis signal flow, taking the group delay δ of **LPF** into account.

If the input is a real signal $s[n]$, we calculate

$$\hat{s}^-[n] \stackrel{\triangle}{=} s[n] - 2\mathrm{Re}\left\{\hat{p}[n]\right\} \tag{4.121}$$

$$\approx s[n] - 2\mathrm{Re}\left\{p[n]\right\} \tag{4.122}$$

$$\stackrel{\triangle}{=} s^-[n] \tag{4.123}$$

instead of $z^-[n]$. The factor of two comes from the fact that $s[n]$ is composed of two partials, $p_1[n]$ and $p_2[n]$, as discussed in Section 4.4. The basic subtraction scheme is shown in Figure 4.7. Since most audio signals are real-valued, the signal-flow diagram has been drawn to reflect the case for real-valued input.

The approach presented here for notch filtering is a strong alternative to those described in Section 1.2.3.

4.9.1.1 High-Quality Subtractive Analysis

As discussed in the previous section, the estimate $\hat{p}[n]$ of Eqn. (4.116) has some disadvantages, including a suboptimal $f[n]$ estimate and uneven group delay in the envelope extraction, due to **LPF** . Also, the estimate $\hat{p}^\dagger[n]$ given in Eqn. (4.117) is a statistically more efficient estimate of $p[n]$. Finally, since $\mathbf{LPF}_\mathrm{R}$ is linear-phase, we can align the phases perfectly after taking the group delay δ_3 into account. We then calculate the high-quality notch-filtered signal as

$$\hat{z}^{-\dagger}[n] \stackrel{\triangle}{=} z[n] - \hat{p}^\dagger[n]. \tag{4.124}$$

If the input is a real signal $s[n]$, we calculate

$$\hat{s}^{-\dagger}[n] \stackrel{\triangle}{=} s[n] - 2\mathrm{Re}\left\{\hat{p}^\dagger[n]\right\}. \tag{4.125}$$

The signal-flow diagram for calculating $\hat{s}^{-\dagger}[n]$ is given in Figure 4.8.

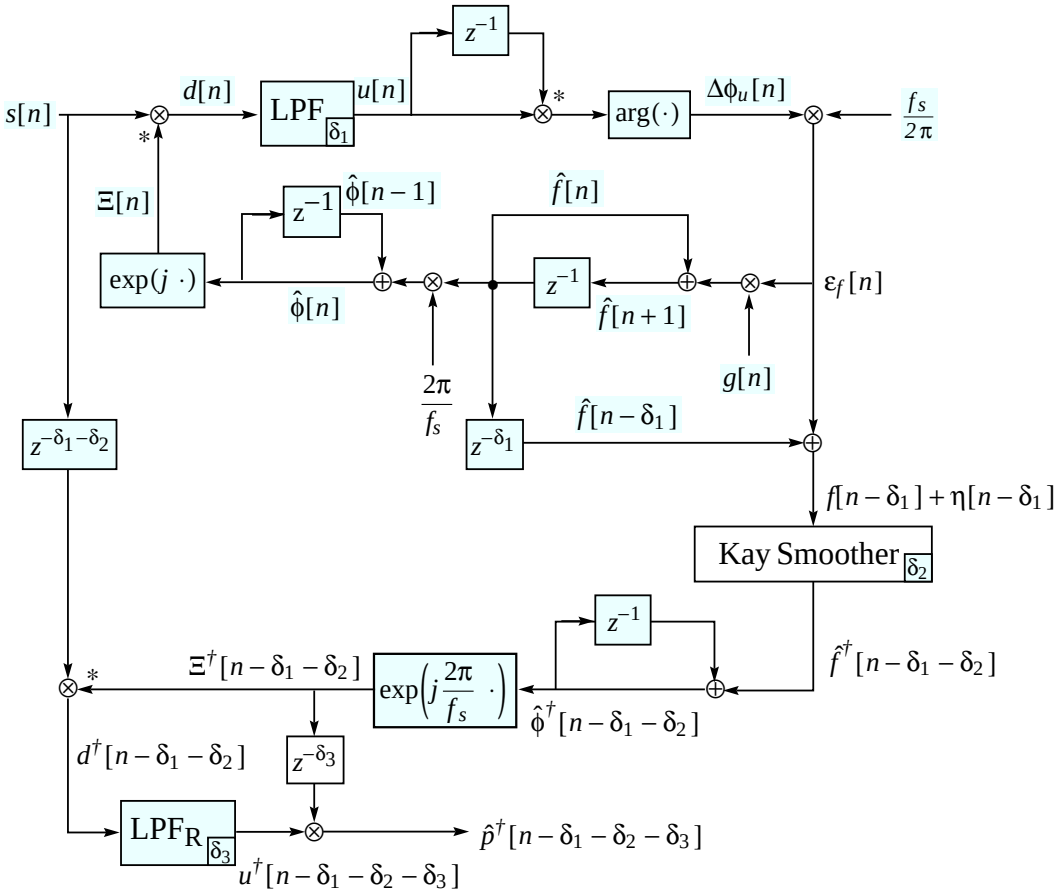

Figure 4.6: Resynthesis flow diagram which takes group delays δ_1, δ_2, and δ_3 into account, and uses the Kay optimal phase-difference smoother, a second demodulating phasor, and a second, linear-phase filter for resynthesis.

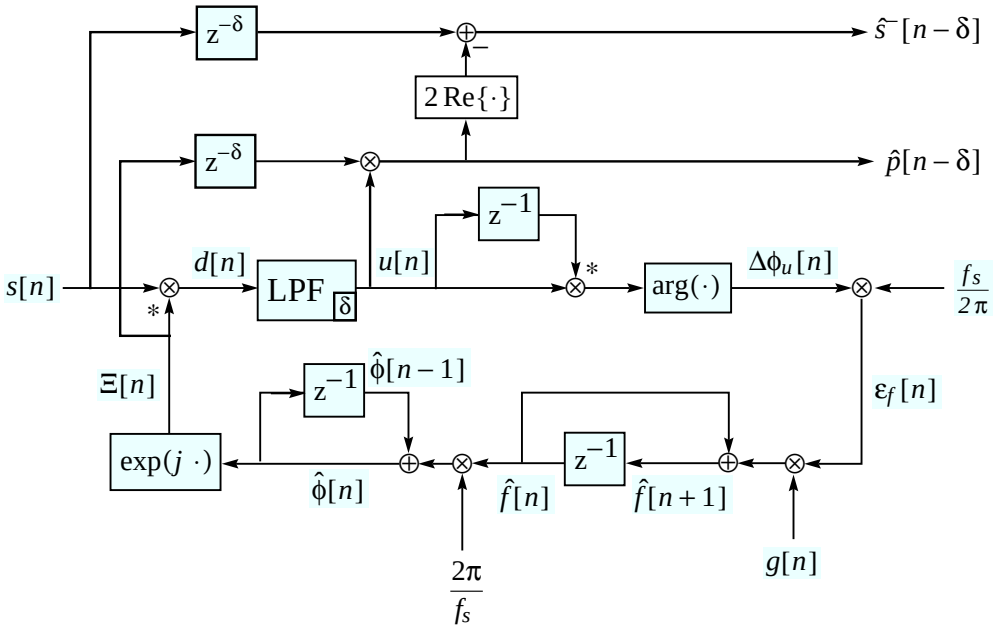

Figure 4.7: Simple method for subtractive analysis.

4.10 Summary

We have seen how to apply the results from Section 2.3 regarding the winding rate of the analytic signal representation of a target partial $p[n]$ to build a novel, complex-valued frequency-locked loop tracker. The tracker forms an estimate of the instantaneous frequency and dynamically frequency-warps the target signal to DC according to that estimate. This tracker gives us the instantaneous frequency estimate necessary to apply the ideas from Chapter 3 for isolating energy due to frequency-varying sinusoids. The algorithm is robust for signals which have a filtered signal-to-noise ratio $\mathrm{SNR}_1 > 1$.

The filtered, demodulated signal may be remodulated to reconstruct the original partial. Phase information is preserved so that the target signal may be removed from the original mixture, in a new formulation of adaptive notch filtering.

We have considered issues such as tracking stability, group delay, and loop filter design. Additionally, we showed how the basic tracking loop could be modified to compute a high-quality estimate of the instantaneous frequency using a statistically efficient smoothing filter due to Kay [75]. This frequency estimate, coupled with fast FIR linear-phase filtering, can be used to calculate a high-quality, computationally inexpensive estimate of $p[n]$, which has many potential applications in commercial digital audio signal processing.

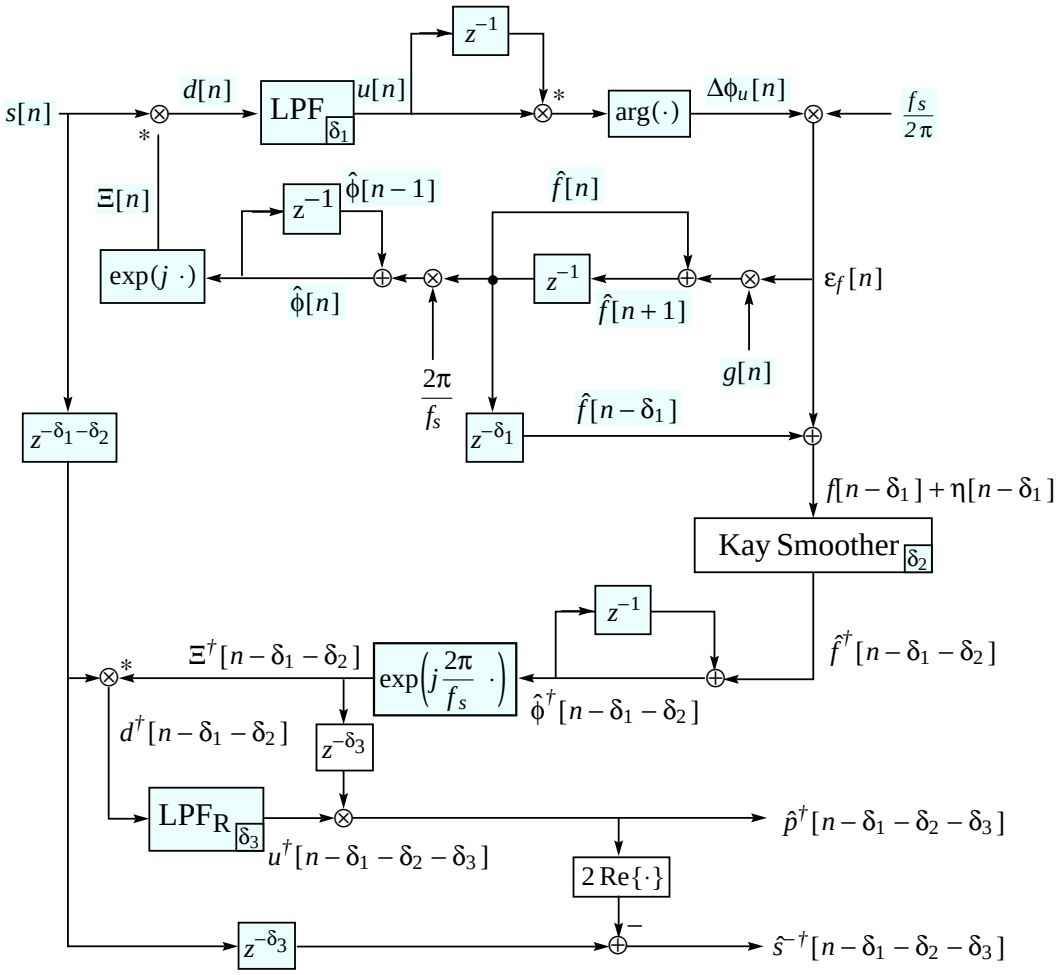

Figure 4.8: Signal flow diagram for high-quality subtractive analysis. All group delays have been taken into account. Optimal frequency smoothing is used. A second, high-quality, linear-phase filter is used for resynthesis.

Chapter 5

Harmonic-Locked Loop Signal Tracking

The frequency-locked loop (FLL) algorithm of the previous chapter performs fast and accurate tracking of the instantaneous frequency of a single target partial in isolation. However, if the signal-to-noise ratio is too large, tracking may break down. Acoustical signals are often composed of complex mixtures of signals which bring the signal-to-noise ratio for target partials down below the level needed for tracking by the FLL method. Hence, for analyzing natural signals, the FLL algorithm is an interesting, but fragile, tool for signal analysis. In this chapter, we find that we may take advantage of the harmonic structure of many natural acoustical signals to increase the robustness of tracking significantly.

A *harmonic signal* $\Gamma[n]$ is the sum

$$\Gamma[n] \stackrel{\triangle}{=} \sum_{k=1}^{M} p_k[n] \tag{5.1}$$

of the members $p_k[n]$ of a *harmonic set* Γ, which is defined to be a set of M harmonic partials $\Gamma = \{p_k[n]\}_{k=1}^{M}$, where each $p_k[n]$ is of the form in Eqn. (2.76) and also has

$$f_k[n] \stackrel{\triangle}{=} k f_0[n]. \tag{5.2}$$

$f_0[n]$ is the *instantaneous fundamental frequency*, or *pitch*, of $\Gamma[n]$.[1] The continuous-time equivalents are self-evident.

The problem, then, is to estimate $f_0[n]$ and the amplitudes $a_k[n]$ for some specified range of n from the signal

$$z[n] = \Gamma[n] + \nu[n], \tag{5.3}$$

where $\nu[n]$ is some unknown signal satisfying certain conditions to be given later.

There are several choices available to us: we may estimate the instantaneous frequency of each harmonic independently and then combine the estimates to form $\hat{f}_0[n]$, or we may constrain the center frequency of each tracker to be the appropriate integer multiple of the estimated $f_0[n]$ while

[1] Some authors prefer to call f_2 the "first harmonic" and in general, "f_k" the "$(k-1)$-th harmonic." We adopt the convention that f_k be called the "k-th harmonic," since it is more convenient. Thus, under our convention, $f_1 \stackrel{\triangle}{=} f_0$ is the "first harmonic."

tracking. We take the latter approach since we may then avoid the difficult problem of having to sort out the individual instantaneous frequency tracks belonging to $\Gamma[n]$ out of a potentially complicated mixture. Also, the constrained $f_0[n]$ estimate is more robust; the tracking variance is reduced by pooling information from several sources, thus incorporating *a priori* knowledge of the harmonic structure.

5.1 Fundamental Frequency Estimation

We take advantage of the information from each tracker by combining each tracker's instantaneous frequency correction term $\varepsilon_{f,k}[n]$ to form a weighted average of the ensemble correction as

$$\hat{\varepsilon}_{f,0}[n] = \sum_{k=1}^{M} w_k[n] \frac{\varepsilon_{f,k}[n]}{k}, \tag{5.4}$$

where the $\varepsilon_{f,k}[n]$ are defined as in Eqn. (4.28) and

$$\sum_{k=1}^{M} w_k[n] = 1. \tag{5.5}$$

There are many possible weighting schemes. A useful scheme is to weight each update estimate by the reciprocal of its ε_f-variance. If we assume that

$$\varepsilon_{f,k}[n] = f_k[n] - \hat{f}_k[n] + \eta_k[n], \tag{5.6}$$

where $\eta_k[n]$ is assumed to have a zero-mean Gaussian distribution of variance $\sigma^2_{\eta,k}[n]$ and is independent across k, but not necessarily across n, then the k-th estimate of the fundamental update is

$$\hat{\varepsilon}^{(k)}_{f,0}[n] \stackrel{\triangle}{=} \varepsilon_{f,k}[n]/k \tag{5.7}$$

$$= f_0[n] - \hat{f}_0[n] + \eta_k[n]/k \tag{5.8}$$

and the maximum-likelihood fundamental frequency update, under the stated assumptions, is

$$\hat{\varepsilon}^{\dagger}_{f,0}[n] = \frac{\sum_{k=1}^{M} \left(k^2/\sigma^2_{\eta,k}[n] \right) \hat{\varepsilon}^{(k)}_{f,0}[n]}{\sum_{k=1}^{M} \left(k^2/\sigma^2_{\eta,k}[n] \right)}. \tag{5.9}$$

We may form the refined updates of the $f_k[n]$ by setting

$$\hat{\varepsilon}^{\dagger}_{f,k}[n] \stackrel{\triangle}{=} k \hat{\varepsilon}^{\dagger}_{f,0}[n]. \tag{5.10}$$

Eqn. (5.9) can be seen to be the maximum-likelihood estimator by maximizing the probability of measuring $\{\varepsilon_{f,1}[n], \ldots, \varepsilon_{f,M}[n]\}$ with respect to $\varepsilon_{f,0}[n]$. Using the assumption that the $\eta_k[n]$ are independent, zero-mean Gaussian random variables across k, we have

$$p\left(\varepsilon_{f,1}[n], \ldots, \varepsilon_{f,M}[n] \middle| \varepsilon_{f,0}[n]\right) = \tag{5.11}$$

$$\frac{1}{(2\pi)^{M/2} \prod_{k=1}^{M} \sigma_{\eta,k}[n]} \exp\left(- \sum_{k=1}^{M} \frac{(\varepsilon_{f,k}[n] - k\varepsilon_{f,0}[n])^2}{2\sigma^2_{\eta,k}[n]} \right).$$

Maximizing this expression is equivalent to finding the minimum of the quadratic sum in Eqn. (5.11) with respect to $\varepsilon_{f,0}$; this is satisfied uniquely when

$$\sum_{k=1}^{M} \frac{k\left(\varepsilon_{f,k}[n] - k\varepsilon_{f,0}[n]\right)}{\sigma^2_{\eta,k}[n]} = 0, \tag{5.12}$$

which is equivalent to $\varepsilon_{f,0}[n] = \hat{\varepsilon}^{\dagger}_{f,0}[n]$ of Eqn. (5.9).

From Eqn. (5.9) and the assumption that the $\hat{\varepsilon}^{(k)}_{f,0}[n]$ are independent across k, we find that the variance of this result is

$$\sigma^2_{\hat{\varepsilon}^{\dagger},0}[n] = \frac{\sum_{k=1}^{M}\left(k^2/\sigma^2_{\eta,k}[n]\right)^2\left(\sigma^2_{\eta,k}[n]/k^2\right)}{\left\{\sum_{k=1}^{M}\left(k^2/\sigma^2_{\eta,k}[n]\right)\right\}^2} \tag{5.13}$$

$$= \left\{\sum_{k=1}^{M}\left(k^2/\sigma^2_{\eta,k}[n]\right)\right\}^{-1} \tag{5.14}$$

$$< \min_k\left\{\sigma^2_{\eta,k}[n]/k^2\right\}. \tag{5.15}$$

The variance of $\hat{\varepsilon}^{\dagger}_{f,k}[n]$ is thus

$$\sigma^2_{\hat{\varepsilon}^{\dagger},k}[n] = k^2\sigma^2_{\hat{\varepsilon}^{\dagger},0}[n] \tag{5.16}$$

$$< k^2 \min_m\left\{\sigma^2_{\eta,m}[n]/m^2\right\} \tag{5.17}$$

$$\leq \sigma^2_{\eta,k}[n], \tag{5.18}$$

where the last inequality may be quite substantial.

Eqns. (5.9) and (5.10) may be used to update the individual frequency trackers, using Eqn. (4.31a), constraining the harmonic frequency estimates to being exact integer multiples of the fundamental. The variance reduction in Eqn. (5.18) yields a powerful algorithm which can track a harmonic signal through interfering noise. All of the harmonic estimators pool their estimates together, sharing their mutual information so that the ensemble $f_0[n]$ update estimate becomes at least as good as the best single-harmonic estimator. Weighting with the reciprocal of the ε_f-error variance is equivalent to weighting by the signal-to-noise ratio SNR_2 for large SNR_2, due to the small-angle approximation (cf. Eqns. (2.130e) and (2.135)).

5.2 Variance Estimation

To use the above results for maximum-likelihood weighted f_0 estimation it is necessary to estimate the variances $\sigma^2_{\eta,1}[n], \ldots, \sigma^2_{\eta,M}[n]$. We realize from Eqn. (4.29) that

$$\eta_k[n] = \frac{f_s}{2\pi}(\zeta[n] - \zeta[n-1]), \tag{5.19}$$

hence the $\eta_k[n]$ are correlated across n. However, the optimality of Eqn. (5.9) only depends on independence across k, and not n. To estimate the variance $\sigma^2_{\eta,k}[n]$ we assume that $\eta_k[n]$ is a stochastic process with slowly-varying parameters, and also that $\hat{f}_k[n] \approx f_k[n]$, giving

$$\eta_k[n] \approx \varepsilon_{f,k}[n], \tag{5.20}$$

We then calculate the variance estimate

$$\widehat{\sigma^2}_{\eta,k}[n] = \overline{\varepsilon^2}_{f,k}[n] \tag{5.21}$$

$$\triangleq \sum_{m=1}^{n} w_{n,k}[m]\varepsilon^2_{f,k}[m] \tag{5.22}$$

$$\approx \langle \varepsilon^2_{f,k}[n] \rangle \tag{5.23}$$

$$\approx \sigma^2{}_{\eta,k}[n], \tag{5.24}$$

where $w_{n,k}[\cdot]$ is some weighting function such that

$$\sum_{m=1}^{n} w_{n,k}[m] = 1. \tag{5.25}$$

Recall that the frequency estimate $\hat{f}[n]$ for a single tracker, as described in Section 4.2, will generally be a weighted sum of terms

$$\hat{f}[n] = \sum_{m=1}^{n} w_n[m] \left[f[m] + \frac{f_s}{2\pi}(\zeta[m] - \zeta[m-1]) \right] \tag{5.26}$$

$$= \sum_{m=1}^{n} w_n[m] \left(f[m] + \eta[m] \right), \tag{5.27}$$

where the specific form of $w_n[m]$ is dependent on the exact smoothing scheme used. For example, Eqn. (4.108) shows an exponentially weighted scheme where

$$w_n[m] = (1 - g_\ell) g_\ell^{n-m} \tag{5.28}$$

$$= g(1-g)^{n-m}, \tag{5.29}$$

and Eqn. (5.25) holds approximately, assuming that the loop gain g_ℓ is a constant. In general, the weighting coefficients are generated by the recursion of Eqn. (4.31c). Therefore, we may use the same difference equation to calculate

$$\overline{\varepsilon^2}_{f,k}[n] = g_{\ell,k}[n]\overline{\varepsilon^2}_{f,k}[n-1] + (1 - g_{\ell,k}[n])\varepsilon^2_{f,k}[n] \tag{5.30}$$

where we allow the loop gain $g_{\ell,k}[n]$ to be time-varying.

The approximation in Eqn. (5.23) does not take into account possible constant offsets in the tracking noise $\eta_k[n]$, due to factors such as interfering partials near a tracker's center frequency. However, we note that if a tracker is tracking a partial in the presence of zero-mean noise, so that $\hat{f}[n] \approx f[n]$, the main contributor to the magnitude of $\varepsilon_f[n]$ is the noise $\eta_k[n]$, rather than the slew, assuming that the frequency $f[n]$ changes relatively slowly with respect to the tracking loop time constant τ_ℓ given in Eqn. (4.33). An unbiased variance estimate would require the calculation of

$$\langle \varepsilon_{f,k}[n] \rangle \approx \bar{\varepsilon}_{f,k}[n] \tag{5.31}$$

$$\triangleq \sum_{m=1}^{n} w_{n,k}[m]\varepsilon_{f,k}[m] \tag{5.32}$$

so that

$$\widehat{\sigma^2}_{\eta,k}[n] = \overline{\varepsilon^2}_{f,k}[n] - \bar{\varepsilon}^2_{f,k}[n], \tag{5.33}$$

reflecting

$$\sigma^2{}_{\eta,k}[n] \triangleq \langle \varepsilon^2{}_{f,k}[n] \rangle - \langle \varepsilon_{f,k}[n] \rangle^2. \tag{5.34}$$

However, this scheme is more complicated than Eqn. (5.22) and even has some disadvantages. We see first that if the noise terms $\eta_k[n]$ are zero-mean, the variance estimates given by Eqns. (5.33) and (5.22) are the same. In this case, using Eqn. (5.22) instead of Eqn. (5.33) makes little difference.

The scheme of Eqn. (5.22) has the feature that if there is a strong interfering partial $p_i[n]$ near a tracked harmonic $p_k[n]$ of a harmonic set Γ , i.e., if

$$|p_i[n]| > |p_k[n]| \tag{5.35}$$

and $f_i[n] - \hat{f}_k[n]$ is within the passband of $\mathbf{LPF}_k$, then the constant pull by $p_i[n]$ on the tracker on $p_k[n]$ causes a large, relatively constant tracking error signal $\varepsilon_{f,k}[n]$ and consequently causes the fundamental update $\hat{\varepsilon}^{(k)}_{f,0}[n]$ to be weighted appropriately low in Eqn. (5.9). The unbiased variance estimate $\widehat{\sigma^2}_{\eta,k}[n]$ of Eqn. (5.33) discounts the DC offset in $\eta_k[n]$ caused by the constant pull and thus causes the fundamental update estimate $\hat{\varepsilon}^{(k)}_{f,0}[n]$ to be weighted too high in Eqn. (5.9), possibly causing derailment of the harmonic tracker ensemble on Γ.

Finally, we note that if $\eta_k[n]$ has a constant, non-zero mean then the assumptions for deriving the maximum-likelihood estimator in Eqn. (5.11) break down. It is then necessary to take the mean of $\eta_k[n]$ into account, but it is impossible to distinguish an offset in $\eta_k[n]$ from the tracking error $f_k[n] - \hat{f}_k[n]$ solely by observing $\varepsilon_{f,k}[n]$.

It seems that there are more advantages to using Eqn. (5.22) than Eqn. (5.33) as the variance estimate. Therefore, we shall use the mean-square error of Eqn. (5.22) as the preferred variance estimate for weighting the fundamental update $\hat{\varepsilon}^{(k)}_{f,0}[n]$.

As the assumptions used in Eqn. (5.11) about the statistics of $\eta_k[n]$ break down, the issues of "optimality" and "maximum-likelihood" begin to get murky and one begins to grasp at theoretical straws to justify computational hacks in one's algorithms.

5.3 LPF Bandwidth ε_f-Variance Saturation

In this section we deal with one of the above-mentioned deficiencies of the noise model due to underestimates in $\eta_k[n]$ due to correlations in $\zeta_k[n]$ (cf. Eqn. (5.19)) across time.

If the input signal's SNR_1 is too low, i.e., if $\mathrm{SNR}_1 \leq 1$, spurious windings begin to occur and the winding count will begin to be dominated by noise, due to the violation of Eqn. (2.95). In this case the winding rate becomes an unreliable estimator of the instantaneous frequency $f[n]$ of a single target partial $p[n]$. However, the variance $\sigma^2_\eta[n]$ of the frequency update $\varepsilon_f[n]$ may be limited by the *bandwidth* of **LPF** rather than by the magnitude of the additive disturbance $\nu[n]$. We may see this by assuming that the input to the system is given by

$$z[n] = p[n] + \nu[n], \tag{5.36}$$

where $\nu[n]$ is zero-mean complex white noise with independent real and imaginary components, variance σ^2_ν, and uncorrelated across n, and

$$p[n] = a[n] \exp\left(\frac{j2\pi}{f_s} \sum_{k=1}^{n} f[n] \right). \tag{5.37}$$

We recall Section 4.2 and assume that we have frequency lock on $p[n]$ so that $\hat{f}[n] = f[n]$. Hence,

$$d[n] = a[n] + \Xi^*_f[n]\nu[n], \tag{5.38}$$

and, assuming that $a[n]$ is a constant a_0,

$$u[n] = a_0 + h_{\text{LPF}} * (\Xi_f^*[n]\nu[n]). \tag{5.39}$$

Define $v[n] \triangleq h_{\text{LPF}} * (\Xi_f^*[n]\nu[n])$. Then

$$u[n]u^*[n-1] = (a_0 + v[n])(a_0 + v^*[n-1]). \tag{5.40}$$

We see that as the signal-to-noise ratio decreases, i.e., as a_0 decreases, the phase of $u[n]u^*[n-1]$ becomes dominated by that of $v[n]v^*[n-1]$. We need to calculate the limiting value of $\langle \arg^2(v[n]v^*[n-1])\rangle$ as a_0 goes to zero. Attempting to derive an exact, closed-form expression for the variance of $\arg(v[n]v^*[n-1])$ proved to be exceptionally difficult, so we must leave it as an open problem for the reader. Intuitively, we may expect that if **LPF** has a rectangular bandwidth BW then the values of $\arg(v[n]v^*[n-1])$ should be distributed approximately uniformly throughout the passband. Hence, we should have

$$\frac{1}{M}\sum_{n=1}^{M} \frac{f_s^2 \arg^2(v[n]v^*[n-1])}{4\pi^2} \approx \frac{1}{\text{BW}} \int_{-\text{BW}/2}^{\text{BW}/2} f^2\, df \tag{5.41}$$

$$= \frac{\text{BW}^2}{12} \tag{5.42}$$

$$\triangleq \sigma^2_{\eta,\text{sat}}. \tag{5.43}$$

For the k-th filter $\mathbf{LPF}_k$ the bound is $\sigma^2_{\eta,k,\text{sat}}$. Simulations show that this expression is approximately correct, with increasing deviations as the filter passband deviates from being rectangular.

If $\sigma^2_{\eta,k}[n]$ is saturated by the bandwidth of $\mathbf{LPF}_k$ then problems arise in the estimation of $\hat{f}_0[n]$ using Eqn. (5.9) because the quality of $\hat{f}_k[n]$ is then overestimated. We see, then, that by filtering the signal to improve the signal-to-noise ratio we end up trading bias for variance, a well-known issue in statistical data analysis [73].

This is especially a problem for higher harmonics, which are often mixed with broad-band noise in audio signals. The weighting given to $\hat{f}_k[n]$ is proportional to $k^2/\sigma^2_{\eta,k}[n]$. Hence, if the estimate $\sigma^2_{\eta,k}[n]$ is underestimated by being saturated at some constant value $\sigma^2_{\eta,k,\text{sat}}$, then the higher harmonics are given an unfairly high weighting. Implicit in the weighting by $k^2/\sigma^2_{\eta,k}[n]$ is that the bandwidth of $\mathbf{LPF}_k$ is not the limiting factor for the magnitude of $\sigma^2_{\eta,k}[n]$. If the unsaturated (unbiased) variance of $\hat{f}_k[n]$ is $\sigma^2_{\eta,k}[n]$, it naturally follows that the fundamental estimate $\hat{f}_k[n]/k$ should have an unbiased variance of $\sigma^2_{\eta,k}[n]/k^2$. However, in the saturated case, it is not known how much of the variance $\sigma^2_{\eta,k}[n]$ was clipped through filtering.

One possible but inelegant way to fix the estimate of Eqn. (5.9) is to limit the weighting of the estimate due to the k-th tracker in cases where the variance $\sigma^2_{\eta,k}$ estimate saturates. Using the bound from Eqn. (5.43), if $\widehat{\sigma^2}_{\eta,k}[n] > \sigma^2_{\eta,k,\text{sat}}/2$ then the tracking variance $\widehat{\sigma^2}_{\eta,k}[n]$ is considered to be close to being saturated by the bandwidth, and is thus underestimated. In this case, the weighting for the k-th estimate is set to a value such as $\{\widehat{\sigma^2}_{\eta,k}[n]\}^{-1}$. Under this scheme, if all the filter bandwidths are the same, the worst estimates will still receive the worst weightings, though the question of whether this scheme is "optimal" in any sense becomes problematic. The estimate of Eqn. (5.9) then becomes

$$\hat{\varepsilon}^{\ddagger}_{f,0}[n] = \frac{\sum_{k=1}^{M} w_k[n](\hat{\varepsilon}^{(k)}_{f,0}[n])}{\sum_{k=1}^{M} w_k[n]}, \tag{5.44}$$

where

$$w_k[n] = \begin{cases} k^2/\widehat{\sigma^2}_{\eta,k}[n], & \text{for } \widehat{\sigma^2}_{\eta,k}[n] < \sigma^2_{\eta,k,\text{sat}}[n]/2 = \text{BW}^2/24 \\ \left\{\widehat{\sigma^2}_{\eta,k}[n]\right\}^{-1}, & \text{otherwise.} \end{cases} \tag{5.45}$$

Any of many equivalent weighting schemes that take into account the phase variance saturation effect of $\mathbf{LPF}_k$ may be used. In further work one may attempt to study further the properties of the phase variation of $\zeta_k[n]$ due to the $\arg(\cdot)$ and multiplicative nonlinearity in order to provide a better weighting scheme with stronger theoretical justification.

5.4 Harmonic Tracker Architecture

The foregoing fundamental estimation may be implemented in a number of ways. We show in this section how some redundancy in the parallel trackers of a harmonic set Γ may be removed for a somewhat more efficient implementation. Recall the basic tracker of Figure 4.1. We notice that if we have an array of such trackers, with the k-th tracker constrained such that $f_k[n] = kf_0[n]$, then the complex exponential is somewhat redundant. We see that for the k-th tracker,

$$\Xi_k[n] = \exp\left(j2\pi \sum_{\ell=1}^{n} f_k[\ell]\right) \tag{5.46}$$

$$= \exp\left(j2\pi k \sum_{\ell=1}^{n} f_0[\ell]\right) \tag{5.47}$$

$$= \Xi_0^k[n]. \tag{5.48}$$

Thus, only one complex exponential needs to be evaluated per step. In a real-time system the complex exponential would probably be implemented by a table lookup, but even so, it is not necessary to calculate $\Xi_k[n]$ for $k > 1$. We see that the k-th demodulated signal may be computed recursively as

$$d_k[n] \stackrel{\triangle}{=} \Xi_k^*[n]s[n] \tag{5.49}$$

$$= \Xi_0^{k*}[n]s[n] \tag{5.50}$$

$$= \Xi_0^*[n]d_{k-1}[n]. \tag{5.51}$$

Additionally, because the frequencies $f_k[n]$ are constrained to multiples of the fundamental, we see it is never necessary to compute $\hat{f}_k[n] = k\hat{f}_0[n]$ explicitly. The output of the k-th phase differencing $\arg(\cdot)$ function is

$$\Delta\phi_{u,k} \stackrel{\triangle}{=} \arg(u_k[n]u_k^*[n-1]) \tag{5.52}$$

$$= \frac{2\pi}{f_s}\left(f_k[n] - \hat{f}_k[n]\right) + \zeta_k[n] - \zeta_k[n-1] \tag{5.53}$$

$$= \frac{2\pi}{f_s}\left(kf_0[n] - \hat{f}_k[n]\right) + \zeta_k[n] - \zeta_k[n-1]. \tag{5.54}$$

We scale the output of the k-th phase differencing $\arg(\cdot)$ function by $2\pi/k$ to scale the update to $f_0[n]$,

$$\varepsilon_{f,k}[n] \stackrel{\triangle}{=} \frac{f_s}{2\pi k}\Delta\phi_{u,k}[n] \tag{5.55}$$

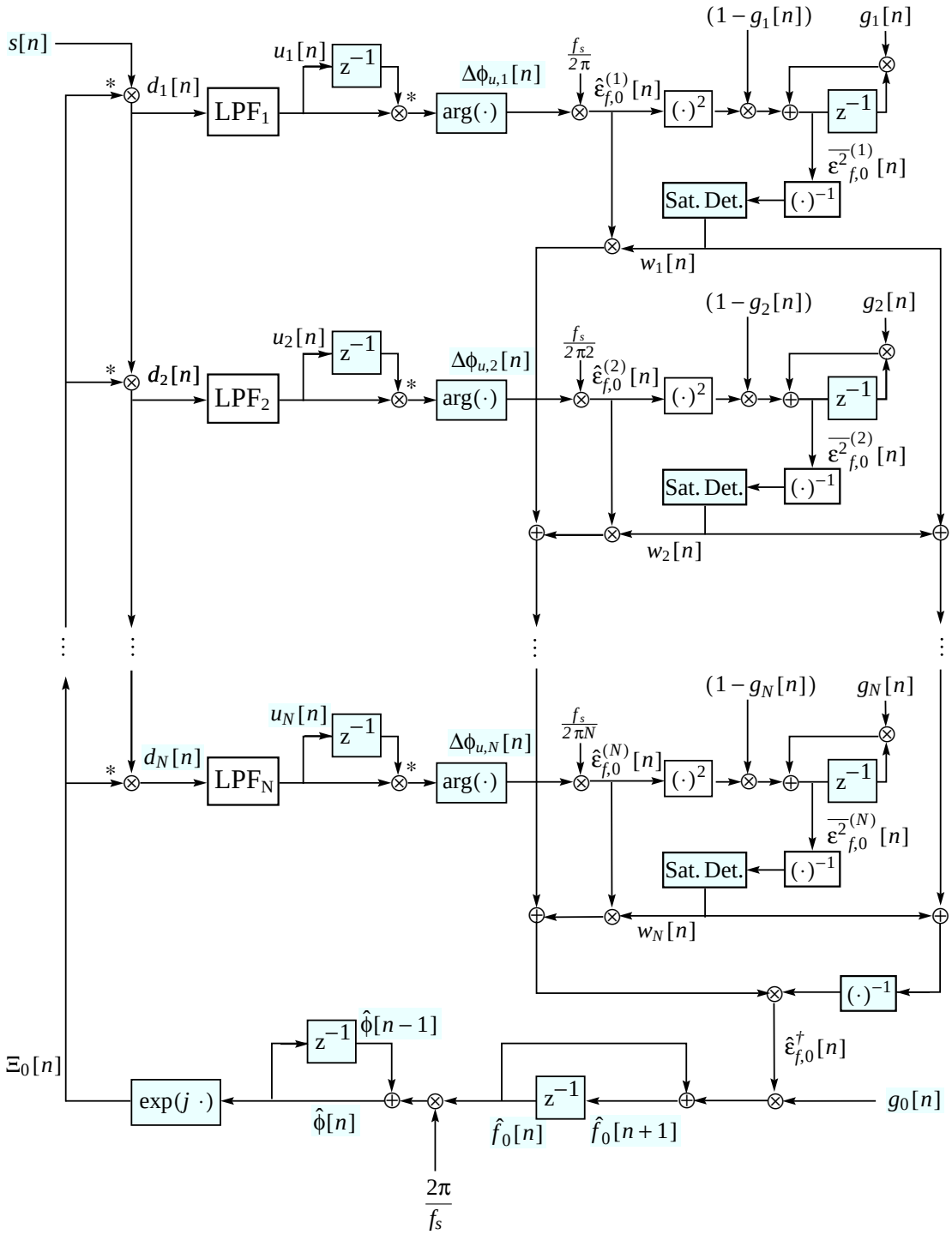

Figure 5.1: Flow diagram for harmonic-locked loop. See text for description.

$$= \frac{f_k[n] - \hat{f}_k[n]}{k} + \frac{f_s}{2\pi k}(\zeta_k[n] - \zeta_k[n-1]) \tag{5.56}$$

$$= f_0[n] - \hat{f}_0[n] + \frac{f_s}{2\pi k}(\zeta_k[n] - \zeta_k[n-1]). \tag{5.57}$$

The variance for the k-th estimator is due to the phase disturbance terms $\zeta_k[n]$ and may be estimated by low-pass filtering the terms $\varepsilon^2_{f,k}[n]$:

$$\widehat{\sigma^2}_{f,k}[n] = g_k[n]\widehat{\sigma^2}_{f,k}[n-1] + (1 - g_k[n])\varepsilon^2_{f,k}[n], \tag{5.58}$$

where $g_k[n]$ is the loop gain for the variance averaging for the k-th harmonic at time n. $g_k[n]$ determines the time constant for the variance filtering

$$\tau_{0,k}[n] = \frac{-1}{\log(g_k[n])}, \tag{5.59}$$

assuming that $g_k[n]$ varies slowly.

In future work it may be desirable to use adjustable weighting to adapt, for example, to transient events and discontinuities; however, for present purposes, we may assume that the $g_k[n]$ are fixed. Since the variance measure should reflect the samples used in calculating the fundamental estimate $\hat{f}_0[n]$, we should use the same weighting function $w_{n,k}[\cdot]$ for averaging the variance as well as the frequency estimates.

The modified signal-flow diagram in Figure 5.1 illustrates the algorithm for tracking the fundamental, incorporating Eqns. (5.9) and (5.10). The schematic is a direct adaptation of Figure 4.1. Alternative schemes may incorporate phase-locking, for example, as in Figure 4.2.

5.5 High-Quality Harmonic Tracking

The tracker architecture used in the previous sections is based on the tracker of Section 4.2. The frequency update estimates provided by this scheme are not optimal, as discussed in Section 4.8. On the other hand, the estimate provided by the enhanced method in Section 4.8 does have some optimality properties, reaching the Cramér-Rao bound for estimating the frequency of a single stationary sinusoid in Gaussian white noise using N signal samples. We may import those results into the harmonic tracking algorithm directly. Referring to Figure 4.3 and Eqn. (4.111), we may form the high-quality estimate of the k-th harmonic as follows: first we calculate

$$f^\star_k[n - \delta_1] = \varepsilon_{f,k}[n] + \hat{f}_k[n - \delta_1] \tag{5.60}$$

$$= \varepsilon_{f,k}[n] + k\hat{f}[n - \delta_1]. \tag{5.61}$$

Next, we use Eqn. (4.114) to form the hiqh-quality smoothed estimate

$$\hat{f}^\dagger_k[n - \delta_1 - \delta_2] = \sum_{k=0}^{N-2} w_{\text{Kay}}[k+1] f^\star_k[n - \delta_1 - k], \tag{5.62}$$

where δ_1 and δ_2 are the delays of **LPF** and the Kay smoother, respectively. At the risk of being redundant, we point out that $N = 2\delta_2 + 2$.

A note should be made here to avert possible confusion between the optimal smoothing described in Section 4.8 and the minimum-variance fundamental frequency estimate described in Section 5.1. The concept of "minimum variance" is always relative to a specific parametric model of a signal. If

one chooses a bad model for the data, the minimum-variance estimate of the model parameters for a given data set may not be useful because the model may be badly chosen in the first place. Hence, one should always be wary when encountering the term "minimum variance."

In our case, there are two somewhat independent dimensions in which "minimum variance" estimates may be made of the frequency of a signal. The first, used in Section 4.8, finds the minimum-variance frequency estimate from a block of $N-1$ phase differences. In the present context, this estimate is taken for a single harmonic, as seen in Eqn. (5.62). The second occurrence of the term "minimum variance" is in the context of combining M independent fundamental frequency updates estimates to form a robust estimate, as seen in Eqn. (5.9). The first frequency estimate is based on averaging phase differences across *time* in a narrow frequency range. The second estimate averages across *frequency* across a single time frame in order to derive the fundamental.

In order to combine the two "minimum-variance" estimates, we may take the result of Eqn. (5.62) and use the weighting scheme of Eqn. (5.9) to obtain the minimum-variance estimate of the fundamental frequency

$$\hat{f}_0^\dagger[n-\delta_1-\delta_2] = \frac{\sum_{k=1}^M \left(k^2/\sigma_{\eta,k}^2[n]\right) \hat{f}_k^\dagger[n-\delta_1-\delta_2]/k}{\sum_{k=1}^M \left(k^2/\sigma_{\eta,k}^2[n]\right)} \tag{5.63}$$

$$= \frac{\sum_{k=1}^M \left(k^2/\sigma_{\eta,k}^2[n]\right) \frac{1}{k}\sum_{\ell=0}^{N-2} w_{\text{Kay}}[\ell+1] f_k^\star[n-\delta_1-\ell]}{\sum_{k=1}^M \left(k^2/\sigma_{\eta,k}^2[n]\right)} \tag{5.64}$$

$$= \frac{\sum_{k=1}^M \left(k^2/\sigma_{\eta,k}^2[n]\right) \frac{1}{k}\sum_{\ell=0}^{N-2} w_{\text{Kay}}[\ell+1] (\hat{f}_k[n-\delta_1-\ell] + \varepsilon_{f,k}[n-\ell])}{\sum_{k=1}^M \left(k^2/\sigma_{\eta,k}^2[n]\right)} \tag{5.65}$$

$$= \sum_{\ell=0}^{N-2} w_{\text{Kay}}[\ell+1] \left(\hat{f}_0[n-\delta_1-\ell] + \hat{\varepsilon}_{f,0}^\dagger[n-\ell]\right). \tag{5.66}$$

We have commuted the phase-difference smoothing to the outer summation, leaving us with familiar quantities on the inside. Note that this estimate is done outside of the tracking loop so that it does not affect the tracking dynamics.

As we observed in the Section 4.8.1, the Kay smoother may be implemented efficiently by the Fast-FIR formulation given in Eqn. (G.120) of Appendix G. The resulting high-quality, low-cost fundamental frequency estimate obtained in Eqn. (5.66) may be used in any of the applications where a high-resolution pitch estimate is desirable.

5.6 Inharmonic Tracking

The assumption of harmonic structure is a powerful guide for tracking and encompasses many kinds of signals. However, there are many signals which have well-defined partials that are not harmonically related. Pianos, for example, have stretched partials such that the k-th partial is greater than the k times the fundamental frequency [15].

The harmonic constraint of Eqn. (5.2) sets up a template for the frequency relationship between the k-th partial and the fundamental $f_0[n]$. This template may be changed so as to reflect *inharmonic* partials as well as harmonic partials. Thus, instead of Eqn. (5.2), we could use the *inharmonic constraint*

$$f_k[n] \stackrel{\triangle}{=} \varpi(k) f_0[n], \tag{5.67}$$

where $\varpi(k)$ is the constant inharmonic ratio between the k-th partial and the fundamental. The signal with these frequency relations is then

$$\Lambda[n] \triangleq \sum_{k=1}^{M} p_k[n], \tag{5.68}$$

where $p_k[n]$ has instantaneous frequency $f_k[n]$ given by Eqn. (5.67). There are no major differences in the dynamics for tracking $\Lambda[n]$ using the dynamics and maximum-likelihood combined fundamental updates described for the harmonic case. We simply use Eqn. (5.67) to update the $f_k[n]$, but we must calculate each $\Xi_k[n]$ explicitly since we may no longer use the recursion of Eqns. (5.49)-(5.51), due to the non-integer ratios of $f_k[n]$ to the fundamental. Additionally, $\varepsilon_{f,k}[n]$ and the associated variance estimates must be scaled appropriately to reflect Eqn. (5.67).

If the frequency relation among partials of an inharmonic set Λ depends on the fundamental as well, we may modify Eqn. (5.67) to

$$f_k[n] \triangleq \varpi(f_0[n], k) f_0[n] \tag{5.69}$$

to reflect this dependence. In this case, $\varpi(f_0[n], k)$ must be stored as a table somewhere, or computed analytically on demand. The inharmonic tracking dynamics of the frequency-dependent $\varpi(f_0[n], k)$ are virtually identical to those of the fixed-ratio case $\varpi(k)$.

5.7 Tracking Multiple Harmonic Signals

The Harmonic-Locked Loop algorithm can be used to track multiple harmonic signals in a mixture. Its use of information distributed across a broad range of frequencies through time to minimize the variance of the fundamental causes it to be quite robust in the presence of interfering signals. For example, if a noise source interferes with a subset of the harmonics being tracked, those obscured harmonics will have a low signal-to-noise ratio and thus receive low weighting. The remaining harmonics with no interference will have higher signal-to-noise ratios and be weighted accordingly. We recall from Eqns. (5.13)-(5.18) that the ensemble estimate is at least as good as the best single estimate.[2]

The Crossing Ambiguity Problem When the instantaneous frequencies $f_1[n]$ and $f_2[n]$ of two partials $p_1[n]$ and $p_2[n]$ cross, their frequency tracks may become ambiguous. For example, if $f_1[n]$ decreases while $f_2[n]$ increases and they intersect at some time n_i such that $f_1[n_i - k] > f_2[n_i - k]$ for $k \geq 1$ and $f_1[n_i + k] < f_2[n_i + k]$ for $k \geq 0$ then if we only observe the frequency tracks it is ambiguous if the tracks are actually $\{f_1[n], f_2[n]\}$ or $\{f_1'[n], f_2'[n]\}$ where

$$f_i'[k] = \begin{cases} f_i[k], & k \leq n_i \\ f_{1-i}[k], & \text{otherwise} \end{cases} . \tag{5.70}$$

In the single-partial tracking system with no slew guidance, two trackers, locked onto $p_1[n]$ and $p_2[n]$ respectively, will both have a tendency to lock onto the higher-amplitude partial when they cross. If the two partials have similar amplitudes then the outcome of the intersection (out of four possibilities) is random. As the two partial approach the crossing point, each signal enters into the band-pass region of the other tracker's low-pass filter. The winding count becomes highly perturbed as the instantaneous frequency calculated from the phase difference undergoes large oscillations, as

[2] with equality if there is only one estimate used in the averaging

discussed in Section 2.1.1.1 and shown by Eqn. (2.18). Averaging the phase difference, as treated in Section 2.3.1 helps greatly, but the competition between very close partials of similar magnitude causes the variances of the phase error $\sigma^2_{\zeta,1}[n]$ and $\sigma^2_{\zeta,2}[n]$ to become rather large. This may be seen in Figure 5.3. Notice that the tracking variance increases near the point of intersection. After crossing, the trackers have exchanged identities giving rise to a "bounce".

It is worthwhile to point out that the human auditory system also has problems distinguishing the two possibilities for perceiving crossing time-varying sinusoids. Bregman [23, p. 364] and Tougas [136] show that the crossing of two pure partials is heard as the "bouncing" signal model of Eqn. (5.70) rather than as crossing partials. Figure 5.2 illustrates this problem. Of the four panels, only (C) gives rise to the crossed percept. It is thought that the difference in timbre facilitates grouping of the parallel harmonic tracks and leaves the single track in its own auditory group.

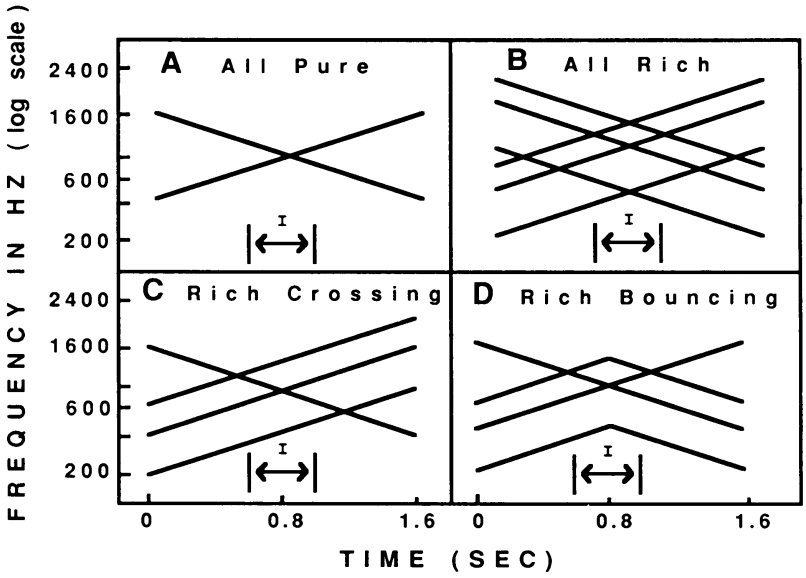

Figure 5.2: The four glide patterns (A-D) used by Tougas and Bregman [136]. Interval I could be filled by glides (as shown), noise, or silence. Used with permission from Bregman [23, Figure 3.28, p. 364], ©1990 MIT Press.

There are several ways to overcome the crossing ambiguity problem. One possibility is to use a slew estimate with second-order tracking dynamics. In this case a slew estimate would provide "inertia" to push two trackers past the point of intersection so they can continue along their proper tracks. Wolcin [147], for example, has used a second-order Markov model incorporating the second difference to provide "inertia" in the short-time FFT peak estimate going from bin to bin. This assumes that the slew rate is a Gaussian random variable centered on its previous value.

5.7.1 Harmonic-Locked Loop Tracking of Multiple Harmonics

Another way to solve the crossing ambiguity problem is to use the harmonic assumption: that the signal being tracked is a member of a harmonic signal. Intuitively, the shared tracking information among member harmonics can resolve the ambiguity as long as there are member harmonics that do not all simultaneously cross. Suppose we have two harmonic signals $\Gamma_1[n]$ and $\Gamma_2[n]$ with instantaneous fundamental frequencies $f_{0,1}[n]$ and $f_{0,2}[n]$, respectively. Suppose that a harmonic from one

set crosses one of the other, i.e.

$$f_{k_1,1}[n_i] = f_{k_2,2}[n_i], \tag{5.71}$$

or equivalently,

$$k_1 f_{0,1}[n_i] = k_2 f_{0,2}[n_i], \tag{5.72}$$

for some some *relatively prime* harmonic numbers k_1 and k_2 respectively and for some time step n_i. Then the harmonic sets Γ_1 and Γ_2 intersect infinitely many times at time n_i, but only at integer multiples of $k_1 f_{0,1}$.[3] To see this result, if it is not already apparent, suppose that for some positive integers m_1 and m_2 that

$$m_1 f_{0,1}[n_i] = m_2 f_{0,2}[n_i].$$

Then from Eqn. (5.72),

$$m_1 = \frac{m_2 k_1}{k_2} \tag{5.73}$$

so that

$$m_1 f_{0,1}[n_i] = \frac{m_2 k_1}{k_2} f_{0,1}[n_i]. \tag{5.74}$$

But, since k_1 and k_2 are relatively prime, it follows that

$$\frac{m_2}{k_2}$$

must be an integer, and hence $m_1 f_{0,1}[n_i]$ is an integral multiple of $k_1 f_{0,1}[n_i]$, and so is $m_2 f_{0,2}[n_i]$.

Hence, for integers $m \not\equiv 0 \pmod{k_1}$, the partial $p_{m,1}[n_i]$ is not a member of Γ_2. Similarly, for integers $m \not\equiv 0 \pmod{k_2}$, we see that $p_{m,2}[n_i] \notin \Gamma_1$.

If we assume that the non-intersecting harmonics from each set are being tracked robustly by the algorithm then their variances will be low. On the other hand, as shown empirically above, when two trackers cross their tracking variances increase due to the tracking ambiguity. Hence, using Eqns. (5.9) and (5.10), as our fundamental frequency updates, we see that $\hat{f}_{0,1}[n]$ and $\hat{f}_{0,2}[n]$, and hence $\hat{f}_{k,1}[n]$ and $\hat{f}_{k,2}[n]$, respectively, will be weighted towards the correct value. The larger the value of k_1 is the more robust the estimate $\hat{f}_{0,1}[n]$ because of the greater proportion of non-intersecting harmonics.

If, on the other hand, a pair of harmonics intersects for some pair of integers k_1 and k_2 such that $k_1 | k_2$, then all of the harmonics of Γ_2 will be subsumed into Γ_1, i.e.,

$$\Gamma_2 \subset \Gamma_1,$$

at time n_i. This is known as the *harmonic crossing ambiguity problem.*

In speech processing, in order for this problem to occur with two voices, either the two voices must cross at the fundamental or one voice would have to be at least an octave higher than the other.

The harmonic crossing ambiguity may not be as bad as it seems; if *the power distribution among the harmonics of each harmonic set,* Γ_1 *and* Γ_2*, are sufficiently different at the crossing frequencies,* then the ambiguity may be resolved. In other words, if Γ_1 has strong harmonics where Γ_2 has weak ones, *and vice versa,* then the signal-to-noise ratios of some subsets of each harmonic set will be different coming into the intersection. The weaker partial, say $p_1[n]$ coming into a given intersection will be overwhelmed by the stronger partial, say $p_2[n]$, and hence variance of the tracker on $p_1[n]$

[3] Of course, we know that the highest harmonic is bound by the sampling rate, but this makes little difference in our argument.

will be high, and thus its weighted contribution to its ensemble fundamental frequency estimate will be low. Conversely, if the stronger partial $p_2[n]$ satisfies the $\mathcal{M}_1$-condition

$$|p_2[n]| > |p_1[n]| + |\nu[n]| \tag{5.75}$$

where $\nu[n]$ is some unaccounted-for signals, such as noise, then according to the Winding Theorem (2.2), the tracking estimator for $p_2[n]$ will be robust, and hence have small variance. Thus $p_2[n]$ would be weighted strongly in its harmonic set Γ_2.

As long as each harmonic set has some member harmonics that are stronger than their intersecting counterparts, both harmonic sets will be track properly through a harmonic intersection. For example, even if two voices crossed their fundamental frequencies at some point, if the *formants* are different, i.e., if one person is producing a frequency-varying "\ü\" vowel, as in "loot," and the other person is saying "\ē\," as in "eat," then, as long as the two fundamental frequencies do not evolve in parallel, the temporary intersection presents no problems! However, problems do arise when these conditions are violated, e.g. either when one harmonic sound source subsumes the harmonics of another over a time interval of non-zero length, or when two intersecting harmonic signals do not have significantly differing formant profiles. Preliminary simulations seem to indicate that even vibrato at the same pitch provides enough of a distinguishing difference to separate two voices.

Some extensions to our harmonic tracking algorithm could incorporate some form of "inertia" for guiding tracking. If slew were incorporated into the single-partial tracking dynamics then the system could track trends in the instantaneous frequency of a the target partial being tracked. The work by Wolcin [147], for example, incorporates knowledge about the slew into the tracking dynamics by assuming that the slew is distributed as a zero-mean Gaussian process. In this context, the addition of slew to the tracking dynamics could then provide the extra "push" needed to get a tracker past an ambiguous intersection of partials. However, accounting for slew in the dynamics may result in overshoot in cases where the slew is changing with time, i.e., if the instantaneous frequency track has non-zero curvature, as is the case with vibrato.

5.8 Harmonic Resynthesis

Resynthesizing an extracted harmonic signal $\Gamma[n]$ is straightforward once its parameters $f_0[n]$ and $\{a_k[n]\}_{k=1}^N$, have been extracted. We simply use one of the procedures listed in Section 4.9 for the resynthesis of a single partial, applying it to each partial $p_k[n]$ in the harmonic set Γ with the understanding that $\hat{f}_k[n] = k\hat{f}_0[n]$. The estimate of the harmonic signal is simply

$$\hat{\Gamma}[n] = \sum_{k=1}^{N} \hat{p}_k[n]. \tag{5.76}$$

As was seen in Section 4.9, this estimation can be done on-line, given sufficient computational power.

5.8.1 Adaptive Harmonic Notch Filtering

Removing the harmonic signal $\Gamma[n]$ from the original input signal $z[n]$ is a straightforward matter, once $\hat{\Gamma}[n]$ has been identified. We follow the discussion in Section 4.9.1 and form

$$\hat{z}^{=}[n] \stackrel{\triangle}{=} z[n] - \hat{\Gamma}[n] \tag{5.77}$$

$$\approx z[n] - \Gamma[n] \tag{5.78}$$

$$\stackrel{\triangle}{=} z^{=}[n]. \tag{5.79}$$

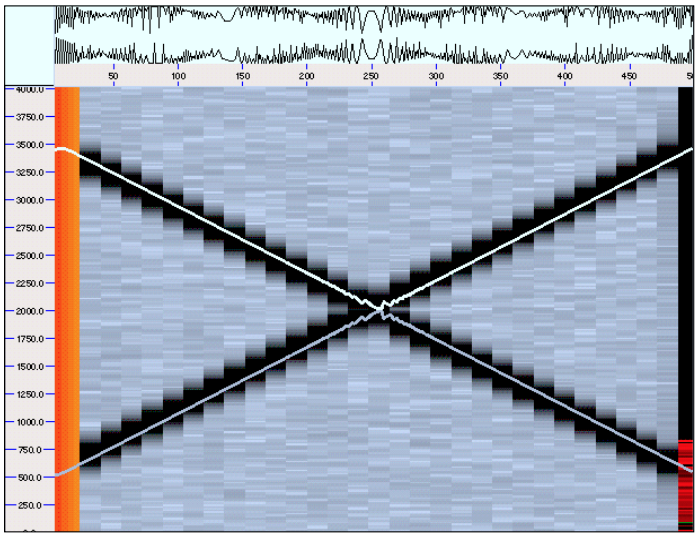

(a)

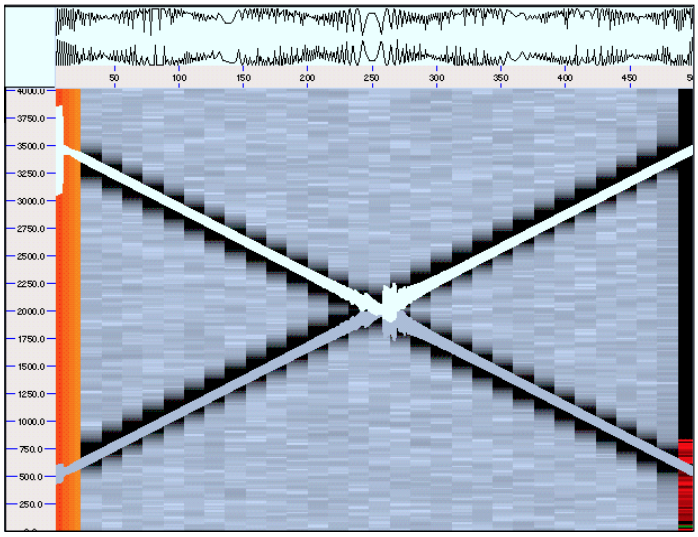

(b)

Figure 5.3: Result of equal-amplitude partials crossing. The two single FLL trackers are initialized to the partials' starting frequencies of 500 Hz and 3500 Hz. The partials have a frequency slew rate of ±6000 Hz/sec and equal amplitude. The results of the collision are drawn **(a)** without variance and **(b)** with vertical thickness proportional to the standard deviation. The background is a short-time Fourier spectrogram; the trackers are drawn in grey and white. The result is that each tracker "bounces."

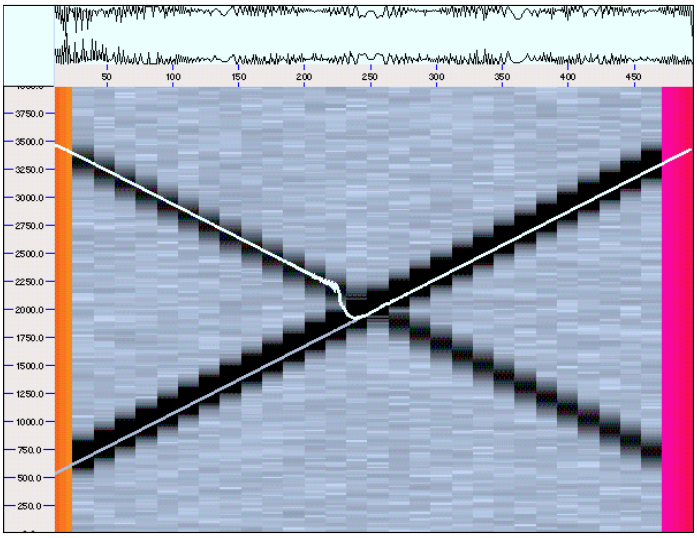

(a)

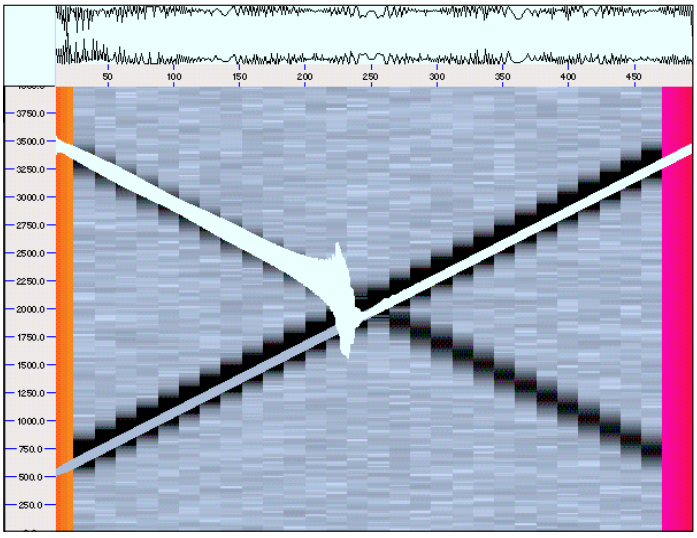

(b)

Figure 5.4: Result of unequal-amplitude partials crossing. Same signal parameters as in Figure 5.3, except that the upwardly slewing partial has amplitude 1.0 and the downwardly slewing partial has amplitude 0.2. The stronger partial captures both trackers and its tracker has almost no change in its direction and tracking variance, while the tracker initially on the weaker partial becomes unstable and is captured by the stronger partial. Notice how its variance grows drastically as it loses tracking on its own signal and is pulled away by the stronger partial.

Here, the superscript "=" is used to make a distinction from the case of single partial subtraction in Section 4.9.1, which uses the superscript "−."

The harmonic notch filtering algorithm described here is a novel and fast technique that should be compared against adaptive comb filters as described by Nehorai [103] and others.

5.9 Summary

In this chapter, we saw how to extend the algorithm of the previous chapter to be able to track harmonic signals. An array of frequency trackers of the kind described in Section 4.2 is constrained so as to track the frequencies of the harmonic set Γ. By using *a priori* information about the frequency relation among partials in a harmonic signal $\Gamma[n]$, we are able to form a robust estimate of the update $\varepsilon_{f,0}[n]$ of the fundamental frequency by pooling together information from each of the trackers. This estimate is better than the best single estimate among the array of trackers. The high-quality fundamental frequency estimate is then fed back to the trackers using the harmonic constraint to guide their tracking. Hence, every tracker benefits from the pooled information. Tracking performance is fast and robust, tolerating a large frequency modulation. A high-quality fundamental frequency estimate may also be calculated efficiently by using Kay's optimal phase-difference smoothing coefficients.

Additionally, inharmonic partials may also be tracked by using known, inharmonic constraints instead of the usual integer-multiple constraint.

The individual harmonics may be resynthesized and added together to form an estimate $\hat{\Gamma}[n]$ of the target harmonic signal. Since phase is preserved, this signal may be subtracted from the original signal to remove it.

Chapter 6

Conclusions

In this chapter, we discuss some results and applications of the ideas contained in the previous chapters.

6.1 Analysis Results

Figures 6.1 through 6.6 show the some examples of voice separation using the Harmonic-Locked Loop algorithm of Chapter 5. The algorithm is reasonably fast; it takes about 150 seconds to process 22 seconds of a 44.1 KHz sampled sound file with 8 harmonic trackers on a 90 MHz Pentium-based computer running NeXTStep. As discussed in Section 4.7.1, a generous amount of decimation can help speed up the algorithm by several orders of magnitude. Also, the algorithm was written in unoptimized C++ where no attempt was made to handle the special case of the Harmonic-Locked Loop.

6.2 Sound Examples

Sound examples illustrating a simple application of the ideas contained in this thesis are available for anonymous FTP from CCRMA. The site and directory are

`ccrma-ftp:/pub/Publications/Theses/AveryWangThesis/sound_demos`.

The exact composition of the example files in this directory are subject to change, due to ongoing improvements in the algorithms. The current contents are documented here.

These sounds are in 44.1KHz, 16-bit, mono NeXT snd format.

- baritone.diff.snd
- baritone.isolated.snd
- baritone.orig.snd

This is a 4.1 second segment of a baritone and orchestra from the "Barber of Seville". The voice and orchestra have been separated from each other. The algorithm does well on vibrato.

- soprano.diff.snd
- soprano.isolated.snd
- soprano.orig.snd

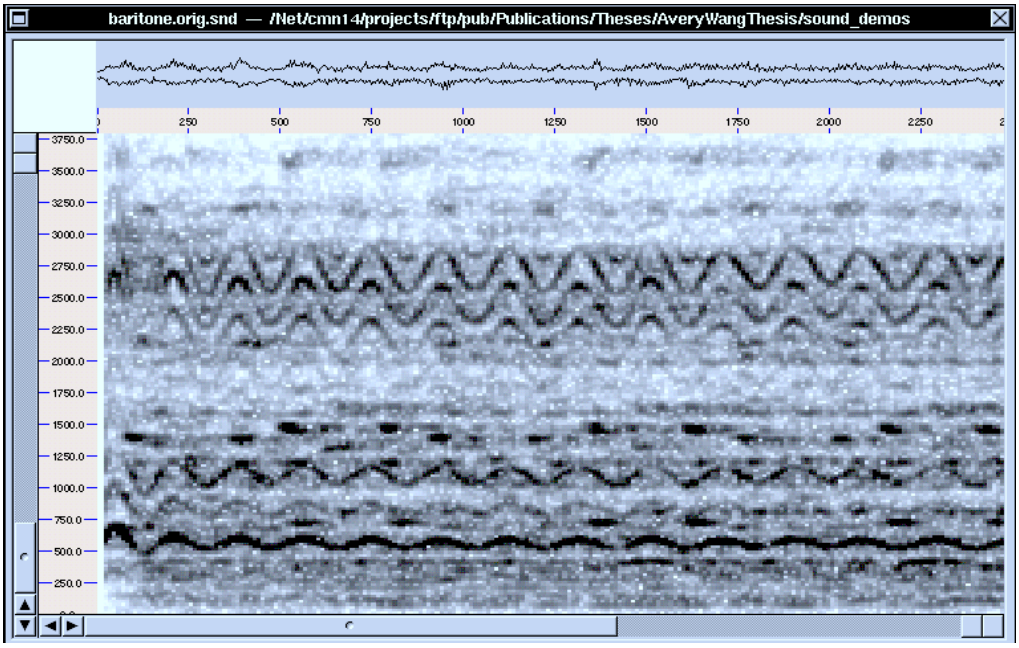

(a)

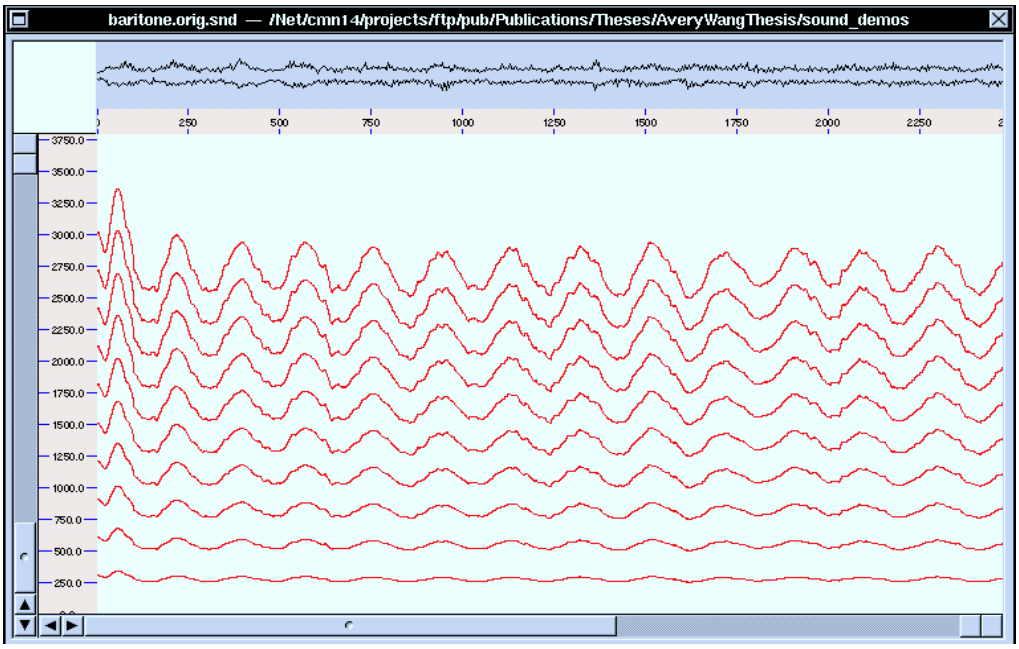

(b)

Figure 6.1: Baritone voice in an orchestral mixture tracked by a set of 10 harmonics. Initial fundamental frequency was set at 300 Hz, tracking gain = 0.002, analysis filter bandwidth = 60Hz. Sampling rate = 44.1 KHz. **(a)** Spectrogram of mixture. **(b)** Harmonic trackers locked onto voice.

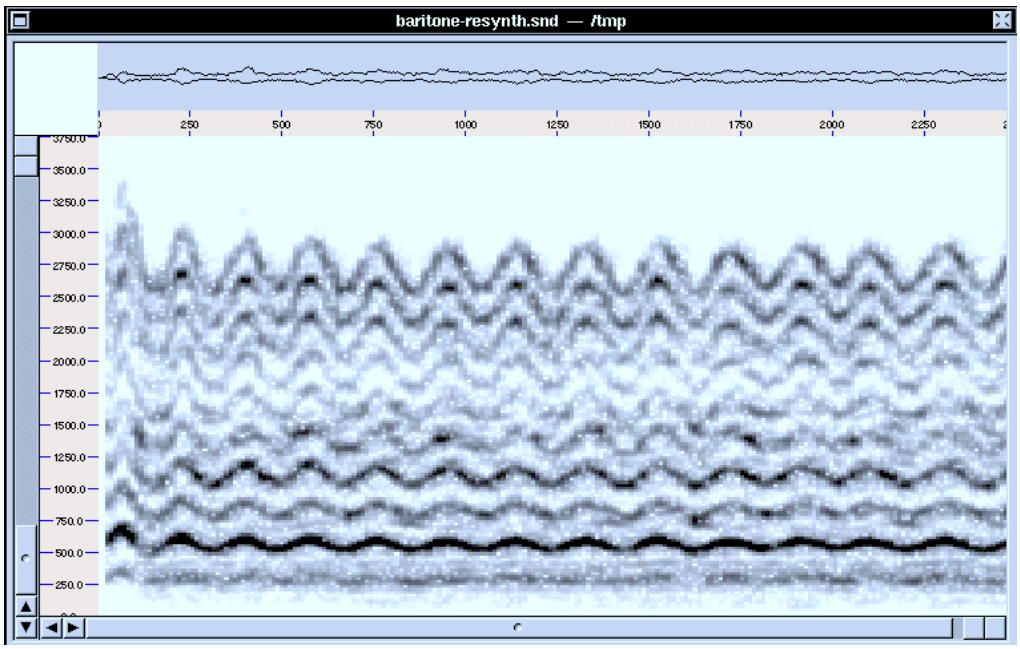

(a)

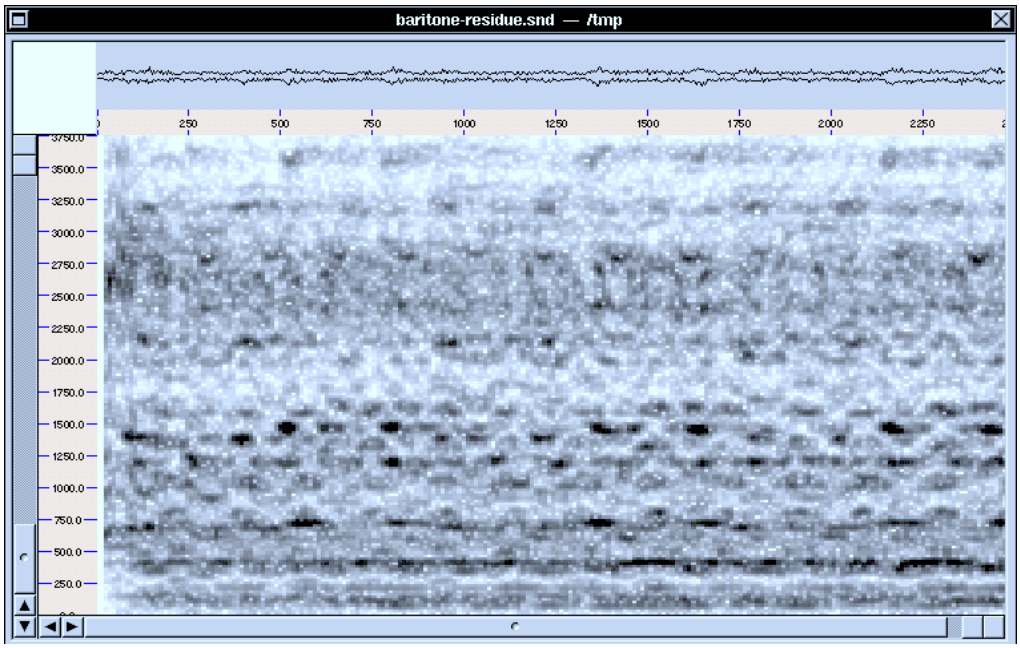

(b)

Figure 6.2: **(a)** Spectrogram of resynthesized baritone voice using the harmonic tracks of Figure 6.1(b). **(b)** Spectrogram showing the result of subtracting the signal of (a) from the original signal. This is the orchestral accompaniment with the baritone voice removed. Note the "negative" image of the vocal partials on the orchestral background.

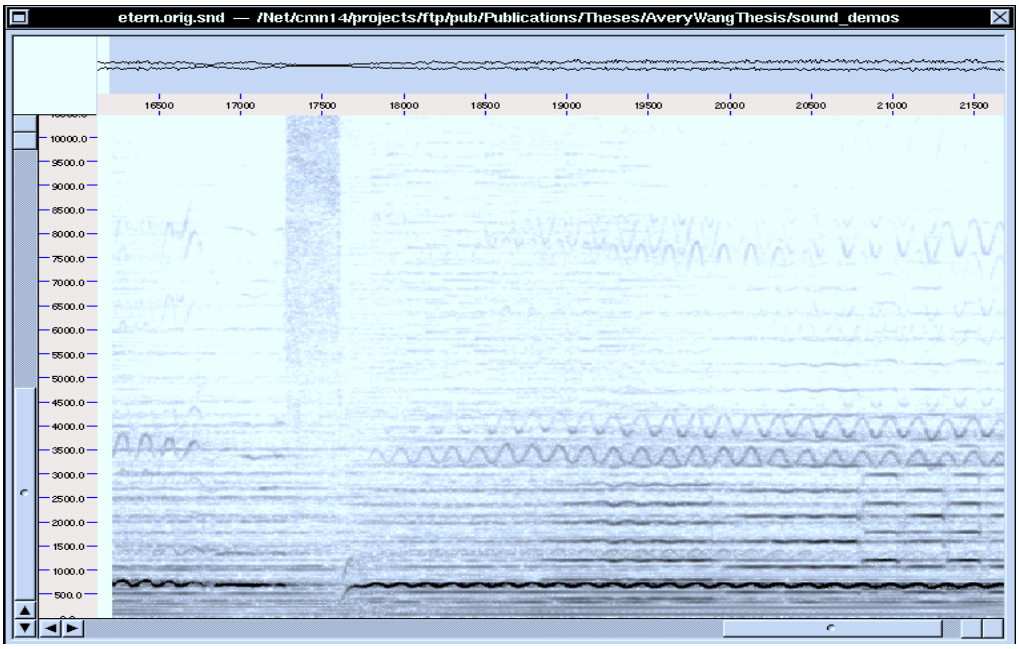

(a)

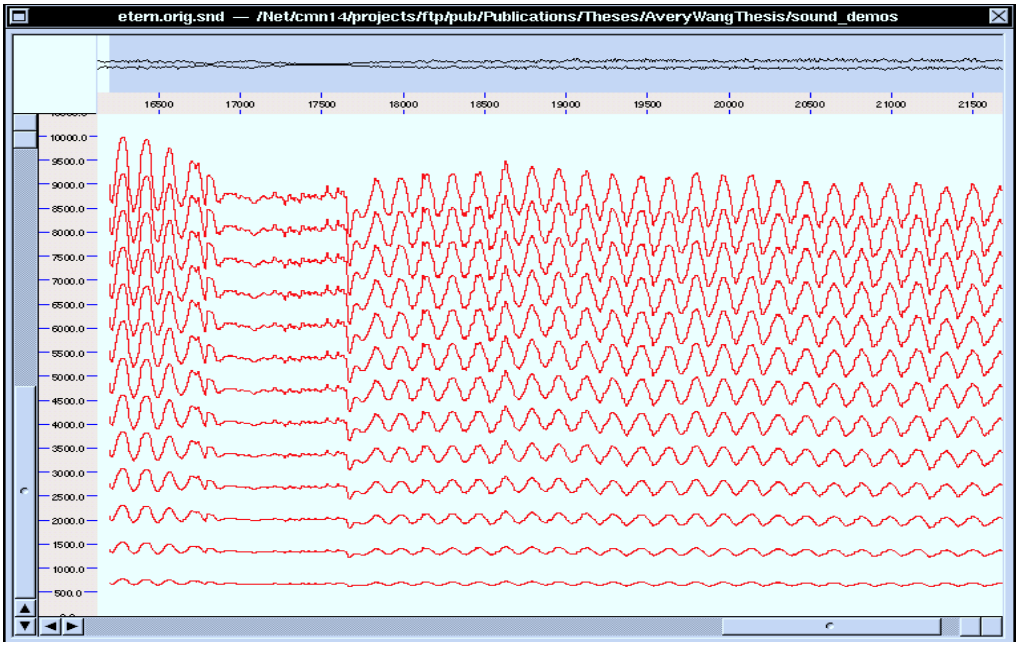

(b)

Figure 6.3: Soprano voice accompanied by a small ensemble and trumpet, tracked by a set of 13 harmonics. Initial fundamental frequency was set at 700 Hz, tracking gain = 0.002, analysis filter bandwidth = 60Hz. Sampling rate = 44.1 KHz. **(a)** Spectrogram of mixture. **(b)** Harmonic trackers locked onto voice.

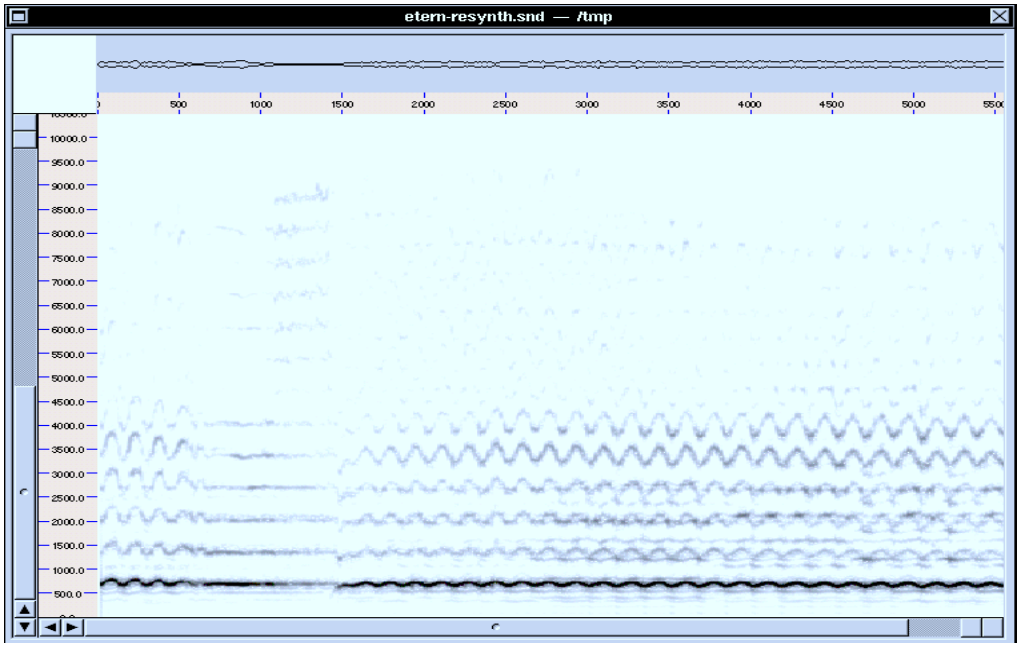

(a)

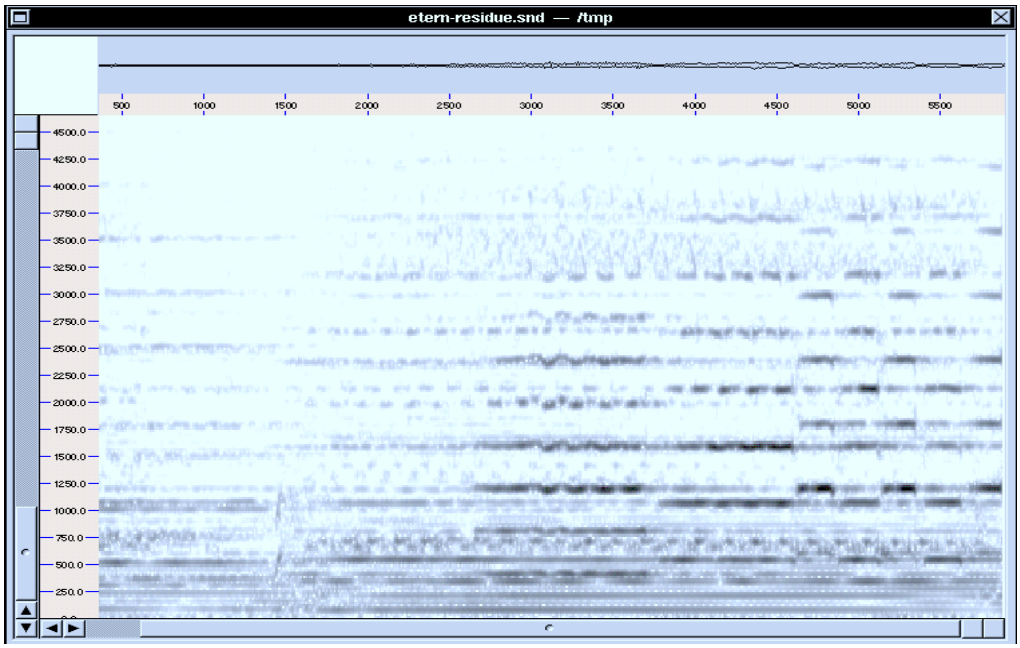

(b)

Figure 6.4: **(a)** Spectrogram of resynthesized soprano voice using the harmonic tracks of Figure 6.3(b). **(b)** Spectrogram showing the result of subtracting the signal of (a) from the original signal. This is the ensemble accompaniment, including a trumpet in the second half.

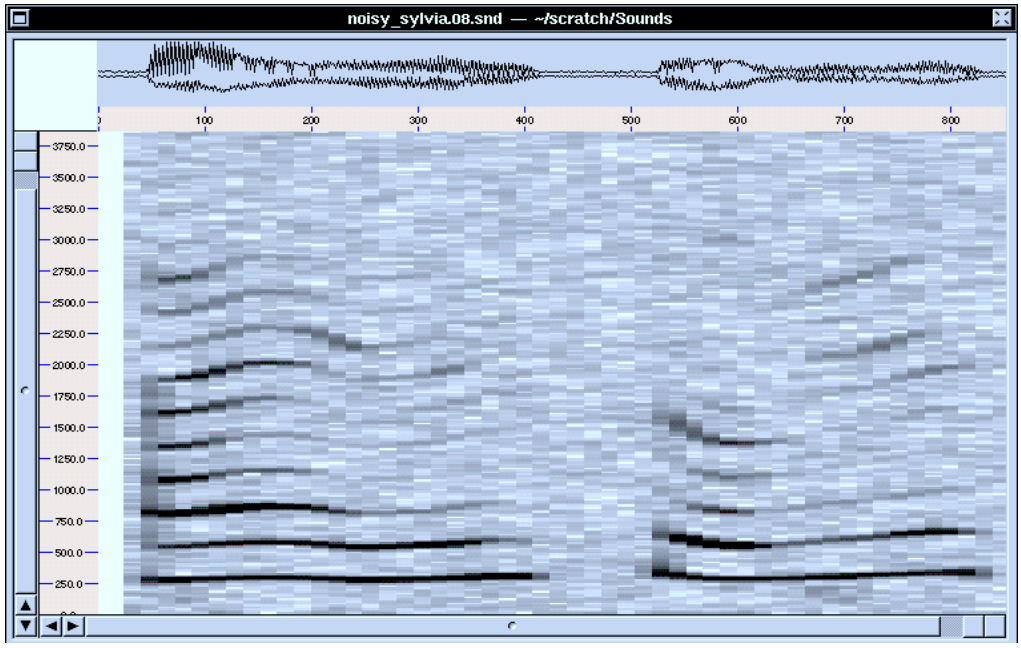

(a)

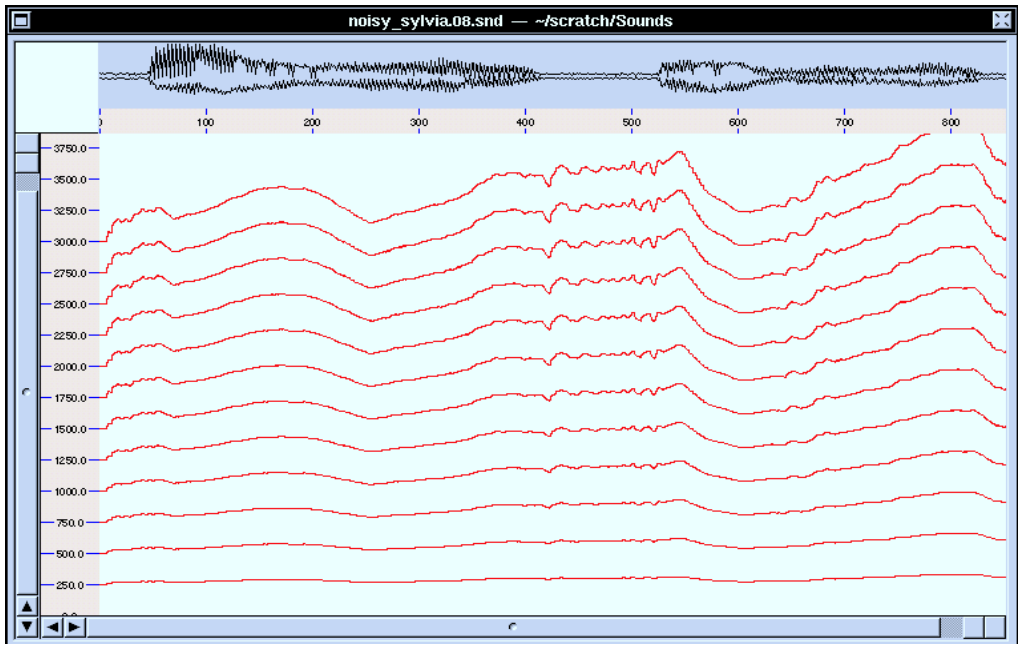

(b)

Figure 6.5: Female voice with noise tracked by a set of 12 harmonics. Initial fundamental frequency was set at 250 Hz, tracking gain = 0.02, analysis filter bandwidth = 60Hz. Sampling rate = 8012 Hz. **(a)** Spectrogram of mixture. **(b)** Harmonic trackers locked onto voice. Note that during the pause between about 425-525 ms the trackers wander around randomly since there is no harmonic energy to track.

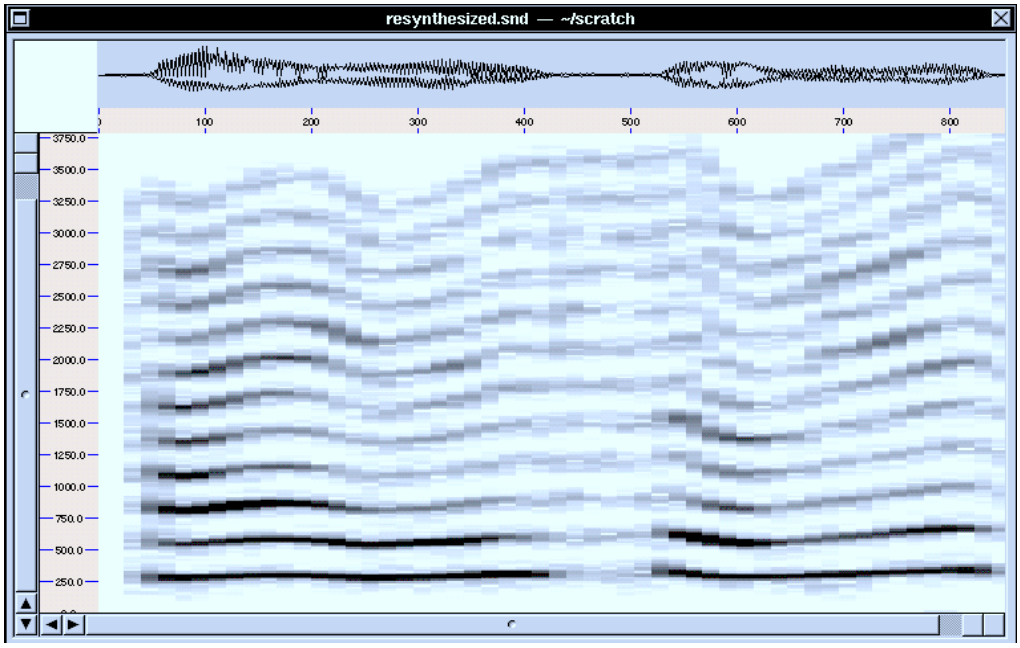

(a)

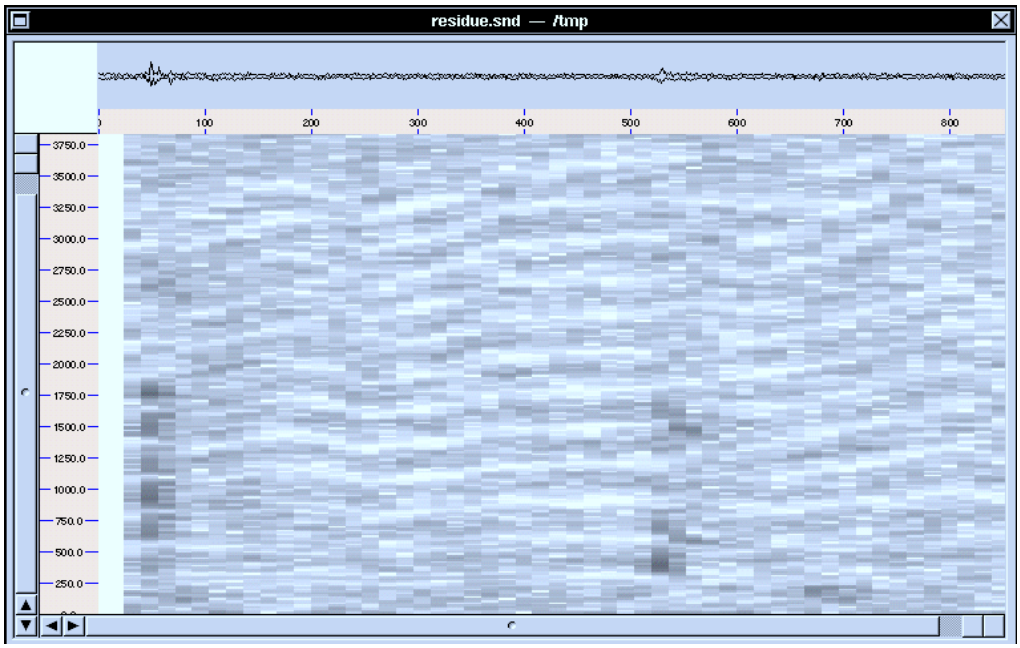

(b)

Figure 6.6: **(a)** Spectrogram of resynthesized female voice using the harmonic tracks of Figure 6.5(b). The resynthesis algorithm has captured signal energy that is close to each tracker's frequency, pulling along a fair amount of the noise. This also occurs during the pause between 425 and 525 ms, when the trackers are freely wandering without a signal to track. **(b)** Spectrogram showing the result of subtracting the signal of (a) from the original signal. This is the residual noise. Note the "negative" image of the vocal partials on noise background.

Another snippet from the "Barber of Seville." This 4.1 second example contains a soprano, baritone, and orchestra. The soprano has been separated. The voice is distorted in the first half, but then again, the mixture really is quite complex and the soprano is almost inaudible in the first half.

- days.diff.snd
- days.isolated.snd
- days.orig.snd

This is an 8.4 second segment from 10,000 Maniacs' "These are the days". Natalie sings in a mix with melody and harmony parts as well as instrumentals. The melody part has been separated from the harmony and instruments. Despite the articulations, the algorithm manages to track the melody through the mixture.

- etern.diff.snd
- etern.isolated.snd
- etern.orig.snd

This is a 22 second snippet of Kathleen Battle and Wynton Marsalis together in "eternal source of light divine" by Handel. Battle is accompanied by soft harpsichord plus some trumpet at the end by Marsalis. Again, the voice has been separated from the mixture.

6.3 Applications

There are many applications for the techniques described in this thesis. The fact that care has been taken to attain both statistical and computational efficiency makes the harmonic-locked loop algorithm attractive for commercial audio purposes. John Pierce has said that there is a world of difference between what would make the CIA happy and what would make the music people happy. Our goal is to please the latter. The voice extraction experiments on such diverse and complex musical sounds as opera and pop music have shown encouraging results on the ability to extract the instantaneous frequency tracks and the envelopes of individual voices and instruments from music. We list some the applications that come immediately to mind.

6.3.1 Voice Isolation

As is documented above in Section 6.2, vocal and other harmonic signals may be tracked, parameterized, resynthesized in isolation, and removed from the original sound. This fact suggests the applicability of this technique to do-it-yourself karaoke systems for the home market. Additionally, the technique could be applied to instruments with harmonic structure and facilitate the creation of "Music Minus One" recordings from existing soundtracks.

6.3.2 Speech Processing

Speech can be cleaned up dramatically using the harmonic-locked loop algorithm. Since the process has relatively low cost, especially for the 8KHz CODEC rates used for telephones, the algorithm may be applied in real-time as a front-end to a speech recognition system to improve recognition rates in noisy environments.

Additionally, since the fundamental frequency track and the envelopes for each harmonic can be estimated accurately, this information may also be used directly in a speech recognition system for such tasks as formant recognition.

6.3.3 Pitch Shifting

It is a simple matter to shift the pitch of a voice, once the instantaneous amplitudes $a_k[n]$ and the fundamental frequency $f_0[n]$ of the target harmonic set have been extracted. One way to attempt this is to scale the instantaneous frequencies of a harmonic signal by a frequency scaling factor α before resynthesizing as in Eqn. (5.76). However, this simplistic scaling model is actually incorrect because of the way voiced speech is produced physically.

6.3.3.1 Formant Factorization

As is well known, voiced speech may be modeled as a train of glottal impulses filtered through a vocal tract formant filter [39] which is largely independent of the glottal impulse rate. If we model the glottal impulses as a train of delta impulses

$$x(t) = \sum_{-\infty}^{\infty} \delta(t - k/f_0) \tag{6.1}$$

we know that the Fourier transform of this sequence is [21]

$$X(f) = \sum_{-\infty}^{\infty} \delta(f - kf_0). \tag{6.2}$$

Hence, if the vocal tract filter has a transfer function $H_v(f)$ then we obtain the vocal output as

$$Y(f) = X(f)H_v(f) \tag{6.3}$$

$$= \sum_{k=-\infty}^{\infty} H_v(kf_0)\delta(f - kf_0). \tag{6.4}$$

Since we assume that the signal is stationary, we see that the Fourier spectrum is the same as the instantaneous spectrum (cf. Section 2.1.4). The time-domain signal is then

$$y(t) = \sum_{k=-\infty}^{\infty} a_k \exp(j2\pi k f_0 t), \tag{6.5}$$

where the amplitudes are

$$a_k = H_v(kf_0). \tag{6.6}$$

Thus, we see that the instantaneous amplitudes of the harmonics of a voice signal may be thought of as sampled values of the vocal filter transfer function.

We can thus model the formant filter by interpolating the sampled envelope values $a_k[n]$ across k. For example, a crude approximation would be a simple linear interpolation across k, so that

$$\left|\hat{H}_v(f)\right| \approx a_k[n] + (a_{k+1}[n] - a_k[n])(f - kf_0[n]), \tag{6.7}$$

where $k = \lfloor f/f_0[n] \rfloor$. Alternatively, polynomial interpolation may be used.

Once the formant transfer function has been estimated it is a simple matter to shift the pitch of the voice using additive resynthesis by using the estimated magnitude transfer function $\left|\hat{H}_v(f)\right|$

excited at frequencies $\{\alpha k f_0[n]\}_{k=1}^{N}$, where α is the frequency scaling factor. Hence, the pitch-shifted signal is implemented as

$$y_\alpha[n] = \sum_{k=1}^{N} \left| \hat{H}_v(\alpha k f_0[n]) \right| \exp\left(\frac{j2\pi\alpha k}{f_s} \sum_{\ell=1}^{n} f_0[\ell] \right). \tag{6.8}$$

The harmonic-locked loop algorithm may be used to extract speech parameters in a simple way. Assuming that a HLL tracker has acquired lock onto a voiced speech sound, the instantaneous amplitudes $\{a_k[n]\}_{k=1}^{N}$ are the estimated sampled values of the magnitude formant filter.

A voice can be resynthesized with a different pitch and formant structure to provide chorus and harmony effects.

6.3.4 Pitch Tracking MIDI Control

Since the algorithm can lock tightly onto a harmonic signal and adapt very quickly to follow it, it is possible to track the pitch of a singing voice, even in the midst of much disturbance, such as in an orchestra. The harmonic locked loop algorithm can be used to provide instantaneous pitch information, including tight following of vibrato. This information can be used for coaching of voice students. Additionally, the parameters can potentially be used in conjunction with Perry Cook's SPASM [39] for realistic modeling of singing voices.

For some bizarre applications, the instantaneous pitch information can be fed in real-time to a MIDI controller, thereby allowing a singer to transform his or her voice into any synthesizeable musical sound with the same fundamental frequency. Additionally, transformations such as linear scaling or even non-linear warping can be used for interesting effects. For example, a synthesizer can be programmed which can play in harmony with a singer. If a singer uses vibrato, the MIDI pitch parameter may be quantized so that only allowable notes on a piano, for example, are played in accompaniment with the singer.

Also, the formant factorization described above may be used to control other MIDI parameters, such as timbre or even instrument type, translating "\ü\" vowels into gongs and "\ē\," vowels into trumpets.

Additionally, such tracking could be applied to instruments such as violins and cellos, giving that violist who always wanted to branch out the possibility of "playing" trombone.

The potential applications of harmonic-tracking MIDI controllers are endless.

6.3.5 Audio Compression Techniques

The best way to compress a signal is to be able to synthesize it parametrically. In lossy compression, it is desirable to extract the parts of the signal that matter most and ignore the parts that make no difference perceptually [69]. If a good, sparse, parametric model of the relevant parts of a signal can be found, then there is a great potential for compression. The extracted envelopes of a time-varying harmonic signal are quite narrow-band, after frequency warping removes their FM bandwidth. Hence, the envelope signals may be drastically subsampled. Additionally, the instantaneous frequency track for most sound sources does not vary more than a few dozen Hertz per second, so it, too, is quite band-limited. Hence, signals such as speech may be compressed drastically while maintaining a high quality of resynthesis. A compression factor of 100-to-1 is quite possible using harmonic resynthesis.

To use the harmonic tracking algorithm in such a context, work must be done to process transients and other stochastic components of signals which are coherent entities composed of both harmonic and stochastic components [126].

6.3.6 De-noising

The applications of compression an de-noising go hand-in-hand, conceptually. The point in compression is to remove unused information and to keep what is perceptually relevant. The requirement in de-noising is similar: Given that there is a signal buried in noise, and given that it is possible at all to extract it, chances are that it has relatively low complexity and has deterministic, i.e., sinusoidal, components. To extract the signal out of noise, it is necessary to estimate the parameters representing the deterministic part of the signal to be de-noised. By using the harmonic locked loop algorithm, it is possible to extract these parameters, assuming a harmonic relationship. Preliminary experiments on de-noising using such an approach show enormous potential. Again, as with audio compression, work needs to be done to extract transients and other stochastic signal components belonging to the target signal.

6.4 Future Work

Much remains to be done to extend the work described in this thesis. Many of the applications listed in the previous section imply some future directions to go with the harmonic-locked loop tracker.

It is encouraging to have been able to obtain the clean auditory source separation results using just the harmonic loop tracking algorithm. However, the possibilities for future work in this direction are tremendous. There are more things to do to build a more complete auditory scene analysis system, including incorporating some of the *gestalt* grouping rules given by Bregman [23] and used by others [26, 40, 50, 96] in their systems.

The most obvious currently is to use some kind of automatic pitch estimation algorithm to seed the harmonic tracking. Currently, the seeding is done manually at the beginning of each analysis run. Automatic pitch detection, for example, could be implemented using a cepstral technique [20]. Since the cepstrum technique is somewhat expensive computationally, and since we only need seed values in case of new harmonic signals, the cepstrum could be run periodically, perhaps spaced every one or two hundred milliseconds. When a new cepstral peak has been detected, a harmonic tracker may be launched to track the corresponding harmonic signal.

A powerful cue which must be incorporated eventually is that of common onsets. Currently, the HLL algorithm runs continuously through its input sound record, from beginning to end. The use of onsets and offsets, along with automatic seeding of the fundamental frequency, is the next step towards fully automatic segmentation of harmonic signals. Most notes, including inharmonic ones, have well-defined onsets in their partials which can be grouped by onsets which occur within a few milliseconds of each other. Offsets must also be detected to determine the extent of phrasing, either in voices or musical instruments. Techniques from abrupt-change theory [11] may be used to detect sudden increases in variance to decide when tracking is lost. Such information has great potential for parsing of auditory signals.

Another issue with tracking of sinusoids is that often frequency lock does not happen at the onset of a signal, but rather some time after it starts. This is a consequence of the non-zero tracking time constant. As may be noticed in the some of the sound examples, the tracker did not attain lock on beginnings of each word so some voicing residue was left behind along with the start transients. A promising hack for this, which has been tried successfully on test data, is to run the tracking algorithm backwards once harmonic lock is obtained. The tracker is then run to the beginning of the note or phrase while having lock on the signal and then run forward again, thereby having lock during the extent of the harmonic signal's existence.

Spatial cues have been completely ignored in the present work. One may employ the PLL, FLL, and HLL algorithms to analyze different views of the same signal from multiple microphones. By

comparing relative phases and intensities one may derive estimates of object positions.

Techniques for detecting and tracking inharmonic series should also be developed. For example, a fixed template system for the frequency relationships among inharmonic partials for a given instrument could be used for inharmonic tracking as described in Section 5.6. The template could be pre-programmed or learned, perhaps using common onsets as a cue to start training.

6.5 Conclusion

The list of possibilities employing the algorithms described in this thesis is quite large. My expectation is that cocktail-party processors will continue to grow in power and sophistication, perhaps building on top of my work. I am looking forward to the day when I will have a meaningful argument with an artificial entity in a crowded airport lobby.

Appendix A

The Bedrosian Product Theorem

Given two complex functions $x(t)$ and $y(t)$ we consider the Hilbert transform [21] of the product $x(t)y(t)$. For example, if one of the functions, say $y(t)$, is the carrier and the other the modulator, such that

$$y(t) = \cos(\omega t)$$

and

$$x(t) = a(t),$$

where $a(t)$ is some real amplitude function, we may define the signal

$$\begin{aligned} s(t) &\stackrel{\triangle}{=} x(t)y(t) \\ &= a(t)\cos(\omega t). \end{aligned}$$

For many purposes we wish to derive the signal

$$\tilde{q}(t) = -a(t)\sin(\omega t),$$

in which the cosine function is phase-lagged by 90°. We know that the Hilbert transform [21] delays the sinusoidal components of a signal by a quarter-cycle, i.e.

$$\mathcal{H}\{\sin(\omega t)\} = \cos(\omega t)$$

and

$$\mathcal{H}\{\cos(\omega t)\} = -\sin(\omega t)$$

for all $\omega \in \Re$. The Hilbert transform of the signal $s(t)$ yields the *quadrature function* $q(t)$ of $s(t)$ such that the signal

$$z(t) \stackrel{\triangle}{=} s(t) - j\,\mathcal{H}\{s(t)\} \tag{A.1}$$

$$= s(t) - j\,q(t) \tag{A.2}$$

is an *analytic signal* [21].

For constant $a(t)$ it is clear that $\tilde{q}(t) = \mathcal{H}\{s(t)\} = q(t)$. It is not immediately obvious that this should hold for time-varying $a(t)$. Since multiplication is commutative we cannot say which of $x(t)$ and $y(t)$ is the carrier and which is the modulator. For example, if $x(t) = \sin(t)$ and $y(t) = \sin(10t)$ does the Hilbert transform yield $\sin(t)\cos(10t)$, $\cos(t)\sin(10t)$, or neither? A quick calculation reveals that $\mathcal{H}\{x(t)y(t)\} = \sin(t)\cos(10t)$.

We wish to find the general conditions for $x(t)$ and $y(t)$ under which

$$\mathcal{H}\{x(t)y(t)\} = x(t)\mathcal{H}\{y(t)\}. \tag{A.3}$$

These conditions are given by the Bedrosian Product Theorem [12].

First prove a lemma, adapted from a result by Bedrosian [12].

Lemma A.1 *Let $x(t)$ and $y(t)$ be complex functions in $L_2(-\infty,\infty)$ with Fourier transforms $X(f)$ and $Y(f)$ respectively. Then the support of $X(u)$ and $Y(v)$ is in the region*

$$\mathcal{B} = \{(u,v) : \operatorname{sgn}(u+v) = \operatorname{sgn}(v)\} \tag{A.4}$$

if and only if the Hilbert transforms satisfy

$$\mathcal{H}\{x(t)y(t)\} = x(t)\mathcal{H}\{y(t)\}. \tag{A.5}$$

Proof: The product may be written

$$x(t)y(t) = \int_{-\infty}^{\infty} du \int_{-\infty}^{\infty} dv\, X(u)G(v)e^{j2\pi(u+v)t}. \tag{A.6}$$

By the definition of the Hilbert transform,

$$\mathcal{H}\{e^{j2\pi at}\} = \frac{-1}{\pi t} * e^{j2\pi at} \tag{A.7}$$

$$= \mathcal{F}^{-1}\{j\operatorname{sgn}(f)\delta(f-a)\} \tag{A.8}$$

$$= j\operatorname{sgn}(a)e^{j2\pi at} \tag{A.9}$$

Therefore

$$\mathcal{H}\{x(t)y(t)\} = j\int_{-\infty}^{\infty} du \int_{-\infty}^{\infty} dv \operatorname{sgn}(u+v)X(u)G(v)e^{j2\pi(u+v)t}. \tag{A.10}$$

Also,

$$x(t)\mathcal{H}\{y(t)\} = j\,x(t)\int_{-\infty}^{\infty} dv \operatorname{sgn}(v)G(v)e^{j2\pi vt} \tag{A.11}$$

$$= j\int_{-\infty}^{\infty} du \int_{-\infty}^{\infty} dv \operatorname{sgn}(v)X(u)G(v)e^{j2\pi(u+v)t}, \tag{A.12}$$

so that Eqn. (A.3) holds when the support of $X(u)$ and $Y(v)$ occur on (u,v) where

$$\operatorname{sgn}(u+v) = \operatorname{sgn}(v), \tag{A.13}$$

except on a set of measure zero. Q.E.D.

The Bedrosian Product Theorem [12, 17] follows immediately:

Theorem A.1 (Bedrosian Product Theorem) *Let $x(t)$ and $y(t)$ be complex functions in $L_2(-\infty,\infty)$. If*

(1) the Fourier transform $X(f)$ of $x(t)$ is zero for $|f| > a$ and the Fourier transform $Y(f)$ of $y(t)$ is zero for $|f| < a$ for some arbitrary positive constant a, or
(2) $x(t)$ and $y(t)$ are analytic [21],

then the Hilbert transform of the product $x(t)y(t)$ is given by Eqn. (A.3).

Condition (1) is of particular interest to us. It simply states that the bandwidth of $x(t)$ must be less than the lowest magnitude frequency component of the carrier $y(t)$. In the particular application to the frequency tracking algorithm described in Section 4, we are concerned about the case where we have a signal $s(t)$ of the form

$$s(t) = a(t)\cos(2\pi f(t) + \phi) \tag{A.14}$$

and we want to derive the signal

$$z(t) = a(t)\exp(j2\pi f(t) + j\phi) \tag{A.15}$$

as in Section 2.3. If condition (1) holds with $x(t) = a(t)$ and $y(t) = \cos(2\pi f(t) + \phi)$ then $-\mathcal{H}\{s(t)\}$ is the imaginary part of $z(t)$.

Thus we see that if the conditions for the Bedrosian Product Theorem hold the ambiguity between the amplitude modulator and carrier is resolved: the signal with the smaller bandwidth is taken to be the amplitude envelope.

In the amplitude and frequency estimation procedure described in Section 4 the time-varying estimate of instantaneous-frequency is the output of a tracking loop with a memory which is windowed by a decaying exponential. Thus the Fourier spectra of the carrier and the envelope may in fact intersect when considered over the entire time extent of the signal, but because of the decaying memory the overlap does not lead to ambiguity as long as the instantaneous frequency is always greater than the instantaneous bandwidth of the envelope function. The measured instantaneous bandwidth of the envelope function $a(t)$ depends on the frequency response of the low-pass filter used to window the estimate (cf. Section 2.1.3).

Appendix B

The Pitfalls of Using Zero-Crossings as a Phase-Locking Criterion in Digital PLLs

Digital phase-lock loops use zero crossing detectors to track the frequency and phase of an input signal. Zero-crossings of the input signal increment a counter, and zero-crossings of the tracking reference signal decrement the counter [14, 87, 146]. The frequency of the reference signal is made proportional to the value of the counter. Asynchrony in the zero-crossings causes temporary fluctuations in the frequency of the reference signal which bring the two signals into phase so that the zero-crossings become simultaneous. The digital PLL is suited for applications such as digital frequency synthesis for logic clocks, and are able to achieve phase-lock with any initial frequency disparity, as opposed to conventional analog PLLs which have a limited pull-in and lock-in range.

Digital PLLs may not be suited, however, for situations with noise or phase distortion. We present here a contrived example of how phase distortion in a square wave may leave the magnitude spectrum the same, but induce arbitrarily many zero-crossings.

Let a square wave $s(t)$ be defined with period 1

$$s(t) = \begin{cases} 1 & : \quad t \in [k - 1/4, k + 1/4), \forall k \in \mathcal{Z} \\ -1 & : \quad \text{otherwise.} \end{cases} \tag{B.1}$$

Then, the Fourier series decomposition is:

$$s(t) = \frac{4}{\pi} \sum_{k=0}^{\infty} \frac{(-1)^k \cos(2\pi(2k+1)t)}{2k+1}. \tag{B.2}$$

This Fourier series expansion of $s(t)$ has a phase signature of $(+-+-)$, i.e. the sign alternates with consecutive non-zero harmonics. The result of summing the first 400 non-zero harmonics of $s(t)$ is shown in Figure B.1.

By inducing a rather unnatural phase distortion, such that the signal has the same magnitude spectrum, we obtain the function

$$\tilde{s}(t) = \frac{4}{\pi} \sum_{k=0}^{\infty} \frac{\tilde{\phi}(k) \cos(2\pi(2k+1)t)}{2k+1}, \tag{B.3}$$

where the phase function $\tilde{\phi}(\cdot)$ is defined as

$$\tilde{\phi}(k) = \begin{cases} 1 & : \quad k \equiv 0,1 (\mathrm{mod} 4) \\ -1 & : \quad k \equiv 2,3 (\mathrm{mod} 4), \quad \forall k \in \mathcal{Z}. \end{cases} \tag{B.4}$$

Thus, $\tilde{s}(\cdot)$ is the result of multiplying the spectrum of $s(\cdot)$ by the function $\sqrt{2}\cos(2\pi f/8)$, which produces the correct sign change at the non-zero spectral components of Eqn. (B.2), yielding the phase signature of $(++--)$. This is the same as convolving the time domain signal $s(t)$ by $1/\sqrt{2}\{\delta(t-1/8)+\delta(t+1/8)\}$. We see more or less immediately that the resulting time-domain signal is

$$\tilde{s}(t) = \begin{cases} \sqrt{2} & : \quad t \in [k-1/8, k+1/8), \\ -\sqrt{2} & : \quad t \in [k+3/8, k+5/8), \forall k \in \mathcal{Z}, \quad \text{and} \\ 0 & : \quad \text{otherwise.} \end{cases} \tag{B.5}$$

The result of summing the first 400 non-zero harmonics is shown in Figure B.2. Notice that the time-domain signal lies on the time axis for half the period.

We can now make an obvious further modification of the phase described in Eqn. (B.4. Define $\tilde{s}_n(t)$ and $\tilde{\phi}_n(k)$ as follows:

$$\tilde{s}_n(t) = \frac{4}{\pi} \sum_{k=0}^{\infty} \frac{\tilde{\phi}_n(k) \cos\left(2\pi(2k+1)t\right)}{2k+1}, \tag{B.6}$$

and

$$\tilde{\phi}_n(k) = \begin{cases} \tilde{\phi}(k) & : \quad k \neq n \\ -\tilde{\phi}(k) & : \quad k = n. \end{cases} \tag{B.7}$$

Thus, we have inverted the sign of one of the harmonics of Eqn. (B.3). The result for $n = 15$ is seen in Figure B.3.

As n increases, the number of zero crossings per cycle of $\tilde{s}_n(t)$ approaches infinity. This contrived example illustrates how a naïve zero-crossing detector scheme for digital phaselock loops could be fooled into deciding that the frequency being tracked was far different from the fundamental of the harmonic series. Although the phase distortion in this example is rather artificial and drastic, more natural kinds of phase distortion will also produce spurious zero crossings.

One might suggest placing some sort of hysteresis on the zero-crossing detector so that it is no longer a zero-crossing detector, but rather a level-crossing detector. With $n = 1$, however, we see that there are 10 zero crossings of $\tilde{s}_n$ in Figure B.4. We see that the hysteresis threshold must be set high (outside ± 0.5) in order to avoid spurious zero-crossing counts. regions near $\tilde{s}(t) = 1$ and -1 may also present some problems. Also, if the phase relation $\tilde{\phi}$ varies unpredictably, no preset system would be able to track the fundamental period of the distorted square wave.

A conclusion to be drawn about the widely-used zero-crossing digital PLL technique is that it may be unreliable if there is significant phase distortion in the signal. In general, the digital PLL technique is best suited for applications where the SNR is high and signal detection is not a problem. Such conditions are usually met in applications such as digital frequency synthesis, but not necessarily for such applications as audio signal detection and identification.

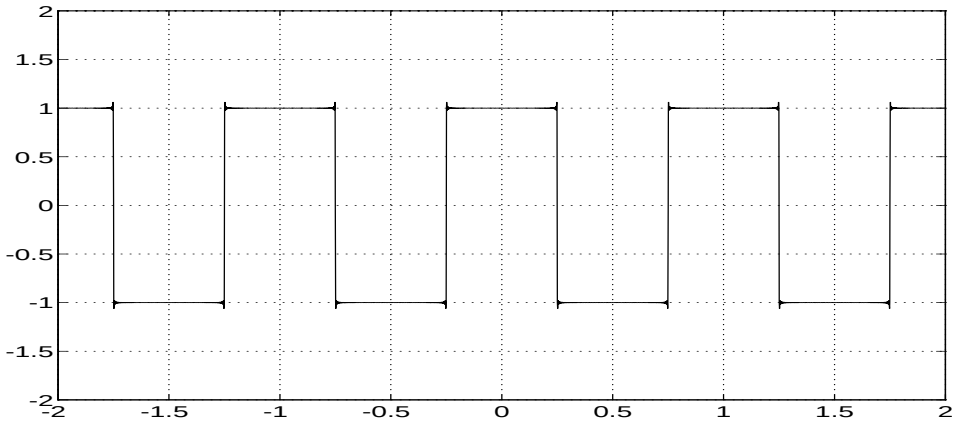

Figure B.1: Square Wave

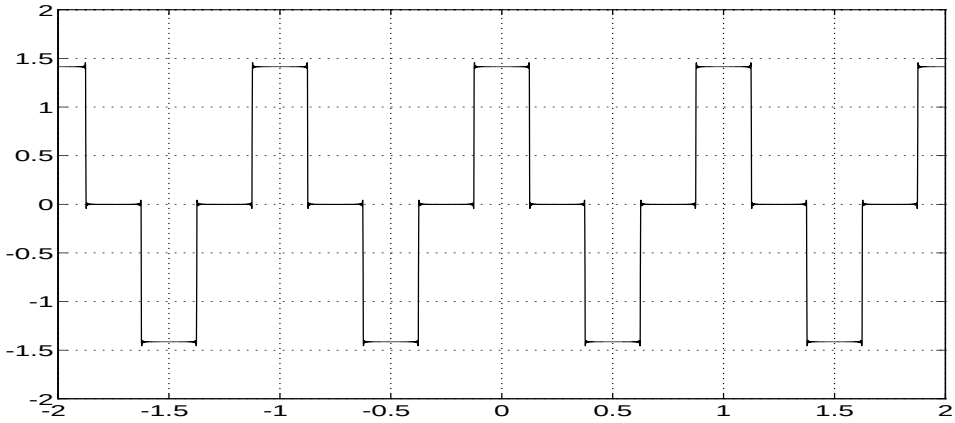

Figure B.2: Square wave with $(++--)$ phase distortion

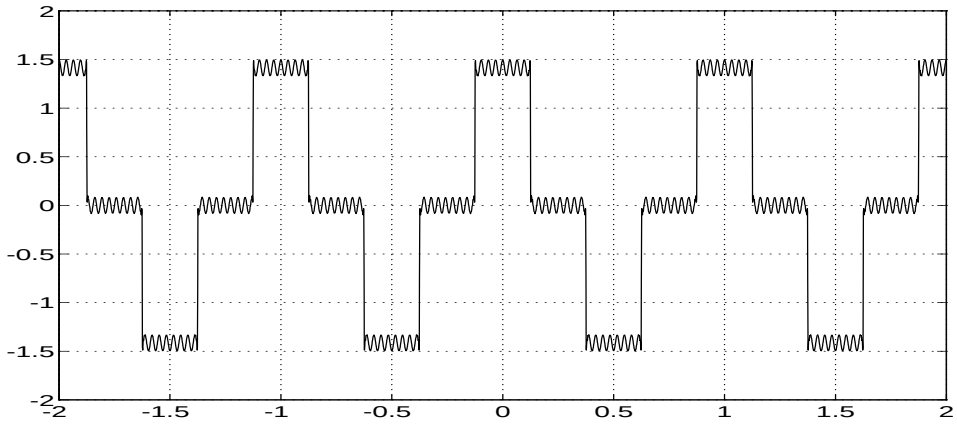

Figure B.3: Square wave with $(++--)$ phase distortion and negation of the 15th non-zero harmonic

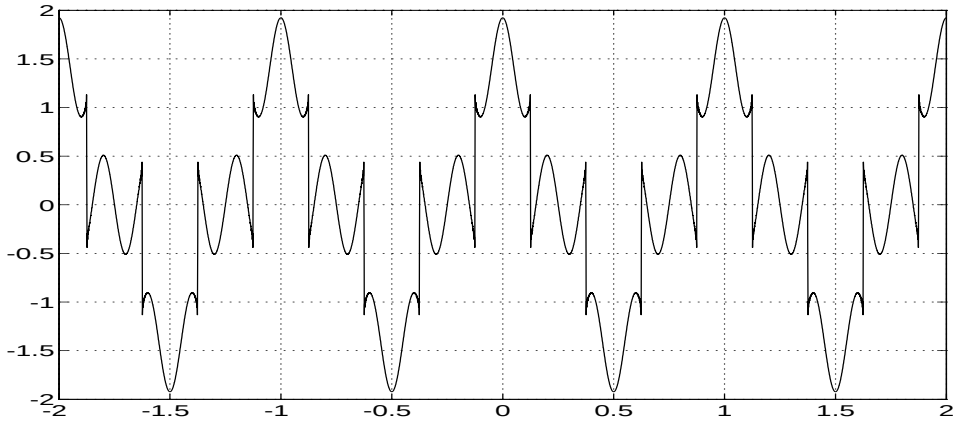

Figure B.4: Square wave with $(++--)$ phase distortion and negation of the 2nd non-zero harmonic.

Appendix C

Some Signals Which Violate the $\mathcal{M}_1$-Condition, but for Which the Winding Measure is Robust

It turns out that the $\mathcal{M}_1$-condition given by Eqn. (2.103) is sufficient, but not necessary, for the winding number of $z(t)$ to give a robust estimate of the winding of the strongest partial $p(t)$. We present two examples.

C.1 Geometric Series

Certain geometric series have the property that the winding number is proportional to the frequency of the fundamental, even though Eqn. (2.82) may not hold. This may be seen by considering the signal

$$z(t) = \sum_{k=1}^{N} \alpha^{k-1} w^k(t) \tag{C.1}$$

$$= w(t) \frac{1 - \alpha^N w^N(t)}{1 - \alpha w(t)}. \tag{C.2}$$

where

$$w(t) \stackrel{\triangle}{=} e^{j\omega_0 t}. \tag{C.3}$$

We see that if $|\alpha| \in [1/2, 1)$ then the signals have the property that

$$1 \not> \left| \sum_{k=2}^{N} \alpha^{k-1} w^k(t) \right|, \quad \text{for some } t, \tag{C.4}$$

notably at times $t = (2\pi n - \arg(\alpha))/\omega_0$, thus violating Eqn. (2.82). Also, for an infinite geometric series with $|\alpha| > 1/\sqrt{2}$ the power of the harmonics is greater than that of the fundamental, i.e.

$$\sum_{k=2}^{\infty} |\alpha|^{2(k-1)} = \frac{|\alpha|^2}{1 - |\alpha|^2} \tag{C.5}$$

$$> 1. \tag{C.6}$$

However, we see that the absolute phase of the term

$$\frac{1-\alpha^N w^N(t)}{1-\alpha w(t)} \tag{C.7}$$

is restricted to $(-\pi, \pi)$, and thus the phase winding count is dominated by the multiplicative factor $w(t)$.

C.2 Harmonic Series

Consider the signal

$$z(t) \triangleq \sum_{k=1}^{\infty} \frac{-1^{(k-1)}}{(2k-1)} w^{2k-1}(t), \tag{C.8}$$

where, as before,

$$w(t) \triangleq e^{j\omega_0 t}. \tag{C.9}$$

This signal may be expressed in closed form as

$$z(t) = \arctan\{w(t)\}. \tag{C.10}$$

We note that the arctan$(\cdot)$ function performs a conformal mapping from points $w(t)$ on the unit circle to an infinite strip bounded by $\mathrm{Re}\{z(t)\} = \pm\pi/4$ [101]. As $w(t)$ makes a counterclockwise circuit along the unit circle around time axis, $z(t)$ also makes a counterclockwise circuit around the time axis along the boundary of the infinite strip, approaching the point $z(t) = +j\infty$ as $w(t)$ approaches $+j$ and $z(t) = -j\infty$ as $w(t)$ approaches $-j$. Figure C.1 shows the mapping from the unit circle to the infinite strip.

It is interesting to point out that the real part of $z(t) = \arctan\{w(t)\}$ is a square wave of amplitude $\pi/4$ and period $\omega_0/2\pi$.

C.3 Rational Functions

The results of Section C.1 may be extended quite easily. Any two sets of (complex) numbers $\{\alpha_k\}_{k=1}^N$ and $\{\beta_\ell\}_{\ell=1}^M$ such that $|\alpha_k|, |\beta_\ell| < 1$ will generate a waveform $z(t)$ defined as

$$z(t) = w(t)\frac{\prod_{\ell=1}^{M}(1-\beta_\ell w(t))}{\prod_{k=1}^{N}(1-\alpha_k w(t))} \tag{C.11}$$

will have an average winding rate of ω_0 radians per second. The proof is left as an exercise for the reader. These functions represent a way of taking the transfer function $H(z)$ of a minimum-phase, time-invariant linear filter and generating a waveform $w(t)H(w(t))$ whose winding rate will always be dominated by the fundamental, regardless of whether the $\mathcal{M}_1$-condition is satisfied. In general, any analytic function whose poles and zeros are within the unit circle may be used as $H(\cdot)$.

The general approach of generating a waveform by applying a function to a sinusoid is called *waveshaping*, studied by Le Brun [85].

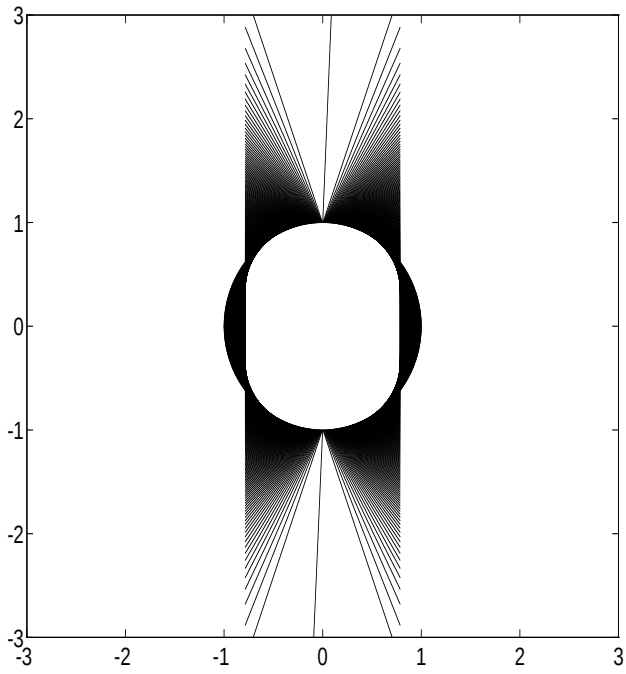

Figure C.1: The conformal mapping from the unit circle $w(t) = \exp(j2\pi\omega_0 t)$ to the infinite strip $\mathrm{Re}\{z(t)\} = \pm\pi/4$, as performed by the mapping $z(t) = \arctan(w(t))$. Line segments are drawn between corresponding points $w(t)$ and $z(t)$ for 2000 values of $w(t)$ uniformly spaced on the unit circle. $z(t)$ winds once around the time axis as $w(t)$ makes a single circuit for $t \in [0, 1]$.

Appendix D

Cramér-Rao Bounds for Polynomial Phase Signals

Several authors have presented interesting analyses of the Cramér-Rao minimum-variance bounds (CRBs) for sinusoidal signals. Brennan [24] presents a derivation of the CRBs for the parameters of a sinusoidal signal in noise for which the phase and amplitude are unknown. Rife and Boorstyn [119] present an excellent generalization of the analysis to all combinations of cases where the amplitude, frequency, and phase of a sinusoidal signal are either known or unknown.

The CRBs for the frequency and phase estimates for a single partial with additive Gaussian noise are treated in Peleg, *et al* [111]. In this reference the authors present an analysis of M-th order polynomial fits to the phase of a continuous measured complex signal presumed to have constant amplitude. The polynomial fit in their analysis is performed over a continuous interval $[T_1, T_2]$ by projection onto a basis of the first M Legendre polynomials. Because the fit is performed over the entire interval simultaneously, this method is suitable for off-line processing or on-line blocked estimation where some estimate delay is permitted. Matching of endpoints for phase and frequency continuity in the case of blocked estimation is an issue to be considered in this approach.

The Cramér-Rao bounds for M-th degree polynomial phase functions are given by Peleg, *et al* [111, Eqns. (18),(21)] as

$$\mathrm{CRB}(\phi_M(t)) = \frac{N_0}{2A^2T} \sum_{m=0}^{M} (2m+1) P_m^2 \left(\frac{2t - T_1 - T_2}{T} \right), \tag{D.1}$$

and

$$\mathrm{CRB}(f_M(t)) = \frac{N_0}{2\pi^2 A^2 T^3} \sum_{m=1}^{M} (2m+1) f_m^2 \left(\frac{2t - T_1 - T_2}{T} \right), \tag{D.2}$$

where $T \triangleq T_2 - T_1$, A is the amplitude of the signal, N_0 is the noise density, $P_m(t)$ is the m-th order Legendre polynomial, and $f_m(t)$ is its derivative. The CRBs for instantaneous frequency are shown to grow as M^3 at the middle of the interval and as M^6 at the endpoints; the instantaneous phase CRB grows as M and M^2 for the respective points. Additionally, the CRBs diminish as $1/T$ and $1/T^3$ for instantaneous phase and frequency respectively.

The explicit CRBs for polynomial-phase signals for cases $M = 1, 2$, and 3 are given as

$$\mathrm{CRB}(\phi_1(t)) = \frac{N_0}{A^2 T} \left(6\tau^2 + 0.5 \right) \tag{D.3a}$$

$$\mathrm{CRB}(f_1(t)) = \frac{6N_0}{4\pi^2 A^2 T^3}, \tag{D.3b}$$

$$\mathrm{CRB}(\phi_2(t)) = \frac{N_0}{A^2 T}\left(90\tau^4 - 9\tau^2 + 1.125\right) \tag{D.4a}$$

$$\mathrm{CRB}(f_2(t)) = \frac{N_0}{4\pi^2 A^2 T^3}\left(360\tau^2 + 6\right), \tag{D.4b}$$

$$\mathrm{CRB}(\phi_3(t)) = \frac{N_0}{A^2 T}\left(1400\tau^6 - 330\tau^4 + 22.5\tau^2 + 1.125\right) \tag{D.5a}$$

$$\mathrm{CRB}(f_3(t)) = \frac{N_0}{4\pi^2 A^2 T^3}\left(12600\tau^4 - 900\tau^2 + 37.5\right), \tag{D.5b}$$

respectively, where for convenience, we have defined

$$\tau \triangleq \frac{2t - T_1 - T_2}{T_2 - T_1}. \tag{D.6}$$

Case $M = 1$ given by Eqns. D.3a-D.3b give the Cramér-Rao bounds for estimating the frequency and phase of a fixed-frequency complex sinusoid, and Eqns. D.4a-D.4b give the Cramér-Rao bounds for a time-varying signal with a constant frequency slew rate.

For the case of non-polynomial phase functions, there is an additional bias term corresponding to higher-order terms of the infinite series expansion of the phase function not accounted for by a finite polynomial approximation. The curious reader is referred to section IV. of Peleg, *et al* [111] for a thorough analysis of the estimation error, including approximations for sufficiently large signal-to-noise ratios.

Appendix E

Optimal Frequency and Slew Estimation from Smoothed Phase Differences

In this appendix we present the results by Kay [75] for the optimal smoothed phase-difference frequency estimator. Additionally, we present an extension of Kay's derivation to the optimal estimate of the *slew* of a signal.

E.1 Kay's Optimal Phase-Difference Frequency Estimator

As shown in Section 2.1.1.1, taking the phase derivative or the finite difference of the phase can lead to questionable results for estimating the frequency of a sinusoidal component in the presence of other signals such as noise or interfering sinusoids. The results are unreliable, due to the sensitivity of the phase derivative or difference to noise. However, if the derivative or phase difference is smoothed the results may be quite useful. Kay has derived the optimal weighting coefficients in [75]. Since the results are so useful in this dissertation, the results and derivations are repeated here.

In this appendix, we assume that the signal $z[n]$, for $0 \leq n \leq N-1$, consists of a single pure-frequency sinusoid of frequency f plus complex Gaussian white noise $\nu[n]$ with uncorrelated real and imaginary parts and variance σ_ν^2, and sampling rate f_s, so that

$$z[n] = A \exp\left(\frac{j2\pi nf}{f_s} + j\phi_0\right) + \nu[n]. \tag{E.1}$$

To estimate the frequency, we might try averaging $N-1$ samples of the phase difference:

$$f[n] = \sum_{k=1}^{N-1} \frac{f_s}{2\pi} w[k]\{\mathrm{Arg}(z[n-k]) - \mathrm{Arg}(z[n-k-1])\} \tag{E.2}$$

$$= \sum_{k=1}^{N-1} \frac{f_s}{2\pi} w[k] \arg\{z[n-k]z^*[n-k-1]\}, \tag{E.3}$$

where it is understood in Eqn. (E.2) that the argument function $\mathrm{Arg}(\cdot)$ formally gives the absolute phase, and that $\arg(\cdot)$ returns the phase modulo 2π in $(-\pi, \pi)$. The weighting coefficients $w[k]$ are

normalized, so that

$$\sum_{k=1}^{N-1} w[k] = 1. \tag{E.4}$$

We would like to know what the "optimal" weighting coefficients $w[k]$ are. Certainly, the answer depends on the statistics of the signal and noise.

It is clear that if $w[k] = 1/(N-1)$ then

$$f[n] = \frac{1}{N-1} \sum_{k=1}^{N-1} \frac{f_s}{2\pi} \{\text{Arg}(z[n-k]) - \text{Arg}(z[n-k-1])\} \tag{E.5}$$

$$= \frac{f_s}{2\pi} \frac{\text{Arg}(z[n]) - \text{Arg}(z[n-N+1])}{N-1}, \tag{E.6}$$

which is the average phase difference, scaled by $f_s/2\pi$. Intuitively, one might think that this is the best window because each of the phase difference samples are equally weighted. However, this reasoning is flawed, as the following analysis due to Kay [75] will reveal.

If signal-to-noise ratio is fairly small,[1] we may make the approximation

$$z[n] \approx (A + u_1[n]) \exp\left(\frac{j2\pi nf}{f_s} + j\phi_0 + ju_2[n]\right), \tag{E.7}$$

where $u_1[n]$ and $u_2[n]$ are zero-mean Gaussian white noise processes with variances $\sigma_\nu^2/2$ and $\sigma_\nu^2/2A^2$ respectively. We may take the complex argument at this stage, but then we are faced with the phase-unwrapping problem to get the absolute phase encountered by Tretter [137]. However, since we are interested in the phase difference anyway, the absolute phase is irrelevant. Therefore, we may calculate the phase difference by using the conjugate-product as in Eqn. (E.3) and thus set

$$\Delta\phi_z[n] \triangleq \arg(z[n]z^*[n-1]) \tag{E.8}$$

$$\approx \frac{2\pi}{f_s} f + u_2[n] - u_2[n-1]. \tag{E.9}$$

For notational convenience, we define

$$\omega \triangleq \frac{2\pi}{f_s} f. \tag{E.10}$$

Given $N-1$ observations of $\Delta\phi_z[n]$,[2] we find the optimal frequency estimate

$$\hat{f} = \frac{f_s}{2\pi} \hat{\omega} \tag{E.11}$$

by finding the value of ω which minimizes [75, 152]

$$J(\omega) = (\mathbf{\Delta} - \omega\mathbf{1})^T \mathbf{C}^{-1} (\mathbf{\Delta} - \omega\mathbf{1}) \tag{E.12}$$

where $\mathbf{1}$ is the $(N-1) \times 1$ vector of ones,

$$\mathbf{\Delta} \triangleq [\Delta\phi_z[1], \ldots, \Delta\phi_z[N-1]]^T, \tag{E.13}$$

[1] In Section 2.3.1 we give a novel analysis of the conditions for the robustness of using the averaged phase difference as a frequency estimator.

[2] Kay [75] uses N data points and thus obtains $N-1$ phase differences.

and $\mathbf{C}^{-1}$ is the inverse of the covariance matrix $\mathbf{C}$ of $\mathbf{\Delta}$ defined in Eqn. (E.27). This is simply the maximum likelihood estimate of f, given that $u_2[k]$ is zero-mean IID Gaussian noise [74]. Minimizing $J(\omega)$ is the same as finding the maximum of the Gaussian distribution $\exp(-J(\omega)/2)$. By taking the derivative $dJ(\omega)/d\omega$ and setting it equal to zero, we find

$$\hat{\omega} = \frac{\mathbf{1}^T\mathbf{C}^{-1}\mathbf{\Delta}}{\mathbf{1}^T\mathbf{C}^{-1}\mathbf{1}}. \tag{E.14}$$

We see that $\hat{\omega}$ is an unbiased estimator because, for each k,

$$E\{\Delta\phi_z[k]\} = E\{\frac{2\pi}{f_s}f + u_2[k] - u_2[k-1]\} \tag{E.15}$$

$$= \omega \tag{E.16}$$

since for all m, $E\{u_2[m]\} = 0$. Therefore,

$$E\{\hat{\omega}\} = \frac{\mathbf{1}^T\mathbf{C}^{-1}E\{\mathbf{\Delta}\}}{\mathbf{1}^T\mathbf{C}^{-1}\mathbf{1}} \tag{E.17}$$

$$= \frac{\mathbf{1}^T\mathbf{C}^{-1}\mathbf{1}}{\mathbf{1}^T\mathbf{C}^{-1}\mathbf{1}}\omega \tag{E.18}$$

$$= \omega. \tag{E.19}$$

Kay gives the variance of this estimator as [75]

$$\mathrm{var}(\hat{f}) = \frac{1}{\mathbf{1}^T\mathbf{C}^{-1}\mathbf{1}}. \tag{E.20}$$

This may be seen by using calculating

$$\hat{\omega} - E\{\hat{\omega}\} = \frac{\mathbf{1}^T\mathbf{C}^{-1}\mathbf{\Delta}}{\mathbf{1}^T\mathbf{C}^{-1}\mathbf{1}} - \omega \tag{E.21}$$

$$= \frac{f_s}{2\pi}\frac{\mathbf{1}^T\mathbf{C}^{-1}\mathbf{U}}{\mathbf{1}^T\mathbf{C}^{-1}\mathbf{1}}, \tag{E.22}$$

where

$$\mathbf{U} \stackrel{\triangle}{=} [u_2[1] - u_2[0], \ldots, u_2[N-1] - u_2[N-2]]^T. \tag{E.23}$$

The variance of $\hat{\omega}$ is then given by

$$E\left\{|\hat{\omega} - E\{\hat{\omega}\}|^2\right\} = E\left\{\frac{\mathbf{1}^T\mathbf{C}^{-1}\mathbf{U}\mathbf{U}^T\mathbf{C}^{-1}\mathbf{1}}{(\mathbf{1}^T\mathbf{C}^{-1}\mathbf{1})^2}\right\} \tag{E.24}$$

$$= \frac{\mathbf{1}^T\mathbf{C}^{-1}\mathbf{C}\mathbf{C}^{-1}\mathbf{1}}{(\mathbf{1}^T\mathbf{C}^{-1}\mathbf{1})^2} \tag{E.25}$$

$$= \frac{1}{\mathbf{1}^T\mathbf{C}^{-1}\mathbf{1}}, \tag{E.26}$$

where in Eqn. (E.25) we have used the fact that

$$\mathbf{C} \stackrel{\triangle}{=} E\left\{\mathbf{U}\mathbf{U}^T.\right\} \tag{E.27}$$

We see from Eqn. (E.23) that

$$\mathbf{C}_{k,k} = E\left\{\left|u_2[k] - u_2[k-1]\right|^2\right\} \tag{E.28}$$

$$= \left(\frac{\sigma_\nu^2}{2A^2} + \frac{\sigma_\nu^2}{2A^2}\right) \tag{E.29}$$

$$= \frac{\sigma_\nu^2}{A^2}, \tag{E.30}$$

and

$$\mathbf{C}_{k,k+1} = E\left\{(u_2[k] - u_2[k-1])(u_2[k+1] - u_2[k])\right\} \tag{E.31}$$

$$= -\frac{\sigma_\nu^2}{2A^2}. \tag{E.32}$$

Furthermore, $\mathbf{C}_{m,n} = 0$ for $|m-n| > 1$. Thus,

$$\mathbf{C} = \frac{\sigma_\nu^2}{2A^2}\begin{bmatrix} 2 & -1 & 0 & \cdots & 0 \\ -1 & \ddots & \ddots & \ddots & \vdots \\ 0 & \ddots & 2 & -1 & 0 \\ \vdots & \ddots & -1 & 2 & -1 \\ 0 & \cdots & 0 & -1 & 2 \end{bmatrix}. \tag{E.33}$$

The inverse of this matrix is given by [75, 92]

$$\left[\mathbf{C}^{-1}\right]_{i,j} = \frac{2A^2}{\sigma_\nu^2}\left|\min(i,j) - \frac{ij}{N}\right|. \tag{E.34}$$

After some algebra, we have [75]

$$\mathbf{1}^T\mathbf{C}^{-1}\mathbf{1} = \frac{A^2N\left(N^2-1\right)}{6f_s^2\sigma_\nu^2} \tag{E.35}$$

and therefore

$$\mathbf{W}_{\text{Kay}} \triangleq [w_{\text{Kay}}[1], \ldots, w_{\text{Kay}}[N-1]]^T \tag{E.36}$$

$$= \frac{\mathbf{C}^{-1}\mathbf{1}}{\mathbf{1}^T\mathbf{C}^{-1}\mathbf{1}}. \tag{E.37}$$

After some algebraic manipulation, we arrive at

$$w_{\text{Kay}}[k] = \frac{3N}{2\left(N^2-1\right)}\left\{1 - \left[\frac{2k-N}{N}\right]^2\right\}, \quad k = 1, \ldots, N-1. \tag{E.38}$$

Therefore, using Eqn. (E.14), we have

$$\hat{f} = \frac{f_s}{2\pi}\hat{\omega} \tag{E.39}$$

$$= \frac{f_s}{2\pi}\sum_{k=1}^{N-1} w_{\text{Kay}}[k]\Delta\phi_z[k]. \tag{E.40}$$

We note that Eqn. (E.4) holds. Eqns. (E.20) and (E.35) yield

$$\mathrm{var}\left\{\hat{f}\right\} = \frac{3f_s^2\sigma_\nu^2}{2\pi^2 A^2 N\left(N^2-1\right)}, \tag{E.41}$$

which is the Cramér-Rao bound [24, 75, 111, 119].

The frequency estimator given by Eqn. (E.5) is suboptimal because the variance is simply [75] (cf. Eqns. (2.136))

$$\mathrm{var}\left\{\hat{f}_{\mathrm{subopt}}\right\} = \frac{f_s^2\sigma_\nu^2}{4\pi^2 A^2\left(N-1\right)^2}. \tag{E.42}$$

One may wonder why the phase differences should be weighted differently. To shed some light on this issue, we note that the estimator given in Eqn. (E.5) is a telescoping sum, utilizing only two data points, with the other phase differences canceling out! Consequently, the frequency estimate is as noisy as those two points. On the other hand, we see that, in Eqn. (E.39), every phase difference is used. If we formally substitute the absolute phase into the phase differences in Eqn. (E.39), we see that

$$\hat{f} = \frac{f_s}{2\pi}\sum_{k=1}^{N-1} w_{\mathrm{Kay}}[k]\Delta\phi_z[k] \tag{E.43}$$

$$= \frac{f_s}{2\pi}\sum_{k=1}^{N-1} w_{\mathrm{Kay}}[k]\{\mathrm{Arg}(z[k]) - \mathrm{Arg}(z[k-1])\} \tag{E.44}$$

$$= \frac{f_s}{2\pi}\sum_{k=0}^{N-1} (w_{\mathrm{Kay}}[k] - w_{\mathrm{Kay}}[k+1])\mathrm{Arg}(z[n]) \tag{E.45}$$

$$= \frac{f_s}{2\pi}\sum_{k=0}^{N-1} \frac{6(2k-N-1)}{\left(N^2-1\right)N}\mathrm{Arg}(z[n]) \tag{E.46}$$

$$= \frac{3f_s}{\pi(N^2-1)\,N}\sum_{k=0}^{N-1}(2k-N-1)\mathrm{Arg}(z[n]), \tag{E.47}$$

which provides the slope of the least-squares linear regressor fit to the absolute phase data.

E.1.1 Fast FIR Filter Implementation

An efficient implementation of the Kay smoothing filter based on Fast FIR theory is given in Appendix G, in Eqn. (G.121), reproduced here for convenience:

$$w_{\mathrm{Kay}}[n] = \frac{6N}{N^2-1}\left\{\frac{n}{N} - \left(\frac{n}{N}\right)^2\right\} \tag{E.48}$$

for $1 \le n \le N-1$.

$$H_{\mathrm{Kay}}(z) = \frac{6}{N(N^2-1)} \times \frac{(N-1)z^{-1} - (N+1)z^{-2} + (N+1)z^{-N-1} - (N-1)z^{-N-2}}{\left(1-z^{-1}\right)^3}. \tag{E.49}$$

We see that this may be realized with as few as two multiplies and six adds per input sample if a running estimate is desired.

E.2 Slew Estimation

In this section, we assume a signal model similar to the one in Section E.1, but with a non-zero slew. The signal $z[n]$, for $0 \leq n \leq N-1$, consists of a single frequency-slewing sinusoid of initial frequency f_0 and slew rate of $\dot{f}$ plus complex Gaussian white noise $\nu[n]$ with uncorrelated real and imaginary parts and variance σ_ν^2, so that

$$z[n] = A \exp\left(\frac{j2\pi n f_0}{f_s} + \frac{j\pi n(n+1)\dot{f}}{f_s^2} + j\theta\right) + \nu[n]. \tag{E.50}$$

To estimate the slew rate

$$\dot{f}[n] \stackrel{\triangle}{=} f_s(f[n] - f[n-1]) \tag{E.51}$$

we may try calculating the second phase difference

$$\hat{\dot{f}} = \frac{f_s^2}{2\pi}\Delta^2\phi_z[n] \tag{E.52}$$

$$= \frac{f_s^2}{2\pi}(\Delta\phi_z[n] - \Delta\phi_z[n-1]) \tag{E.53}$$

$$= \frac{f_s^2}{2\pi}(\phi_z[n] - 2\phi_z[n-1] + \phi_z[n-2]) \qquad \text{(formally)}, \tag{E.54}$$

where $\phi_z[n]$ is the phase of $z[n]$. We see that if $\nu[n] = 0$ then the second difference gives $\dot{f}$ exactly.

However, since taking differences greatly amplifies noise, we wish to average this result over some interval of n. To do this, we must find the optimal slew weighting coefficients $w_s[k]$. We extend Kay's derivation [75] of the optimal frequency estimator coefficients to find the optimal weighting coefficients for estimating slew from a vector $\mathbf{\Delta}$ of phase-differences, given by Eqn. (E.13).

The expression in Eqn. (E.54) shows that consecutive slew estimates are correlated, and therefore must be whitened to minimize the variance of the estimate. Given N phase samples[3] $\phi_z[k]$, each with variance $\sigma_{\phi_u}^2 = \sigma_\nu^2/2A^2$, we calculate $N-2$ second phase differences $\Delta^2\phi_z[k]$

$$\mathbf{\nabla} \stackrel{\triangle}{=} \left[\Delta^2\phi_z[2], \ldots, \Delta^2\phi_z[N-1]\right]^T \tag{E.55}$$

$$= \begin{bmatrix} \Delta\phi_z[2] - \Delta\phi_z[1] \\ \vdots \\ \Delta\phi_z[N-1] - \Delta\phi_z[N-2] \end{bmatrix} \tag{E.56}$$

$$= \mathbf{D}\mathbf{\Delta} \tag{E.57}$$

where

$$\mathbf{D} \stackrel{\triangle}{=} \begin{bmatrix} 1 & -1 & 0 & \cdots & 0 \\ 0 & 1 & -1 & \ddots & \vdots \\ \vdots & \ddots & \ddots & \ddots & 0 \\ 0 & \cdots & 0 & 1 & -1 \end{bmatrix} \tag{E.58}$$

is the $(n-2) \times (n-1)$ differencing matrix.

[3] Since we are working with the phase *differences* there is no phase ambiguity resulting from extracting the complex phase from $z[k]$.

Hence, the $(n-2)\times(n-2)$ correlation matrix of $\boldsymbol{\nabla}$ is

$$\begin{aligned}
\mathbf{K} &\stackrel{\triangle}{=} E\{\boldsymbol{\nabla}\boldsymbol{\nabla}^T\} && \text{(E.59)}\\
&= \mathbf{D}E\{\boldsymbol{\Delta}\boldsymbol{\Delta}^T\}\mathbf{D}^T && \text{(E.60)}\\
&= \mathbf{D}\mathbf{C}\mathbf{D}^T && \text{(E.61)}\\
&= \frac{\sigma_\nu^2}{2A^2}\begin{bmatrix} 6 & -4 & 1 & 0 & \cdots & 0 \\ -4 & \ddots & \ddots & \ddots & \ddots & \vdots \\ 1 & \ddots & \ddots & \ddots & \ddots & 0 \\ 0 & \ddots & \ddots & 6 & -4 & 1 \\ \vdots & \ddots & \ddots & -4 & 6 & -4 \\ 0 & \cdots & 0 & 1 & -4 & 6 \end{bmatrix}, && \text{(E.62)}
\end{aligned}$$

where $\mathbf{C}$ is the $(n-1)\times(n-1)$ phase difference correlation matrix

$$\mathbf{C} = \frac{\sigma_\nu^2}{2A^2}\begin{bmatrix} 2 & -1 & 0 & \cdots & 0 \\ -1 & \ddots & \ddots & \ddots & \vdots \\ 0 & \ddots & 2 & -1 & 0 \\ \vdots & \ddots & -1 & 2 & -1 \\ 0 & \cdots & 0 & -1 & 2 \end{bmatrix}, \qquad \text{(E.63)}$$

also found in Eqn. (E.33).

The maximum-likelihood, or minimum-variance,[4] estimator for $\dot{f}$, given the phase difference samples $\Delta\phi_z[1],\ldots,\Delta\phi_z[N-1]$, is the value of $\dot{f}$ minimizing [74]

$$J(\dot{f}) = (\boldsymbol{\nabla} - \frac{2\pi\dot{f}}{f_s^2}\mathbf{1})^T\mathbf{K}^{-1}(\boldsymbol{\nabla} - \frac{2\pi\dot{f}}{f_s^2}\mathbf{1}), \qquad \text{(E.64)}$$

which is given by

$$\hat{\dot{f}}^\dagger = \frac{f_s^2}{2\pi}\frac{\mathbf{1}^T\mathbf{K}^{-1}\boldsymbol{\nabla}}{\mathbf{1}^T\mathbf{K}^{-1}\mathbf{1}}, \qquad \text{(E.65)}$$

and this attains the Cramér-Rao minimum variance bound given as

$$\sigma^2_{\dot{f},\min} = \left(\frac{f_s^2}{2\pi}\right)^2\frac{1}{\mathbf{1}^T\mathbf{K}^{-1}\mathbf{1}} \qquad \text{(E.66)}$$

for small disturbances (i.e., with $\mathbf{SNR}_1 > 1$). The optimal weighting coefficients are then given by

$$\mathbf{W}_s \stackrel{\triangle}{=} \frac{\mathbf{K}^{-1}\mathbf{1}}{\mathbf{1}^T\mathbf{K}^{-1}\mathbf{1}}. \qquad \text{(E.67)}$$

By working through some rather uninteresting algebra, using Eqns. (E.13) and (E.34), we find that the window is a fourth degree polynomial:

$$w_s[k] = \frac{30k(k-1)(k-N)(k-N-1)}{N(N^2-1)(N^2-4)}, \qquad \text{(E.68)}$$

[4] A prerequisite for reading this dissertation is knowing that ML, MV, LMS, etc. are all the same for Gaussian random variables.

for $k = 2, \ldots, N-1$. More tedious algebraic manipulations yield that the variance is

$$\sigma_f^2 = \frac{f_s^4 \sigma_\nu^2}{8\pi^2 A^2} \frac{720}{N(N^2-1)(N^2-4)}, \tag{E.69}$$

which is the Cramér-Rao bound.

We present the derivation of a fast FIR filter which has as its impulse response,

$$h_k = \begin{cases} w_s[k], & k = 2, \ldots, N-1 \\ 0, & \text{otherwise,} \end{cases} \tag{E.70}$$

as an exercise for the reader. Refer to Appendix G and Eqn. (E.49) for hints.

Appendix F

A Fuzzy Euclidean Algorithm

Given the frequency estimates $\hat{f}_1$ and $\hat{f}_2$ of two partials and their corresponding variances σ_1^2 and σ_2^2, we wish to determine if they are members of the same harmonic series, and if so, what the best estimate of their common fundamental frequency f_0 is, and with what certainty.

We make use of a modified form of the Euclidean Algorithm which finds the greatest common divisor (GCD) of a pair of positive integers (cf. [104] for a description of the standard Euclidean Algorithm).

The Fuzzy Euclidean Algorithm: If the variances σ_1^2 and σ_2^2 are zero, we are then simply searching for relatively prime integers m_1 and m_2 such that $\hat{f}_0 = \hat{f}_1/m_1 = \hat{f}_2/m_2$, where $\hat{f}_0$ is the desired common fundamental. Otherwise, we are searching for m_1 and m_2 such that $\hat{f}_1/m_1 - \hat{f}_2/m_2$, or equivalently,

$$m_2\hat{f}_1 - m_1\hat{f}_2 \tag{F.1}$$

is within one standard deviation of zero. Assuming independence of the uncertainty in $\hat{f}_1$ and $\hat{f}_2$, the variance of the expression (F.1) is $m_2^2\sigma_1^2 + m_1^2\sigma_2^2$, and thus we try to satisfy the condition

$$\left(m_2\hat{f}_1 - m_1\hat{f}_2\right)^2 < m_2^2\sigma_1^2 + m_1^2\sigma_2^2. \tag{F.2}$$

We also specify a ceiling $f_{\max}$ above which it makes no sense to search for a least common multiple for $\hat{f}_1$ and $\hat{f}_2$, i.e.,

$$m_2\hat{f}_1,\, m_1\hat{f}_2 < f_{\max}. \tag{F.3}$$

The Euclidean Algorithm is normally used to find the GCD of a pair of integers but it may be perfectly well applied to positive real numbers with no modification, provided that $\hat{f}_1$ and $\hat{f}_2$ are exact integer multiples of $\hat{f}_0$. A slight modification is necessary to incorporate condition (F.2) to account for imprecision due to measurement errors.

The "Fuzzy" Euclidean Algorithm finds m_1 and m_2 as follows: Assume that $\hat{f}_1 \geq \hat{f}_2$, otherwise just swap the indices for "1" and "2" in the following. Initialize the recursion with

$$x_0 = \hat{f}_1, \tag{F.4}$$

$$y_0 = \hat{f}_2, \tag{F.5}$$

$$p_1^{(x,0)} = 1, \tag{F.6}$$

$$p_2^{(x,0)} = 0, \tag{F.7}$$

$$p_1^{(y,0)} = 0, \quad \text{and} \tag{F.8}$$
$$p_2^{(y,0)} = 1. \tag{F.9}$$

Then perform the recurrence starting with $n = 0$,

$$a_n = \lfloor x_n / y_n \rfloor, \tag{F.10}$$
$$r_n = x_n - a_n y_n, \tag{F.11}$$
$$x_{n+1} = y_n, \tag{F.12}$$
$$y_{n+1} = r_n, \tag{F.13}$$
$$p_1^{(x,n+1)} = p_1^{(y,n)}, \tag{F.14}$$
$$p_2^{(x,n+1)} = p_2^{(y,n)}, \tag{F.15}$$
$$p_1^{(y,n+1)} = p_1^{(x,n)} - a_n p_1^{(y,n)}, \quad \text{and} \tag{F.16}$$
$$p_2^{(y,n+1)} = p_2^{(x,n)} - a_n p_2^{(y,n)}. \tag{F.17}$$

The expression $\lfloor x \rfloor$ denotes "round x down to the nearest integer less than or equal to x." The p variables have been added to the standard Euclidean Algorithm to keep account of the multiples of $\hat{f}_1$ and $\hat{f}_2$ in each of the x_n and y_n, such that

$$x_n = p_1^{(x,n)} \hat{f}_1 + p_2^{(x,n)} \hat{f}_2 \quad \text{and} \tag{F.18}$$
$$y_n = p_1^{(y,n)} \hat{f}_1 + p_2^{(y,n)} \hat{f}_2. \tag{F.19}$$

If

$$r_n^2 < \left(p_1^{(y,n+1)}\right)^2 \sigma_1^2 + \left(p_2^{(y,n+1)}\right)^2 \sigma_2^2, \tag{F.20}$$

we successfully terminate the iteration, otherwise we continue the recurrence with $n + 1$. On the other hand, if

$$\left|p_1^{(y,n)}\right| \hat{f}_1 > f_{\max} \quad \text{or} \tag{F.21}$$
$$\left|p_2^{(y,n)}\right| \hat{f}_2 > f_{\max} \tag{F.22}$$

then the search for the least common integer multiple of $\hat{f}_1$ and $\hat{f}_2$ exceeds the maximum range, and the algorithm terminates unsuccessfully. It is apparent that if either σ_1^2 or σ_2^2 is non-zero then Eqn. (F.20) will necessarily eventually be fulfilled if conditions (F.21) and (F.22) are not posited. Alternatively, absolute bounds may be placed on $p_1^{(y,n)}$ and $p_2^{(y,n)}$, for example

$$\left|p_1^{(y,n)}\right|, \left|p_2^{(y,n)}\right| < P_{\max}. \tag{F.23}$$

If condition (F.20) has been satisfied at step N, we have that

$$m_2 = \left|p_1^{(y,N+1)}\right| \quad \text{and} \tag{F.24}$$
$$m_1 = \left|p_2^{(y,N+1)}\right|. \tag{F.25}$$

When we have found m_1 and m_2, we have two estimates of the fundamental: $\hat{f}_1/m_1$ and $\hat{f}_2/m_2$. The estimates have variances σ_1^2/m_1^2 and σ_2^2/m_2^2 respectively. We consolidate the two estimates by

weighting each with the reciprocal of its variance:

$$\hat{f}_0 = \frac{\left(\sigma_1^2/m_1^2\right)^{-1}\hat{f}_1/m_1 + \left(\sigma_2^2/m_2^2\right)^{-1}\hat{f}_2/m_2}{\left(\sigma_1^2/m_1^2\right)^{-1} + \left(\sigma_2^2/m_2^2\right)^{-1}} \tag{F.26}$$

$$= \frac{m_1\sigma_2^2\hat{f}_1 + m_2\sigma_1^2\hat{f}_2}{m_2^2\sigma_1^2 + m_1^2\sigma_2^2}. \tag{F.27}$$

If $\hat{f}_1$ and $\hat{f}_2$ are independent Gaussian random variables then this is the maximum likelihood estimate, given $\hat{f}_1$, $\hat{f}_2$, m_2, m_1, σ_1^2 and σ_2^2. This may be seen by calculating the joint conditional probability density of $\hat{f}_1/m_1$ and $\hat{f}_2/m_2$ given f_0, and maximizing with respect to f_0. Thus, assuming independence of $\hat{f}_1$ and $\hat{f}_2$, we have

$$p(\hat{f}_1/m_1, \hat{f}_2/m_2|f_0) = p(\hat{f}_1/m_1|f_0)p(\hat{f}_2/m_2|f_0) \tag{F.28}$$

$$= \frac{m_1 m_2}{2\pi\sigma_1\sigma_2}\exp\left(-\frac{\left(f_0 - \hat{f}_1/m_1\right)^2}{2\sigma_1^2/m_1^2} - \frac{\left(f_0 - \hat{f}_2/m_2\right)^2}{2\sigma_2^2/m_2^2}\right). \tag{F.29}$$

We need to maximize this expression with respect to f_0. We may equivalently minimize

$$\frac{\left(f_0 - \hat{f}_1/m_1\right)^2}{2\sigma_1^2/m_1^2} + \frac{\left(f_0 - \hat{f}_2/m_2\right)^2}{2\sigma_2^2/m_2^2},$$

yielding Eqn. (F.26). The variance of $\hat{f}_0$ is then

$$\sigma_0^2 = \frac{m_1^2\sigma_2^4\sigma_1^2 + m_2^2\sigma_1^4\sigma_2^2}{\left(m_2^2\sigma_1^2 + m_1^2\sigma_2^2\right)^2} \tag{F.30}$$

$$= \frac{\sigma_1^2\sigma_2^2}{\left(m_2^2\sigma_1^2 + m_1^2\sigma_2^2\right)}. \tag{F.31}$$

These results may be easily extended, to an arbitrarily large number of harmonic frequency estimates. If we have determined $(\hat{f}_1, \sigma_1, m_1), \ldots, (\hat{f}_N, \sigma_N, m_N)$, we may estimate f_0 as

$$\hat{f}_0 = \frac{\left(\sigma_1^2/m_1^2\right)^{-1}\hat{f}_1/m_1 + \ldots \left(\sigma_N^2/m_N^2\right)^{-1}\hat{f}_N/m_2}{\left(\sigma_1^2/m_1^2\right)^{-1} + \ldots \left(\sigma_N^2/m_N^2\right)^{-1}}. \tag{F.32}$$

The proof that this is the maximum-likelihood estimate is the same as the case for $N = 2$ given above, assuming independence of $\hat{f}_1, \ldots, \hat{f}_N$. The variance is given similarly as

$$\sigma_0^2 = \frac{\left(\sigma_1^2/m_1^2\right)^{-1} + \ldots \left(\sigma_N^2/m_N^2\right)^{-1}}{\left(\left(\sigma_1^2/m_1^2\right)^{-1} + \ldots \left(\sigma_N^2/m_N^2\right)^{-1}\right)^2} \tag{F.33}$$

$$= \frac{1}{m_1^2/\sigma_1^2 + \ldots m_N^2/\sigma_N^2}. \tag{F.34}$$

Appendix G

Fast Finite Impulse Response (FIR) Digital Filter Implementations

G.1 Introduction

Infinite impulse response (IIR) recursive linear digital filters are widely used because of their low computational cost and low storage overhead requirements. Finite impulse response (FIR) filters, on the other hand, allow the possibility of implementing linear-phase linear digital filters which have constant group delay across all frequencies. The tradeoff is that to achieve similar magnitude transfer functions, FIR filters usually require much larger filter orders than their IIR counterparts. For example, a general N-th order FIR filter requires $N+1$ multiplies and N adds. In certain cases, however, FIR filters may be designed which have an operation count comparable to that of an IIR filter while maintaining the linear phase property.

The set of finite impulse responses which may be efficiently implemented includes those which are truncated IIR (TIIR) sequences of low order. Although the following results were derived independently of Saramäki and Fam [52, 123], the idea of using truncated IIR filters to generate linear-phase filters was originally introduced by Fam [52]. Fam and Saramäki [52, 123] deal with unstable hidden modes due to pole-zero cancellations outside of the unit circle by employing a switching and resetting algorithm to reduce the effects of quantization error buildup. We introduce a slightly more efficient version of this idea, as well as an error analysis.

In this paper, we describe a similar algorithm for the efficient implementation of certain classes of FIR filters. We introduce an extension of the TIIR algorithm which allows the truncation of arbitrary IIR filter tails. Our algorithm allows the possibility of implementing polynomial impulse responses. Additionally, we present an analysis of the effects of limited numerical precision and provide design guidelines for designing systems with acceptable noise tolerance.

G.2 Definitions

A general causal N-th order FIR filter consists of a tapped delay line N elements long and a table of $N+1$ impulse response coefficients $\{h_0, \ldots, h_N\}$ such that at each time step n the output

$$y[n] = \sum_{k=0}^{N} h_k x[n-k] \tag{G.1}$$

is formed. The transfer function has the simple form

$$\begin{aligned} H_{\mathrm{FIR}}(z) &\stackrel{\triangle}{=} h_0 + h_1 z^{-1} + \ldots + h_N z^{-N} && \text{(G.2)} \\ &= z^{-N} C(z), && \text{(G.3)} \end{aligned}$$

where $C(z)$ is the N-th degree polynomial formed by the h_k. On the other hand, a causal P-th order IIR filter has the relation

$$y[n] = -\sum_{k=1}^{P} a_k y[n-k] + \sum_{\ell=0}^{P} b_\ell x[n-\ell]. \tag{G.4}$$

The corresponding transfer function is

$$\begin{aligned} H_{\mathrm{IIR}}(z) &\stackrel{\triangle}{=} \frac{b_0 + b_1 z^{-1} + \ldots + b_P z^{-P}}{1 + a_1 z^{-1} + \ldots + a_P z^{-P}} && \text{(G.5)} \\ &= \frac{b_0 z^P + b_1 z^{P-1} + \ldots + b_P}{z^P + a_1 z^{P-1} + \ldots + a_P} && \text{(G.6)} \\ &= \frac{B(z)}{A(z)} && \text{(G.7)} \\ &= h_0 + h_1 z^{-1} + h_2 z^{-2} + \ldots, && \text{(G.8)} \end{aligned}$$

where both

$$A(z) = z^P + a_1 z^{P-1} + \ldots + a_P \tag{G.9}$$

and

$$B(z) = b_0 z^P + b_1 z^{P-1} + \ldots + b_P \tag{G.10}$$

may be assumed to be relatively prime P-th degree polynomials in z, and $A(z)$ is monic by construction.[1] We use the forms in Eqns. (G.5) and (G.6) interchangeably. Eqn. (G.8) is the expansion of the transfer function in terms of the impulse response $\{h_0, h_1, \ldots\}$. $A(z)$ is also known as the *characteristic polynomial* of the filter, and its roots, i.e., the poles, determine the filter dynamics.

Group delay [108] is defined by

$$\delta(\omega) \stackrel{\triangle}{=} -\frac{d \arg\{H(e^{j\omega})\}}{d\omega}. \tag{G.11}$$

The group delay at normalized frequency $\omega = 2\pi f/f_s$, where f_s is the sampling frequency, is the number of samples of delay experienced by the amplitude envelope of a narrow-band input signal centered at ω.

[1] A *monic* polynomial of degree N has 1 as the coefficient of the highest degree term z^N.

A *linear-phase filter* is one such that the phase response at a given frequency is a linear function of frequency, i.e. $\arg\left\{H(e^{j\omega})\right\} = K_1\omega + K_2$ for some constants K_1 and K_2. From this property we see immediately that the group delay is constant for all frequencies. Filters with linear phase response are often desirable because they have no frequency-dependent temporal distortion. A stable IIR filter with non-zero poles cannot have linear phase. However, an FIR filter with coefficients $\{h_0, \ldots, h_N\}$ has linear phase if there exists a ψ such that for all $k \in \{0, \ldots, N\}$

$$h_{N-k} = e^{j\psi} h_k^*, \tag{G.12}$$

i.e., if the reversed coefficients are the complex conjugates of the forward sequence plus a constant phase shift. This may be seen by considering

$$\begin{aligned}
H(e^{j\omega}) &= \sum_{k=0}^{N} h_k e^{-jk\omega} \\
&= \frac{1}{2}\sum_{k=0}^{N} \left(h_k e^{-jk\omega} + h_{N-k} e^{-j(N-k)\omega}\right) \\
&= \frac{e^{-jN\omega/2}}{2}\sum_{k=0}^{N} \left(h_k e^{-j(2k-N)\omega/2} + e^{j\psi} h_k^* e^{j(2k-N)\omega/2}\right) \\
&= \frac{e^{-j(N\omega-\psi)/2}}{2}|h_k|\sum_{k=0}^{N} \left(e^{-j((2k-N)\omega/2-\theta_k+\psi/2)} + e^{j((2k-N)\omega/2-\theta_k+\psi/2)}\right) \\
&= e^{-j(N\omega-\psi)/2}\sum_{k=0}^{N} |h_k| \cos\left(\frac{(2k-N)\omega + 2\theta_k + \psi}{2}\right),
\end{aligned} \tag{G.13}$$

where $\theta_k \stackrel{\triangle}{=} \arg(h_k)$. Thus,

$$\arg\left(H\left(e^{j\omega}\right)\right) = \frac{-N\omega + \psi}{2}, \tag{G.14}$$

and the group delay is

$$\delta(f) = \frac{N}{2}. \tag{G.15}$$

G.3 Truncated IIR (TIIR) Filters

Consider an FIR filter having a truncated geometric sequence $\{h_0, h_0 p, \ldots, h_0 p^N\}$ as an impulse response. This filter has the same impulse response for the first $N+1$ terms as the one-pole IIR filter with transfer function

$$H_{\mathrm{IIR}}(z) = \frac{h_0}{1 - pz^{-1}}. \tag{G.16}$$

If we subtract off the tail of the impulse response we obtain

$$H_{\mathrm{FIR}}(z) = h_0 + h_0 p z^{-1} + \ldots + h_0 p^N z^{-N} \tag{G.17}$$

$$\begin{aligned}
&= \left\{h_0 + h_0 p z^{-1} + \ldots\right\} \\
&\quad - \left\{h_0 p^{N+1} z^{-(N+1)} + h_0 p^{(N+2)} z^{-(N+2)} + \ldots\right\}
\end{aligned} \tag{G.18}$$

$$= \frac{h_0}{1 - pz^{-1}} - \frac{h_0 p^{N+1} z^{-(N+1)}}{1 - pz^{-1}} \tag{G.19}$$

$$= h_0 \frac{1 - p^{N+1} z^{-(N+1)}}{1 - p z^{-1}}. \tag{G.20}$$

The output relation for this filter is

$$y[n] = \sum_{k=0}^{N} h_0 p^k x[n-k] \tag{G.21}$$

$$= p y[n-1] + h_0 \left(x[n] - p^{N+1} x[n-(N+1)] \right). \tag{G.22}$$

We see that the first formulation, Eqn. (G.21), requires $N+1$ multiplies and N adds to implement directly, whereas the second formulation, Eqn. (G.22), requires only 3 multiplies and 2 adds, independent of N. Thus we see that if we can represent an FIR sequence as a truncated exponential sequence, a tremendous savings in computation can be achieved. Note that the $x[n-(N+1)]$ term in Eqn. (G.22) still requires a delay line to be maintained, and thus there are no savings in storage. With modern digital signal processing (DSP) chips, however, ring buffers may be implemented with virtually no computational overhead and the full savings in computational cost may be achieved.

Notice that there is a pole-zero cancellation in the representation given by Eqn. (G.20). If $|p| < 1$ there is no problem since the system is inherently stable. If $|p| \geq 1$, however, then there is a potential problem due to the hidden mode. We will deal with this in Section G.4 where we will see how to run TIIR filters with unstable modes.

The idea of this section was used by Fam [52] where a partial fraction expansion of a transfer function is taken and each mode is truncated separately using Eqn. (G.20). This method works only for cases in which the multiplicity of each pole is one, so that the each mode exhibits a simple exponential decay.

G.3.1 Extension to Higher-Order TIIR Sequences

We may extend the idea of the previous section for computing the TIIR sequence of any rational $H(z)$. The general procedure is to find the "tail" IIR transfer function

$$\begin{aligned} H'_{\mathrm{IIR}}(z) &= h'_0 z^{-1} + h'_1 z^{-2} + \ldots \\ &\triangleq h_{N+1} z^{-1} + h_{N+2} z^{-2} + \ldots \end{aligned} \tag{G.23}$$

whose impulse response, except for a time shift of N steps, matches the tail of the transfer function $H_{\mathrm{IIR}}(z)$ which we would like to truncate after time step N.

We multiply Eqn. (G.8) by z^N and obtain

$$\begin{aligned} z^N H_{\mathrm{IIR}}(z) &= h_0 z^N + \ldots + h_{N-1} z + h_N \\ &\quad + h_{N+1} z^{-1} + h_{N+2} z^{-2} + \ldots \end{aligned} \tag{G.24}$$

$$= C(z) + H'_{\mathrm{IIR}}(z) \tag{G.25}$$

$$= \frac{z^N B(z)}{A(z)} \tag{G.26}$$

$$= C(z) + \frac{B'(z)}{A(z)}, \tag{G.27}$$

where $\mathrm{Deg}\{B'(z)\} < \mathrm{Deg}\{A(z)\} = P$. We may assume that $\mathrm{Deg}\{B'(z)\} = P-1$. $B'(z)$ is unique and may be obtained by performing synthetic division on $z^N B(z)$ by $A(z)$ and finding the remainder. Thus, $z^N B(z) \equiv B'(z) \pmod{A(z)}$.

Once we have obtained $B'(z)$ we have $H'_{\rm IIR}(z) = B'(z)/A(z)$ and we may write

$$H_{\rm FIR}(z) = H_{\rm IIR}(z) - z^{-N} H'_{\rm IIR}(z) \tag{G.28}$$

$$= \frac{B(z) - z^{-N} B'(z)}{A(z)} \tag{G.29}$$

The corresponding system is

$$y[n] = -\sum_{k=1}^{P} a_k\, y[n-k] + \sum_{\ell=0}^{P} b_\ell x[n-\ell] - \sum_{m=0}^{P-1} b'_m x[n-m-(N+1)], \tag{G.30}$$

using the representation in Eqn. (G.29).

The fact that the denominators of the transfer functions $H_{\rm IIR}(z)$ and $H'_{\rm IIR}(z)$ are the same allows additional savings in computational cost due to the fact that the original IIR and tail IIR dynamics are the same and do not need to be performed twice. The term $z^{-(N+1)} z^{-(P-1)} B'(z)$ serves to zero out the dynamics at the end of the delay line and requires only an additional P multiplies and $P-1$ adds. The computational cost of this general truncated P-th order IIR system is $3P+1$ multiplies and $3P-2$ adds, independent of N. Thus, a net computational savings with this class of FIR filters is achieved if $N > 3P$.

The storage costs for this filter are P output samples for the IIR feedback dynamics, N input samples of the FIR filter, and an additional P input samples for the tail-cancellation dynamics, yielding $N+P$ input delay samples, of which only the first and last P are used, and P output delay samples. Thus, the fast FIR algorithm actually requires $2P$ more storage samples than a direct FIR implementation.

As in the previous section, we observe cautiously that the effect of subtracting the tail IIR response $z^{-N} H'_{\rm IIR}(z)$ from $H_{\rm IIR}(z)$ is to cancel all the poles in Eqn. (G.29), which is to be expected since an FIR filter is an all-zero filter.

G.3.2 Other Architectures

The direct implementation specified by Eqn. (G.30) may not be desirable for various reasons. For example, one may choose to use a factored structure such as the cascaded biquad or the parallel partial fraction form.

The basic biquad factorization for a $P = 2Q$-th degree transfer function is given by

$$H(z) = b_0 \prod_{k=1}^{Q} \frac{1 + b_{1,k} z^{-1} + b_{2,k} z^{-2}}{1 + a_{1,k} z^{-1} + a_{2,k} z^{-2}}. \tag{G.31}$$

Each sample is calculated in a cascade

$$x_0[n] = b_0 x[n], \tag{G.32}$$

$$x_k[n] = x_{k-1}[n] - a_{1,k} x_k[n-1] - a_{2,k} x_k[n-2] + b_{1,k} x_{k-1}[n-1] + b_{2,k} x_{k-1}[n-2], \quad k \geq 1, \text{ and} \tag{G.33}$$

$$y[n] = x_Q[n], \tag{G.34}$$

thus requiring $4Q+1 = 2P+1$ multiplies and $4Q = 2P$ adds per sample. Biquad structures are especially suited for the efficient and numerically stable computation of large-order IIR filters which

often have large coefficients when left unfactored. Additionally, complex-conjugate pole pairs may be conveniently grouped together. Since the TIIR filter structure does not lend itself to biquad factorization, the form in Eqn. (G.28) must be taken and the recursive dynamics must be computed twice, resulting in a computational cost of $8Q + 1 = 4P + 1$ multiplies and $8Q + 1 = 4P + 1$ adds per sample. Thus, this realization is somewhat more computationally expensive than the direct realization.

We may also factor $H(z)$ modally into a partial fraction expansion:

$$H(z) = \sum_{k=1}^{N_p} \sum_{\ell=1}^{M_k} \frac{C_{k,\ell}}{(1 - p_k z^{-1})^\ell}, \tag{G.35}$$

where N_p is the number of distinct poles, and M_k is the multiplicity of the k-th pole. The (k, ℓ) partial fraction gives rise to a filter which has as impulse response

$$h_{k,\ell,n} = C_{k,\ell} \binom{n + \ell - 1}{\ell - 1} p_k^n. \tag{G.36}$$

To form the TIIR filter, a tail IIR filter is derived for each partial fraction using synthetic division as outlined in Section G.3.1. Each TIIR response is calculated separately, and the results are added together to form the complete response. The factorization need not be as complete as outlined in Eqn. (G.35). one may choose an intermediate level of factorization, leaving some factors lumped together and others separated from each other. For example, one may want to group complex-conjugate pairs together, thus avoiding complex arithmetic.

Alternatively, one may wish to leave terms with the same poles together as in

$$H(z) = \sum_{k=1}^{N_p} \frac{B_k(z)}{(z - p_k)^{M_k}}, \tag{G.37}$$

since calculating the tail IIR response for each n-th order multiplicity term yields a degree $n - 1$ polynomial numerator anyway. The impulse response of the k-th partial fraction in this case is

$$h_{k,n} = \sum_{\ell=0}^{M_k} b_{k,\ell} \binom{n - \ell + M_k - 1}{M_k - 1} p_k^{n-\ell} \tag{G.38}$$

where the $b_{k,\ell},\ \ell = 0, \ldots, M_k$ are the coefficients of $B_k(z)$.

Another example is to group together the stable factors, i.e., with poles p_k such that $|p_k| < 1$, and implement the unstable poles with $|p_k| < 1$ separately. These strategies will become useful in Section G.5.

G.4 Unstable Hidden Modes

We now address the issue of pole-zero cancellation and the resulting hidden modes in the fast FIR algorithm. Although the naïve Fast FIR algorithm of Eqn. (G.30) works in theory there is the practical matter of quantization error due to finite register lengths when dealing with truncated unstable IIR systems, i.e., those with poles p_k such that $|p_k| > 1$. Consider the system in equation (G.22). We may model quantization error as an independent, identically distributed (IID) noise

$n \equiv 0 \pmod N$	$n \not\equiv 0 \pmod N$
Primary TIIR Filter	
$w_1[N+k] \leftarrow 0, \quad k = 1, \ldots, P-1$ $w_1[k] \leftarrow w_1[k-1], \quad k = N, \ldots, 1$ $w_1[0] \leftarrow x[n]$ $q_1[k] \leftarrow q_2[k-1], \quad k = P, \ldots, 1$ $q_1[0] \leftarrow -\sum_{k=1}^{P} a_k q_1[k] + \sum_{\ell=0}^{P} b_\ell w_1[\ell]$ $y[n] \leftarrow q_1[0]$	$w_1[k] \leftarrow w_1[k-1], \quad k = N+P, \ldots, 1$ $w_1[0] \leftarrow x[n]$ $q_1[k] \leftarrow q_1[k-1], \quad k = P, \ldots, 1$ $q_1[0] \leftarrow -\sum_{k=1}^{P} a_k q_1[k] + \sum_{\ell=0}^{P} b_\ell w_1[\ell] - \sum_{m=0}^{P-1} b'_m w_1[m+N+1]$ $y[n] \leftarrow q_1[0]$
Auxiliary TIIR Filter	
$w_2[k] \leftarrow 0, \quad k = 1, \ldots, P-1$ $w_2[0] \leftarrow x[n]$ $q_2[k] \leftarrow 0, \quad k = 1, \ldots, P-1$ $q_2[0] \leftarrow b_0 w_2[0]$	$w_2[k] \leftarrow w_2[k-1], \quad k = P, \ldots, 1$ $w_2[0] \leftarrow x[n]$ $q_2[k] \leftarrow q_2[k-1], \quad k = P, \ldots, 1$ $q_2[0] \leftarrow -\sum_{k=1}^{P} a_k q_2[k] + \sum_{\ell=0}^{P} b_\ell w_2[\ell]$

Table G.1: Fast FIR algorithm for an unstable Truncated IIR (TIIR) filter.

$n \equiv 0 \pmod N$	$n \not\equiv 0 \pmod N$
Primary TIIR Filter	
$w_1[N+k] \leftarrow 0, \quad k = 1, \ldots, P-1$ $w_1[k] \leftarrow w_1[k-1], \quad k = N, \ldots, 1$ $w_1[0] \leftarrow x[n]$ $q_1[k] \leftarrow q_2[k-1], \quad k = P, \ldots, 1$ $q_1[0] \leftarrow -\sum_{k=1}^{P-1} \frac{a_k^* q_1[P-k]}{a_P^*} - \frac{q_1[P]}{a_P^*} + \sum_{m=0}^{P-1} \frac{b_m'^* w_1[P-1-m]}{a_P^*}$	$w_1[k] \leftarrow w_1[k-1], \quad k = N+P, \ldots, 1$ $w_1[0] \leftarrow x[n]$ $q_1[k] \leftarrow q_1[k-1], \quad k = P, \ldots, 1$ $q_1[0] \leftarrow -\sum_{k=1}^{P-1} \frac{a_k^* q_1[P-k]}{a_P^*} - \frac{q_1[P]}{a_P^*} + \sum_{m=0}^{P-1} \frac{b_m'^* w_1[P-1-m]}{a_P^*} - \sum_{\ell=0}^{P} \frac{b_\ell^* w_1[N+P-\ell]}{a_P^*}$ $y[n] \leftarrow q_1[0]$
Auxiliary TIIR Filter	
$w_2[k] \leftarrow 0, \quad k = 1, \ldots, P-1$ $w_2[0] \leftarrow x[n]$ $q_2[k] \leftarrow 0, \quad k = 1, \ldots, P-1$ $q_2[0] \leftarrow \frac{b_{P-1}'^* w_2[0]}{a_P^*}$	$w_2[k] \leftarrow w_2[k-1], \quad k = P, \ldots, 1$ $w_2[0] \leftarrow x[n]$ $q_2[k] \leftarrow q_2[k-1], \quad k = P, \ldots, 1$ $q_2[0] \leftarrow -\sum_{k=1}^{P-1} \frac{a_k^* q_2[P-k]}{a_P^*} - \frac{q_2[P]}{a_P^*} + \sum_{m=0}^{P-1} \frac{b_m'^* w_2[P-1-m]}{a_P^*}$

Table G.2: Fast FIR algorithm for a reversed unstable Truncated IIR (TIIR) filter derived from a stable TIIR filter.

signal $\nu[n]$ with zero mean and variance σ_ν^2 input to the system of Eqn. (G.22).[2] The output equation is then

$$y[n] = py[n-1] + h_0\left(x[n] - p^{N+1}x[n-(N+1)]\right) + \nu[n] \tag{G.39}$$

$$= h_0 \sum_{k=0}^{N-1} p^k x[n-k] + \sum_{k=0}^{n} p^k \nu[n-k]. \tag{G.40}$$

Thus, the accumulated noise has zero mean, but its variance grows as

$$\sigma_{\text{acc}}^2[n] = \sum_{k=0}^{n} |p|^{2k}\sigma_\nu^2 \tag{G.41}$$

$$= \sigma_\nu^2 \frac{1-|p|^{2(n+1)}}{1-|p|^2} \tag{G.42}$$

so that

$$\lim_{n\to\infty} \sigma_{\text{acc}}^2[n] = \begin{cases} +\infty, & |p| \geq 1 \\ \dfrac{\sigma_\nu^2}{1-|p|^2}, & |p| < 1. \end{cases} \tag{G.43}$$

For a higher-order system, as described in Section G.3.1, this analysis gives an estimate of the noise accumulation behavior if p is the largest-magnitude pole since its dynamics dominates the behavior of the system. A direct implementation of an FIR system, such as in equation (G.21) does not have noise accumulation problems because of its finite memory. We trade computational cost for noise sensitivity in TIIR systems.

Recalling the discussion in Section G.3.2, we may factor the unstable modes of a system apart from the transfer function so that

$$H(z) = H^{\downarrow}(z) + H^{\uparrow}(z) \tag{G.44}$$

$$= \frac{B^{\downarrow}(z)}{A^{\downarrow}(z)} + \frac{B^{\uparrow}(z)}{A^{\uparrow}(z)}, \tag{G.45}$$

where the "$\downarrow$" and "$\uparrow$" superscripts denote "stable hidden modes" and "unstable hidden modes," respectively. Thus, we may implement the two filters of orders $P^{\downarrow}$ and $P^{\uparrow}$, where $P^{\downarrow} + P^{\uparrow} = P$, and add together the outputs. $H^{\downarrow}(z)$ may be implemented as described in Section G.3.1, but $H^{\uparrow}(z)$ must be handled carefully.

Alternatively, we may factor the transfer function into stable and unstable parts

$$H(z) = H^{\downarrow}(z)H^{\uparrow}(z) \tag{G.46}$$

$$= \frac{B^{\downarrow}(z)}{A^{\downarrow}(z)}\frac{B^{\uparrow}(z)}{A^{\uparrow}(z)}, \tag{G.47}$$

in which case the stable and unstable filters are cascaded. Note that in this factorization $B^{\downarrow}(z)$ and $B^{\uparrow}(z)$ are not uniquely determined.

[2] Finite-register effects may be modeled as the sum of q uniformly distributed IID $[-\epsilon, +\epsilon]$, where $\epsilon > 0$ is the smallest quantity such that $x + \epsilon \neq x$ in machine arithmetic, and q is the number of additive terms. If q is relatively large, the total noise may be modeled as a Gaussian distribution. For fixed-point arithmetic ϵ is constant $\forall x$. Floating point arithmetic presents difficulties since the effective ϵ varies proportionally to the magnitude of x. Assuming independence and fixed-point arithmetic, we may model quantization noise as a Gaussian random variable with variance $\sigma_\nu^2 = q\epsilon^2/3$. A thorough analysis of quantization noise statistics is beyond the scope of this paper.

A possible algorithm for stabilizing an unstable TIIR filter using two parallel sets of state variables is given in Table G.1. The algorithm cycles with a period of N time steps. Given a cycle number k, at time step $n = kN$ the auxiliary filter's input delay line $w_2[\cdot]$ of length P and P state variables $q_2[\cdot]$ are cleared to zero. Otherwise the primary and auxiliary systems evolve with the same dynamics. We have taken into account the fact that during the first N time steps the tail canceling terms due to $z^{-N}B'(z)$ in the auxiliary filter are identically zero, hence those terms are not included. Since the FIR impulse response has length $N+1$ we see that at time $n = kN + N$ the two systems have identical output values, except for the amount of accumulated noise. The state variables $q_1[\cdot]$ and $q_2[\cdot]$ are not identical because the input histories are slightly different. However, since we are only concerned with the output, this does not matter. We then copy the auxiliary system's state variables to the primary system and repeat the cycle. This algorithm may be optimized by realizing that the values for $w_2[m]$ are zero for $m > N$ during each cycle. Thus the last summation in the dynamics for the auxiliary system shown in Table G.1 is omitted for the cases where $n \equiv 1, \ldots, N \pmod{N}$.

Under this scheme the amount of time that quantization errors can accumulate varies from a minimum of N time steps to a maximum of $2N$, depending on when each error occurs. The minimum is due to the amount of time necessary to allow the auxiliary system to evolve to having the same output value as the primary system. For noise accumulation analysis in this system, we may assume that the unstable system dynamics are dominated by the mode with the largest eigenvalue $p_{\max}$ such that $|p_{\max}| > 1$. We assume for the present analysis that the multiplicity of $p_{\max}$ is one. Thus we must reckon for tolerable performance with

$$\sigma^2_{\max} \geq \sigma^2_\nu \frac{1 - |p_{\max}|^{4N}}{1 - |p_{\max}|^2}. \tag{G.48}$$

If the maximum tolerable noise variance is σ^2_{tol} then we must have $\sigma^2_{\max} < \sigma^2_{\text{tol}}$ so that, approximately,

$$N < \frac{\log\left(1 + \frac{(|p_{\max}|^2 - 1)\sigma^2_{\text{tol}}}{\sigma^2_\nu}\right)}{4\log(|p_{\max}|)}. \tag{G.49}$$

Thus, given $p_{\max}$, σ^2_{tol}, and quantization noise variance σ^2_ν, we have a fundamental limitation on the length of the effective impulse response. A refinement of this bound is given below in Section G.5.3.

The computational cost for implementing an unstable TIIR filter is at most twice the cost of a stable TIIR filter. The extra cost is due to the cost of implementing the auxiliary TIIR filter, which costs about $2P$ operations per sample. Thus the computational cost of the unstable TIIR filter is approximately $5P$ multiples per input sample. The number of adds is about the same. If we take into account the fact that the feed-forward terms due to $B(z)$ are the same (except for cases where $w_2[k]$ has been set to zero) in both the primary and auxiliary systems, we may optimize by avoiding duplicate calculation of these terms and thus reduce the total number of multiplies and adds to about $4P$ per input sample. The shifts of the state variables and input delay lines may be simulated by using pointer arithmetic, and need not actually be performed.

G.5 Fast Linear-Phase FIR Filters

The implementation of filters as TIIR systems is rather pointless unless there is an advantage that is unavailable to untruncated IIR filters. That advantage is that it is possible to implement exactly linear-phase filters. We present two basic strategies for designing filters based on TIIR filters. The first uses the factorization given in Eqn. (G.44), and the second uses the factorization used in Eqn. (G.46).

G.5.1 Additive Factorization Design Method

We saw in Section G.2 that an FIR filter has linear phase if Eqn. (G.12) holds. It is possible to attain such a relation using TIIR filters. Let $H^+_{\rm FIR}(z)$ be a TIIR transfer function such that

$$H^+_{\rm FIR}(z) = \sum_{k=0}^{N} h^+_k z^{-k} \tag{G.50}$$

$$= \frac{B^+(z) - z^{-N} B'^+(z)}{A^+(z)}. \tag{G.51}$$

We form the time-reversed truncated transfer function

$$H^-_{\rm FIR}(z) = \sum_{k=0}^{N} h^-_k z^{-k} \tag{G.52}$$

$$= \sum_{k=0}^{N} h^{+*}_k z^{k-N} \tag{G.53}$$

$$= z^{-N} \left\{H^+_{\rm FIR}\left(1/z^*\right)\right\}^* \tag{G.54}$$

$$= \frac{z^{-N} \left\{B^+\left(1/z^*\right)\right\}^* - \left\{B'^+\left(1/z^*\right)\right\}^*}{\left\{A^+\left(1/z^*\right)\right\}^*} \tag{G.55}$$

$$= \frac{z^{-N} z^{-P} B^-(z) - z^{-(P-1)} B'^-(z)}{z^{-P} A^-(z)} \tag{G.56}$$

$$= \frac{-z B'^-(z) + z^{-N} B^-(z)}{A^-(z)}, \tag{G.57}$$

where the "+" and "−" superscripts denote "forward" and "reverse-conjugated" filter respectively, and the "*" superscript denotes complex conjugation, as usual. Thus, comparing with Eqns. (G.9) and (G.10), we have

$$A^-(z) = 1 + a^*_1 z + \ldots + a^*_P z^P, \tag{G.58}$$

$$B^-(z) = b^*_0 + b^*_1 z + \ldots + b^*_P z^P, \tag{G.59}$$

and

$$B'^-(z) = b'^*_0 + b'^*_1 z + \ldots + b'^*_{P-1} z^{P-1}. \tag{G.60}$$

We have assumed that $B^+(z)$ and $B'^-(z)$ have degrees P and $P-1$, respectively. If we assume that $H^+_{\rm FIR}(z)$ is a stable TIIR filter then $H^-_{\rm FIR}(z)$ is an unstable TIIR filter whose hidden modes are conjugate-reciprocals of those of $H^+_{\rm FIR}(z)$. An example implementation for $H^-_{\rm FIR}(z)$ is given in Table G.2. There we have normalized the numerator and denominator of the filter by dividing through by a^*_P.

Using the arbitrary time shift $M \geq 0$ and phase shift ψ we define the filter

$$H_{\rm LPFIR}(z) \stackrel{\Delta}{=} H^+_{\rm FIR}(z) + e^{j\psi} z^{-M} H^-_{\rm FIR}(z) \tag{G.61}$$

$$= \sum_{k=0}^{N} h^+_k z^{-k} + e^{j\psi} \sum_{k=0}^{N} h^{+*}_k z^{k-N-M} \tag{G.62}$$

We note that this new FIR filter of length $M+N+1$ is invariant with respect to reversing the order, conjugating the coefficients, and multiplying by the phase factor $\exp(j\psi)$. Eqn. (G.12) holds, and

thus $H_{\mathrm{LPFIR}}(z)$ is a linear-phase FIR filter. We may see the linear-phase property more directly by first noticing that, on the unit circle,

$$H^-_{\mathrm{FIR}}\left(e^{j\omega}\right) = e^{-jN\omega}\left\{H^+_{\mathrm{FIR}}\left(e^{j\omega}\right)\right\}^*, \tag{G.63}$$

so that

$$\begin{aligned} H_{\mathrm{LPFIR}}\left(e^{j\omega}\right) &= H^+_{\mathrm{FIR}}\left(e^{j\omega}\right) + e^{j\psi}e^{-jM\omega}H^-_{\mathrm{FIR}}\left(e^{j\omega}\right) && \text{(G.64)}\\ &= H^+_{\mathrm{FIR}}\left(e^{j\omega}\right) + e^{j\psi}e^{-j(N+M)\omega}\left\{H^+_{\mathrm{FIR}}\left(e^{j\omega}\right)\right\}^* && \text{(G.65)}\\ &= e^{-j((N+M)\omega+\psi)/2}\mathrm{Re}\left\{e^{j((N+M)\omega+\psi)/2}H^+_{\mathrm{FIR}}\left(e^{j\omega}\right)\right\}. && \text{(G.66)} \end{aligned}$$

Eqn. (G.15) gives us the result

$$\delta = \frac{M+N}{2}. \tag{G.67}$$

It is rather difficult to design fast FIR filters to a given set of specifications using this additive factorization design method because it is not intuitively obvious how to control the magnitude $\left|H_{\mathrm{LPFIR}}\left(e^{j\omega}\right)\right|$ due to Eqn. (G.66). Nonetheless, for certain impulse response waveforms which are well characterized, this technique provides a useful tool for designing corresponding fast FIR filters to realize them. Some examples are given in Section G.6.2.

G.5.2 Magnitude-Squared Design Method

We begin by choosing a desired non-negative real-valued transfer function $H^2(z) > 0$ for which there exists a stable transfer function $H(z)$ such that

$$\begin{aligned} H^2\left(e^{j\omega}\right) &\triangleq \left|H\left(e^{j\omega}\right)\right|^2 && \text{(G.68)}\\ &= H\left(e^{j\omega}\right)^* H\left(e^{j\omega}\right) && \text{(G.69)} \end{aligned}$$

and polynomials $A^+(z)$ and $B^+(z)$ such that

$$\begin{aligned} H(z) &= \sum_{k=0}^{\infty} h_k z^{-k} && \text{(G.70)}\\ &= \frac{B^+(z)}{A^+(z)}. && \text{(G.71)} \end{aligned}$$

If the coefficients of $A^+(z)$ and $B^+(z)$ are real then Eqn. (G.68) yields

$$H^2\left(e^{j\omega}\right) = H\left(e^{j\omega}\right)H\left(e^{-j\omega}\right). \tag{G.72}$$

We form the TIIR transfer function

$$\begin{aligned} H^+_{\mathrm{FIR}}(z) &= \sum_{k=0}^{N} h_k z^{-k} && \text{(G.73)}\\ &= \frac{B^+(z) - z^{-N}B'^+(z)}{A^+(z)}, && \text{(G.74)} \end{aligned}$$

as in Eqn. (G.51). Similarly, we form $H^-_{\mathrm{FIR}}(z)$, as in Eqn. (G.57). We see immediately, in light of Eqn. (G.63) that the filter

$$H^2_{\mathrm{FIR}}(z) \triangleq H^+_{\mathrm{FIR}}(z)H^-_{\mathrm{FIR}}(z) \tag{G.75}$$

has the property that

$$H^2_{\rm FIR}\left(e^{j\omega}\right) = e^{-jN\omega}\left|H^+_{\rm FIR}\left(e^{j\omega}\right)\right|^2, \tag{G.76}$$

and this is obviously a linear-phase filter with group delay

$$\delta = N. \tag{G.77}$$

This filter may be simply implemented as a cascade of $H^+_{\rm FIR}(z)$ and $H^-_{\rm FIR}(z)$, which may be implemented by Eqn. (G.30) and Table G.2, respectively.

The relationship between $H^2_{\rm FIR}(z)$ and $H^2(z)$ is seen by considering the cyclic convolution [105]

$$H^+_{\rm FIR}\left(e^{j\omega}\right) = \sum_{k=0}^{\infty} w_k h_k e^{-ik\omega} \tag{G.78}$$

$$= \frac{1}{2\pi}\int_0^{2\pi} H\left(e^{j\theta}\right) W_N\left(e^{j(\omega-\theta)}\right) d\theta \tag{G.79}$$

where

$$w_k = \begin{cases} 1, & -N \le k \le N \\ 0, & \text{otherwise,} \end{cases} \tag{G.80}$$

and

$$W_N(z) = \sum_{k=-N}^{N} z^k \tag{G.81}$$

$$= \frac{z^{-N} - z^{N+1}}{1-z} \tag{G.82}$$

so that

$$W_N\left(e^{j\omega}\right) = \frac{\sin\{(N+1/2)\omega\}}{\sin(\omega/2)} \tag{G.83}$$

The extension of the window to negative values does not affect the result and is made to simplify the periodic convolution by eliminating the phase modulation of the window transfer function $W_N(z)$ as well as narrowing its main lobe by a factor of two. Thus,

$$H^2_{\rm FIR}\left(e^{j\omega}\right) = e^{-jN\omega}\left|(W_N * H)\left(e^{j\omega}\right)\right|^2, \tag{G.84}$$

where the "$*$" is understood to be periodic convolution as in Eqn. (G.79).

We notice that the phase of the filter $H(z)$ utilized in the design of $H^2_{\rm FIR}(z)$ is irrelevant, and thus, IIR filters which are usually considered to have excessive phase distortion near sharp cutoffs may be used. Additionally, the fact that the magnitude response for $H^2(z)$ is twice the distance from 0 dB compared to the magnitude response of $H(z)$ implies that constraints in the stop band of $H(z)$ need only be half the desired dB design specification, whereas, on the other hand, the ripples in the passband of $H(z)$ must be better than half the desired dB design specification. Thus, any stable discrete-time IIR filter design such as elliptic, Chebyshev, and Butterworth filters may be chosen as $H(z)$ in Eqn. (G.68) and transformed into a magnitude-squared filter with linear phase. The filter length N for $H^+_{\rm FIR}(z)$ and $H^-_{\rm FIR}(z)$ must be chosen long enough so that the blurring induced by the periodic convolution of $H\left(e^{j(\omega-\theta)}\right)$ by $W_N\left(e^{j(\omega-\theta)}\right)$ does not induce too much distortion in the frequency response. Indeed, disregarding quantization noise for the moment, as N grows to infinity, $W_N\left(e^{j\omega}\right)$ approaches an impulse centered at $\omega = 0$, and $H^+_{\rm FIR}(z)$ converges to $H(z)$. There are constraints due to Eqn. (G.49) on the filter length which are considered in the next section.

G.5.3 A Refined Truncation Algorithm

In both the additive and multiplicative designs of the previous two sections, the length N is constrained by the growth of quantization error in the unstable, reverse-conjugated filter $H^-_{\mathrm{FIR}}(z)$. This bound is given in Eqn. (G.49). We note that it is the most *stable* hidden mode of $H^+_{\mathrm{FIR}}(z)$ which gives rise to the most unstable hidden mode of $H^-_{\mathrm{FIR}}(z)$ due to the conjugate-reciprocal correspondence between their modes. These problematic conjugate-reciprocal modes may restrict the direct implementation in Table G.2 to undesirably short lengths. One way around this problem is to set a significance floor λ_S above the floor for numerical precision λ_P so that errors with magnitude less than λ_S are insignificant, and quantization errors are bounded by λ_P. Let $H(z)$ be the untruncated IIR impulse response associated with $H^+_{\mathrm{FIR}}(z)$ as in Eqn. (G.71). Since $H(z)$ is stable, we have

$$|p_k| < 1, \tag{G.85}$$

where the p_k's are the poles of $H(z)$, and consequently the hidden modes of $H^+_{\mathrm{FIR}}(z)$. The hidden modes of $H^-_{\mathrm{FIR}}(z)$ are thus $1/p_k^*$ and are unstable. We perform a partial fraction expansion on $H(z)$ as in Eqns. (G.37) and (G.38). We then observe the impulse response for each partial fraction. We set the cutoff point N_k for the k-th partial fraction response to be the smallest time after which the maximum impulse response becomes insignificant, i.e., $\forall n > N_k,\ |\mu h_{k,n}| \leq \lambda_S$, where μ is the largest magnitude input. We may solve

$$|h_{k,N_k}| = \lambda_S/\mu \tag{G.86}$$

numerically for N_k by using Eqn. (G.38) or by using the approximation

$$h_{k,n} \approx \sum_{\ell=0}^{M_k} \frac{b_{k,\ell}(n-\ell)^{M_k-1}p_k^{n-\ell}}{(M_k-1)!} \tag{G.87}$$

$$\approx n^{M_k-1}p_k^n \sum_{\ell=0}^{M_k} \frac{b_{k,\ell}p_k^{-\ell}}{(M_k-1)!} \tag{G.88}$$

$$= B_k n^{M_k-1}p_k^n \tag{G.89}$$

for large n, where B_k is implicitly defined by Eqns. (G.88) and (G.89). For $M_k = 1$, we have exactly

$$N_k = \frac{\log\left(\left|\frac{\lambda_S}{\mu B_k}\right|\right)}{\log(|p_k|)}. \tag{G.90}$$

Thus, if $N_k < N$ we may truncate the k-th partial fraction response at N_k instead of N without losing significance. However, since $H(z)$ is stable and responses due to the k-th partial fraction beyond the N_k-th time step are below the significance floor, this does not make any difference. The refinement comes from implementing $H^-_{\mathrm{FIR}}(z)$ as a sum of reversed partial fractions based on Eqn. (G.37) and Eqn. (G.57) but with the k-th partial fraction truncated after $n = N_k$ samples instead of $n = N$ if $N_k < N$. Thus, the unstable mode of $H^-_{\mathrm{FIR}}(z)$ due to the pole at $1/p_k^*$ only needs to grow from having an initial magnitude above the significance floor λ_S and has less time to accumulate exponentially growing quantization noise. We have

$$H^-_{\mathrm{FIR}}(z) = \sum_{k=1}^{N_p} \frac{-zB_k'^-(z) + z^{-N_k'}B_k^-(z,N_k')}{(1-p_k^*z)^{M_k}}, \tag{G.91}$$

where

$$N_k' = \begin{cases} N_k, & N_k \leq N \\ N, & N_k > N. \end{cases} \tag{G.92}$$

Eqn. (G.48) indicates how much quantization noise will accumulate due to the truncated response of length $N = N_k$ of the k-th partial fraction of $H_{\mathrm{FIR}}^-(z)$. Assuming that quantization error occurs on the order of the precision floor λ_P, we have

$$\sigma_\nu^2 \approx \lambda_P^2. \tag{G.93}$$

Also, the significance floor sets a convenient level of noise tolerance, so that may set

$$\sigma_{\mathrm{tol}}^2 = \lambda_S^2. \tag{G.94}$$

We may recast Eqn. (G.48) as

$$\lambda_S^2 \geq \lambda_P^2 \frac{1 - |p_k|^{-4N_k'}}{1 - |p_k|^{-2}} \tag{G.95}$$

$$\approx \lambda_P^2 \frac{|p_k|^{-4N_k'}}{|p_k|^{-2} - 1} \tag{G.96}$$

and thus

$$\lambda_P \leq \lambda_S |p_k|^{2N_k' - 1} \sqrt{1 - |p_k|^2}. \tag{G.97}$$

Combining Eqns. (G.97) and (G.90), assuming $M_k = 1$, we arrive at

$$\lambda_P \leq \frac{\lambda_S^3 \sqrt{1 - |p_k|^2}}{\mu^2 |p_k| |B_k|^2}. \tag{G.98}$$

We see that the precision, in bits, for the state variables must be about 3 times greater than the precision of the data in order to prevent significant noise accumulation. This result is intuitive since the significant part of the impulse response must span the dynamic range specified by the largest magnitude output (which may be assumed to be normalized to 1) and λ_S over a period of N_k' samples, whereas the noise in $H_{\mathrm{FIR}}^-(z)$ may grow over a period of up to $2N_k'$ samples using the same dynamics. The preceding analysis is not generally applicable when dealing with floating point quantities because the range of significance varies with the exponent. Assuming a constant-energy input, we see that the analysis still holds since the significance and precision floors are approximately constant at steady-state.

G.5.3.1 Unit-Magnitude Mode TIIR filters

A third class of linear-phase filters consisting of pure TIIR responses is available. If we choose $H_u(z)$ to be a TIIR filter of length N such that all of its (hidden) modes are on the unit circle and each mode has multiplicity one, then we are assured that $H_u(z)$ will have linear phase. This may be seen by observing that such a filter must satisfy Eqn. (G.12). If there are modes with multiplicity greater than one, then Eqn. (G.12) is not generally satisfied. However, care may be taken to place the zeros so that Eqn. (G.12) holds.

Applying the analysis of the previous section, we see from Eqn. (G.90) that the N_k's for this type filter will all be infinity. In this case, it is not necessary to reset the state variables very often because the growth of quantization error will be additive, and not exponential.

From a worst-case point of view, the number of samples in which error in the least significant bit may accumulate before reaching the significance floor λ_s is approximately

$$N = \lambda_s/\lambda_p, \tag{G.99}$$

assuming that there is one bit's worth of error in the LSB per sample processed. If the noise is zero-mean, then the accumulated error is a random walk whose standard error grows proportionally to the square root of the number of samples processed. We would like the standard error to be some distance away from the least significant bit of the output signal. For an error accumulation such that the 3-sigma error is below the significance floor, we have the relation

$$3\lambda_p\sqrt{N} < \lambda_s, \tag{G.100}$$

giving

$$N < (\lambda_s/3\lambda_p)^2 \tag{G.101}$$

$$\approx 4^G/10, \tag{G.102}$$

where G is the number of guard bits. Hence, we see that TIIR filters with hidden modes only on the unit circle have desirable stability properties over the filters described in the previous two sections.

Since unit-magnitude mode TIIR filters are quasi-stable and do not need to be reset every N cycles, the number of computations necessary to stabilize them may be reduced by performing the state-variable reset infrequently. Since an FIR filter has finite memory, it is sufficient to run two parallel filters starting only N steps before the state-variable transfer.

The impulse responses of TIIR filters with unit-magnitude hidden modes are sums of modal responses of the form

$$h_k[n] = P_k(n)p_k^n \tag{G.103}$$

$$= P_k(n)exp(j\omega_k n) \tag{G.104}$$

for $n = 0, \ldots, N$, where p_k is the k-th unique pole and $P_k(n)$ is an m_k-1-th degree polynomial, where m_k is the multiplicity of the k-th pole; these are truncated polynomials times complex exponentials.

Some examples of TIIR filters of the unit-magnitude-modes class are given in Section G.6.2.

G.5.4 Time-Varying TIIR Filters

The ability to change filtering characteristics in real-time may be a desirable characteristic for discrete-time filters. FIR filter coefficients in conventional tapped delay-line implementations may be adjusted dynamically without much regard to stability; such FIR systems are intrinsically stable. One simply needs to take care not to change the coefficients so quickly that transients are introduced into the filter output.

Stable IIR systems may also have their coefficients changed on-line, if the changes are slow enough. It is possible to inject energy into an IIR system by changing the filter coefficients in such a way as to make the filter output unbounded, even though the filter coefficients at each instant in time may correspond to a stable fixed-coefficient IIR system. If the coefficient changes are slow enough with respect to the filter time constant then mismatches between the state variables and coefficients are absorbed by the exponential decay of the filter.

Since the TIIR formulation depends on the careful cancellation between the impulse responses of two IIR systems, changes in filter coefficients of a TIIR system would result in a very complicated

mixture of modes which are difficult to cancel out exactly. The behavior of such non-steady state operation of TIIR filters is beyond the scope of this paper. Hence, it may seem at first glance that TIIR filters would not be suited for deployment in situations where adjustable filters are necessary.

There do exist several possibilities for time-varying TIIR implementations, however. One way is to change the coefficients of the TIIR system dynamically as we would change the coefficients of a stable IIR system, taking care to match the tail-canceling IIR filter according to the impulse-generating filter using synthetic division. In this case, we must depend on the resetting algorithm given in Section G.4 used to stabilize unstable TIIR systems. The use of this algorithm induces a finite memory into the state variables of the system; after $2N$ samples are processed, the system will again have the normally expected steady-state behavior. However, the period between the coefficient change and the state-variable refresh gives plenty of time for an unstable TIIR system to accumulate significant, exponentially growing errors. The result would then be quite unacceptable.

A better solution is to leave the filters invariant in time, thus avoiding the difficult analysis. We simply need to calculate the desired target TIIR filter of length N, say $H_2(z)$, with its states initialized to zero. At the appropriate time, the input stream into $H_2(z)$ is turned on and the filter begins operating. After N time steps, the filter's input delay line is full and its output has no startup transients. Given that $H_1(z)$ is the starting filter, we may then transition to $H_2(z)$ by cross-fading. Let $\alpha[n]$ be some kind of ramping function such that

$$\alpha[n] = \begin{cases} 0, & n = 0 \\ 1, & n = T, \end{cases} \tag{G.105}$$

and has smoothly changing values in between, and where T is the transition time. For example, $\alpha[n]$ could be a linear ramp or some kind of exponential decay. T is assumed to be sufficiently long that any transients induced by the transition are negligible. Then, the time-varying filter response may be given by the cross-faded output

$$y[n] = \begin{cases} h_1 * x[n], & n \le n_0 \\ (1-\alpha[n-n_0])h_1 * x[n] + \alpha[n-n_0]h_2 * x[n], & n_0 < n < n_0 + T \\ h_2 * x[n], & n \ge n_0 + T, \end{cases} \tag{G.106}$$

where n_0 is the time step at which the transition begins. It is assumed that $H_2(z)$ has been properly initialized, starting at least N time steps before the transition begins. At time $n_0 + T$ the filter output is determined by $H_2(z)$ so that $H_1(z)$ may be turned off and its computational and storage resources reclaimed.

Such a set-up may be used where $H_1(z)$ and $H_2(z)$ are linear-phase FFIR filters. In order to preserve phase alignment, $H_1(z)$ and $H_2(z)$ should have the same FIR length of N.

Hence, we see that the TIIR and linear-phase FFIR algorithms may be used where time-varying filters are required.

G.5.5 Computational Cost

Assuming that $H^+_{\mathrm{FIR}}(z)$ is a stable filter, we may implement it with $3P+1$ multiplies and $3P$ adds per sample. $H^-_{\mathrm{FIR}}(z)$ is then unstable and must be calculated with parallel state variables as outlined in Section G.4, Table G.2, and the previous section. Table G.2 reflects a few changes from the algorithm outlined in Table G.1 which are necessary to implement the reversed filter $H^+_{\mathrm{FIR}}(z)$. The cost for $H^-_{\mathrm{FIR}}(z)$ is about $4P$ adds and multiplies per sample, as discussed in Section G.4. We see, then, that the number of operations is about $7P$ multiplies and adds per sample.

It is interesting to note that implementing a partial fraction (parallel) structure for a transfer function as opposed to a direct implementation, as in Eqn. (G.30) does not significantly alter the

number of multiply-accumulates used as long as the characteristic polynomials are monic and the numerators have degree one less than the denominator. However, each separate factor requires an additional input delay line of length $N_k + M_k$, which might be avoided by clever indexing. Also, the algorithmic overhead may increase, not to mention a greater amount of design effort. The advantage is that greater numerical stability is achieved, and N may then be chosen arbitrarily large. Also, each mode is present only where it is above the significance threshold λ_S. Of course, a full factorization is not necessary: it is sufficient to group together modes with the same magnitude, or to implement only the troublesome modes separately.

The unit-magnitude-mode, linear-phase filters described in Section G.5.3.1 are particularly computationally efficient. Since such filters are intrinsically self-hermitian, there is no need to implement a mirror filter as in the additive and magnitude-squared design methods. Additionally, the resetting only needs to be implemented infrequently, and may be absorbed into the overhead cost. Hence, the computational cost should be approximately $3P$ operations per sample, plus the refresh overhead.

G.6 Simulations and Examples

To illustrate the basic idea of a truncated IIR (TIIR) system, we examine the system

$$H(z) = \frac{z^2}{z^2 - 1.9z + 0.98} \tag{G.107}$$

$$= \frac{B^+(z)}{A^+(z)} \tag{G.108}$$

which we wish to truncate after $N = 300$ samples; thus we wish to have an FIR response of 301 steps. We first form the tail-canceling polynomial as in Eqn. (G.29). We perform synthetic division on $z^{300}B(z)$ by $A(z)$ and obtain the remainder

$$B'^+(z) = -0.162126z + 0.139770 \tag{G.109}$$

so that $H^+_{\mathrm{FIR}}(z)$ of Eqn. (G.51) is defined. We plot the impulse response of the direct implementation given in Eqn. (G.30) in Figures G.1(a) and G.1(b). We see that at step $n = 301$ the tail of the response has been subtracted off and the response magnitude drops by about 115 dB. Due to quantization errors, there is a residual response. Figures G.1(c) and G.1(d) show the same system, but implemented using the algorithm presented in Section G.4 and Table G.1. Here, the system is forced to have a finite memory and thus the residual response is completely canceled at time step $n = 600$ because the state variables are refreshed every $N = 300$ time steps.

We next form the reverse-conjugated system $H^-_{\mathrm{FIR}}(z)$ as described by Eqn. (G.57) and arrive at

$$H^-_{\mathrm{FIR}}(z) = \frac{-zB'^-(z) + z^{-N}B^-(z)}{A^-(z)} \tag{G.110}$$

$$= \frac{-0.139770z^2 + 0.162126z - z^{-N}}{0.98z^2 - 1.9z + 1} \tag{G.111}$$

$$= \frac{-0.142622z^2 + 0.165435z - 1.020408z^{-N}}{z^2 - 1.938776z + 1.020408}, \tag{G.112}$$

where, in the last equation, we have normalized by 0.98 in order to have a monic characteristic polynomial. This system has unstable hidden modes and its impulse response is plotted in Figures G.1(e) and G.1(f). The tail is canceled with about 125 dB attenuation, but the quantization noise grows without bound to overwhelm the signal eventually. Figures G.1(g) and G.1(h) show how the state variable refresh technique completely cancels the quantization noise before it becomes significant.

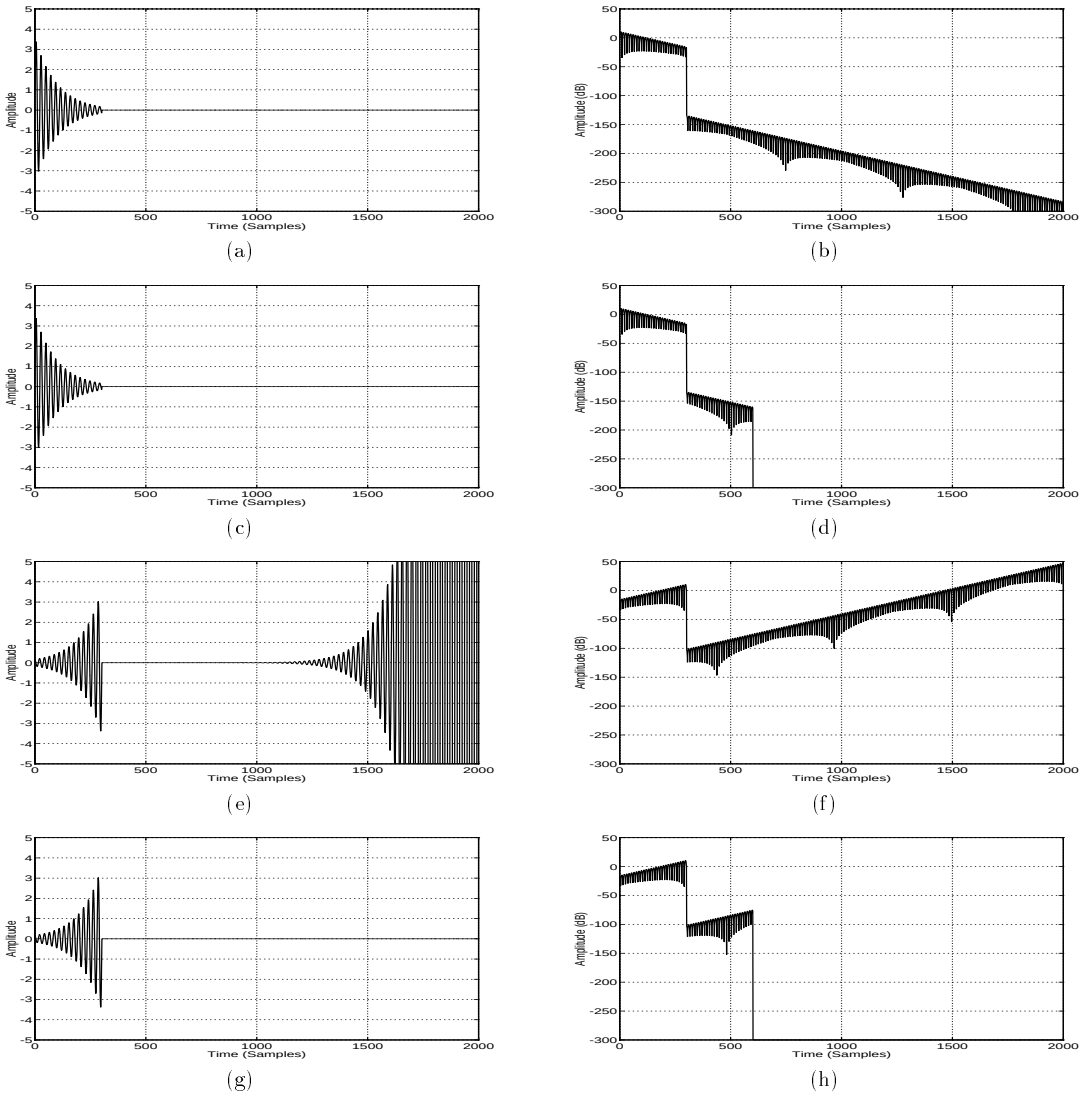

Figure G.1: **(a)** Impulse response of TIIR system of Eqn. (G.107) truncated after 300 steps using stable implementation. **(c)** Same as (a) except using unstable implementation–state variables refreshed every 300 steps; thus the system has finite memory. **(e)** TIIR impulse response of reversed system of Eqn. (G.112) using the stable implementation. Note that the quantization error grows without bound. **(g)** Same as (e) except using unstable implementation. Again, state variables refreshed every 300 steps. **(b,d,f, and h)** Same as (a,c,e, and g), respectively, except on a decibel scale. The arithmetic was done using double-precision floating point, but with 32-bit single-precision floating-point state variables.

G.6.1 Elliptic-Filter-Based FFIR Design Example

Elliptic Filter Coefficients			
a_0	1.00000000	b_0	0.05149489
a_1	−5.20086294	b_1	−0.25706694
a_2	11.46455205	b_2	0.57645267
a_3	−13.68525876	b_3	−0.74102189
a_4	9.32002688	b_4	0.57645267
a_5	−3.43103178	b_5	−0.25706694
a_6	0.53331689	b_6	0.05149489

Table G.3: Elliptic filter coefficients for the example in Section G.6.1

k	Poles	Residue	N_k	$\lambda_P(dB)$
1	$0.93560805 + j0.31706231$	$0.00710587 + j0.01100914$	497	−211.6943
2	$0.93560805 - j0.31706231$	$0.00710587 - j0.01100914$	497	−211.6943
3	$0.88941945 + j0.28954430$	$-0.06609826 + j0.02150355$	116	−233.0556
4	$0.88941945 - j0.28954430$	$-0.06609826 - j0.02150356$	116	−233.0556
5	$0.77540397 + j0.15290736$	$0.06436785 - j0.21546997$	38	−247.2166
6	$0.77540397 - j0.15290736$	$0.06436785 + j0.21546997$	38	−247.2166
Direct term: $h_0 = 0.05149489$				

Table G.4: Elliptic filter poles, magnitudes and decay times to significance level λ_S for the example in Section G.6.1. The N_k's are calculated using Eqn. (G.90) with $\lambda_S = 2^{-15}$ and maximum input amplitude $\mu = 1$. The λ_P's denote the precision floor necessary to implement this filter.

	$\ell = 1$	$\ell = 2$
$a_{1,\ell}$	−1.87121609	0.97589092
$b_{1,\ell}$	0.01421174	−0.02027779
$b'_{1,\ell}$	6.08847078e–05	−5.74152962e–05
$a_{2,\ell}$	−1.77883890	0.87490286
$b_{2,\ell}$	−0.13219652	0.10512570
$b'_{2,\ell}$	−3.88583695e–06	−1.38234153e–05
$a_{3,\ell}$	−1.55080795	0.62463198
$b_{3,\ell}$	0.12873570	−0.03392829
$b'_{3,\ell}$	5.80618310e–05	−4.35418795e–05

Table G.5: Coefficients for the modal decomposition of the elliptic filter in Eqn. (G.113) and Eqn. (G.114). The $b'_{k,\ell}$ are calculated using synthetic division as outlined in Table G.6 and N_k from Table G.4.

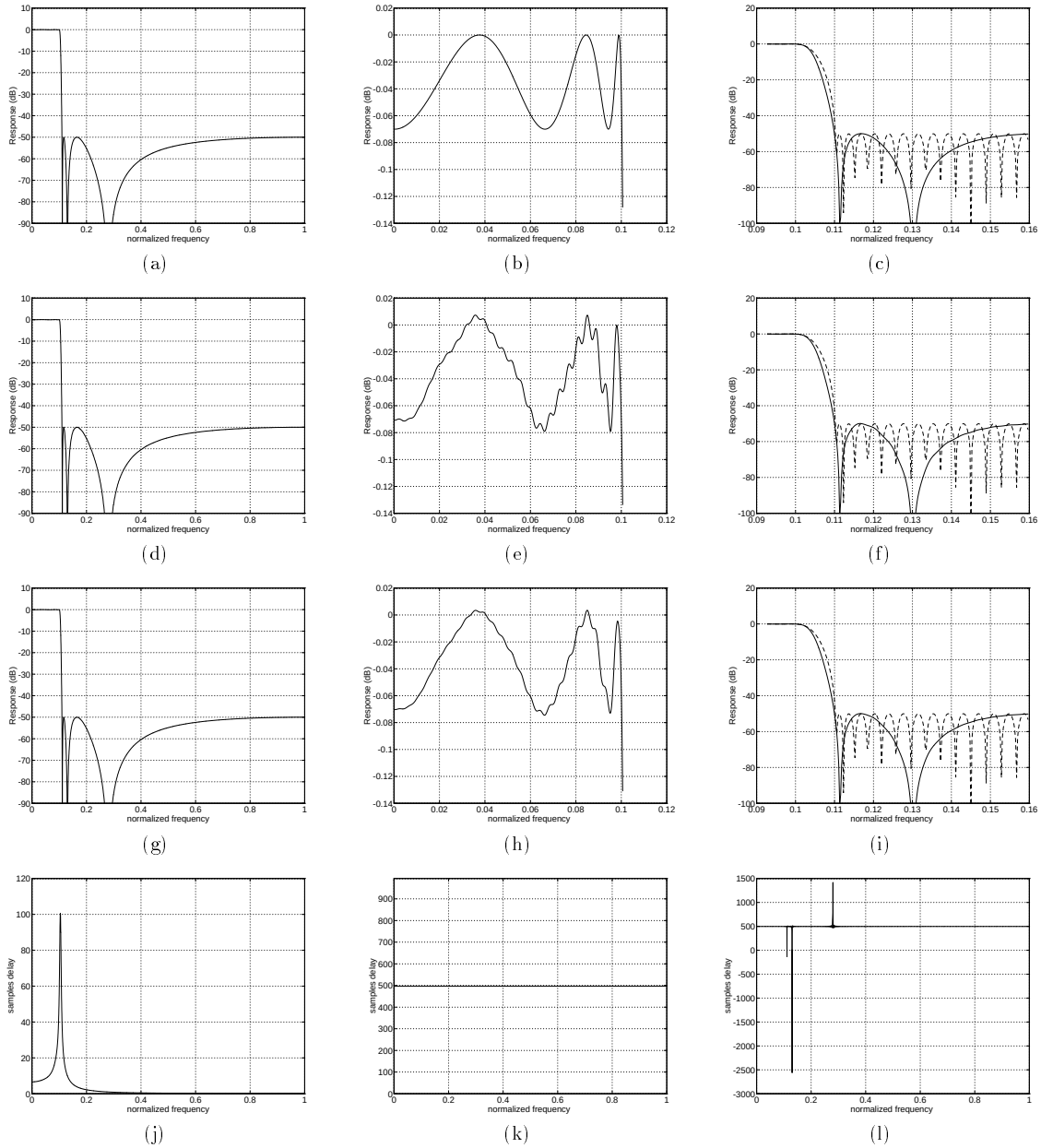

Figure G.2: Filter responses from the linear-phase elliptic filter design example in Section G.6.1. **(a-c)** Views of the untruncated response of $H^2\left(e^{j\omega}\right)$. **(d-f)** Views of the response of $H^2_{\mathrm{FIR}}\left(e^{j\omega}\right)$, with truncation at $N = 497$. Note the ringing in the passband in **(e)** due to Gibb's effect. **(g-i)** Views of the hybrid filter $H\left(e^{j\omega}\right) H^-_{\mathrm{FIR}}\left(e^{j\omega}\right)$. Views **(c), (f), and (i)** have portions of an order 500 FIR filter designed by the Parks-McLellan algorithm to have the same specs as the target filter, superposed for comparison. **(j)** Group delay of the forward filter $H(z)$ used as the design basis of $H^2_{\mathrm{FIR}}(z)$. **(k)** Group delay of the $H^2_{\mathrm{FIR}}\left(e^{j\omega}\right)$. It is exactly 497 time steps. **(l)** Group delay of the hybrid filter $H\left(e^{j\omega}\right) H^-_{\mathrm{FIR}}\left(e^{j\omega}\right)$.

We illustrate here the design of a low-pass linear-phase FFIR filter using the magnitude-squared technique outlined in Section G.5.2. We wish to design a filter which meets the following criteria:

(1) Passband $(0.00, 0.10)$, in fractions of $f_s/2$ with at most 0.080dB maximum peak-to-peak ripple, where f_s is the sampling frequency
(2) Stopband $(0.11, 1.00)$ with at least 50 dB minimum attenuation
(3) Linear phase
(4) 15 bits of fixed point significance in the mantissa.
(5) Maximum input amplitude is $\mu = 1.0$

Because of the sharp transition band in the interval $(0.10, 0.11)$, we select an elliptic filter as the basis for our design [61]. We realize that our choice of $H(z)$ only needs to meet half the specifications of (1) and (2) above, and that (3) is irrelevant. Using Matlab, we find that an order 6 filter suffices to give us a filter $H(z)$ with the desired properties such that $H^2(z)$ satisfies the above criteria. The arguments to the **ellip** function are

- $N = 6$
- Passband ripple = 0.035 dB
- Stopband attenuation = 25 dB
- Cutoff frequency = 0.10 (normalized units).

We have allowed an additional 0.005 dB margin in the passband to anticipate Gibbs ringing due to sequence truncation expressed in Eqn. (G.78). For the form given in Eqn. (G.5) the coefficients are given in Table G.3. Since the multiplicity of each pole is one, we may use Eqn. (G.90) to calculate the decay times N_k to the significance floor. We round up in each case. The poles are given in Table G.4 as well as the magnitude and N_k for each pole. Because the coefficients come in complex-conjugate pairs we may rearrange $H(z)$ into three 2nd-order real terms so that

$$\begin{aligned} H(z) = h_0 &+ \frac{b_{1,1}z^{-1} + b_{1,2}z^{-2}}{1 + a_{1,1}z^{-1} + a_{1,2}z^{-2}} \\ &+ \frac{b_{2,1}z^{-1} + b_{2,2}z^{-2}}{1 + a_{2,1}z^{-1} + a_{2,2}z^{-2}} + \frac{b_{3,1}z^{-1} + b_{3,2}z^{-2}}{1 + a_{3,1}z^{-1} + a_{3,2}z^{-2}}, \end{aligned} \tag{G.113}$$

where the coefficients are given in Table G.5. We then implement each term separately in the truncated form given in Eqn. (G.30) to form $H^+_{\rm FIR}(z)$ using each term's decay-to-significance times N_1, N_3, and N_5 for the cutoffs. The coefficients are calculated by using synthetic division as explained in Table G.6 and are listed in Table G.5. We choose $N = 497$ as the cutoff point for truncating the filter since this is the largest N_k. Thus we may implement the forward filter as

$$\begin{aligned} H^+_{\rm FIR}(z) = h_0 &+ \frac{b_{1,1}z^{-1} + b_{1,2}z^{-2} - b'_{1,1}z^{-(N_1+1)} - b'_{1,2}z^{-(N_1+2)}}{1 + a_{1,1}z^{-1} + a_{1,2}z^{-2}} \\ &+ \frac{b_{2,1}z^{-1} + b_{2,2}z^{-2} - b'_{2,1}z^{-(N_3+1)} - b'_{2,2}z^{-(N_3+2)}}{1 + a_{2,1}z^{-1} + a_{2,2}z^{-2}} \\ &+ \frac{b_{3,1}z^{-1} + b_{3,2}z^{-2} - b'_{3,1}z^{-(N_5+1)} - b'_{3,2}z^{-(N_5+2)}}{1 + a_{3,1}z^{-1} + a_{3,2}z^{-2}}. \end{aligned} \tag{G.114}$$

Using Eqn. (G.57) we form

$$H^-_{\rm FIR}(z) = h_0 + z^{-N-N_1}\frac{-b'_{1,2} - b'_{1,1}z^{-1} + b_{1,2}z^{-N_1} + b_{1,1}z^{-(N_1+1)}}{a_{1,2} + a_{1,1}z^{-1} + z^{-2}} \tag{G.115}$$

$$+ z^{-N-N_3} \frac{-b'_{2,2} - b'_{2,1} z^{-1} + b_{2,2} z^{-N_3} + b_{2,1} z^{-(N_3+1)}}{a_{2,2} + a_{2,1} z^{-1} + z^{-2}}$$
$$+ z^{-N-N_5} \frac{-b'_{3,2} - b'_{3,1} z^{-1} + b_{3,2} z^{-N_5} + b_{3,1} z^{-(N_5+1)}}{a_{3,2} + a_{3,1} z^{-1} + z^{-2}}$$

from the corresponding parts in Eqn. (G.114). Notice that each term is delayed by an appropriate $N - N_k$ steps in order to align the phases of the response properly. To implement this filter we use the algorithm of Table G.2 and Section G.4 due to the unstable hidden modes of each dynamic term. We may wish to normalize the coefficients by $a_{k,2}$ so that the characteristic polynomials are monic in each term. At this point we form $H^2_{\rm FIR}(z)$ by cascading the output of $H^-_{\rm FIR}(z)$ into the input of $H^+_{\rm FIR}(z)$. This order may be preferable since the state-variable reinitialization scheme used in Section G.4 may introduce some discontinuities near or below the significance floor λ_S. Thus, postfiltering by $H^+_{\rm FIR}(z)$ attenuates any such additional noise, however insignificant.

We show in Figure G.2 the results of our filter implementation. Figures G.2(a)-(c) show the ideal untruncated $H^2(z)$ response from our design. Its decibel response is simply double that of $H(z)$ from Eqn. (G.113). Figures G.2(d)-(f) show the truncated response of $H^2_{\rm FIR}(z) = H^-_{\rm FIR}(z)H^+_{\rm FIR}(z)$. Notice the presence of Gibbs overshoot due to the truncation of the filter response. Figures G.2(g)-(i) show the implementation $H^-_{\rm FIR}(z)H(z)$ in which the tail of the forward response is not truncated. The response is smoother, but there may be some slight deviations from phase linearity due to the asymmetry. The error due to the tail response of $H(z)$ should be small, however, since the tail of each mode for $H^+_{\rm FIR}(z)$ is cut off at the significance floor λ_S. The phase responses for $H(z)$, $H^2_{\rm FIR}(z)$, and $H^-_{\rm FIR}(z)H(z)$ are shown in Figures G.2(j)-(l).

G.6.2 Windows and Polynomials

Unit-magnitude mode TIIR responses are convenient for generating well-known impulse response functions for computing weighted averages of an input sequence. Often in signal processing applications, an exponential window is undesirable for averaging highly non-stationary data because of the long tail. Finite-length windows with polynomial terms may be generated using multiple poles at $z = 1$ and using Eqn. (G.38). The terms due to the binomial coefficients generate the polynomial coefficients. The FFIR algorithm provides a cost-effective method for implementing such weighting sequences. For example, the simple N-point rectangular window may be generated as a quasi-stable TIIR filter with filter dynamics

$$H_{\rm rectangular}(z) = \frac{1 - z^{-N}}{1 - z^{-1}}. \tag{G.116}$$

The $2N$-point Bartlett window is

$$H_{\rm Bartlett}(z) = \frac{1}{N} \frac{1 - z^{-N} - z^{-(N+1)} + z^{-(2N+1)}}{1 - 2z^{-1} + z^{-2}}. \tag{G.117}$$

The N-point Hanning window, also known as the *Hann* window, is

$$H_{\rm Hanning}(z) = \frac{1}{2} \left(\frac{1 - z^{-N}}{1 - z^{-1}} - \frac{1 - \cos\left(\frac{2\pi}{N-1}\right)(z^{-1} + z^{-N}) + z^{-(N+1)}}{1 - 2\cos\left(\frac{2\pi}{N-1}\right) z^{-1} + z^{-2}} \right). \tag{G.118}$$

The N-point Hamming window is

$$H_{\rm Hamming}(z) = 0.54 \frac{1 - z^{-N}}{1 - z^{-1}} - 0.46 \frac{1 - \cos\left(\frac{2\pi}{N-1}\right)(z^{-1} + z^{-N}) + z^{-(N+1)}}{1 - 2\cos\left(\frac{2\pi}{N-1}\right) z^{-1} + z^{-2}}. \tag{G.119}$$

An example of a useful polynomial impulse response is the Kay window [75] used for statistically efficient frequency estimation based on averaged phase differences with weighting coefficients

$$w_{\mathrm{Kay}}[n] = \frac{6N}{N^2-1}\left\{\frac{n}{N} - \left(\frac{n}{N}\right)^2\right\} \tag{G.120}$$

for $1 \leq n \leq N-1$.

$$H_{\mathrm{Kay}}(z) = \frac{6}{N(N^2-1)} \times \frac{(N-1)z^{-1} - (N+1)z^{-2} + (N+1)z^{-N-1} - (N-1)z^{-N-2}}{(1-z^{-1})^3}. \tag{G.121}$$

This implementation requires only six adds and two multiplies, independent of N.

G.7 Applications

We list here some of the many possible applications for TIIR filters.

G.7.1 Digital speaker crossover networks and mixers for digital audio applications

In the past, commercial digital audio systems designers have had to choose between efficient, nonlinear-phase IIR filters and linear-phase, but computationally expensive, FIR filters. Mixing the outputs from non-linear phase filters may result in unwanted nulls in the combined frequency response due to cancellation of signals with different frequency-dependent group delays. The linear-phase TIIR algorithm combines the best of these features from both types of filter.

Group delay remains a potential problem, however, for real-time mixing applications with feedback to a performing musician. Delays of greater than 10ms have been known to be disorienting to performers. Given an allowance of about 6ms for miscellaneous system delays in a digital mixer, we may have about 4ms group delay in which to perform filtering. Quite reasonable filtering can be performed within 4ms at studio sampling rates.

Consider that, with a 48kHz stereo sampling rate, a 25MHz Motorola DSP56001 can devote at most 130 operations per sample to filtering, corresponding to an FIR group delay of about 1.46ms. Thus, the DSP56001 would fall behind real-time performance with one stereo channel pair before excessive group delay became a problem. On the other hand, a nice 2-pole Chebyshev type II filter may be converted into a linear-phase TIIR filter with a cost of about 14 multiply-accumulates per sample. This example illustrates the expense of FIR filtering and the potential gains from the application of linear-phase TIIR filtering.

For off-line applications, group delay is not a large concern. In either case, considerable computational savings may be attained, depending on the filter specifications. Even in the age of rapidly expanding hardware capabilities, a factor of N increase in algorithmic efficiency is valuable because it allows N times more discrete-time filters to be simulated on the same hardware with the same time requirements.

G.7.2 Multirate Filtering

One disadvantage of the fast FIR filtering methods is that, although they are computationally efficient, they are limited to hop sizes of one. Multirate [138] or STFT techniques, which decimate

the data stream to account for a reduction in bandwidth, can be quite efficient, thus reducing the relative advantage of TIIR filtering over FIR filters. However, polyphase interpolating filters for upsampling in multirate systems may be easily implemented as TIIR filters, providing a great savings in computation, thus gaining the best features of both filter design ideologies. The development of applications of TIIR theory to multirate filter design is beyond the scope of this paper.

G.7.3 High-Resolution, Optimal Frequency Estimator

Kay derived the optimal weighting sequence for estimating the frequency of a pure-frequency sinusoid in Gaussian noise from finite phase differences [76]. The window given in Eqn. (G.120) attains the Cramér-Rao bound for moderate SNR. Eqn. (G.121) shows how a running average may be computed using only 2 multiplies and 6 adds per sample, independent of the window length. Such a system may be used for computing a running estimate of instantaneous frequency.

G.7.4 Polynomial Impulse Responses

Sometimes a finite-length window is desired for processing non-stationary signals where long exponential tails are undesirable. Running windows such as the Bartlett, Hamming, or Hanning Window give a more localized and symmetric average than a decaying exponential. Additionally, polynomial responses with sinsuoidal modulation may be constructed easily, as seen in Section G.5.3.1.

G.8 Summary

The power of the fast FIR algorithm stems from the ability to form complicated FIR sequences as the quotient of two polynomials with relatively few non-zero coefficients. The resulting cancellation of all the dynamic modes yields the desired FIR sequence. This may be thought of as "filter compression," in which low-entropy redundancies in certain kinds of FIR sequences are encoded using generating functions based on IIR dynamics. We utilize unstable as well as stable IIR dynamics in creating our TIIR responses by exploiting a state-variable-resetting technique which takes advantage of the fact that FIR responses have finite memory. Another technique introduced here is the use of synthetic division to generate a tail-canceling complement filter. Finally, the technique described in Section G.5.2 allows the straightforward use of conventional IIR filter design methods for creating linear-phase fast FIR filters.

```
     int i,j;
     double *w=(double *)malloc((P+1)*sizeof(double));
/*** load the numerator coefficients for B(z) ***/
     for(i=0;i<P+1;i++){
          w[i]=b[i];
     }
/*** do synthetic division ***/
     for(i=0; i<=N; i++){
          factor=w[0];
          for(j=0;j<P;j++){
               w[j]=w[j+1]+factor*a[j];
          }
          w[P]=0;
/**** The remainder after the i-th step is in w[0..(P-1)] ***/
     }
/*** copy the result to the output array ***/
     for(i=0;i<P;i++) {
          bb[i]=w[i];
     }
```

Table G.6: Algorithm for performing synthetic division to generate the tail-canceling polynomial $B'(z)$.

Appendix H

A Software Framework for Auditory Source Separation

I have built a software framework for the auditory source separation for the NeXT computer. The system, currently named *Tracker.app*, was written using the native programming tools on the NeXT, including Interface Builder, Project Builder, and Objective-C++. The interface portions were written in Objective-C and the main grouping engine was implemented in a combination of Objective-C++ and C++, all supported by the Gnu 2.2 compiler supplied with the NeXTStep 3.2 developer system software. Program development was carried out on both a Color Turbo NeXTStation and an ALR Pentium platform with the Intel version of NeXTStep 3.2.

The application shell provides a general purpose analysis framework for implementing assorted kinds of analysis and displaying the results together. The user is presented with a sound editor interface which allows recording, inspection, and playback of sounds through the built-in microphone at the CODEC rate of 8012Hz. Sound files may also be opened as well and played back or edited. A scrolling SoundView controls the display of the digitized sound. Supported sound sample formats are mu-law compressed 8-bit, 16-bit linear, 32-bit float, and ATC compressed. Other formats are also automatically supported through the comprehensive -[Sound convertTo:] Objective-C method supplied in NeXT's Sound Kit. All sampling rates are supported for analysis, but only the 8012, 22050, and 44100 Hz rates are supported directly for sound playback on native NeXT hardware. The application can also save sound documents to either its own format or a combination of the playback-supported formats and sampling rates, with the appropriate conversion being performed upon request.

The user may make a sound selection for playback, editing, or analysis by using either the mouse, by clicking and dragging with the mouse, or by specifying start, and end or duration intervals in either milliseconds or samples. Pressing the **play** button plays the sound, **record** records over the selection; selecting **cut**, **copy**, or **paste** performs the appropriate action using the pasteboard; and finally, pressing the **analysis** button performs the analyses that have been selected in the **Preferences** panel.

H.1 Analysis Modules

When the **analysis** button is pressed the program copies and converts the selected samples in the SoundView to a standard 32-bit floating-point format available for all analysis modules to use. Each selected analysis module is then called in turn to perform its specific analysis calculations. Next,

each selected analysis module is called in turn to create a a graphical representation of its analysis. Finally, each selected analysis module is called in turn to display its graphical representation in the analysis View, which has been programmed to scroll synchronously underneath the selected samples in the SoundView. The analysis View has a time ordinate and frequency abscissa, providing a time-frequency plane for representation. A number of nice user features are included in the display of the analysis results. The user may zoom and scroll along both axes using scroll bars. Additionally, the user may scroll the time-frequency plot by clicking with the mouse on a point inside the graphics view and dragging in any direction; the graphics display scrolls to keep the point centered.

Analysis functionality is supplied by modules which are required to adhere to an Objective-C Protocol consisting of three Objective-C modules:

−calculate,
−makeDrawing, and
−drawLayer:(const NXRect *)rects :(int)rectCount,

which implement the three analysis steps mentioned above. The **−calculate** and **−makeDrawing** methods are called only once, but the **−drawLayer::** method is called each time the module needs to update its drawing. The arguments to **−drawLayer::** are similar to the View class's **−drawSelf::** method. **rectCount** is the number of rectangles that are provided in the **rects** array–either one or three. If it is one, the entire area enclosed by **rects[0]** must be updated. If it is three, **rects[1]** and **rects[2]** contain regions which must be updated, and **rects[0]** is the smallest rectangle enclosing both **rects[1]** and **rects[2]**.

There are currently only two analysis modules supplied with the application.

H.1.1 Spectrogram Analyzer

The first module is a spectrogram analyzer which performs blocks of FFTs windowed with either the rectangular, Bartlett, Hamming, Hanning, or Blackman window, depending on the user's selection in the **Preferences** panel. The FFT block size is a power of 2, from 16 to 16384, again depending on the user's choice. The hop-size may also be set by the user. The spectrogram is displayed on a hue scale with a decibel dynamic range from 0 dB down to a floor specified by the user down to -400 dB, but with a preset of -150 dB. The color saturation and brightness are also user-adjustable.

The spectrogram analyzer is provided as a reality check over which to display extracted parameters such as the instantaneous frequency tracks of sinusoidal components in the signal.

H.1.2 Tracking Analyzer

A general auditory grouping analysis system is provided in the other analysis module currently provided in Tracker.app. The system provides a master grouping controller object which runs each grouping object registered with it in a round-robin fashion. Each grouping object owns a set of general tracker objects, each of which extracts some feature of the auditory object it is tracking in the time-frequency plane. The general tracker object is free to implement its frequency tracking algorithm by any means, such as the FLL algorithm of Chapter 4 or any of various spectral peak-tracking methods [76, 94, 119, 126, 128, 137, 147]. Other signal object parameters besides instantaneous frequency, such as onsets, amplitude envelope, tracking variance, and others, can also be made available. The current implementation only supports FLL tracking. Each grouping object is responsible for maintaining grouping relationships of the tracking objects it owns. Possible grouping relationships include onset grouping, harmonicity, common FM, common AM, and other kinds of Gestalt grouping relations described by Bregman [23]. Currently, the only kind of grouping supported is based on harmonicity and common FM. Each harmonic grouping object takes the

frequency updates generated by each tracker and computes a weighted sum of the N fundamental estimates, as described in Chapter 5.1. Due to the lack of an automatic pitch detection component, the application has been set to track only one harmonic series.

Using the **Inspector** panel, the user may provide the parameters of initial fundamental frequency, tracking gain, low-pass filter bandwidth, and number of harmonics. Upon pressing the **Analyze** button in the sound document window, the application processes the selected sound through each layer of analysis in turn. The result in the current version of the program is a spectrogram background with harmonic tracks corresponding to the target sound, if there is indeed one present at the given initial fundamental frequency. Examples of typical analysis results are shown in Figures 6.1 through 6.6, with different combinations of layers turned on.

H.2 Resynthesis

The user may resynthesize a target sound by selecting bandwidth for the resynthesis filter in the **Inspector** panel and pressing the **Resynthesize** button. The fundamental frequency track extracted in the analysis described above is used to demodulate each of the harmonics. Each harmonic's envelope is isolated by using the resynthesis filter. This provides the opportunity to use linear-phase filters with sharp cut-offs, though this has not yet been implemented. Each isolated harmonic is reconstructed by remodulating its phase-aligned envelope with the original demodulating function. The results are then added together to create a sound file consisting of the resynthesized target sound. This sound is played upon pressing the **Replay Resynthesis** button. A copy of the generated sound is placed in the NeXT system pasteboard.

H.2.1 Harmonic Notch Filtering

The user may also remove the target sound from a mixture. The user selects a bandwidth for the resynthesis filter and then presses the **Notch** button in the **Inspector** panel. To play the residual sound the user presses the **Replay Notch** button. A copy of the generated sound is placed in the NeXT system pasteboard.

H.2.2 Pitch Shifting

Pitch shifting is also supported. The user selects a ratio for the **Resynth Freq Scale** field in the **Inspector** panel. The remodulator is then generated with the frequency scaled by this factor. The harmonics are hence simply stretched in frequency. This mode does not make sense for performing harmonic notch filtering so it only modifies the resynthesis function.

H.3 Faster Performance

I have also written a version of the Harmonic-Locked Loop algorithm presented in Chapter 5 for the Motorola 56001 DSP chip on the NeXT computer. The analysis loop is called with arguments supplying the number of harmonics, the tracking gain, the filter coefficients for a biquad instantiation of **LPF**, the low-pass filter in the HLL algorithm, a variance saturation threshold, the initial fundamental frequency, and the output decimation factor. After initialization, the DSP routine consumes input samples fed to it via host-DSP DMA. The DSP routine provides a series of output frames at the sampling rate divided by the decimation factor. Each output frame consists of the fundamental estimate followed by N pairs of numbers denoting the real-and imaginary components of the complex envelope of each of the harmonics. The output results are sent to the host

by DSP-host DMA. All frequencies are represented in units of normalized angle per sample, i.e., a frequency of 1.0 corresponds to the sampling rate. The full tracking loop shown in Figure 5.1 is implemented, including phase error discrimination, variance estimation, variance saturation detection, and maximum-likelihood weighting for each harmonic. The weighted sum of the fundamental update estimates is normalized by the sum of the inverse variances, and finally the fundamental estimate is updated.

The DSP implementation currently does not attempt to estimate the initial pitch, nor does it attempt to segment based on abrupt changes in variance conditions, though these could be added quite easily. On the 25MHz DSP56001 resident on every NeXT computer, real-time performance may be attained using two harmonics at a 44.1 KHz sampling rate. At a 8 KHz sampling rate, one may use up to 11 harmonics and stay within real-time performance. This DSP routine should provide a basis for applications using the HLL algorithm, such as real-time voice or instrument pitch extraction suitable for MIDI code generation.

As of this writing, the DSP version has not yet been incorporated into Tracker.app.

H.4 Future directions

There are some obvious issues that need to be addressed. A current limitation in the software is the lack of an automatic pitch detector. This is discussed in Section 6.4, and may be implemented easily. Automatic phrasing detection is another simple extension that has not been undertaken due to time constraints. With automatic pitch detection and automatic phrasing detection it should be easy to have automatic detection and tracking of multiple harmonic sources. Further kinds of grouping rules should be incorporated into this object-oriented source separation framework.

Further analysis modules may be created using the Objective-C Protocol listed above. For example, a Wigner-Ville Distribution [17, 18, 35, 66] analysis module could be provided as a background instead of the Fourier spectrogram. Other quadratic distributions, such as the Affine or Cohen energetic classes may be implemented as an extension of the WVD.

In the near future, I plan to extend Tracker.app to allow the user to inspect the object hierarchy. The user should be able to select an object in the object browser and perform such tasks as resynthesizing its constituent parts. For example, in a mixture of several voices, each voice should be represented by an HLL grouping object. Each of the harmonics should be represented as daughter nodes. A resynthesis message should be sent recursively to all dependent nodes of a given node. Hence, the user should be able to listen to any grouped auditory object as well as its individual components.

Bibliography

[1] Abatzoglou, "A fast local maximum likelihood estimator for time delay estimation," *IEEE ASSP*, vol. 34, Apr. 1986.

[2] M. Abramowitz and I. A. Stegun, *Handbook of Mathematical Functions.* New York: Dover Publications, ninth ed., 1972.

[3] L. V. Ahlfors, *Complex Analysis.* New York: McGraw-Hill Book Co., third ed., 1979.

[4] H. Akaike, "Fitting autoregressive models for prediction," *Ann. Inst. Stat. Math.*, vol. 21, pp. 243–347, 1969.

[5] L. B. Almeida and J. M. Tribolet, "Nonstationary spectral modeling of voiced speech," *IEEE Trans. Acoustics, Speech, and Signal Processing*, vol. ASSP-31, pp. 664–677, 1983.

[6] B. D. Anderson and J. B. Moore, *Optimal Filtering.* Englewood Cliffs, NJ: Prentice-Hall, Inc., 1979.

[7] G. Arfken, *Mathematical Methods for Physicists.* New York: Academic Press, third ed., 1985.

[8] R. G. Baraniuk and D. L. Jones, "Shear madness: New orthogonal bases and frames using chirp functions," *IEEE Trans. Signal Processing*, vol. 41, pp. 3543–3549, Dec. 1993.

[9] R. G. Baraniuk and D. L. Jones, "Warped wavelet bases: Unitary equivalence and signal processing," in *Proc. ICASSP*, (Piscataway, NJ), pp. 320–323, IEEE Service Center, 1993.

[10] R. G. Baraniuk and D. L. Jones, "Unitary equivalence: A new twist on signal processing," *IEEE Trans. Signal Processing*, 1993, submitted.

[11] M. Basseville and I. V. Nikiforov, *Detection of abrupt changes: theory and application.* Englewood Cliffs, NJ: Prentice-Hall, Inc., 1993.

[12] E. Bedrosian, "A product theorem for Hilbert transforms," *Proc. IEEE*, vol. 51, pp. 868–869, 1963.

[13] A. Benveniste, "Design of adaptive algorithms for the tracking of time-varying systems," *Int. J. Adaptive Contr. Signal Processing*, vol. 1, pp. 3–29, 1987.

[14] R. E. Best, *Phase-locked loops: theory, design, and applications.* New York: McGraw-Hill, second ed., 1993.

[15] E. D. Blackham, "The physics of the piano," in *The Physics of Music* (C. M. Hutchins, ed.), San Francisco: W. H. Freeman and Co., 1978.

[16] J. Blauert, *Spatial Hearing: the psychophysics of human sound localization.* Cambridge, Mass.: MIT Press, 1983.

[17] B. Boashash, "Estimating and interpreting the instantaneous frequency of a signal–part 1: Fundamentals," *Proc. IEEE*, vol. 80, pp. 519–538, Apr. 1992.

[18] B. Boashash, "Estimating and interpreting the instantaneous frequency of a signal–part 2: Algorithms and applications," *Proc. IEEE*, vol. 80, pp. 540–568, Apr. 1992.

[19] B. Boashash and P. O'Shea, "Use of the cross Wigner-Ville distribution for estimation of instantaneous frequency," *IEEE Trans. Signal Processing*, vol. 41, pp. 1439–1445, Mar. 1993.

[20] B. P. Bogert, M. J. R. Healy, and J. W. Tukey, "The quefrency alanysis of time series for echoes: Cepstrum, pseudo-autocovariance, cross-cepstrum, and saphe cracking," in *Proc. Symposium Time Series Analysis* (M. Rosenblatt, ed.), (New York), pp. 209–243, John Wiley and Sons, 1963.

[21] R. N. Bracewell, *The Fourier Transform and its Applications.* New York: McGraw-Hill, second, revised ed., 1986.

[22] J. N. Bradley and R. L. Kirlin, "Phase-locked loop cancellation of interfering tones," *IEEE Trans. Signal Processing*, vol. 41, pp. 391–395, Jan. 1993.

[23] A. S. Bregman, *Auditory Scene Analysis: the perceptual organization of sound.* Cambridge, Mass.: MIT Press, 1989.

[24] L. Brennan, "Angular accuracy of a phased array radar," *IRE Trans. Antennas Propagat.*, pp. 268–275, May 1961.

[25] Y. Bresler and A. Macovski, "Exact maximum likelihood parameter estimation of superimposed exponential signals in noise," *IEEE Trans. Acoust. Speech Signal Process.*, vol. ASSP-34, pp. 1081–1089, Oct. 1986.

[26] G. J. Brown, *Computational Auditory Scene Analysis: A Representational Approach.* PhD dissertation, University of Sheffield, Department of Computer Science, Sept. 1992.

[27] W. A. Brown and J. Herschel H. Loomis, "Digital implementations of spectral correlation analyzers," *IEEE Trans. Signal Processing*, vol. 41, pp. 703–720, Feb. 1993.

[28] D. Cahan, ed., *Hermann von Helmholtz and the Foundations of Nineteenth-Century Science.* No. 12 in California Studies in the History of Science, Berkeley: University of California Press, 1994.

[29] B. Carlsson and P. Händel, "Analysis and interpretation of a constrained notch filter," in *Proc. ICASSP*, (Piscataway, NJ), pp. 293–296, IEEE Service Center, 1992.

[30] C. Chafe and D. Jaffe, "Source separation and note identification in polyphonic music," Tech. Rep. STAN-M-34, Center for Computer Research in Music and Acoustics (CCRMA), Department of Music, Stanford University, Stanford, CA 94305, Apr. 1986.

[31] E. C. Cherry, "Some experiments on the recognition of speech with one, and with two ears," *J. Acoust. Soc. Am.*, vol. 25, pp. 975–979, 1953.

[32] J. Chowning, "The synthesis of complex audio spectra by means of frequency modulation," *J. Audio Engineering Society*, vol. 21, pp. 526–534, Sept. 1973.

[33] C. K. Chui, *Wavelets: a tutorial in theory and applications.* Boston: Academic Press, 1992.

[34] L. Cohen, "Generalized phase-space distribution functions," *J. of Math. Phys.*, vol. 7, pp. 781–786, 1966.

[35] L. Cohen, "Time-frequency distributions–a review," *Proc. IEEE*, vol. 77, pp. 941–981, 1989.

[36] L. Cohen and C. Lee, "Instantaneous frequency, its standard deviation, and multicomponent signals," in *Advanced Algorithms and Architectures for Signal Processing III, Proc. SPIE* (F. T. Luk, ed.), vol. 975, pp. 186–208, 1988.

[37] L. Cohen and C. Lee, "Standard deviation of instantaneous frequency," in *Proc. ICASSP*, vol. 4, (Piscataway, NJ), pp. 2238–2241, IEEE Service Center, 1989.

[38] L. Cohen and C. Lee, "Instantaneous bandwidth for signals and spectrogram," in *Proc. ICASSP*, vol. 5, (Piscataway, NJ), pp. 2451–2454, IEEE Service Center, 1990.

[39] P. R. Cook, *Identification of Control Parameters in an Articulatory Vocal Tract Model, with Applications to the Synthesis of Singing.* PhD dissertation, Stanford University, Department of Music, 1991.

[40] M. P. Cooke, *Modelling Auditory Processing and Organisation.* PhD dissertation, University of Sheffield, Department of Computer Science, May 1991.

[41] J. P. Costas, "Residual signal analysis–a search and destroy approach to spectral analysis," in *Proc. of the first ASSP Workshop on Spectral Estimation*, (Hamilton, Canada), pp. 6.5.1–6.5.8, Aug. 1981.

[42] A. de Cheveigné, "Strategies for voice separation based on harmonicity." To be presented at ICSLP, Yokohama.

[43] A. de Cheveigné, "Separation of concurrent harmonic sounds: Fundamental frequency estimation and a time-domain cancellation model of auditory processing," *J. Acoust. Soc. Am.*, vol. 93, pp. 3271–3290, June 1993.

[44] A. de Cheveigné, "Time-domain comb filtering for speech separation," Technical Report TR-H-016, ATR Human Information Processing Research Laboratories, 2-2, Hikaridai, Seika-cho, Soraku-gun, Kyoto 619-02 Japan, July 1993.

[45] A. de Cheveigné, H. Kawahara, K. Aikawa, and A. Lea, "Speech separation for speech recognition," *Journal de Physique IV*, vol. 4, pp. C5–545–C5–548, May 1994.

[46] A. de Cheveigné, S. McAdams, J. Laroche, and M. Rosenberg, "Identification de voyelles simultanées harmoniques et inharmoniques," *Journal de Physique IV*, vol. 4, pp. C5–553–C5–556, May 1994.

[47] D. J. De Fatta, J. G. Lucas, and W. S. Hodgekiss, *Digital Signal Processing: A System Design Approach.* New York: John Wiley and Sons, 1988.

[48] D. C. Dennett, *Consciousness Explained.* Boston: Little, Brown, and Co., 1991.

[49] N. R. Draper and H. Smith, *Applied Regression Analysis.* New York: Wiley, 2nd ed., 1981.

[50] D. P. W. Ellis, "A computer implementation of psychoacoustic grouping rules," Tech. Rep. 224, MIT Media Lab, Perceptual Computing Section, MIT Media Lab E15-368C, Cambridge, MA 02139, Aug. 1993.

[51] D. P. W. Ellis, "Hierarchical models of hearing for sound separation and reconstruction," Tech. Rep. 219, MIT Media Lab, Perceptual Computing Section, MIT Media Lab E15-368C, Cambridge, MA 02139, Mar. 1993.

[52] A. T. Fam, "FIR filters that approach IIR filters in their computational efficiency," in *Twenty-First Asilomar Conference on Signals, Systems, and Computers, Pacific Grove*, pp. 28–30, Nov. 1987.

[53] D. J. Felleman and D. C. Van Essen, "Distributed hierarchical processing in the primate cerebral cortex," *Cerebral Cortex*, vol. 1, pp. 1–47, Jan. 1991.

[54] F. M. Gardner, "Characteristics of frequency-tracking loops," in *Phase-Locked Loops* [87], pp. 226–240.

[55] W. A. Gardner, *Statistical Spectral Analysis: A Non-probabilistic Theory.* Englewood Cliffs, NJ: Prentice-Hall, 1987.

[56] W. A. Gardner, "Exploitation of spectral redundancy in cyclostationary signals," *IEEE Signal Processing Magaine*, pp. 14–36, Apr. 1991.

[57] W. A. Gardner, "On the spectral coherence of nonstationary processes," *IEEE Trans. Signal Processing*, vol. 39, pp. 424–430, Feb. 1991.

[58] W. A. Gardner, ed., *Cyclostationarity in communications and signal processing.* New York: IEEE Press, 1994.

[59] G. H. Golub, *Matrix computations.* Baltimore: Johns Hopkins University Press, 2nd ed., 1989.

[60] I. S. Gradshteyn and I. M. Ryzhik, *Table of Series Integrals and Products.* New York: Academic Press, fifth ed., 1993.

[61] A. Gray and J. Markel, "A computer program for designing elliptic filters," *IEEE Trans. Acoust. Speech Signal Process.*, vol. 24, pp. 529–538, Dec. 1976.

[62] P. Händel and A. Nehorai, "Tracking analysis of a constrained adaptive notch filter," in *Proc. ICASSP*, (Piscataway, NJ), pp. 3209–3212, IEEE Service Center, 1991.

[63] S. Haykin, *Adaptive Filter Theory.* Englewood Cliffs, NJ: Prentice-Hall, Inc., second ed., 1991.

[64] P. Hedelin, "Models for non-linear estimation of speech." Draft Manuscript, 1977.

[65] H. v. Helmholtz, *On the Sensations of Tone as a Physiological Basis for the Theory of Music.* New York: Dover Publications, second English ed., 1859.

[66] F. Hlawatsch and G. F. Boudreaux-Bartels, "Linear and quadratic time-frequency signal representations," *IEEE Signal Processing Magazine*, pp. 21–67, Apr. 1992.

[67] P. G. Hoel, S. C. Port, and C. J. Stone, *Introduction to stochastic processes.* Boston: Houghton Mifflin, 1972.

[68] C. M. Hutchins, *The Physics of Music.* San Francisco: W. H. Freeman and Co., 1978.

[69] N. Jayant, J. Johnston, and R. Safranek, "Signal compression based on models of human perception," *Proc. IEEE*, vol. 81, pp. 1383–1422, Oct. 1993.

[70] D. Johnson, "The application of spectral estimation methods to bearing estimation problems," *Proc. IEEE*, vol. 70, pp. 1018–1028, 1982.

[71] E. R. Kandel, J. H. Schwartz, and T. M. Jessell, *Principles of Neural Science.* New York: Elsevier, third ed., 1991.

[72] Y. Katznelson, *An Introduction to Harmonic Analysis.* New York: Dover Publications, 1976.

[73] S. M. Kay, *Modern Spectral Estimation–Theory and Application.* Englewood Cliffs, NJ: Prentice-Hall, Inc., 1988.

[74] S. M. Kay, *Fundamentals of Statistical Signal Processing: Estimation Theory.* Englewood Cliffs, NJ: Prentice-Hall, Inc., 1993.

[75] S. Kay, "Statistically/computationally efficient frequency estimation," in *Proc. ICASSP*, (Piscataway, NJ), pp. 2292–2295, IEEE Service Center, 1988.

[76] S. Kay, "A fast and accurate single frequency estimator," *IEEE Trans. Acoustics, Speech, and Signal Processing*, vol. 37, pp. 1987–1990, Dec. 1989.

[77] M. Konishi, T. T. Takahashi, H. Wagner, W. E. Sullivan, and C. E. Carr, "Neurophysiological and anatomical substrates of sound localization in the owl," in *Auditory Function: Neurobiological Bases of Hearing* (G. M. Edelman, W. E. Gall, and W. M. Cowan, eds.), pp. 721–745, New York: Wiley, 1988.

[78] R. Kumaresan and C. S. Ramalingam, "On separating voiced-speech into its components," in *Twenty-Seventh Asilomar Conference on Signals, Systems, and Computers*, (Pacific Grove, California), pp. 1041–1046, Nov. 1993.

[79] R. Kumaresan, C. S. Ramalingam, and A. Rao, "RISC: an improved Costas estimator-predictor filter bank for decomposing multicomponent signals," in *Proc. Seventh SSAP Workshop*, (Quebec City), June 1994.

[80] U. K. Laine, "MSE filter design and spectrum parametrization by orthogonal FAM transformation." Draft.

[81] U. K. Laine, "Famlet, to be or not to be a wavelet?." Draft, 1992.

[82] U. K. Laine, "Speech analysis using complex orthogonal auditory transform (COAT)." Draft, 1992.

[83] U. K. Laine, M. Karjalainen, and T. Altosaar, "Warped linear prediction (WLP) in speech and audio processing," in *Proc. ICASSP*, (Piscataway, NJ), IEEE Service Center, 1994.

[84] J. Lamperti, *Stochastic processes : a survey of the mathematical theory.* New York: Springer-Verlag, 1977.

[85] M. Le Brun, "Digital waveshaping synthesis," *J. Audio Engineering Society*, vol. 27, pp. 250–266, Apr. 1979.

[86] W. Lindemann, *Die Erweiterung eines Kreuzkorrelationsmodells der binauralen Signalverarbeitung durch kontralaterale Inhibitionsmechanismen.* PhD dissertation, Ruhr-Universität Bochum, Germany, Fakultät für Elektrotechnik, 1985.

[87] W. C. Lindsay and C. M. Chie, *Phase-Locked Loops.* New York, NY: IEEE Press, 1986.

[88] L. Ljung and Gunnarsson, "Adaptation and tracking in system identification–a survey," *Automatica*, vol. 26, pp. 7–21, Jan. 1990.

[89] L. Ljung, *System Identification: Theory for the User.* Englewood Cliffs, NJ: Prentice-Hall, Inc., 1987.

[90] A. Macovski, *Medical Imaging Systems.* Englewood Cliffs, NJ: Prentice-Hall, Inc., 1983.

[91] L. Mandel, "Interpretation of instantaneous frequency," *Amer. J. Phys.*, vol. 42, pp. 840–846, 1974.

[92] M. Marcus, *Basic theorems in matrix theory.* Appl. Math. Series, National Bureau of Standards, 1960.

[93] D. Marr, *Vision.* San Francisco: W. H. Freeman and Co., 1982.

[94] R. J. McAulay and T. F. Quatieri, "Speech analysis/synthesis based on a sinusoidal representation," *IEEE Trans. Acoustics, Speech, and Signal Processing*, vol. 34, pp. 744–754, Aug. 1986.

[95] R. J. McAulay and T. F. Quatieri, "Pitch estimation and voicing detection based on a sinusoidal speech model," in *Proc. ICASSP*, (Piscataway, NJ), pp. 249–252, IEEE Service Center, 1990.

[96] D. K. Mellinger, *Event Formation and Separation of Musical Sound.* PhD dissertation, Stanford University, Department of Music, 1991.

[97] J. A. Moorer, "The optimum comb method of pitch period analysis of continuous digitized speech," *IEEE Trans. Acoust. Speech Signal Process.*, vol. ASSP-22, pp. 330–338, Oct. 1974.

[98] J. A. Moorer, *On the segmentation and analysis of continuous musical sound by digital computer.* PhD dissertation, Stanford University, Department of Computer Science, May 1975.

[99] T. Nakatani, H. G. Okuno, and T. Kawabata, "Auditory stream segregation in auditory scene analysis with a multi-agent system," in *AAAI Conference Proceedings*, 1994.

[100] F. D. Natali, "AFC tracking algorithms," *IEEE Trans. Commun.*, vol. 32, pp. 935–947, Aug. 1984.

[101] Z. Nehari, *Conformal Mapping.* New York: Dover Publications, Inc., 1975.

[102] A. Nehorai, "A minimal parameter adaptive notch filter with constrained poles and zeros," *IEEE Trans. Acoustics, Speech, and Signal Processing*, vol. 33, pp. 983–996, Aug. 1985.

[103] A. Nehorai and B. Porat, "Adaptive comb filtering for harmonic signal enhancement," *IEEE Trans. Acoustics, Speech, and Signal Processing*, vol. 34, pp. 1124–1138, Oct. 1986.

[104] I. M. Niven, H. S. Zuckerman, and H. L. Montgomery, *An Introduction to the Theory of Numbers.* New York: Wiley, fifth ed., 1991.

[105] A. V. Oppenheim and R. W. Schafer, *Discrete-Time Signal Processing.* Englewood Cliffs, N.J.: Prentice Hall, 1989.

[106] A. V. Oppenheim, R. W. Schafer, and T. G. Stockham, "Nonlinear filtering of multiplied and convolved signals," *Proc. IEEE*, vol. 56, pp. 1264–1291, Aug. 1968.

[107] P. F. Panter, *Modulation , Noise, and Spectral Analysis.* New York: McGraw-Hill, 1965.

[108] A. Papoulis, *Signal Analysis.* New York: McGraw-Hill, 1977.

[109] T. W. Parsons, "Separation of speech from interfering speech by means of harmonic selection," *J. Acoust. Soc. Am.*, vol. 60, pp. 911–918, 1976.

[110] R. D. Patterson, J. Holdsworth, I. Nimmo-Smith, and P. Rice, "Appendices B and C of *the svos final report: the auditory filterbank*," Tech. Rep. 2341, MRC Applied Psychology Unit, 15 Chaucer Road, Cambridge CB2 2FF, Dec. 1987.

[111] S. Peleg, B. Porat, and B. Friedlander, "The acheivable accuracy in estimating the instantaneous phase and frequency of a constant amplitude signal," *IEEE Trans. Signal Processing*, vol. 41, pp. 2216–2224, June 1993.

[112] J. R. Pierce, *The science of musical sound.* New York: W. H. Freeman and Co., revised ed., 1992.

[113] G. Pólya and G. Szegö, *Problems and Theorems in Analysis, Parts I and II.* Berlin: Springer-Verlag, 1972.

[114] B. Porat, *Digital Processing of Random Signals.* Englewood Cliffs, NJ: Prentice-Hall, Inc., 1994.

[115] W. H. Press, B. P. Flannery, S. A. Teukolsky, and W. T. Vetterling, *Numerical Recipies in C.* Cambridge, England: Cambridge University Press, 1988.

[116] L. R. Rabiner and R. W. Schafer, *Digital Processing of Speech Signals.* Englewood Cliffs, NJ: Prentice-Hall, Inc., 1978.

[117] C. S. Ramalingam and R. Kumaresan, "Voiced-speech analysis based on the residual interfering sinal canceler (RISC) algorithm," in *Proc. ICASSP*, (Piscataway, NJ), pp. 473–476, IEEE Service Center, Apr. 1994.

[118] B. D. Rao and R. Peng, "Tracking characteristic of the constrained IIR adaptive notch filter," *IEEE Trans. Acoust. Speech Signal Process.*, vol. 36, pp. 1466–1479, Sept. 1988.

[119] D. C. Rife and R. R. Boorstyn, "Single tone parameter estimation from discrete-time observations," *IEEE Trans. Inform. Theory*, vol. 20, pp. 591–598, Sept. 1974.

[120] R. S. Roberts, W. A. Brown, and J. Herschel H. Loomis, "Computationally efficient algorithms for cyclic spectral analysis," *IEEE Signal Processing Magazine*, pp. 38–49, Apr. 1991.

[121] H. Royden, *Real Analysis.* New York: MacMillan Publishing Co., second ed., 1968.

[122] W. Rudin, *Real and Complex Analysis.* New York: McGraw-Hill Book Co., third ed., 1986.

[123] T. Saramäki and A. T. Fam, "Properties and structures of linear-phase FIR filters based on switching and resetting of IIR filters," in *Proc. IEEE International Symposium on Circuits and Systems*, (Piscataway, NJ), pp. 3271–3274, IEEE Service Center, 1990.

[124] R. O. Schmidt, *A signal subspace approach to multiple emitter location and spectral estimation.* PhD dissertation, Stanford University, 1981.

[125] M. R. Schroeder, "Period histogram and product spectrum: new methods for fundamental-frequency measurement," *J. Acoust. Soc. Am.*, vol. 43, pp. 829–834, 1968.

[126] X. Serra, *A System for Sound Analysis/Transformation/Synthesis Based on a Deterministic Plus Stochastic Decomposition.* PhD dissertation, Stanford University, Department of Music, Oct. 1989.

[127] J. Smith, "Analysis and performance evaluation of an adaptive notch filter," *IEEE Tr. Info. Th.*, vol. 30, Mar. 1984.

[128] J. O. Smith and X. Serra, "PARSHL: An analysis/synthesis program for non-harmonic sounds based on a sinusoidal representation," in *Proc. of the International Computer Music Conference, 1987*, (Urbana, Illinois), pp. 290–297, 1987.

[129] D. Starer and A. Nehorai, "Polynomial factorization algorithms for adaptive root estimation," in *Proc. ICASSP*, (Glasgow, Scotland), pp. 1158–1161, 1989.

[130] Y. Stettiner, D. Malah, and D. Chazan, "Estimation of the parameters of a long-term model for accurate representation of voiced speech," in *Proc. ICASSP*, (Piscataway, NJ), pp. 534–537, IEEE Service Center, 1993.

[131] T. G. Stockham, T. M. Cannon, and R. B. Ingerbretsen, "Blind deconvolution through digital signal processing," *Proc. IEEE*, vol. 63, pp. 678–692, Apr. 1975.

[132] P. Stoica and A. Nehorai, "Music, maximum likelihood, and Cramér-Rao bound," *IEEE Trans. Acoustics, Speech Signal Process.*, vol. 37, pp. 720–741, 1988.

[133] P. Stoica and A. Nehorai, "Performance analysis of an adaptive notch filter with constrained poles and zeros," *IEEE Trans. Acoustics, Speech, and Signal Processing*, vol. 36, pp. 911–919, June 1988.

[134] P. Stoica and A. Nehorai, "Convergence analysis of an adaptive pseudolinear-regression notch filtering algorithm," *Circuits Syst. Signal Processing*, vol. 10, pp. 245–259, 1991.

[135] M. Sun and R. J. Sclabassi, "Discrete-time instantaneous frequency and its computation," *IEEE Trans. Signal Processing*, vol. 41, pp. 1867–1880, May 1993.

[136] Y. Tougas and A. S. Bregman, "Auditory streaming and the continuity illusion," *Perception And Psychophysics*, vol. 47, no. 2, pp. 121–126, 1990.

[137] S. A. Tretter, "Estimating the frequency of a noisy sinusoid by linear regression," *IEEE Trans. Inform. Theory*, vol. 31, pp. 832–835, Nov. 1985.

[138] P. P. Vaidyanathan, *Multirate Systems and filter banks.* Englewood Cliffs, NJ: Prentice-Hall, 1993.

[139] J. Ville, "Theorie et application de la notion de signal analytic," *Cables et Transmissions*, vol. 2A, no. 1, pp. 61–74, 1948.

[140] A. Wang, "Frequency- and phase-lock loop tracking of partials." Abstract from the 1993 CCRMA Affiliates Meeting, May 1993.

[141] A. Wang and J. O. Smith, "On fast FIR filters implemented as tail-canceling IIR filters," *IEEE Trans. Signal Processing*, 1994, submitted.

[142] M. Wax, *Detection and estimation of superimposed signals.* PhD dissertation, Stanford University, Stanford, Calif., 1985.

[143] M. Wax and T. Kailath, "Detection of signals by information theoretic criteria," *IEEE Trans. Acoust. Speech Signal Process.*, vol. 33, pp. 387–392, 1985.

[144] M. Wax and I. Ziskind, "Detection of the number of coherent signals by the MDL principle," *IEEE Trans. Acoust. Speech Signal Process.*, vol. 37, pp. 1190–1196, 1989.

[145] M. Weintraub, *A Theory and Computational Model of Auditory Monaural Sound Separation.* PhD dissertation, Stanford University, Department of Electrical Engineering, Aug. 1985.

[146] D. H. Wolaver, *Phase-locked loop circuit design.* Englewood Cliffs, N.J.: Prentice Hall, second ed., 1991.

[147] J. J. Wolcin, "Maximum *a posteriori* estimation of narrow-band signal parameters," *J. Acoust. Soc. Am.*, vol. 68, pp. 174–178, July 1980.

[148] H. Wold, *A Study in the Analysis of Stationary Time Series.* Stockholm: Almqvist & Wiksell, 1954.

[149] D. Wulich, E. I. Plotkin, M. N. S. Swamy, and W. Tong, "PLL synchronized time-varying constrained notch filter for retrieving a weak multiple sine signal jammed by FM interference," *IEEE Trans. Signal Processing*, vol. 40, pp. 2866–2870, Nov. 1992.

[150] J. F. Yang and M. Kaveh, "Adaptive eigensubspace algorithms for direction or frequency estimation and tracking," *IEEE Trans. Acoust. Speech Signal Process.*, vol. 36, pp. 241–251, 1988.

[151] J. F. Yang and M. Kaveh, "Adaptive algorithms for tracking roots of spectral polyomials," in *Proc. ICASSP*, (Glasgow, Scotland), pp. 1162–1165, 1989.

[152] S. Zacks, *Parametric Statstictcal Inference.* New York: Pergamon, 1981.

Index